CREATION AND MODIFICATION OF POLYMERIC MATERIALS USING ELECTRON BEAM RADIATION

by

DALE C. MCHERRON

Dissertation submitted to the Faculty of the

Virginia Polytechnic Institute and State University

in partial fulfillment of the requirements for the degree of

DOCTOR OF PHILOSOPHY

in

Chemical Engineering

APPROVED:

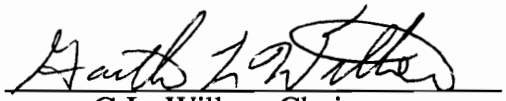

G.L. Wilkes, Chairman

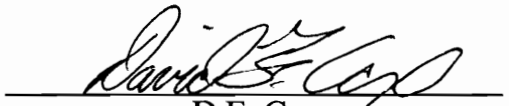

D.F. Cox

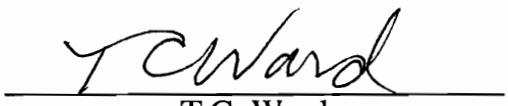

T.C. Ward

R.M. Davis

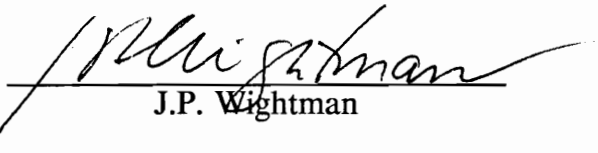

J.P. Wightman

Blacksburg, VA
November, 1991

CREATION AND MODIFICATION OF POLYMERIC MATERIALS USING ELECTRON BEAM RADIATION

by

Dale C. McHerron

Committee Chairman: G.L. Wilkes
Chemical Engineering

(ABSTRACT)

This dissertation begins with a review of radiation chemistry and a number of important variables which can influence the chemistry occurring in irradiated polymeric materials. Following the literature review, four different studies involving the electron beam irradiation and subsequent characterization of various polymeric materials are presented.

The first study describes a novel process that has been developed for producing crosslinked polymeric microspheres. With this process, it is possible to produce polymeric microspheres in an aqueous media with a solids content as high as 67 vol % by incorporating a trifunctional acrylate into a biliquid foam (known as polyaphrons) and exposing it to electron beam radiation. The second study involves characterizing the radiation response of a relatively new crystallizable polyimide, LARC-CPI, primarily in terms of its thermal properties as determined by differential scanning calorimetry (DSC), with some limited x-ray scattering experiments. The third study illustrates the effects of electron beam radiation on four different glassy polymers that have been physically aged prior to irradiation. It is shown that

irradiation reduces the extent of aging present in the material and that this reduction is proportional to the absorbed dose. The last study examines the crosslinking behavior of a polystyrene - poly(vinyl methyl ether) blend as a function of absorbed dose, composition, and phase separation. It is shown that the crosslinking behavior (in terms of the gel fraction produced) is strongly dependent on all three of these factors. Furthermore, the protective nature of the aromatic groups in polystyrene that is typically displayed by this polymer was not observed in this blend system.

ACKNOWLEDGEMENTS

First and foremost, I would like to thank Professor Garth L. Wilkes, for his guidance, support, and patience over the last 3+ years. It has been a truly rewarding and enjoyable experience to learn from Professor Wilkes and his dedication has been inspiring. Working with Professor Wilkes has made me a better scientist and I am indebted to him.

I would like to thank my committee members for their helpful discussions and time during the course of my research.

I am grateful to 3M Corp. and Amoco Corp. for financial support during my graduate career.

I greatly appreciate the help and support of the Chemical Engineering Department Staff: Dr. William Conger, Sandy Simpkins, Diane Cannaday, Sue Stoeckel, Diane Patty and Carol Stables. Their friendly dispositions, willingness to help, and experience with Va. Tech bureaucracy made my day to day activities much easier and fun.

I would like to express my appreciation to all my colleagues in the laboratory for their friendship, assistance, and support. I am especially appreciative to the older folks who helped me in getting established in the lab: Ha-chul (Chris), Cal, Tony, David, and Leo. Working with them and all my other colleagues has been loads of fun and I wish everyone the best of luck in their pursuits.

I would like to give a special acknowledgement to Sheri Bass for her love, friendship, and moral support throughout my graduate career. She has brought much happiness into my life. I would also like to say thanks to all my friends outside of the lab who have offered unlimited diversions away from the many hours I spent working.

Finally, and most importantly, I would like to thank my parents for all their love, support (both financial and moral), encouragement, and guidance over the years, without which this document would not exist today.

TABLE OF CONTENTS

LIST OF TABLES

LIST OF FIGURES

CHAPTER I

1.0 INTRODUCTION

Radiation chemistry is a science that deals with the chemical changes that occur in matter as a result of exposure to high energy ionizing radiation. High energy radiation includes electromagnetic radiation (i.e. x-rays and gamma rays), particles (such as alpha particles, beta particles or electrons, protons, and neutrons), and fission fragments (1).

The origin of radiation chemistry dates back to the discovery of x-rays by Roentgen (2) and radioactivity by Becquerel (3) in the 1890's. By 1900, alpha, beta, and gamma rays had been distinguished with regard to their charges and their respective abilities to ionize and penetrate various materials (4). The radiation chemistry of polymers, however, did not begin until the late 1920's. During this time period, Coolidge irradiated various organic materials with cathode rays (i.e. electrons) and reported on the formation of solid deposits on the walls of his equipment, eluding to the ability of radiation to induce polymerization (5). In 1929, E.B. Newton subjected rubber to cathode rays demonstrating that crosslinking could be achieved by radiation exposure (6). However, this early work was carried out before the development of powerful radiation sources. Hence, radiation chemistry did not really begin to flourish until World War II, when the Manhattan Project was undertaken to develop the atomic bomb. This not only developed interest in nuclear fission, but on the effects of radiation environments on materials as well. Most

notably however, was the work of Charlesby, who in 1952, demonstrated that polyethylene could be transformed into an insoluble, crosslinked material with high thermal stability (7). This work illustrated that desirable physical properties in polymers could be achieved by radiation processing, and since that time radiation chemistry of polymers has been a rapidly growing field in both academic and industrial arenas.

More recently, the crosslinking of radiation sensitive prepolymers and oligomers, particularly for thin film applications, has become a significant area of research, especially in industry. This type of process offers the advantages of reduced energy requirements and solvent free preparations over conventional thermal curing. Especially with growing concerns of environmental impacts from industry, radiation processing will undoubtably continue to be an area of active research.

This dissertation encompasses experiments in both areas of polymer radiation chemistry: the effects of radiation on polymeric materials, and the use of radiation for crosslinking reactive oligomeric species. All of the work involves the use of an electron beam as the radiation source.

A brief account of the history of polymer radiation chemistry has been outlined in this introduction. In subsequent sections, a comparison of various types of radiation, some general features of the interaction of radiation with condensed organic systems, radiation effects on polymers, and electron beam radiation chemistry of acrylated oligomers are discussed, comprising the literature review. Following the

literature review, experimental results and conclusions are reported on: (1) the formation of polymeric microspheres using electron beam radiation, (2) the effects of electron beam radiation on the differential scanning calorimetry (DSC) behavior of LARC-CPI, (3) electron beam effects on several physically aged polymers (polycarbonate, poly(methyl methacrylate), and polystyrene) and (4) electron beam irradiation of polystyrene - poly(vinyl methyl ether) blends.

CHAPTER II

2.0 LITERATURE REVIEW

2.1 COMPARISON OF RADIATION SOURCES

The electromagnetic radiation spectrum spans a wide range of energies and corresponding frequencies. Figure 2-1 depicts the majority of the electromagnetic spectrum (part of the low frequencies are omitted) and the assignments of various types of radiation that are currently known to exist. Along with the spectrum and the assignments are the corresponding types of energies associated with molecules. It should be noted that these assignments are not sharp or distinct; there is some overlap among both the radiation and molecular labels, but it is useful to define the relative energy scales for various radiation sources and molecular energy modes. These assignments are important in that they may indicate how various types of radiation might interact with molecules. For instance, microwaves will primarily affect the translational and rotational energies of molecules since they both have similar characteristic frequencies or energies. Likewise, ultraviolet rays will preferentially interact with the electrons in the outer orbitals of a molecule. Of course, other factors may influence what interactions occur (if any), but this concept does illustrate one necessary prerequisite.

Due to their respective energies and frequencies, many types of radiation have been found to be of utility for various applications in chemical science. For example, x-rays and visible light are useful for discerning molecular superstructure because

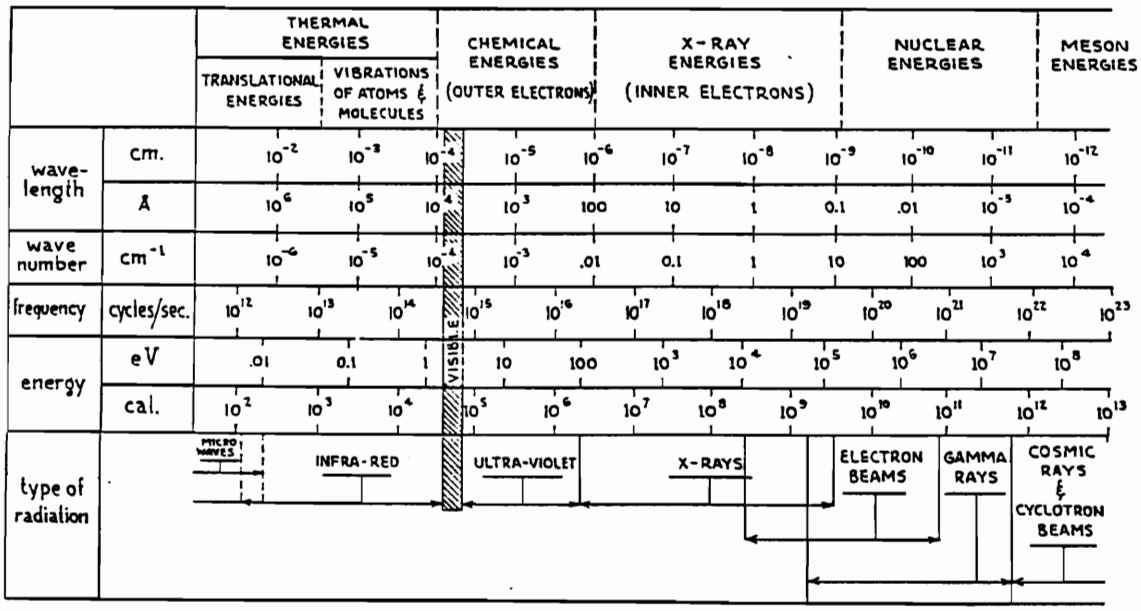

Figure 2-1. The electromagnetic spectrum and assignments of various types of radiation. (ref. 8)

their respective wavelengths are on the same scale as crystalline planes, phase structures in multicomponent systems, etc. Infrared radiation is used for determining the presence of various functional groups and atomic structures because this frequency is in the same region as the vibrational modes of molecules. On the other hand, microwaves (as well as some infra-red radiation), ultra-violet, electron beam, and gamma radiation have all been utilized in the processing of polymers to induce changes in chemical structure. Hence, due to the nature of this research proposal, the interactions of these types of radiations (especially electron beams) with organic matter will be more fully discussed.

2.1.1 Microwaves

Microwaves are electromagnetic radiation with energy in the range of about 0.001 to 0.01 eV. The absorption of microwaves (as well as infra-red radiation) results in the generation of heat which is the primary mechanism for bringing about chemical reaction with this type of radiation. However, the absorption of microwaves is strongly dependent on the chemical structure and composition of the polymer. In particular, the dipole character of the polymer will play a key role in determining the sensitivity to microwave radiation.

Microwave heating is essentially the same as dielectric heating except that the latter is done at a lower frequency. In essence, exposure to microwaves is akin to being in the presence of an alternating electric field. When molecules are placed in an electric field, polarization occurs. If permanent dipoles are present, they will try

to align themselves with the electric field. The electric field may also induce dipoles, depending on the strength of the field and the polarizability of the medium. In any case, for microwave heating to occur, permanent dipoles must be present. When a permanent dipole is present in a microwave field, it will be constantly trying to realign itself as the field alternates. If the frequency is high enough (which will be material dependent) the dipoles will not be able to "keep up" with the alternating field, which will result in dielectric loss (the extent of this is characterized by the dielectric loss factor). This dielectric loss is dissipated through heat to the medium. The higher the dielectric loss factor, the easier it is to heat the material with microwaves. However, structural characteristics of the material must also be considered, especially the glass transition temperature. If the glass transition temperature is significantly higher than the processing temperature, heating may be hindered even if permanent dipoles are present. This is due to the restricted mobility of molecules in the glassy state. If the dipoles are effectively "frozen" in place, microwaves will not increase the translational energy (i.e. temperature) arising from dielectric loss since the molecules are severely restricted.

The fact that some polymers contain dipoles while others do not gives rise to microwave sensitive and microwave transparent materials, respectively. This may be desirable in some multicomponent systems where preferentially heating of one component is necessary. This concept is the basis for microwave drying of polymers. In this process, water (or some other polar solvent) will preferentially absorb energy

and evaporate without excessive heating of the polymer matrix. It has been shown that polyolefins are well suited to this type of process (due to their low dipole character), while materials with more polar groups, such as polyisoprene and hydroxyethyl cellose, have limited applicability (9).

Microwaves have also been utilized for thermally inducing polymerizations (10). This technique gives much more uniform heating than conventional thermal processes because energy is imparted equally to all molecules (assuming the molecules have similar character) thereby eliminating temperature gradients due to conduction in convective thermal processing of bulk materials. It should be noted however, that "hot spots" can occur, which are localized regions with higher temperatures than the surroundings, due to the presence of microwave sensitive groups. In addition, temperature gradients near the surface may arise with microwave processing due to convective heat transfer to the surroundings.

In systems that are not particularly susceptible to microwave heating, it is possible to facilitate heating (and subsequent polymerization) by incorporation of a metallic component. Several studies (11,12) have been made on the polymerization of epoxy resins that have metallic powders of iron or copper dispersed in the epoxy matrix. When exposed to microwaves, the metal heats up very quickly, and conductive heat transfer to the resin occurs, causing polymerization.

Although microwave radiation can induce chemical changes, the mechanism differs sharply from ultra violet, electron beam and gamma radiation processes.

Microwave induced polymerization involves a process of thermally inducing chemical reactions, whereas the other radiation schemes involve direct production of excited species to effect chemical change. Hence, microwave processing is more closely related to conventional thermal treatments (although differences do exist, especially with respect to kinetics) than other forms of radiation processes that will be discussed.

2.1.2 Ultra-Violet

Ultra-violet (UV) light is characterized by electromagnetic radiation with energy in the range of about 5 to 50 eV. The energy associated with UV light is generally not sufficient to cause ionization of molecules, although ionization may occur in some molecules with low electron affinity if exposed to high frequency UV light. Hence, UV light is not considered ionizing radiation unlike x-rays, electron beams, or gamma rays, which do possess the energy necessary for ionization. However, UV light does have the energy required to cause molecular excitation (i.e. movement of an electron to a higher energy level). For excitation and subsequent chemical reaction to occur, a molecule must be able to absorb a photon of light. This is known as the Grotthus - Draper law (13). Molecules capable of absorbing a photon of UV light possess absorption bands in this region of the spectrum and are known as chromophores. Since not all molecules are capable of absorbing photons in the UV region, the absorption of UV light is a selective process which is governed by the Beer - Lambert law (14):

$$\frac{I}{I_0} = 10^{-(\sum_i \epsilon_i c_i)b} \qquad [1]$$

where:

I_0 = incident light intensity
I = light intensity at point "b"
b = sample depth
ϵ_i = molar extinction coefficient of species i
c_i = molar concentration of species i

Assuming a homogeneous material, this law predicts the intensity of light decreases exponentially with sample thickness. The extinction coefficient defines how "strong" an absorber a molecule is and this value may vary from 100 M^{-1} cm^{-1} for "forbidden transitions" (i.e. no photon absorption due to electron spin considerations) to 10^5 M^{-1} cm^{-1} for "fully allowed" transitions (i.e. strong UV absorption bands). Table 2-1 gives some values for extinction coefficients and the maximum of the absorption band for a variety of different polymers. Inspection of this table illustrates the strong dependence of UV absorption on the molecular structure of the polymer and not on the atomic composition. For instance, polyethylene and polystyrene have similar atomic compositions (i.e. they both consist of only carbon and hydrogen) yet their UV absorption characteristics are quite different. This is in sharp contrast to ionizing radiation such as gamma rays or electron beams, where absorption is fairly independent of the molecular structure. This distinction is due to the relative energies of UV and gamma or electron beam radiation compared to the binding

Table 2-1. Extinction coefficients and maximum absorption bands for various polymers. (ref. 15)

Polymer	λ_{max}, nm	ϵ, $M^{-1}cm^{-1}$ [a]
polyethylene	140	
poly(methyl methylacrylate)	214	170
poly(methyl vinyl ketone)	290	18
polystyrene	269	175
	262	222
poly(2-isopropenylnaphthalene)	323.5	242
	280	4550
poly(*N*-vinylcarbazole)	345	4500
	293	12900

[a] In moles of repeating units.

energies of electrons, as well as the fact that energy must be conserved during absorption. Since UV radiation only possesses enough energy to excite molecules, the electron energy levels associated with a molecule (i.e. molecular structure) will determine if it can absorb a photon of UV light; the photon energy must equal the difference between two electron energy levels for the photon to be absorbed and excite the molecule. On the other hand, gamma radiation has photon energies that are in excess of the binding energies. In this case, an electron is completely removed from its parent atom and the energy levels within the atom are of no significance.

Since UV absorption requires the presence of chromophores, photopolymerization must be carried out on species which contain such groups, otherwise a photoinitiator must be added to the system. Once excited, photoinitiators react with monomer to facilitate a chain reaction, producing a polymer. The use of photoinitiators is useful in that the free radical concentration (and subsequently the molecular weight) can be precisely controlled, although they do introduce impurities into the system which may be undesirable for certain applications.

Once chromophores become excited by UV light, a number of processes may occur. Some of these processes result in chemical change, such as those responsible for photopolymerization. However, other processes such as fluorescence and phosphorescence, do not result in any permanent chemical change and are considered in the realm of photophysics. Discussion of these processes is not within the scope of this research proposal, and the reader is referenced to several reviews

(17,18) on this subject. It should be noted however, that the section on chemical changes induced by electron beams will discuss some features that may be pertinent to photoprocesses as well.

2.1.3 Gamma Radiation

Gamma radiation is electromagnetic radiation with energy in the range of approximately 50 keV to about 60 MeV. X-rays overlap into the lower end of this range, so the interactions with matter for these types of radiation are very similar.

As with UV light, the absorption of gamma rays is governed by the Beer - Lambert law. However, the interaction of gamma rays with matter is not a selective process as with UV light, and it depends primarily on the atomic composition and not on the molecular structure (as previously discussed). In particular, absorption depends on the atomic number of the atoms present, i.e. the concentration of electrons in the medium. Gamma rays interact primarily with electrons causing ionization, so as the concentration of electrons increases, more interactions occur and absorption increases. The extent of absorption is quantified by the extinction or absorption coefficient as defined in the Beer - Lambert law (see previous section). For gamma rays, this absorption coefficient is determined by the contributions of three different energy deposition processes. These processes include the photoelectric effect, Compton scattering, and pair production. The relative extent of these interactions depends on the energy of the gamma ray photons. Figure 2-2

illustrates the relative contributions of these processes to the total absorption coefficient in water as a function of photon energy.

Photoelectric Effect

As illustrated in Figure 2-2, the photoelectric effect is negligible for photon energies above 60 kev. In this process, the photon is completely absorbed by an atom and an electron is ejected. The energy of this electron is equal to the energy of the photon minus its own binding energy, in accordance with the conservation of energy. The electron ejected usually occupies an inner orbital, and once ejected, an outer electron may drop down to occupy this vacancy with emission of a low energy x-ray. If the atomic number is low (which is the case for most organic polymers), it may be more likely that this energy will eject another electron from the same atom instead of x-ray production (Auger effect).

The absorption coefficient for the photoelectric contribution per electron is given by (19):

$$\tau_e \sim (\frac{Z}{h\nu})^3(1 + 0.008Z) \qquad [2]$$

Hence, photoelectric absorption is strongly dependent on both the atomic number, Z, and the energy of the incident photon ($h\nu$).

Compton Scattering. Compton scattering predominates in low atomic number species when photons have energies ranging from 60 keV up to about 10 MeV. This

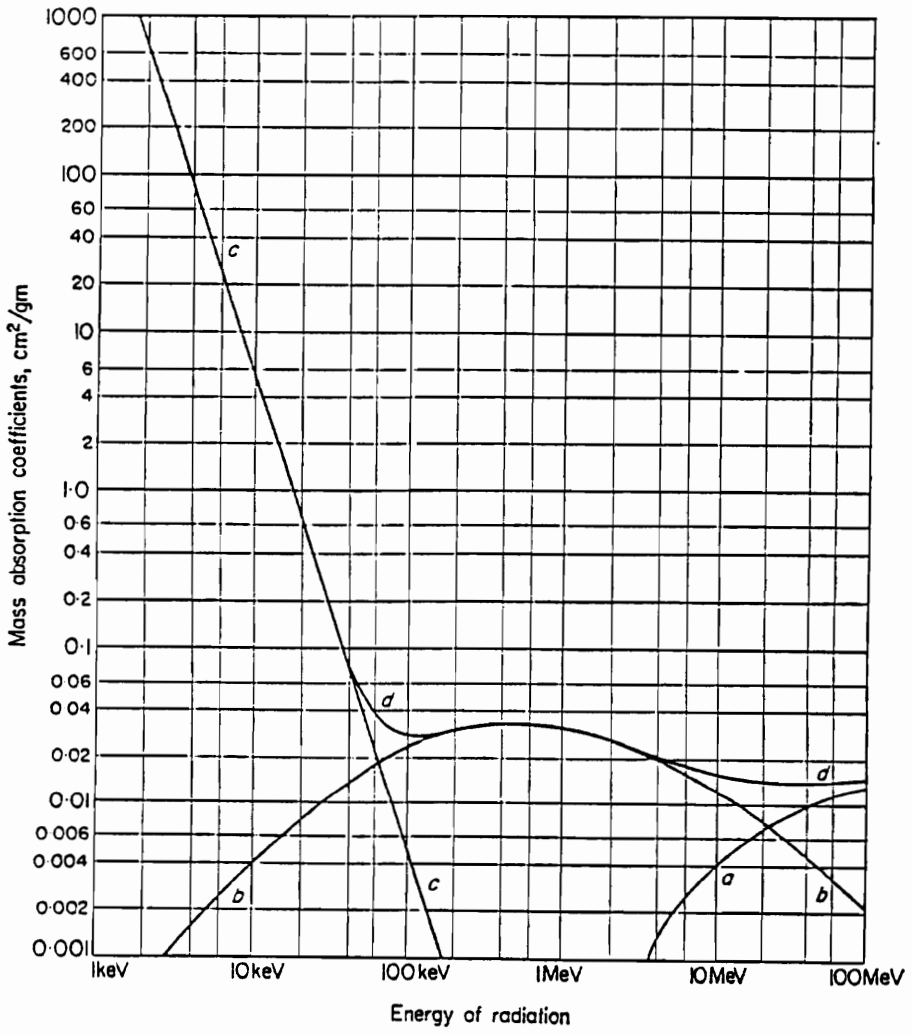

Figure 2-2. Relative contributions of (a) pair production, (b) Compton scattering, and (c) the photoelectric effect to (d) the total absorption coefficient of gamma radiation in water as a function of photon energy. (ref. 16)

phenomenon is the primary mechanism of energy deposition for ^{60}Co radiation, which usually consists of gamma rays with energies around 1.2 MeV. In this process, a photon transfers part of its energy to an electron (usually an outer shell electron) which is subsequently ejected. The photon then continues in another direction with lower energy, to interact further via compton scattering or the photoelectric effect, depending on its energy. If the binding energy of the electron can be considered insignificant compared to the energy of the photon, which is usually the case for low atomic number species, then the compton scattering contribution to the absorption coefficient will depend only on the concentration of the electrons in the medium and not on the photon energy.

Pair Production

Pair production is the only process by which gamma rays interact with the nucleus of an atom. This process only becomes significant at high energies, usually above 3 MeV for atoms with low atomic number. Hence for most applications, pair production is not a significant contribution to the energy deposition process.

In pair production, the photon is completely absorbed by the nucleus of the atom which results in the production of a positron - electron pair. This is an example of the conversion of energy to mass. The kinetic energy of the pair equals the energy of the photon minus 1.02 MeV, which corresponds to the rest mass of the pair. Once ejected from the nucleus, the electron may interact with the medium as will be described in the next section. Once the positron is ejected it will begin to slow down

and will eventually become annihilated by combining with another electron. When this occurs, two photons are created with energies of 0.51 MeV each, and travel in opposite directions, which will further react with the medium (19).

It is quite evident that exposure to gamma radiation results in ionization of the medium and the generation of energetic electrons. Thus, gamma radiation is very similar to electron beam radiation except that free electrons are created within the medium instead of externally, as is the case for electrons beams. In addition, the absorption of gamma radiation obeys the Beer - Lambert law, while the absorption of electron beams is more of a random process. Qualitatively, the results are similar - ionization and excitation of the medium and the production of free electrons. Due to these similarities, the topic on electron beam radiation will only include aspects which make this area unique, while a separate section will be devoted to the interactions of energetic electrons with organic matter.

2.1.4 Electron Beam Radiation

Electron beam radiation, in contrast to other types of radiation discussed, is best described as particulate in nature, rather than possessing wave characteristics. Electron beams are generally produced from electronic equipment, but radioisotopic sources do exist. The latter sources are usually considered as beta ray emitters. The energy of an electron beam produced from an electronic source is monoenergetic and depends on the accelerating voltage of the system. This voltage can be as low as several keV for applications in electron microscopy or as high as 20 MeV for

powerful electron accelerators used in industry. These voltages are necessary to achieve sufficient penetration depth in processing because the penetration of electron beams is much less than for electromagnetic radiation of the same energy. For example, a 1 MeV electron beam can penetrate about 0.5 cm of water, while a gamma ray of the same energy has a half value thickness (thickness required to reduce the initial intensity to half of its original value) of 10 cm (20). Hence, electron beams are well suited for applications in thin films, but are of limited utility where large penetration depths are required, except where extremely high electron energies can be generated. It should also be noted that electrons produced from most commercial accelerators are more energetic than the electrons ejected from atoms through gamma rays. The increased penetration capability of gamma rays is due to the nature of the gamma ray itself, and not the free electrons that are produced.

Since the energy of electrons produced from electronic accelerators is significantly higher than the free electrons generated in a medium from gamma rays, the mechanism of energy deposition may differ. In particular, at higher energies electrons may lose a considerable portion of their energy by deceleration induced by the nuclear field resulting in the emission of x-rays (known as bremsstrahlung). The ratio of energy lost by bremsstrahlung (E_b) to that by ionization (E_i) and excitation is given by (21):

$$\frac{E_b}{E_i} = \frac{EZ}{800} \quad (E \text{ in } MeV) \qquad [3]$$

This phenomena limits the penetration depth of high energy electron beams, but it should be noted that the x-rays produced by this process may cause further ionization and excitation.

Since the mechanism of electron energy deposition which directly results in ionization and excitation of organic matter is pertinent to both gamma and electron beam radiation, a separate section will be devoted to this subject. While some concepts will be focused toward electron beam applications, many of the general features encompass any fast electron moving in condensed media, regardless of whether they are produced by an external source, such as an electron accelerator, or internally by gamma radiation.

2.2 FEATURES OF THE INTERACTIONS OF FAST ELECTRONS WITH ORGANIC MATTER

This section will focus on the energy deposition mechanism of fast electrons in condensed media and the early events that are a result of this energy deposition. In particular, the concepts of ionization and excitation will be discussed as well as stopping power and its influence on ionization and the resulting track structures. This will lead to some of the other events that occur, such as energy transfer and subsequent chemical reactions, which will be covered in the next section.

Fast electrons deposit energy when travelling through condensed organic media primarily by the processes of ionization and excitation. As previously discussed, fast electrons may also interact with nuclei which results in x-ray production, but this process only predominates at very high electron energies. Electrons may also interact with nuclei through elastic collisions, but this is a rare case and usually little energy is lost by the electron. These nuclear interactions typically do not result in any chemical transformation (although x-ray production may cause subsequent chemical reactions). Hence, ionization and excitation are the primary mechanisms that are of concern in radiation chemistry.

2.2.1 Ionization and Excitation

Ionization and excitation of atoms and molecules result from the interaction of free, fast electrons with orbital electrons. This interaction involves inelastic collisions between free and orbital electrons, which results in energy loss of the free electron

(with little change in direction). This energy is transferred to the orbital electron and if this energy is greater than the binding energy of the electron, ionization occurs and the electron is ejected from the atom. If not, the electron will jump to a higher energy level causing excitation, since insufficient energy was imparted to cause complete electron removal.

The kinetic energy of an electron produced from a typical accelerator is much higher than the kinetic or binding energy of a valence electron. Table 2-2 gives the velocity (relative to the speed of light) of electrons as a function of the kinetic energy and accelerating voltage. For instance, electrons with a kinetic energy of 175 keV have a velocity and kinetic energy that are about 100 times and 10,000 times that of a hydrogen atom valence electron, respectively. Hence, one fast electron is capable of interacting with a large number of orbital electrons causing numerous ionization events before all its energy is dissipated to the medium. The number and frequency of these interactions is dependent on the energy of the electron as well as electron density of the medium. As the energy of the electron is dissipated, the electron slows down and interacts more frequently, due to the longer time available for interaction with a particular electron at lower velocities. Hence, more ionization events occur toward the end of the electron's path through a medium than at the beginning. However, as the energy of the electron approaches the energy required for ionization, the number of ionization events decreases. This dictates that the rate of energy transfer will vary along the path of the electron. There are two parameters which

Table 2-2. Velocity of electrons as a function of kinetic energy and accelerating voltage (relative to the speed of light). (ref. 22)

Velocity (Relative to c)	Kinetic Energy (MeV)	Accelerating Voltage (kV)
0.001979	10^{-6}	0.001
0.00730*	----------	-----
0.006257	10^{-5}	0.001
0.00240	1.46×10^{-4}	0.146
0.1950	10^{-2}	10
0.4127	0.05	50
0.5483	0.10	100
0.8629	0.50	500
0.9068	0.70	700
0.9411	1.0	1000
0.9791	2.0	2000
0.9893	3.0	3000
0.9934	4.0	4000
0.9957	5.0	5×10^3
0.9988	10.0	10^4
0.9999871	100.0	10^5

* Bohr velocity of an electron in the ground electronic state of hydrogen

relate to this concept - stopping power and the depth-dose profile or linear energy transfer (LET). Linear energy transfer is defined as the energy absorbed by a medium per unit thickness (dE/dz) and the stopping power is defined as the energy lost by an electron per unit path length (dE/dS). If the thickness of the specimen is small compared to the maximum penetration depth of the electron then the path length (S) can be approximated by the thickness (z). In addition, if the electron energy is not too high, than the energy lost by the electron equals the energy locally absorbed by the medium. Under these conditions, the LET (or depth - dose function) and stopping power are equivalent.

2.2.2 Stopping Power

Stopping power is essentially a function that describes the dissipation of energy of a charged particle as it traverses through a medium. It is dependent on the energy and charge of the particle and the nature of the medium. The Bethe equation is a useful relation for determining the stopping power of electrons, which in one form, is expressed as (23):

$$\frac{dE}{dS} = 7.84x10^{10} \frac{\rho}{E} \sum_i c_i \frac{Z_i}{A_i} ln(\gamma \frac{E}{J_i}) \qquad [4]$$

where:

E = electron energy (eV)
S = electron path length (cm)
ρ = density of medium (gr/cm)

C_i = weight fraction of species i
Z_i = atomic number of species i
A_i = atomic weight of species i
J_i = mean ionization energy of species i (eV)
γ = 1.166

Equation (4) is quite accurate in the range of $10 < E < 10^5$ keV, but corrections do exist for energies below this range (19). This relationship was originally developed from quantum mechanical considerations by Bethe in 1933 (32). It relies on the Born approximation, which is valid only when the incident particle has a much higher velocity than the orbital electrons. Hence, limitations on the electron energy must be made. This relationship assumes simple additivity of the atoms present to determine the overall stopping power of the medium. This reflects the statistical nature of electron energy deposition involving electron - electron inelastic collisions. This relationship indicates that the species which has the greatest contribution to the overall electron concentration will absorb most of the energy lost by the incident electron (which is in sharp contrast to the nature of UV absorption). Inspection of equation (4) reveals two factors. The logarithmic term, which increases quickly at first and rises slowly at high energies, and the front factor which steadily decreases with increasing electron energy. The combination of these two factors is illustrated in Figure 2-3, which gives the stopping power (dE/dS) for polystyrene as a function of incident electron energy (24).

Since stopping power will obviously vary depending on the electron energy and the nature of the medium being traversed, the penetration depth of an electron will

vary as well. The depth - dose function (dE/dz) lends itself to the determination of penetration depths more so than the stopping power because it is based on the energy dissipation as a function of sample depth rather than the actual path length of an individual electron. The Grun range defines the penetration depth of an electron and this parameter can be determined from the depth dose function or the following relation can be used to calculate it directly (25):

$$R_g = \left(\frac{0.047}{\rho}\right) E_0^{1.75} \qquad [5]$$

where:

R_g = Grun range (microns)
ρ = sample density (gr/cm)
E_0 = incident electron energy (keV)

This relationship was developed by Grun through his studies on the energy dissipation of electrons in air. He also demonstrated that the depth - dose function is invariant if the electron position and energy are normalized with respect to Rg and E_0, respectively. The normalized depth - dose function is given by (26):

$$\Lambda(f) = 0.74 + 4.7f - 8.9f^2 + 3.5f^3 \quad 5 < Z < 12$$
$$\Lambda(f) = 0.6 + 6.21f - 12.4f^2 + 5.69f^3 \quad 10 < Z < 15 \qquad [6]$$

where:

$\Lambda(f) = d(E/E_0)/d(z/R_g)$

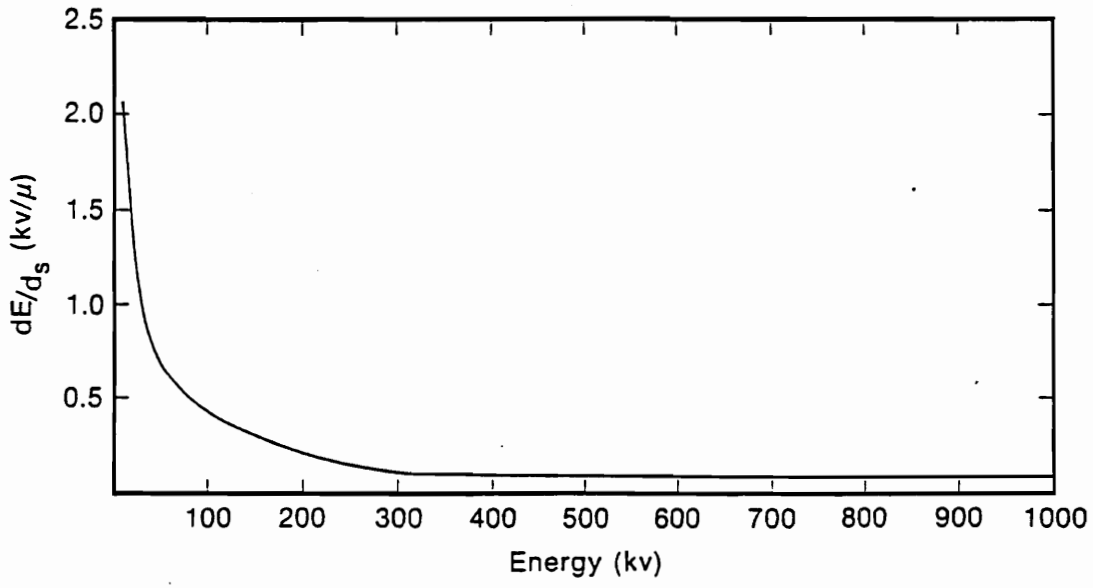

Figure 2-3. Stopping power for polysytrene as a function of incident electron energy. (ref. 24)

$$f = z/R_g$$

Note that the depth - dose function is empirical in nature as opposed to the stopping power, which gives insight into the factors which affect electron energy dissipation, due to its theoretical basis. Figure 2-4 graphically illustrates the normalized depth - dose function. Note that there is a maximum in the rate of energy transfer at about 0.4Rg, which is some distance into the medium and not at the surface. This maximum is the product of two factors. At small penetration depths the stopping power is increasing as the electron slows down, so the rate of energy dissipation increases. Eventually, the energy of the electron decreases to a point where it limits the energy dissipation (i.e at depths greater than $0.4R_g$) and the depth - dose function decreases and approaches zero as the Grun range is reached. In practical applications this depth - dose function may manifest itself by causing non-uniform curing or exposure, especially if the sample thickness approaches the Grun range. To obtain a uniform dosage through a sample, the thickness should be small compared to the Grun range. Thus, in electron beam applications, a significant portion of the electron beam energy is wasted to ensure uniform cure.

2.2.3 Track Structure

Since the energy dissipated from a high energy electron is a strong function of its energy at the particular time, the energy deposition will be non-uniform, as discussed. This non-uniform energy deposition gives rise to a spatial distribution of ionization and excitation within the medium, which will be non-uniform as well. The spatial

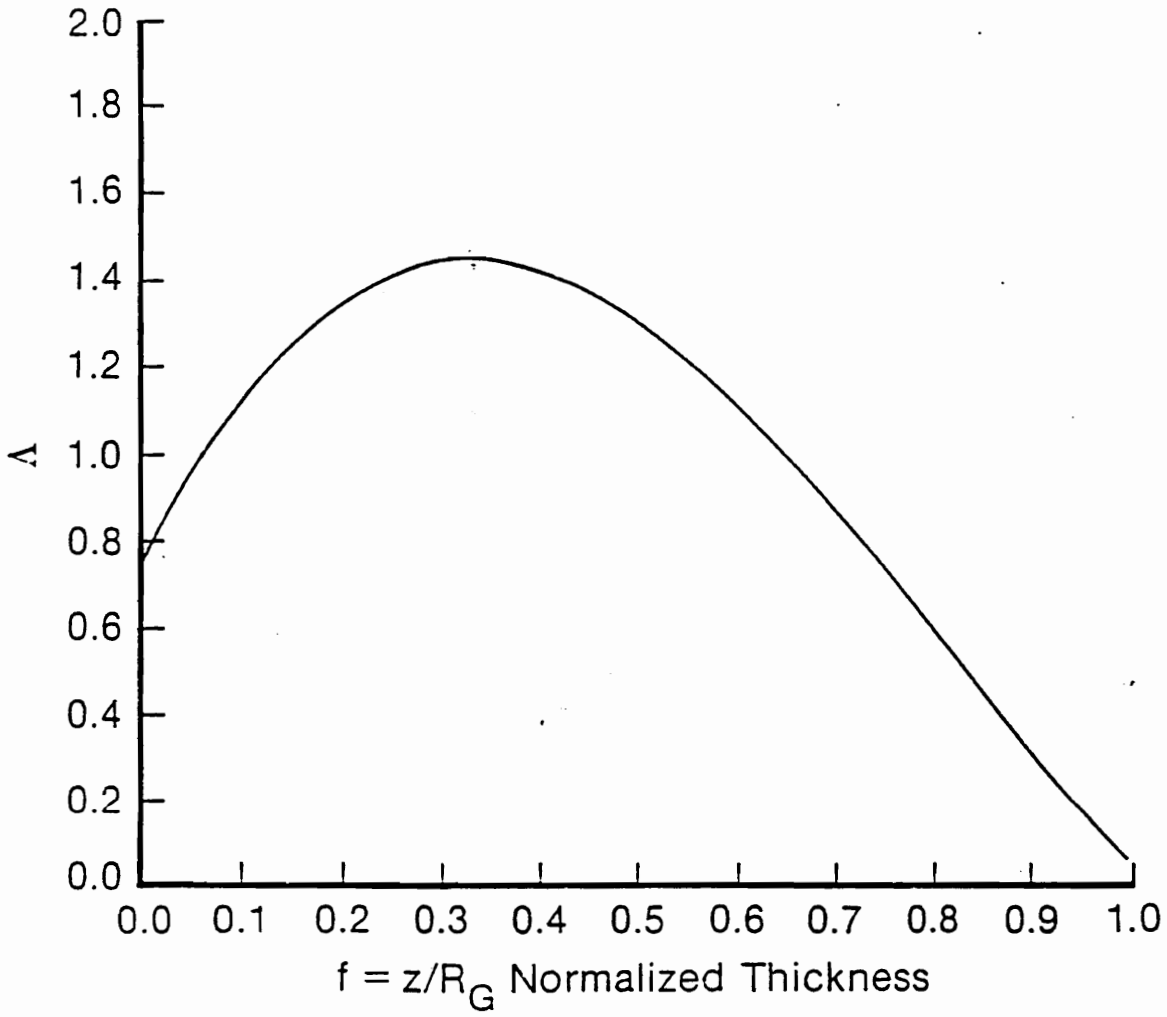

Figure 2-4. Graphical illustration of the normalized depth - dose function. (ref. 26)

distribution of localized regions of ionization is known as the track structure. A track is the path a primary electron takes through a medium and the localized regions of ionization are known as spurs. The stopping power plays an important role in determining the nature of the track structure and how the individual spurs are distributed. To illustrate this, several definitions and their relation to electron beam processing parameters need to be made. First, is the concept of specific ionization (SI), which is defined as the total number of ion pairs formed per unit track length (22):

$$SI = \frac{(dE/dS)}{W} \qquad [7]$$

where: W = total energy consumed per ion pair formed

The two electron beam parameters of interest are the accelerating voltage and the current density. The accelerating voltage determines the kinetic energy of the electron and hence will govern the stopping power as well. As the accelerating voltage increases, the kinetic energy of the electron increases and both the stopping power and specific ionization will decrease. The current density determines the number of incident electrons per unit area. As the current density increases, the number of incident electrons per unit area increases, and hence the distance between individual tracks will decrease. The effects of the accelerating voltage (or stopping power or specific ionization) and the current density are illustrated in Figure 2-5. As

the stopping power increases, the spurs along a single track become closer together, since more energy is dissipated per unit track length. This ability to exert some control over the track structure with electron beam radiation is unique compared to gamma radiation, where the energy of the ejected electrons from photoelectric and compton scattering processes is not so easily controlled. Furthermore, the resulting track structure is a primary difference between various forms of ionizing radiation and hence is also a contributing factor to the different chemical changes which may take place.

It should be noted that the track structures depicted in Figure 2-5 represent only the contribution of the incident electron to the total track structure and assumes no change in the specific ionization (or stopping power) along the path. This assumption is not valid if the sample thickness approaches the Grun range of the electrons. In reality, the track structure can be quite complex. The spurs will become closer together as the electron slows down and the rate of energy dissipation increases. In addition, some electrons ejected from atoms as a result of ionization (known as secondary electrons or delta rays) will have sufficient energy to form short tracks of their own, which will appear as branches off the primary track. This is depicted in Figure 2-6, which shows a typical track structure formed by a 1 MeV electron. The track structure consists of three entities: spurs, short tracks, and blobs. Classification of these ionized regions is based on the energy deposited; spurs are regions with 6 to 100 eV of energy deposited, blobs -- 100 to 500 eV, and short tracks

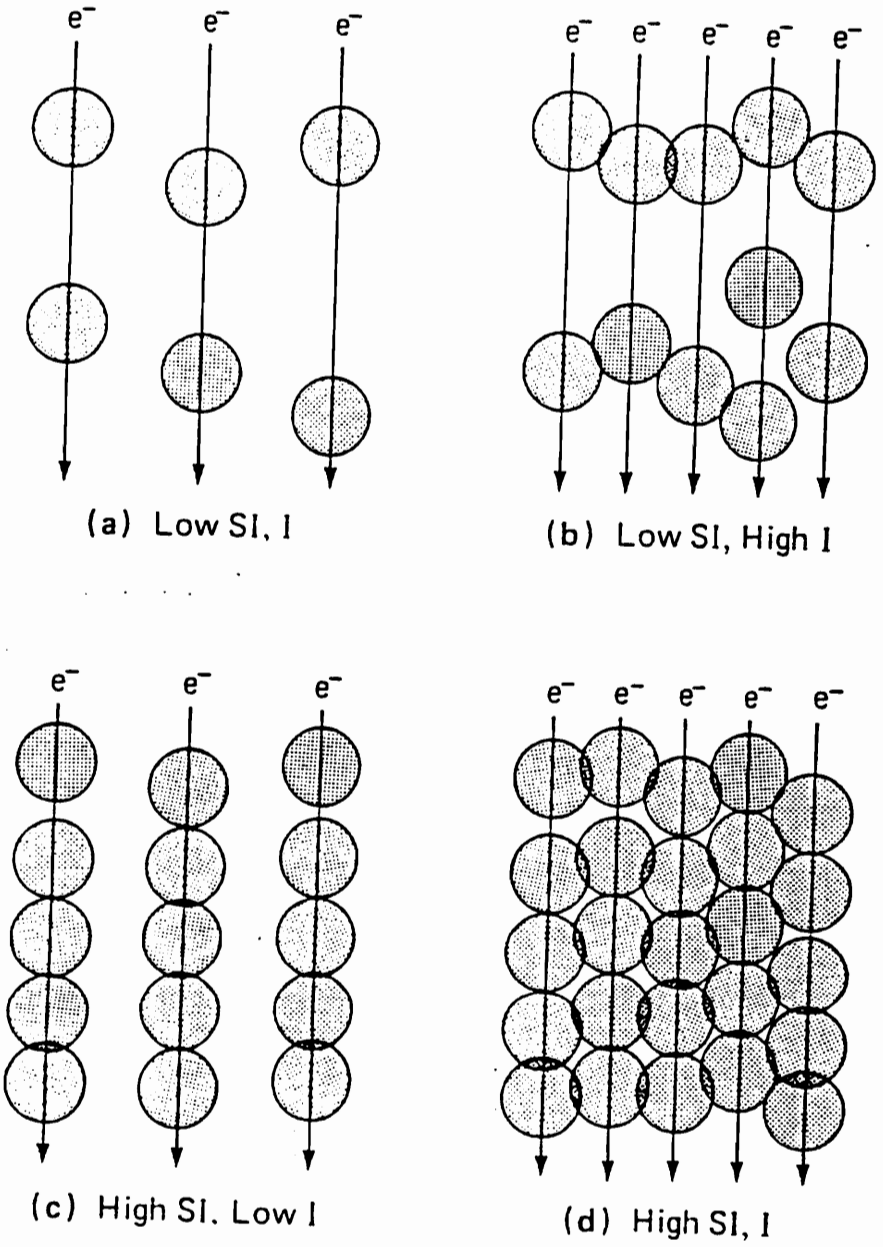

Figure 2-5. Effects of specific ionization (SI) and current density (I) on initial track structure. (ref. 22)

-- 500 to 5000 eV of deposited energy. Isolated spurs contain the least amount of deposited energy and are thought to be spherical regions which contain 1 to 4 ionized species. Short tracks contain much greater amounts of deposited energy and are made up of closely spaced spurs, and may be considered as cylindrical regions of ionization. Blobs are considered to be pear shaped regions and created by ejected electrons that have insufficient energy to escape the attractive field of its parent atom and hence are treated as a separate entity (27). The relative population of these track components depends strongly on the energy of the electron. For example, Mozumder and Magee (28) have calculated that a 20 keV electron dissipates 38% of its energy as isolated spurs and 50% as short tracks, while a 10 MeV electron deposits 76% of its energy as isolated spurs and only 16% as short tracks. This illustrates that as the energy of an electron increases, more isolated spurs are produced (indicative of a lower rate of energy deposition) which is commensurate with a decrease in stopping power.

Eventually, an electron will have lost most of its initial energy and will no longer be able to ionize or excite molecules. These electrons may further dissipate energy through atomic rotational and translational transitions until its energy decreases to the thermal energy level of the medium. These electrons are then likely to be captured by positive ions, neutral molecules (particularly oxygen) or possibly free radicals, although the exact nature of the fate of these thermal electrons is still debatable.

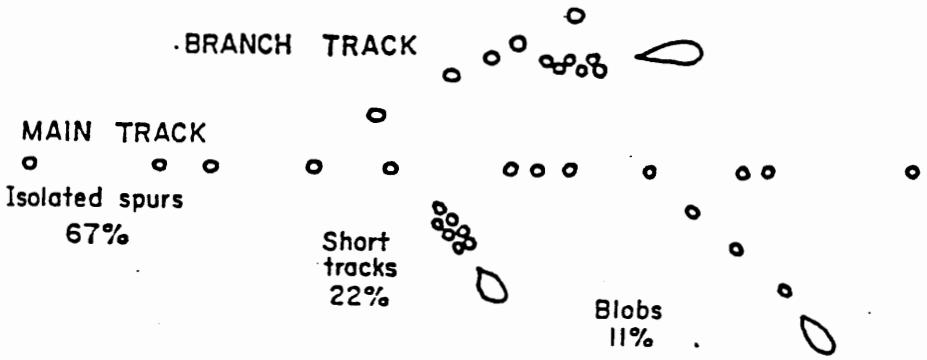

Figure 2-6. Typical track structure for a 1 MeV electron in water. (ref. 27)

This section has covered the interactions of fast electrons in condensed media. It has focused primarily on the concept of stopping power and its influence on the spatial distribution of localized electron - molecule interactions. Once these initial interactions have occurred, processes involving ions, free electrons, excited species, etc. become significant, which is the topic of the next section.

2.3 PROCESSES IN CONDENSED MEDIA FOLLOWING RADIATION EXPOSURE

Upon exposure of a medium to ionizing radiation, ions, excited species, and free electrons are created. Hence, processes occurring after radiation exposure involve interactions among these entities as well as neutral molecules. Before discussing events which produce chemical transformations, the concept of energy transfer will be covered, since it is of extreme importance in the electron beam processing of mixtures, due to its effect on the chemical reactions which subsequently take place.

2.3.1 Energy Transfer

Radiation induced reactions typically use less energy than is absorbed by the reactants. However, in some cases, particularly when a mixture of functional groups are present, the extent of reaction is far greater (or far less) for a given species than would be expected from its contribution to the stopping power of the medium. This suggests that energy is transferred from one type of molecule to another to account for the enhanced (or hindered) reactivity observed. A common example of this is the "shielding" (from radiation) that can be observed in some polymers when aromatic species are added to the system. In this case, the reactivity of a polymer is reduced due to the presence of the aromatic groups which act as an energy sink. It is also possible to create situations where the reactivity of a particular species is enhanced (as will be discussed).

Energy transfer is a very general term and seems to be used loosely, which may be the result of our lack of understanding concerning the actual processes occurring. Most of our knowledge on energy transfer has been developed in the field of photochemistry, and hence our understanding of excitation energy transfer is more thorough than other forms of energy transfer. In general, energy transfer can involve the transport of mass (in conjunction with charge or excitation energy), charge alone, or excitation energy alone. Energy transfer involving mass transport describes the diffusion of hydrogen atoms commonly encountered in irradiated polymers, but this does not radically alter the reactivity of specific functional groups, and as such it will not be given further consideration.

Charge Transfer

Charge transfer in polymers involves migration of electrons or positive charges. The transfer may be electronic in nature (transfer of charge only) or ionic (transfer of charge and mass, such as protons). Hence, charge transfer results in electrical conductivity in polymers, although this may be extremely short lived. Hirsch and Martin (29) have reported that the electrical conductivity in a variety of polymers exposed to pulse radiolysis consists of a "prompt" component and a "delayed" component. The prompt component involves transfer of a significant amount of charge over short distances (on the order of 100 Å). The delayed component involves transfer over longer distances (on the order of a micron), although the

distance traveled is extremely temperature dependent. Both positive and negative charge transfer was observed, depending on the particular polymer in question.

Excitation Energy Transfer

Excitation energy transfer has been well characterized compared to other forms of energy transfer due to the extensive work done on this phenomena in the field of photochemistry. Six classifications of excitation energy transfer have been developed, some of which are found in irradiated polymers more than others. These six types of excitation energy transfer include (30):

1. Radiative Transfer - involves emission and capture of a photon between two molecules with overlapping emission and absorption spectra.

2. Exchange Transfer - transfer by electron exchange interactions between species with overlapping orbitals.

3. Excimer Transfer - involves combination of an excited molecule with a similar unexcited molecule with subsequent dissociation and transfer of energy.

4. Forster Long Range Transfer - caused by columbic interactions between two molecules (usually dissimilar, with overlapping emission and absorption spectra) that make coupled electronic transitions - the donor going from an excited to ground state while the acceptor goes from the ground to an excited state (of lower energy than the donor excited state). Separation distances can approach 100 Å, and the rate of energy transfer has been found to be proportional to the inverse sixth power of the separation distance (31).

5. Molecular Exciton Transfer - similar to Forster transfer, except that the rate of energy transfer is proportional to the inverse cube of the separation distance, due to stronger coupling energies than Forster type transfers.

6. Charge Transfer Excitons - energy transfer process with characteristics of both charge and excitation transfer.

A more complete review of these types of energy transfer is given by Partridge (30). As mentioned previously, energy transfer can significantly alter the radiation chemistry in polymers, particularly when a mixture of functional groups is present. Molecular cross sections provide a useful basis for determining if energy transfer is occurring, which will now be discussed, along with some illustrative experimental results.

Molecular Cross Sections

Cross sections provide insight into the relationship between the physical interactions of radiation with matter and the chemical changes that take place. In particular, it provides a basis for comparing the radiation sensitivities of various species by quantifying the rate and extent of chemical change induced by ionizing radiation.

Consider a molecular system which is exposed to an electron beam. The number of molecules (N) transformed in a given time (t), is given by the following differential equation (23):

$$-\frac{dN}{dt} = \sum_i q_i \sigma_i I_T N \qquad [8]$$

where:

I_T = current of the electron beam
σ_i = inelastic electron scattering cross section for the ith excitation
q_i = probability of a chemical event occurring following the ith excitation

This differential equation states that the number of molecules described by N which change in unit time (t) is equal to the sum of the following products: (1) the probability of an excitation event occurring, (2) the probability that this particular event will result in a chemical reaction, (3) the electron beam current (i.e. the number of electrons per unit area) and (4) the number of molecules under consideration which are present. Rearrangement of Eq. 8 gives:

$$\int_{N_0}^{N} \frac{dN}{N} = -\sum_i q_i \sigma_i I_T \int_0^t dt \qquad [9]$$

where N_0 is the number of molecules under consideration which are present prior to radiation exposure (t=0). Integration gives the following result:

$$\frac{N}{N_0} = e^{-(\sum_i q_i \sigma_i I_T t)} \qquad [10]$$

Let $I_T t = D$, the dose in terms of energy per unit area, and $\Sigma_i \sigma_i q_i = \sigma$, the cross section for chemical transformation of the species described by N, in terms of area per unit energy. This gives:

$$\frac{N}{N_0} = e^{-(\sigma D)} \qquad [11]$$

N/N_0 can be determined by the relative change in the IR absorption band of the species in question at various doses, D. A semi-log plot of N/N_0 versus D should give a straight line with a slope of $-\sigma$. Figure 2-7 shows this type of plot for a variety of different species and illustrates the wide range of radiation sensitivities among polymeric materials. Note that this development assumes that excitation occurs only by direct interaction with the electron beam. Hence, if energy transfer processes are occurring, some deviation will exist, the extent of which depends on the particular chemistry. This deviation can be accounted for by incorporating additional terms into Eq. 8, which describe chemical transformations occurring via energy transfer mechanisms, with corresponding cross sections for each energy transfer mechanism. This leads to a complex model due to the non-linearity of the resulting differential equation. This will not be considered here, but this formalism has been developed by Pacansky (23).

A simple way to discern the overall effects of energy transfer (without having to develop a detailed model) is to make a series of N/N_0 versus D plots for a series of

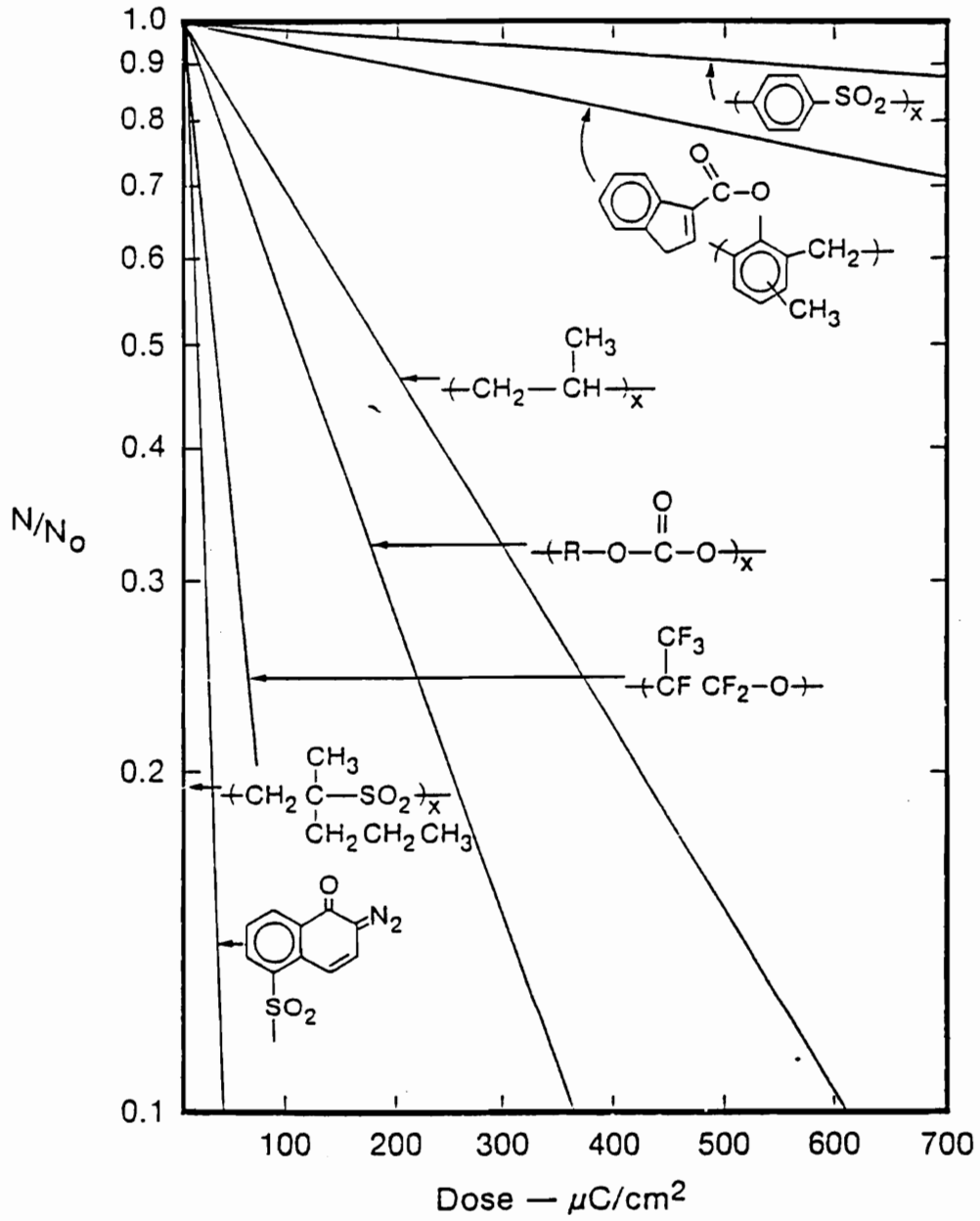

Figure 2-7. Semi-log plot of N/N_o versus Dose for a variety of different polymers. (ref. 23)

mixtures with varying compositions which are thought to display energy transfer between the components. If energy transfer is taking place, the cross section of the component in question should show a strong concentration dependence. This has been illustrated in the literature by Pacansky and Waltman (33). In this experiment, the electron beam exposure of a solid mixture of diazoketone in a host matrix of a phenolic resin was considered (see Figure 2-8 for the component structures). This particular mixture was chosen for several reasons. First, the energy level of the first excited state of the phenolic resin is higher than that of the diazoketone. This condition facilitates energy transfer only from the resin to the diazoketone. Secondly, the phenolic resin is comparatively insensitive to radiation under the dose range studied. This allows the diazoketone decomposition to be monitored with no significant changes to the host matrix. Lastly, the diazoketone has a very short excited state lifetime which greatly restricts energy transfer between diazoketone molecules, and as such, chemical decomposition is the primary mechanism of energy decay. This ensures that IR spectroscopy is an accurate method of following the chemical changes that take place.

Figure 2-9 shows the semi log plots of N/N_0 versus D for the mixture over a wide range of compositions. Notice that most of the plots are non-linear, indicating that non-exponential decay of the diazoketone is occurring, which suggests the transfer of energy. However, this curvature was ignored in calculating the cross sections, which does not introduce much error. In essence, this gives an effective overall cross

(1)

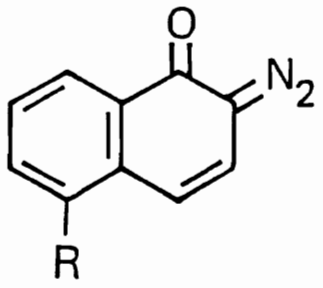

(2)

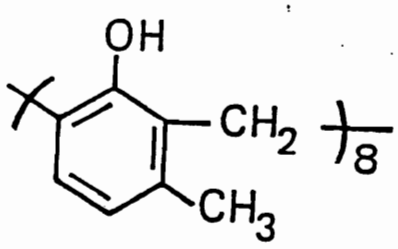

Figure 2-8. Molecular structure of (1) diazoketone and (2) phenolic resin used in the energy transfer study by Pacansky and Waltman. (ref. 33)

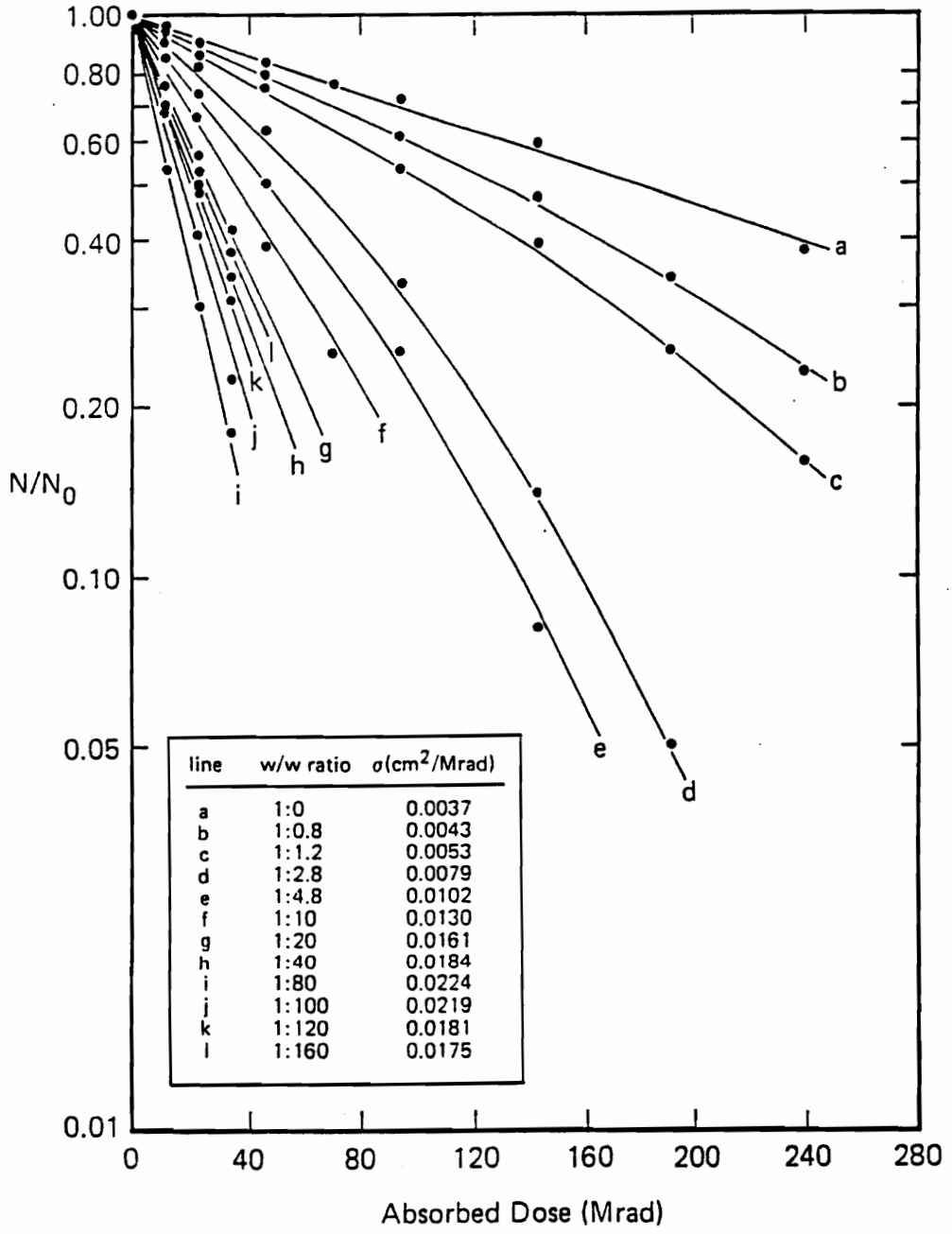

Figure 2-9. Semi-log plot of N/N_o versus Dose for various compositions of the diazoketone - phenolic resin mixture. (ref. 33)

section without having to develop a detailed model of the energy transfer mechanisms. Figure 2-10 shows the dependence of the cross section for decomposition of the diazoketone on the concentration in the resin matrix. The cross section increases with decreasing concentration, which means that decomposition increases with decreasing amounts of diazoketone present. This is totally unexpected if energy transfer is not considered. If anything, a decrease in the cross section would be expected with decreasing concentrations. In any case, the fact that the cross section is showing this type of behavior indicates that energy is being transferred from the phenolic resin to the diazoketone. In fact, the authors have attributed this to a Forster energy transfer mechanism. Also notice that there is a maximum in the curve at about 0.04M, where energy transfer is most efficient. Below this concentration the diazoketone molecules are so far apart that there will be regions where the resin cannot transfer energy to a diazoketone molecule. Above this concentration there begins to be competition among the diazoketone molecules for the energy transferred, and the cross section decreases.

This has illustrated the importance of energy transfer processes in the radiation exposure of mixtures. Energy transfer can alter the rates and extent of reactions occurring from what would be expected if the various chemical transformations of the components were dependent only on their relative contributions to the overall stopping power of the medium. Energy transfer mechanisms are essentially one class of reactions which involve the various species created by ionizing radiation. Energy

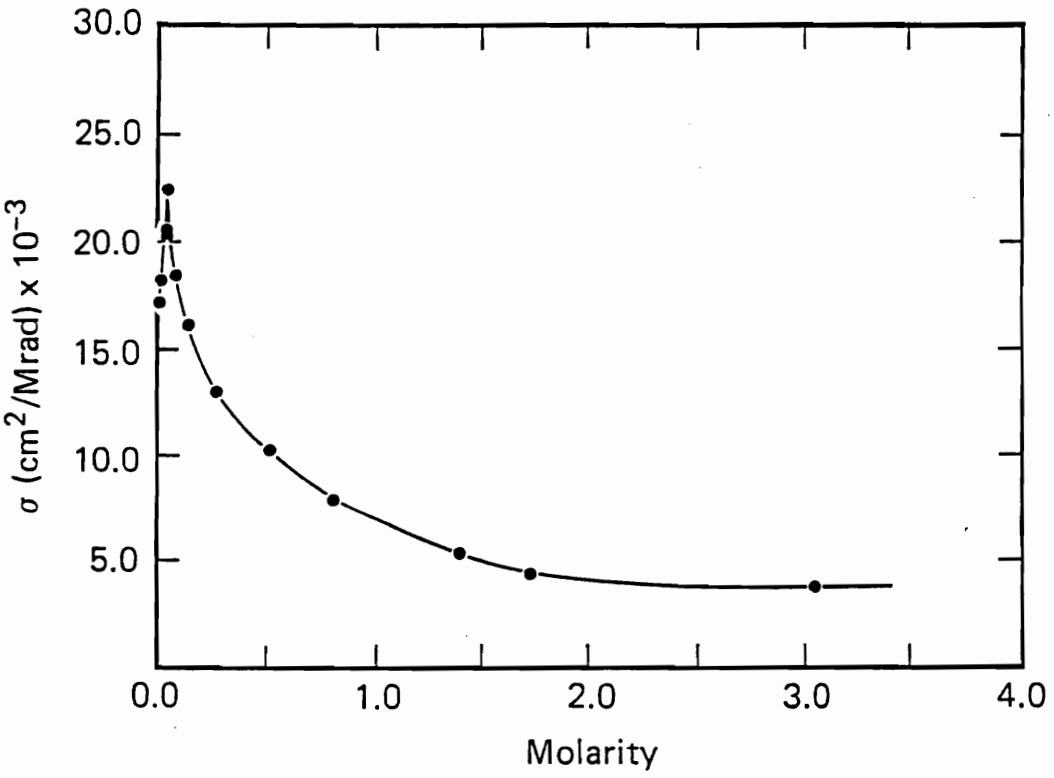

Figure 2-10. Dependence of the decomposition cross section (σ) for the diazoketone in the phenolic resin matrix. (ref. 33)

transfer reactions usually occur prior to other reactions involving radiation products which are responsible for permanent chemical changes in polymers. The reactions of energy transfer products as well as other species created by ionizing radiation will now be covered.

2.3.2 Chemical Reactions

As discussed, energy transfer describes a class of processes in which energy is dissipated from one molecular entity and subsequently absorbed by another species. Once these processes have occurred (and during the course of these energy transfer processes as well), other reactions take place which allow for irradiated molecules to dissipate the energy deposited by high energy radiation. Some of these reactions lead to permanent chemical changes in polymeric systems and some do not. However, all of these radiation induced reactions arise due to the simple fact that all the molecules are trying to reach a state of equilibrium which was disrupted by the radiation exposure. The initial and final equilibrium states of the irradiated system typically are not identical -- i.e. some chemical transformations have taken place. There are numerous reactions which can take place among the ionized, excited and neutral molecules, as well as the free electrons, which produce these chemical transformations. These reactions however, are not always easily discernable; they are extremely fast and typically over in much less than one second, making detection a difficult task. The development of pulse radiolysis techniques has increased our understanding of these fast reactions, but this research area will not

be discussed here. However, some comprehension of these fast reactions is necessary to understand how physical changes in irradiated polymers may occur, which will now be discussed.

Reactions of Ionized Molecules

Ionized molecules typically react by one of several different processes. Probably the most common reaction in irradiated polymers is ion - electron recombination. In this reaction a positive ion reacts with an electron to give a highly excited molecule:

$$AB^+ + e^- \rightarrow AB^* \qquad [12]$$

The electron captured may be the same electron ejected during the ionization process (if little kinetic energy was imparted to the electron) or it may be another electron which has slowed down sufficiently such that it is unable to escape the attractive forces of the positive ion. The excited molecule produced by this process is at a much higher energetic excited state than excited molecules produced directly by radiation. As a result, the molecule will most likely dissociate in order to dissipate this excess energy. Hence, electron capture by positive ions will contribute to the permanent changes found in irradiated polymers.

A second possible reaction of ionized molecules is combination of a positive and negative ion. In this case, positive and negative ions react to form excited species:

$$AB^- + CD^+ \rightarrow AB^* + CD^* \qquad [13]$$

The extent of this reaction will depend on the particular chemistry, since some polymers will be more (or less) susceptible to negative ion production. The excited states produced in this reaction are at a lower energy level than those produced by equation 12, since the reaction energy must be shared between two species. Since dissociation will be less likely at this lower energy state, this process probably contributes less to the total radiation induced changes than the electron capture process.

A third type of reaction that ions may undergo involves interactions with neutral molecules:

$$AH^+ + BH \rightarrow AH_2^+ + B\cdot \qquad [14]$$

or

$$A^+ + BC \rightarrow AB^+ + C \qquad [15]$$

The first reaction is a hydrogen transfer reaction which results in the production of a free radical ($B\cdot$). The second reaction is a condensation type reaction with formation of a stable molecule (C). Less is understood about these types of reactions

in radiation chemistry, and as such the contribution of these reactions to the total chemical transformations occurring in irradiated polymers is not exactly known.

Ions may also react by other mechanisms of by modifications of the above reactions (as well as energy transfer interactions) and the reader is referenced to a review (34) for more detail on the subject.

Reactions of Excited Species

Excited species, like ions, may react by several different mechanisms. The most significant reaction for producing chemical changes in polymers is the dissociation of an excited species to produce free radicals:

$$A^* \rightarrow B\cdot + C\cdot \qquad [16]$$

The free radicals produced can subsequently react to form stable products (as will be discussed). For this reaction to occur, however, the excitation energy of A^* must be sufficient to break a covalent bound to give the free radical products. Any excess energy will be imparted to the free radicals in the form of kinetic energy.

Excited species may also dissociate to form stable molecules:

$$A^* \rightarrow R + S \qquad [17]$$

Where R and S may be saturated or unsaturated molecules. Dissociation of an excited species is a unimolecular process, unlike the previous reactions shown.

Another unimolecular reaction that excited species may undergo involves conversion to the ground state. This may or may not involve the emission of radiation. Fluorescence is a common example of radiative conversion to the ground state. Non-radiative unimolecular conversion to the ground state may be accomplished either by conversion of electronic excitation energy to vibrational energy or to a lower level of excitation energy. Conversion to lower energy levels may or may not involve a change in multiplicity (i.e. total electron spin). Constant multiplicity conversions are known as internal conversions and variable multiplicity conversions (i.e. conversion from a singlet to triplet state) are known as intersystem crossings. These unimolecular conversions to the ground state typically do not result in any transformations and hence are of little interest in the radiation modification of polymers.

Excited species may also react with other molecules to give free radicals (for example, by hydrogen abstraction), or stable molecules. The extent of bimolecular processes involving excited molecules depends on the specific chemistry, but they do not seem to be well characterized and as such, their significance is not well known.

Reactions of Free Radicals

The vast majority of chemical transformations in irradiated polymers has been attributed to reactions involving free radicals. Although other species (such as ions) may be responsible for certain chemical effects, free radicals reactions are surely predominant in most systems. In addition, free radicals have much longer lifetimes

than most ions and excited molecules, making them easier to observe and analyze. The importance of free radical reactions is based on several observations (35):

1. A variety of free radical reactions have been initiated by ionizing radiation and the kinetics and products of such reactions are very similar to those initiated by other means.

2. Inhibitors for conventional free radical reactions are also effective for inhibiting radiation induced reactions. For instance, it has been shown that the products obtained by the polymerization of a equimolar mixture of styrene and methyl methacrylate depends on the reaction mechanism (36). In free radical polymerizations the resulting polymer contains 50% styrene, in cationic reactions, 99% styrene, and in anionic polymerizations, 1% styrene is present in the polymer., Radiation induced polymerization of this system results in a polymer containing 50% styrene indicating a free radical mechanism is operative (37).

3. Radiation induced reactions are extremely sensitive to the presence of oxygen, which will react with free radicals to form peroxides and other oxidized structures. In addition to these observations, electron spin resonance (ESR) analysis of irradiated polymers has identified the presence of free radicals.

Reactions involving free radicals which are thought to bring about chemical changes in irradiated polymers include:

1. Transfer Reactions -- this involves abstraction of a hydrogen or other atom, which may be illustrated as:

$$R_1^{\cdot} + R_2X \rightarrow R_1X + R_2^{\cdot} \qquad [18]$$

This results in the stabilization of the R_1 radical and the production of a new radical, R_2.

2. Addition Reactions -- this involves the addition of a free radical to another species, which is often unsaturated:

$$R^{\cdot} + CH_2{=}CH_2 \rightarrow R{-}CH_2{-}CH_2{-} \qquad [19]$$

This reaction corresponds to the propagation step in free radical chain reaction polymerizations.

3. Termination Reactions -- this type of process results in the destruction of free radicals and the production of stable products, either by combination:

$$R_1^{\cdot} + R_2^{\cdot} \rightarrow R_1R_2 \qquad [20]$$

or by disproportionation:

$$R_1^{\cdot} + R_2CH_2CH_2^{\cdot} \rightarrow R_1H + R_2CH{=}CH_2 \qquad [21]$$

It has been suggested (38) that the former reaction may be responsible for the formation of crosslinks in long chain paraffin molecules while the latter may be

responsible for the increase in unsaturation observed in some polymers (more on this in the next section).

It should be noted that free radicals are extremely reactive with atmospheric oxygen, which can lead to the production of oxidized structures. Hence the presence of oxygen in the radiation environment (as well as absorbed oxygen) will significantly alter the radiation chemistry of polymers, as will be discussed in a later section.

This section has focused on the processes and interactions that occur after the initial physical interactions between radiation and condensed organic matter. In essence, this has described how molecules dissipate energy imparted to them during radiation exposure, in order to obtain a stable state of equilibrium which may or may not be quite different from the initial equilibrium state. It follows that the various "final states" that may be obtained in irradiated polymers should be discussed, as well as how the reactions described here operate to produce these permanent chemical changes in polymeric systems.

2.4 PHYSICAL AND CHEMICAL TRANSFORMATIONS IN IRRADIATED POLYMERS

As discussed, there are numerous chemical reactions which take place in irradiated polymers. Some of these reactions result in profound changes in the physical properties of the polymer, while others do little to alter the system. Since the physical properties of polymeric materials are sensitive to the molecular weight and distribution of the molecular chains, any chemical transformations which affect these parameters will also alter the physical properties of the system. In this regard polymers are unique, in that only one chemical transformation of this type per molecule can have a dramatic effect on the physical properties. This makes polymers well suited for radiation processing since relatively very few chemical transformations are required to alter the physical properties, compared to low molecular weight compounds.

Due to the sensitivity of polymer physical properties to molecular weight, the predominant processes of concern in irradiated polymers are crosslinking and chain scission. Crosslinking is a process where polymeric chains become covalently bonded to each other, with a subsequent increase in molecular weight. Chain scission involves the breaking of covalent bonds within a molecule and results in a decrease in molecular weight. In irradiated polymers, both of these processes occur simultaneously, usually with one process dominating over the other. Table 2-3 shows the classification of a variety of polymers with respect to which process dominates.

Many factors will affect the relative extent of crosslinking and chain scission, as will be discussed. The classifications in Table 2-3 are valid for the radiation exposure of neat polymers in the absence of oxygen. A general rule has been proposed by Miller et al. (40) which classifies predominately crosslinking or chain scission polymers based on the molecular structure. If a vinyl polymer has two side chains attached to the main chain carbon then it will primarily undergo chain scission whereas vinyl polymers with one or two hydrogens attached to the main chain carbon will primarily crosslink. This rule is not universal and exceptions do exist. For instance, some methacrylates with long side chains will undergo crosslinking (21).

Several mechanisms come to mind that may explain this general rule. First, the presence of two side chains may introduce a steric strain on the carbon backbone thereby promoting chain scission. In addition, two side chains may provide some resonance stabilization to a backbone carbon free radical, reducing its reactivity. This could lessen the probability of recombination between to free radical pairs at a scission site. A third possibility is that a hydrogen atom is easily removed from a carbon chain (compared to larger species in a condensed phase) thereby leaving a site for crosslinking to occur.

While the above general rule of the dependence of crosslinking and chain scission on the molecular structure is quite useful, there have also been numerous detailed mechanisms proposed for crosslinking and scission processes. Any mechanism should take into account for early observations (41,42) that the degree of crosslinking and

Table 2-3. Classification of predominately crosslinking and chain scissioning polymers in the absence of oxygen. (ref. 39)

Predominant crosslinking	*Predominant degradation*
Polyethylene	Polyisobutylene
Polypropylene	
Poly(vinyl chloride)	Poly(vinylidine chloride)
Chlorinated polyethylene	Polychlorotrifluoroethylene
Chlorosulphonated polyethylene	Polytetrafluoroethylene
Polyacrylonitrile	Polymethacrylonitrile
Poly(acrylic acid)	Poly(methacrylic acid)
Polyacrylates	Polymethacrylates
Polyacrylamide	
Polyvinylpyrrolidone	
Poly(vinyl alkyl ethers)	
Poly(vinyl methyl ketone)	
Polystyrene	Polyα-methylstyrene
Sulphonated polystyrene	
Natural rubber	Cellulose plastics
Synthetic rubber (except polyisobutylene)	
Polysiloxanes	
Polyamides	
Poly(ethylene oxide)	
Polyesters	

scission is directly proportional to the total dose and relatively independent on the dose rate (in the absence of oxygen). A number of proposed mechanisms have been reviewed by Charlesby (21,43), but there are objections to many of the mechanisms and this subject is still not completely understood. However, it will be illustrative to present the proposed reaction mechanisms for a polymer which primarily crosslinks and one which undergoes chain scission. For this purpose, the proposed reaction mechanisms for irradiated polyethylene (a crosslinker) and polyisobutylene (a scissioner) will be examined.

2.4.1 Free Radical Reactions in Irradiated Polyethylene

Although much research has been done on the irradiation of polyethylene, there still seems to be some controversy the exact nature of the mechanisms resulting in chemical change. Any proposed mechanism should explain the following observations:

1. Formation of crosslinks with eventual production of an insoluble network (7).
2. 98% of the gases evolved during irradiation is molecular hydrogen, the balance being mainly methane, ethane, propane and butane (44,45).
3. The initial disappearance of vinylidene and vinyl unsaturation with an increase in trans - vinylene unsaturation with increasing dose, which may exceed the initial unsaturation level (46,47).

Miller et al. (46) have suggested that unsaturation may be the result of abstraction of adjacent hydrogen atoms along the backbone:

$$-CH_2-CH_2-CH_2-CH_2 \rightarrow -CH_2-CH=CH-CH_2- + H_2 \qquad [22]$$

Pearson (48) has proposed that double bonds are an intermediate in the crosslinking process, as illustrated in Fig. 2.11. It is also thought that atomic hydrogen produced by cleavage of a C-H bond can abstract a hydrogen from a neighboring chain, which results in the formation of a crosslink between the two free radicals left on the main chains. Furthermore, there is evidence (49,50) that free radical migration can occur along the main chain or possibly between chains in polyethylene. This suggest that free radicals on the main chain can migrate until two radicals on separate chains come in close proximity to each other and react to form a crosslink. These mechanisms illustrate the formation of "H-type" crosslinks (tetrafunctional junctions). It is also possible to form "T-type" crosslinks (trifunctional junctions). This type of crosslink is thought to occur by reaction of free radicals produced by main chain scission with neighboring chains:

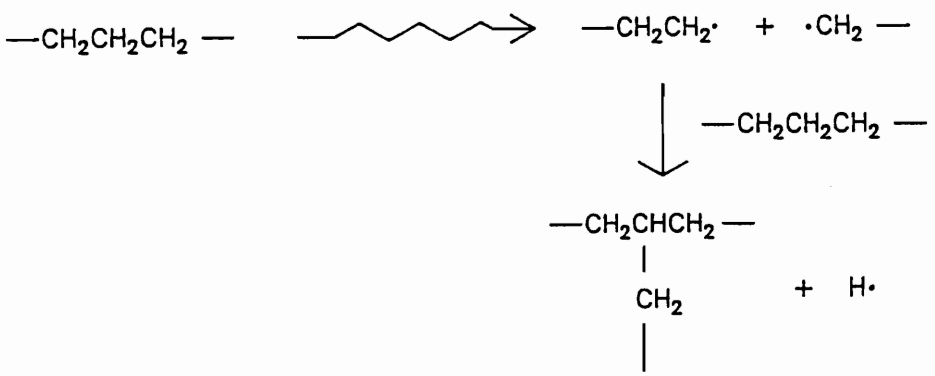

[23]

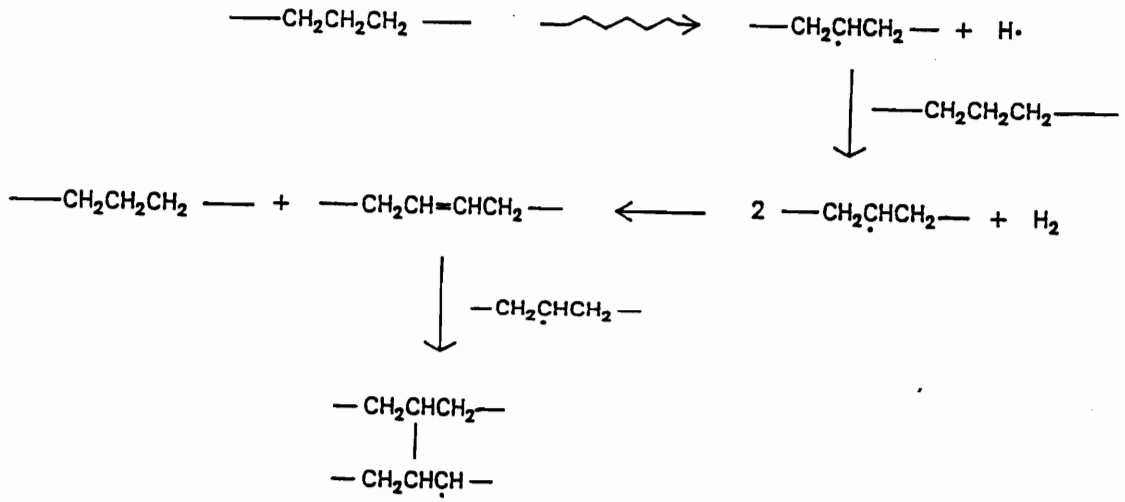

Figure 2-11. Possible free radical mechanism for the formation of double bonds and crosslinks in polyethylene. (ref. 47)

It must be stressed that these mechanisms are suggestions by investigators in this field, and there is actually little direct evidence to establish the exact nature of crosslinking (as well a scission) reactions. It should also be noted that polyethylene is a semi-crystalline material, which can complicate analysis. It may be likely that the predominating mechanisms may be different in crystalline and amorphous regions (as will be discussed) and hence observations may be dependent on the exact state of the system.

2.4.2 Free Radical Reactions in Polyisobutylene

Polyisobutylene is the simplest polymer structure that undergoes primarily chain scission under the effects of ionizing radiation:

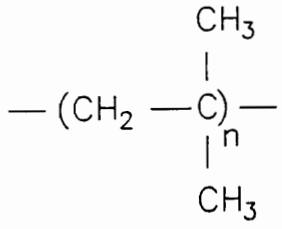

POLYISOBUTYLENE

Irradiation of polyisobutylene results in the following transformations (51):

1. Increase in the degree of vinylidene unsaturation (i.e. side chain unsaturation), with approximately 1.87 double bonds formed per chain scission.
2. Methane and hydrogen are the primary gaseous products, although isobutylene production increases with increasing dose.
3. The efficiency of chain scission reactions increases with increasing temperature.

4. The viscosity average molecular weight (M_v) is inversely proportional to the radiation dose.

The following mechanisms are thought to be operative in the irradiation of polyisobutylene:

Main chain scission to produce two stable molecules:

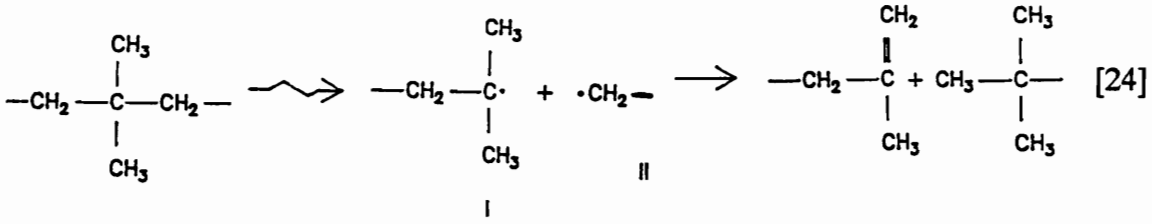

[24]

I II

Structures I and II are likely to react by disproportionation as shown, since this is favored due to the presence of side groups on structure I. Structure I may also dissociate to produce an isobutylene molecule and another free radical. However other reactions must be occurring to account for the 1.87 double bonds formed per chain scission. In particular, a methyl radical may be formed by side chain scission which abstracts a hydrogen from a neighboring methyl group, producing methane and vinylidene unsaturation:

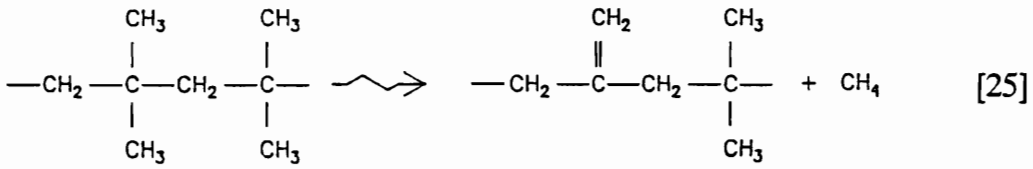

[25]

In addition, Shultz (53) suggested the following mechanism which accounts for the production of methane and two vinylidene groups per scission:

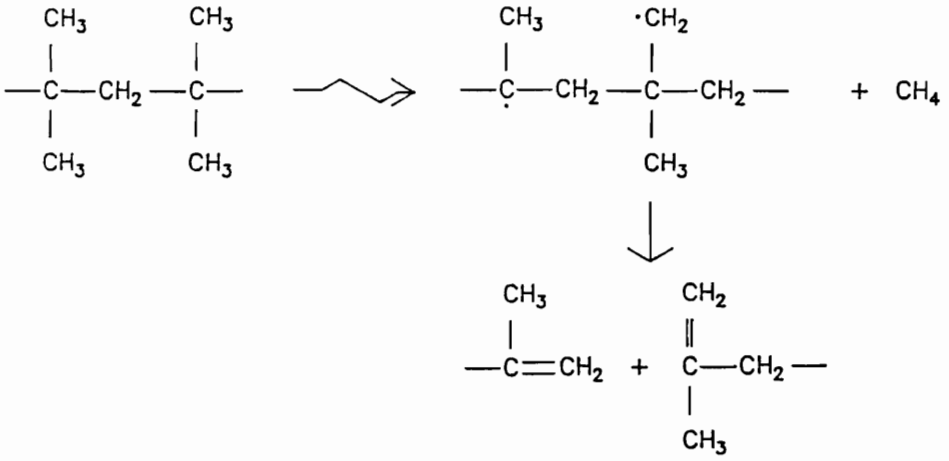

[26]

There does not appear to be any mechanisms suggested that account for the evolution of hydrogen gas since this is thought to be a product of crosslinking reactions or vinylene unsaturation (i.e main chain unsaturation), neither of which are found to occur in irradiated polyisobutylene. However, it has been suggested (54) that since the extent of crosslinking is quite low, hydrogen evolution may be the result of formation of intramolecular cyclic structures.

As is evident from the observations and the proposed mechanisms on crosslinking and chain scission reactions discussed here, the evolution of gas as well as double bond formation (and consumption) also occurs during radiation exposure of polymers. Often the gas produced is trapped within the material, especially in glassy polymers. This may cause internal stresses within the polymer which may lead to

cracking and fracture. In fact, it has been shown (55) that a foamed structure can be created by irradiation of poly(methyl methacrylate) with subsequent heating above the glass transition temperature, which allows the trapped gases to escape.

This section has focused on the transformations that occur in polymers as a result of radiation exposure and the proposed mechanisms that may be operative. As discussed, the primary effect of ionizing radiation is to alter the molecular weight distribution of the polymer. Since the physical properties of polymers are affected by changes in molecular weight, radiation can have a significant impact on these properties. Discussion will now turn to a qualitative description of these changes in physical properties as well as how the relative extent of crosslinking and chain scission can be determined.

2.5 EFFECTS OF RADIATION INDUCED TRANSFORMATIONS ON THE PHYSICAL PROPERTIES OF POLYMERS

Although crosslinking and chain scission processes occur in most (if not all) irradiated polymers, the effects of these transformations on the physical properties will be strongly dependent on the particular polymer. For example, an increase in crosslink density will have a much greater effect on the modulus of an amorphous elastomer than it would on an amorphous glassy polymer. Likewise the presence of crystallinity has a strong influence on mechanical properties, and as such may effectively "mask" the effects of crosslinking. In general, however, an increase in crosslink density can influence the physical properties in a variety of ways, some of which include: increased Young's modulus, decreased elongation at break, increased strength, decreased solubility, and a reduction in swelling. These changes are considered desirable in many cases, and has provided the motivation for industrial radiation processing of polymers. It should be noted however, that excessive crosslinking can lead to embrittlement and deterioration of physical properties. The effects of chain scission processes will be dependent on the initial molecular weight and the extent of chain scission that occurs. In particular, if chain scission results in a decrease in molecular weight below the critical molecular weight necessary for chain entanglements, then marked changes in properties will result. Reductions in Young's modulus, elongation at break, and strength, are just a few of the effects that may be observed. It must be stressed, however, that the extent of most of these

changes is material dependent, as previously discussed. For this reason, a detailed discussion on radiation induced changes in polymer properties will not be given. However, upon discussion of factors which influence the radiation response of polymers, some details of physical property changes will be shown. Fortunately, it is possible to determine the relative extent of crosslinking and chain scission in most polymers regardless of the effects on mechanical properties.

2.5.1 G - Value Determination

The extent of crosslinking and chain scission is characterized by what are known as G - values. The G - value gives the number of crosslinking events (G(x)) or chain scission events (G(s)) that occur per 100 eV of absorbed energy. Hence, G - values indicate the chemical efficiency of a particular process. Although G - values are most commonly used for evaluating crossslinking and scission processes in irradiated polymers, other reactions have been characterized in this way as well. For instance, G - values for hydrogen gas evolution ($G(H_2)$) and decomposition of various functional groups have also been employed. G - values for a number of different polymers are given in Table 2-4. This shows the wide range of G - values that are observed in radiation chemistry. Values from below 1.0, characteristic of radiation resistant aromatic groups, to values above 10,000, indicative of radiation induced chain reactions of unsaturated hydrocarbons have been reported.

The determination of G - values for crosslinking and chain scission is based on one of the physical property changes that is not "masked" by the physical state of the

Table 2-4. G - values for reactions involving various molecular species found in organic polymers. (ref. 57)

Material	Bond Broken	G Value
Saturated Hydrocarbon	C—H or C—C	6-9
Unsaturated Hydrocarbon	C=C	10-11000
Aromatic Hydrocarbon	C—H, C—C	0.2-1
Carboxylic Acids	CH α to COOH	5
Ethers	CH α to COC	7
Halogenated Compounds	C—H, C—C	3

polymer, namely solubility. A polymer which is usually soluble in a particular solvent will become partly insoluble only if the extent of crosslinking is high enough such that a three dimensional network is formed (network formation will be discussed in a later section). The presence of crystallinity, or whether the polymer is a glass or elastomer, has no effect on the ultimate solubility of the polymer, and hence, these factors will not affect the determination of G - values (although the kinetics of solubilization will be strongly affected by these variables). Before detailing this type of analysis several cautions should be pointed out. First, the presence of crystallinity may affect the relative extent of crosslinking and scission and the extent of these reactions may differ in the amorphous and crystalline regions. G - value determinations give values for the overall system so one must realize this when attempting to use this analysis on multiphase systems. In fact, this analysis was developed for use on single phase homogenous systems, although some researchers have applied this to other more complex systems. Secondly, the effects of dissolving the polymer in a solvent must be considered. For instance, it is possible that trapped free radicals (particularly in glasses) may react upon dissolution, effectively altering the true G - values.

G - value determination utilizing solubility changes in irradiated polymers was developed by Charlesby and Pinner (56) in 1959. The following relationship was derived, which describes the relationship between the soluble fraction of polymer and the G - values, as well as the absorbed dose:

$$S + S^{0.5} = \frac{G(S)}{2G(X)} + \frac{100N_a}{M_{w,i}G(X)mD} \qquad [27]$$

where:

S = soluble fraction
G(S) = G - value for chain scission
G(X) = G - value for crosslinking
N_a = Avogadro's Number
m = molecular weight of repeat unit
D = absorbed dose (megarads)
$M_{w,i}$ = initial weight average molecular weight

This relationship was derived assuming an initially random molecular weight distribution. Experimentally, the G - values are determined as follows. First, a series of weighed samples are prepared and irradiated to different doses. The soluble portion is then extracted using a suitable solvent. A Soxhlet extraction apparatus is commonly used here. The insoluble fraction (if any exists) is then thoroughly dried and weighed. The difference between the initial weight of the sample and the weight of the insoluble fraction gives S, the soluble fraction. This is done for each dose level. By plotting ($S + S^{0.5}$) versus 1/D (known as a Charlesby - Pinner plot), the G - values for crosslinking and chain scission can be determined. Pacansky and Waltman (57) have described this procedure for determining G - values in irradiated poly(vinyl butyral). In this analysis, the soluble fraction was determined by extracting irradiated samples with tetrahydrofuran in a Soxhlet extractor for twenty hours. The insoluble fraction was dried at 100°C for two weeks in a vacuum oven until no

differences in successive weighings were found. The Charlesby - Pinner plot for poly(vinyl butyral) is shown in Figure 2-12. the plot displays two regions; a plateau at low doses where no gelation occurs, and a linear sloping region corresponding to increasing levels of gelation with increasing dose (decreasing 1/D). The intercept of this line gives the ratio of G(S)/2G(X), which for this case is 0.86, as shown. If this ratio is greater than or equal to 2.0, then there will be no sloping region on the plot, which indicates no gelation occurring. Hence, if G(S)/G(X) < 4.0, then gelation is predicted to eventually occur for any polymer. Extrapolation of the sloping region of this plot to $(S + S^{0.5}) = 2.0$ gives the dose required for incipient gelation, which for poly(vinyl butyral) is about 65 megarads.

Once the ratio G(S)/G(X) is determined, the individual G - values can be found in one of two ways. First, G(X) can be calculated directly from the slope of the gelation region with knowledge of the initial weight average molecular weight and the molecular weight of the repeat unit (see Eq. 27). The second method requires additional experimental work and can be used as a check for the Charlesby - Pinner analysis. This is done by using the following relationship, which is valid for any initial molecular weight distribution (57):

$$\frac{1}{M_n} = \frac{1}{M_{n,i}} + \frac{GD}{100N_a} \qquad [28]$$

where:

M_n = number average molecular weight after exposure to dose, D
$M_{n,i}$ = initial number average molecular weight
D = absorbed dose (megarads)
G = G(S) - G(X)

Experimentally, the number average molecular weight must be determined at different doses. This is typically done using gel permeation chromatography. By plotting $1/M_n$ versus D, the overall G - value (G(S) - G(X)) can be obtained from the slope of the resulting line. This plot is shown for poly(vinyl butyral) in Figure 2-13. The overall G - value obtained from this plot can be used to check the G - values obtained from the Charlesby - Pinner relationship.

It was previously mentioned that the Charlesby - Pinner relation was derived assuming a random initial molecular weight distribution. Deviations from this type of distribution will be manifested in curvature of the sloping line in the gelation region of the plot. For many distributions, this curvature will be slight and reasonable G - values may be obtained. In addition, since Eq. 28 is valid for any initial distribution, it can be used as a check for accuracy of the Charlesby - Pinner analysis. One point of caution should be noted though. It has been suggested that G - value determination using GPC should be limited to doses that are no greater than half of the critical dose for incipient gelation (58). This is necessary to avoid serious error in the molecular weight determination using the GPC method. Furthermore, doses much greater than the critical gelation dose are utilized in the Charlesby - Pinner analysis. Hence these two different techniques rely on quite

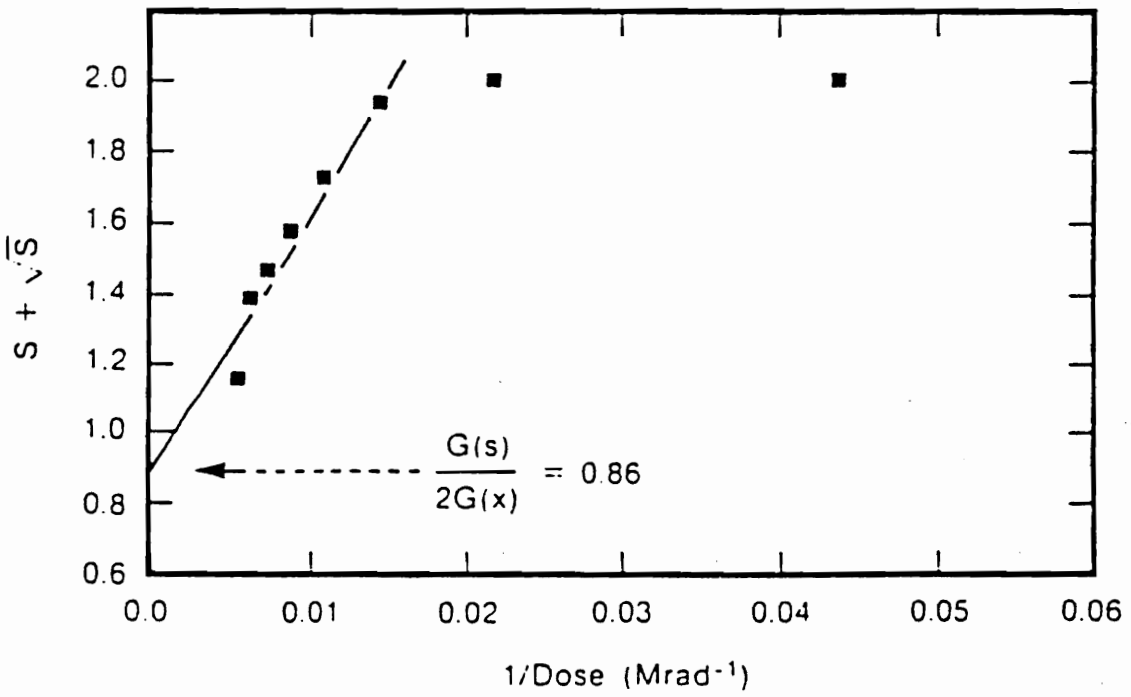

Figure 2-12. Charlesby- Pinner plot for G - value determinations in poly(vinyl butyral). (ref. 63)

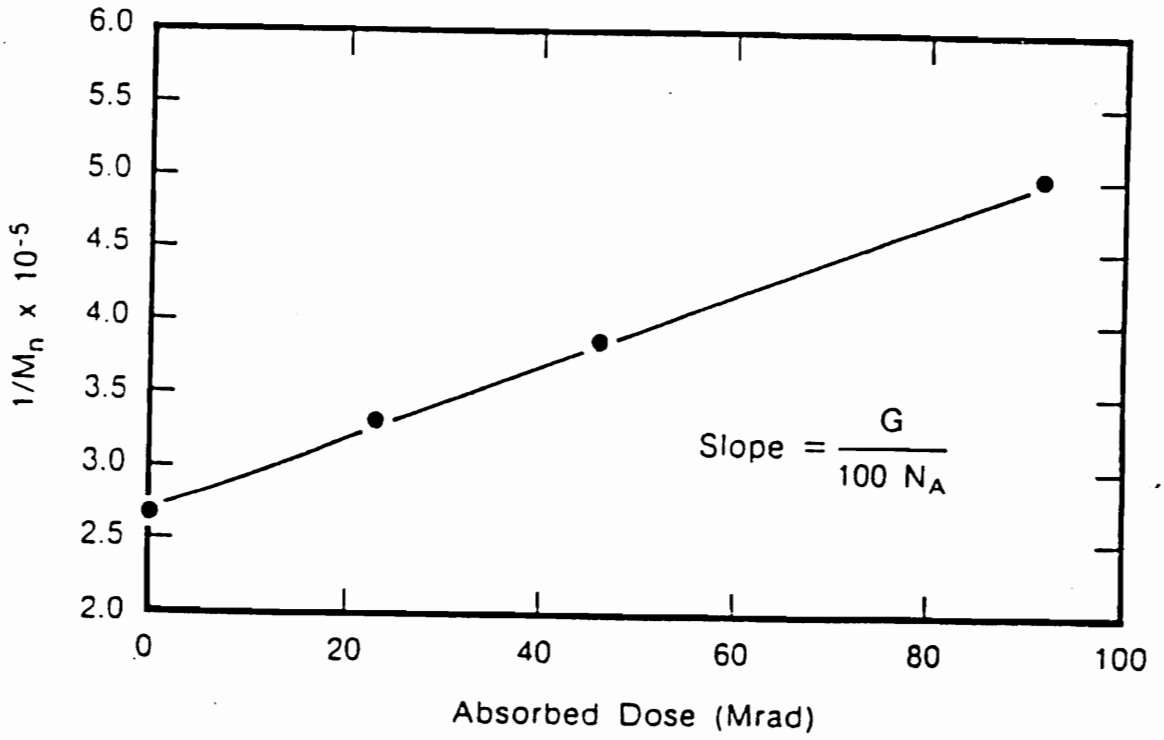

Figure 2-13. Plot of the reciprocal number average molecular weight versus Dose for overall G - value determination in poly(vinyl butyral). (ref. 63)

different dose ranges for the determination of G - values. This may give rise to discrepancies in the results obtained, especially if the extent of chain scission and crosslinking are dependent on the total absorbed dose.

It should be mentioned that the crosslink density can be determined from swelling and elastic modulus measurements in crosslinked polymers. These techniques have been used to determine effective G - values for crosslinking in earlier years, but they are of limited utility, especially in polymers which exhibit significant chain scission. Very recently however, O'Donnell et. al. have reported on G - value determinations using weight average and z - average molecular weights, which may prove to be an effective technique (58).

2.5.2 Other Property Changes

Other radiation effects observed in polymers include changes in optical and electrical properties, as well as modifications to the crystalline state. In particular, yellowing occurs in poly(methyl methacrylate) when exposed to doses of 3 to 5 megarads (59), which has been observed in other polymers as well. In addition, polymers display an increase in electrical conductivity during radiation exposure, although this effect is not usually permanent. However, permanent changes can result, as has been observed in irradiated poly(vinyl chloride) (60) and in thermal and radiation crosslinked polyesters. Fowler and Farmer have done numerous studies in this area, and the reader is referenced to their work for details of this phenomenon (61-64).

The effects of radiation on crystallinity appear to be quite varied, depending on the particular polymer in question. For instance, studies on irradiated polyethylene have indicated that irradiation results in an increase in the crystalline content, with alterations in the interplanar crystalline spacings (65-67). This observation has been attributed to chain scission of tie molecules between crystalline lamella with subsequent crystalline reorganization. On the other hand, irradiation of nylon 6 fibers results in an initial increase in the crystalline content at low doses and a subsequent decrease at higher doses, although no mechanism was suggested for these observations (68). Other work on nylon 66 indicates that radiation decreases the integrated area of the α_1 melting peak, while the α_2 melting peak remains unaffected (a slow cooling rate from the molten state induces the formation of a double melting peak in nylon 66, which are referred to as the α_1 and α_2 melting peaks) (69). These various results further demonstrate the material dependence of radiation induced changes as well as the dependence on the specific morphological state (this point will be considered again in the next section). This also eludes to the difficulties that can be encountered in attempts to extrapolate radiation effects from one material to another. However, work has been done which suggests that there may be a correlation between the melt temperature of semicrystalline polymers (i.e. thermal stability) and the resistance of the crystalline state to radiation.

This section has covered the effects of radiation on the physical properties of polymers. Particular emphasis has been placed on how property changes can be

monitored to determine the relative extents of crosslinking and chain scission. It has been eluded that there are factors which can influence the chemistry and resulting transformations in irradiated polymers, which will now be more fully covered in the following section.

2.6 FACTORS INFLUENCING THE RADIATION RESPONSE OF POLYMERS

Numerous variables can affect the radiation response of polymers and the underlying chemistry, as indicated throughout this review. Discussion will now turn to a more detailed inquiry of some of these influential factors. The effects of these variables to be discussed can vary as much as the radiation induced changes themselves. Some factors have only a slight impact on transformations while others are much more pronounced. In addition, the particular polymer being used to identify influences on radiation effects plays a key role in determining the extent of these changes. Hence, as data is presented to illustrate how certain variables influence radiation induced transformations, it should not be taken as universal phenomena. Results may be quite different depending on the polymer in question. Variations can result when underlying mechanisms interact differently with various polymers. However, in some cases the effects of these influences will be qualitatively similar for many polymers. The following variables which can impact the radiation induced changes in polymers will be discussed: molecular weight and end group effects, temperature, morphology (in particular, effects of crystallinity and orientation), mechanical stress, as well as the most influential factor, the presence of oxygen. During this discussion, detailed effects of radiation on physical properties for a variety of different polymers will become evident as well.

2.6.1 Molecular Weight

The primary direct influence of molecular weight on the radiation response of polymers is manifested in the critical dose required for incipient gelation (R_c). According to the theory of Flory (71) and Stockmayer (72), the critical condition for gel formation is reached when:

$$\rho_c = \frac{1}{\overline{y}_w - 1} \qquad [29]$$

where:

$\underline{\rho}_c$ = fraction of units which are crosslinked
$\overline{y}_w$ = weight average degree of polymerization

This relation assumes that the crosslinks are randomly introduced into a system of long chain molecules, as is typically the case with radiation induced crosslinking of polymers. Hence, as the molecular weight for a given polymer increases, fewer crosslinks (i.e. lower radiation dose) are necessary to produce a gel. This illustrates that the critical dose for incipient gelation (R_c) will decrease as the molecular weight of the polymer increases.

Rijke and Mandelkern (73) have shown that a plot of gel fraction as a function of normalized dose (normalized with respect to R_c) for linear polyethylene results in a single curve. In this work, a series of fractionated polyethylene samples with varying molecular weights were irradiated in the molten state to different doses and

the resulting gel fraction was determined. Figure 2-14 shows the results obtained by plotting the gel fraction versus the normalized dose. The results agree quite well with theoretical predictions (solid line in Figure 2-14).

This effect of molecular weight on the critical gelation dose is further exemplified in Figure 2-15. This shows a log-log plot of the critical gelation dose versus the viscosity average molecular weight for linear polyethylene. As predicted by theory, the critical dose decreases with increasing molecular weight. However, deviations from theory exist at lower molecular weights, which can be attributed to an indirect effect of molecular weight on the irradiation of polymers. As the molecular weight of a polymer decreases, there will be more chain ends (end groups) present per unit volume of polymer. If these end groups are reactive under the effects of ionizing radiation, then marked effects will be observed, as illustrated in Figure 2-15. As the molecular weight of polyethylene drops below 10^5 gr/mol, various deviations from theory (dashed line in Figure 2-15) occur. If irradiation is carried out in the molten state with reactive end groups present (i.e. double bonds) then R_c is less than the theoretical prediction. This is due to enhanced crosslinking resulting from the reactions of the end groups which are not accounted for in theory. However, if the end groups are hydrogenated (i.e. saturated end groups), then the R_c values are closer to theoretical predictions. Deviation from theory for these polymers have been attributed to experimental error and the possibility of oxidation occurring during hydrogenation which will increase the critical gelation dose (73). The largest

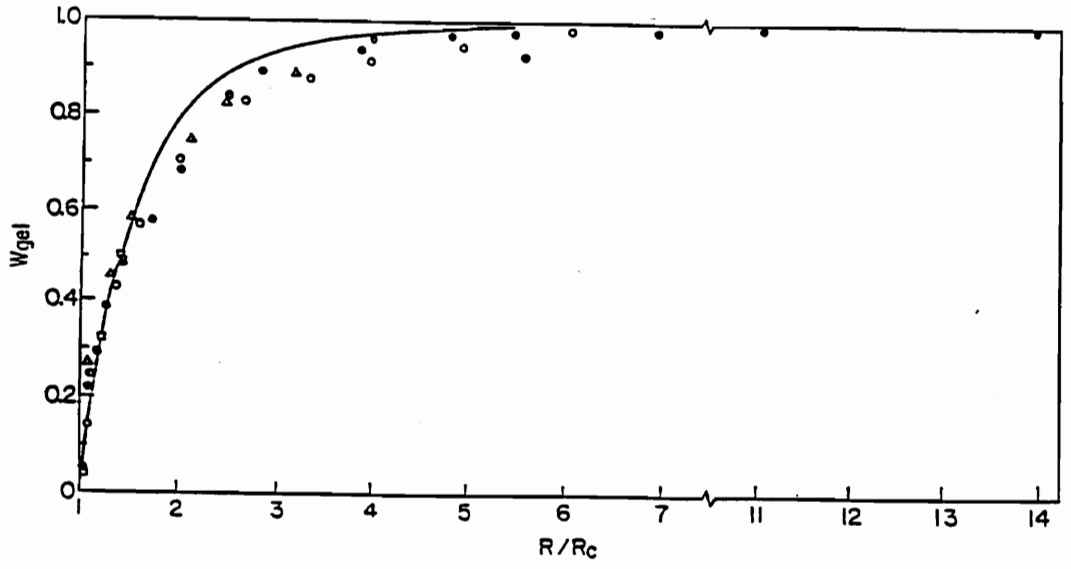

Figure 2-14. Plot of gel fraction (w_{gel}) versus normalized dose (R/R_c) for various molecular weight fractions of polyethylene irradiated in the melt at 133°C. (ref. 73)

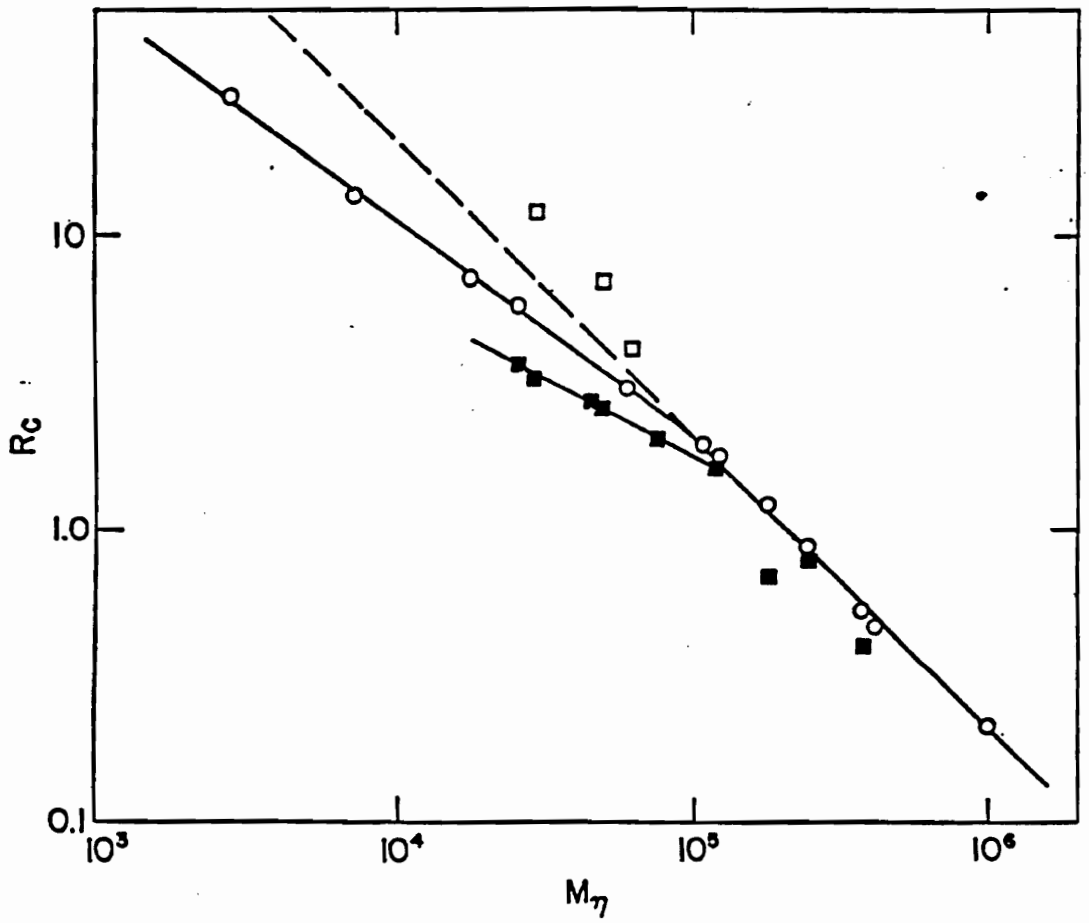

Figure 2-15. Plot of critical gelation dose (R_c) versus M_η for linear polyethylene irradiated in the molten (o) (hydrogenated - □) and crystalline (■) state at 133°C. (ref. 73)

deviations occur when irradiation is carried out on polyethylene in the crystalline state, which brings us to discussion of the next influential variable in irradiated polymers.

2.6.2 Crystallinity

As illustrated in Figure 2-15, irradiation of polyethylene in the crystalline state shows poor agreement with theory. For almost all samples, regardless of molecular weight, R_c is less than the theoretical prediction. This deviation can also be directly attributed to end group effects (and indirectly to the presence of crystallinity). During crystallization of a polymer, end groups are excluded from the crystal lattice since they cannot be incorporated into the unit cell. This increases the concentration of end groups in the amorphous regions, as compared to the completely amorphous state. Hence, end group effects become more pronounced in crystalline polymers, as Figure 2-15 shows. This is further exemplified by the data shown in Table 2-5. These results show that if the end groups are hydrogenated (i.e. rendered unreactive) in linear polyethylene, there is little difference in R_c between amorphous or highly crystalline states, whereas a large difference is noted if the end groups are not hydrogenated. Although the hypothesis has been made (74), the differences in R_c values for amorphous and crystalline polyethylene cannot be attributed to differences in the extent of chain scission processes in the two states of this particular polymer. In fact, it appears that there was some controversy over the years as to whether or not chain scission occurred at all in polyethylene.

Regardless of actual extent of chain scission in polyethylene, it is generally believed that crosslinking occurs primarily in the amorphous regions of this polymer (75). This is likely the result of an increased probability of radical pair recombination in the crystalline phase due to the dense packing and ordered structure of this state. Hence, a direct effect of crystallinity on the irradiation of polyethylene is to alter the spatial distribution of crosslinks. This hypothesis is supported by the work of Lyons (76). In one study, a high density polyethylene (Alathon 7050) was either slow cooled or shock cooled from the melt. The shock cooled sample had a smaller decrease in density upon cooling than the slow cooled sample, indicative of a lower crystallinity content. In addition, the clarity of the shock cooled sample was higher, indicative of a smaller average spherulite size and increased nucleation density (76). These samples were subsequently irradiated and then the elastic modulus was measured *above the melting point* to eliminate effects of crystallinity on the mechanical properties. In essence, modulus measurements were made on an amorphous elastomer, where differences in crosslink density can be readily observed. The results are shown in Figure 2-16. The slow cooled sample has a significantly lower modulus for a given dose than the shock cooled sample. It is proposed (75) that this is a result of greater spatial limitations on where crosslinks can form in the slow cooled sample. The crosslinks are more likely to be bunched together and located near chain ends in the slow cooled sample, due to the presence of larger spherulites and a greater crystallinity content. This effectively decreases the

Table 2-5. Effect of crystallinity on the critical gelation dose (R_c) for hydrogenated and unhydrogenated polyethylene. (ref. 77)

Sample	State	R_c (Mrad)
Nonhydrogenated	Completely amorphous	3.1
	Highly crystalline	1.6
Hydrogenated	Completely amorphous	4.2
	Highly crystalline	4.5

individual contributions of each crosslink to the elastic modulus. Hence a lower modulus is found for a given dose in the slow cooled sample, even though the actual number of crosslinks in the two samples may be similar.

Crystallinity may also affect radiation induced transformations in polymers by reducing the permeability of gases in the polymer. The crystalline state is denser and more orderly than the amorphous state and hence may reduce the ability of gaseous by-products to escape and, more importantly, reduce the permeability of oxygen into the polymer, as will be shown. In addition free radicals may become trapped in the crystalline phase (in addition to recombining), which will affect the post-irradiation processes.

2.6.3 Temperature

The irradiation temperature can affect the radiation chemistry of polymers in several different ways. First, since temperature determines the morphology of polymers (i.e.whether a polymer is glassy or elastomeric, and either crystalline or amorphous), temperature plays a key role in what influential mechanisms are operative. Obviously, the irradiation temperature must be below the melting point of the polymer for the effects of crystallinity just discussed to be of importance. In addition, the relative value of the irradiation temperature with respect to the polymer glass transition temperature (T_g) is another critical consideration. Since polymer chains have reduced mobility in the glassy state, free radicals are more likely to become trapped (i.e. unable to react, yet still active), which can affect post irradiation

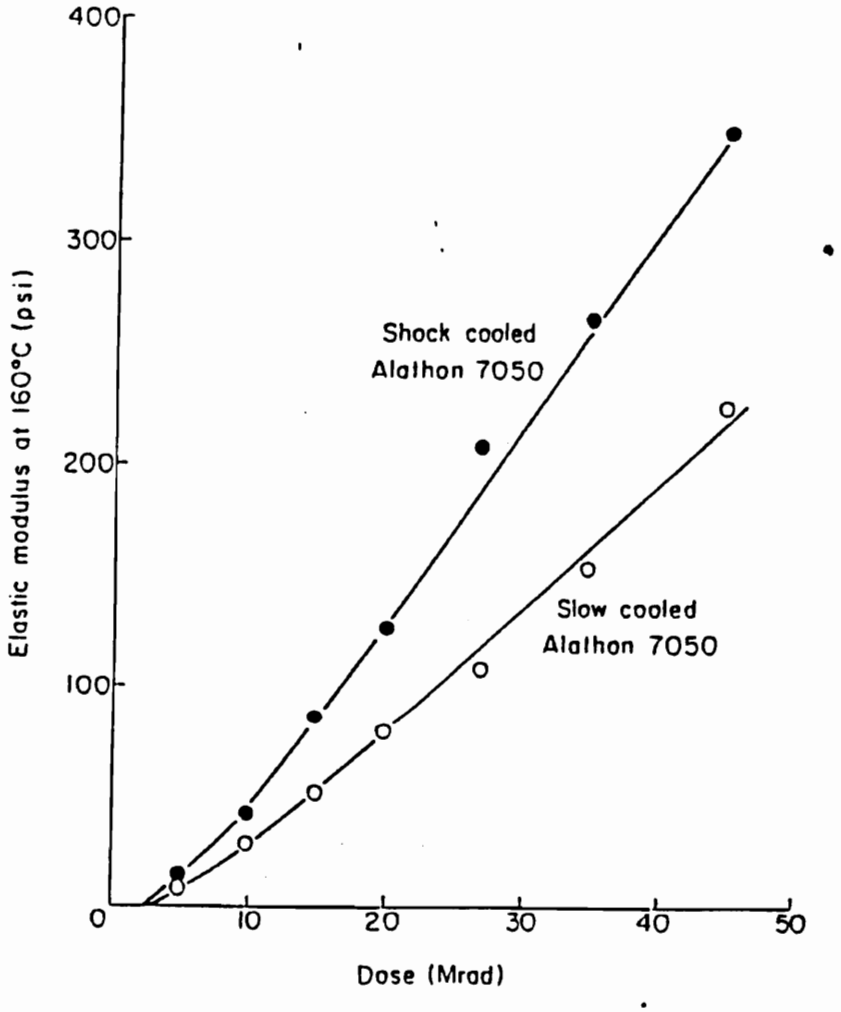

Figure 2-16. Plot of elastic modulus versus Dose for polyethylene with two different thermal treatments. (ref. 69)

processes. For instance, oxidative degradation after radiation exposure will be much more pronounced if there are long - lived, trapped free radicals present to react with atmospheric oxygen (this will be discussed further in the section on oxygen effects). Furthermore, the mobility of the polymer molecules can directly affect the extent of radiation induced changes. One illustration of this is shown in Figure 2-17, which is an arrhenius type plot of $G(H_2)$ versus 1/T for polyethylene. Notice a sharp transition in the curve at ca. -40°C, which roughly corresponds to the glass transition of polyethylene. Below the glass transition $G(H_2)$ is independent of temperature, which is likely due to the "frozen" state of the polymer chains. Once the irradiation temperature is increased above T_g, $G(H_2)$ steadily increases with increasing temperature. This is probably the culmination of two separate effects. First, as the temperature increases above T_g, the polymer chains (and free radicals) gain mobility and are more "free" to react. In addition, the kinetics of free radical reactions increases as the temperature increases. Hence, temperature not only influences transformations via morphological effects, but through its influence on reaction kinetics as well. This notion is further supported by Figure 2-18, which shows that the gel fraction formed in irradiated polyethylene increases with increasing temperature. This is in accord with the increase in $G(H_2)$, since hydrogen is a by-product of the crosslinking process.

2.6.4 Orientation and Stress

The effects of chain orientation and mechanical stress on the radiation response of polymers do not appear to be as well studied as some of the other influential factors presented here. However, several studies have been made which illustrate that stress and orientation can have significant synergistic effects in a radiation environment. A fairly extensive study was carried out by Bell et. al. (78). In this work, the combined effects of ionizing radiation and mechanical stress were analyzed by creep rate measurements on polystyrene, poly(methyl methacrylate), and poly(vinyl chloride). Figure 2-19 shows the relative creep of dogbone samples held in tension at the stresses indicated before, during and after exposure to 3 MeV electrons. As illustrated, the rate of creep increases significantly for all three polymers during radiation exposure and decays after the electron beam was turned off, although the extent of creep is material dependent. Measurements of G - values via a Charlesby - Pinner analysis show no significant effects of applied stress on the relative extents of crosslinking and chain scission in polystyrene. In fact, there was a slight reduction in the extent of chain scission for the stressed samples. This discounts any hypothesis based on chain scission with subsequent flow of chain fragments to explain the accelerated creep. In addition, ESR measurements showed no significant differences in the type or number of free radicals present in the stressed or unstressed states. The effect of temperature was also considered, and it was found that increasing temperature *decreases* the rate of creep for polystyrene. Unexpectedly, the authors found that the polymers expanded in the presence of

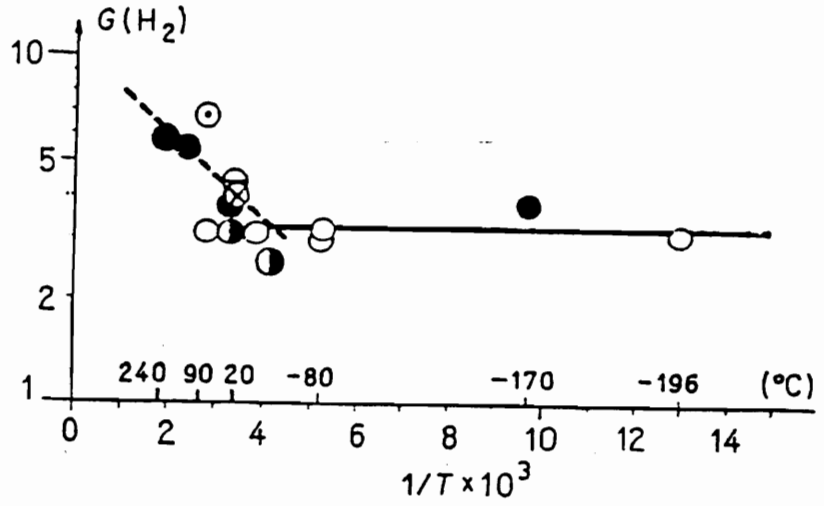

Figure 2-17. Arrhenius plot of $G(H_2)$ versus 1/T for polyethylene compiled from various sources. (ref. 35)

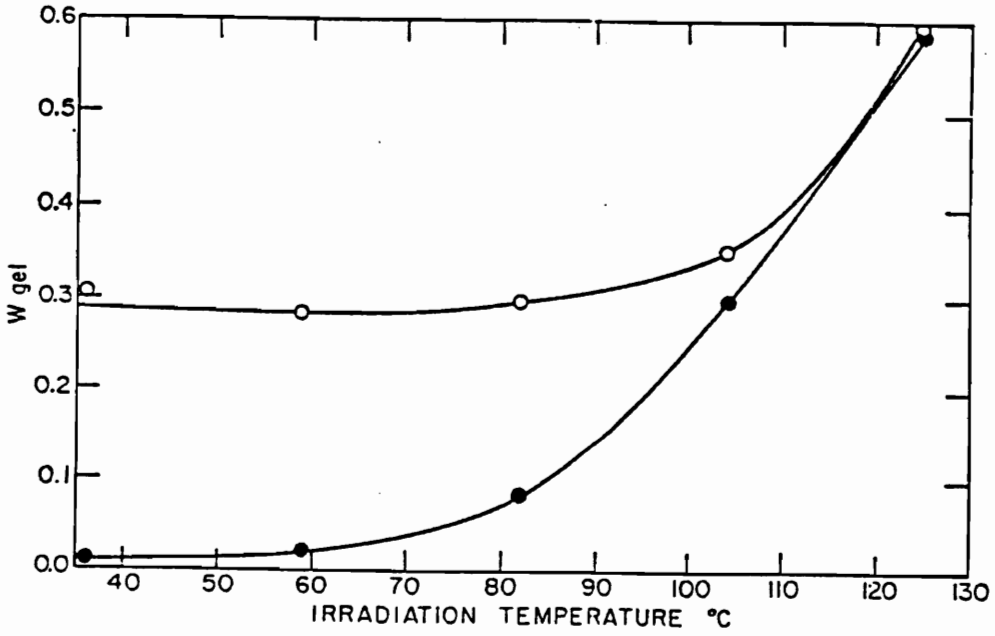

Figure 2-18. Gel fraction versus irradiation temperature for polyethylene post-treated by: (o) - storage at 140°C for two hours and (•) - stored in air for three days. (ref. 73)

radiation. Sample temperature was controlled during irradiation, and hence thermal effects were discounted. The extent of this radiation induced expansion followed the same trend as the extent of creep rate increase. Both of these phenomena were attributed to gas evolution occurring during irradiation, which can increase the free volume within the polymer and subsequently increase the creep rate. Indeed, the relative G - values for gas evolution in these three polymers follows the same trend as the relative increase in the creep rates due to radiation exposure (see Table 2-6). The temperature effects support this hypothesis, since higher temperatures will increase the diffusion rate of gas out of the material. This would lower the free volume increase due to gas evolution, since the equilibrium gas concentration within the polymer will decrease if the rate of gas diffusion out of the sample increases (assuming gas evolution remains constant).

In a less comprehensive study by Akay et. al. (79), the effect of orientation on radiation induced changes in low and high density polyethylene, as well as poly(vinyl chloride) was analyzed by monitoring changes in the carbonyl band of the IR spectra. The production of carbonyl groups in irradiated polymers is indicative of oxidative degradation occurring, as will be discussed. Figure 2-20a-c shows the effect of radiation dose (in the presence of air) on the normalized carbonyl peak height for various extension ratios in these three polymers. Notice that increasing orientation has opposite effects on poly(vinyl chloride) and polyethylene. Increasing the extension ratio of drawn poly(vinyl chloride) causes an initial decrease and

subsequent increase in the carbonyl peak height. This observation was attributed to the effects of drawing on the solubility and diffusivity of oxygen in poly(vinyl chloride). It has been shown (80) that the solubility of oxygen increases while its diffusivity decreases as poly(vinyl chloride) is drawn. Hence, the effect of orientation on the carbonyl peak height of this polymer is attributed to the decreased diffusivity of oxygen at low extension ratios and increased solubility at higher extension ratios.

The steady decrease of the carbonyl peak height in polyethylene with increasing extension ratios is attributed to a reduction in the diffusion rate of oxygen resulting from orientation, which has been reported by Yasuda and Peterlin (81). The decrease in carbonyl groups is much greater for high density polyethylene because of the generation of a fibril structure at high extension ratios (i.e. strain induced crystallization) (79). This work illustrates that different effects can arise in irradiated polymers as the result of the same influential factor (i.e. orientation). Again, one must be careful not to assume universality of a phenomena without understanding the underlying mechanisms.

2.6.5 The Presence of Oxygen

The effects of oxygen on the radiation chemistry and resulting transformations in polymers is by far the most pronounced influential factor that is known to exist. This is due to the ability of oxygen to significantly alter the actual chemical reactions occurring, while the other influences discussed do not. In particular, oxygen is highly reactive with the free radicals generated during irradiation, and hence alters the

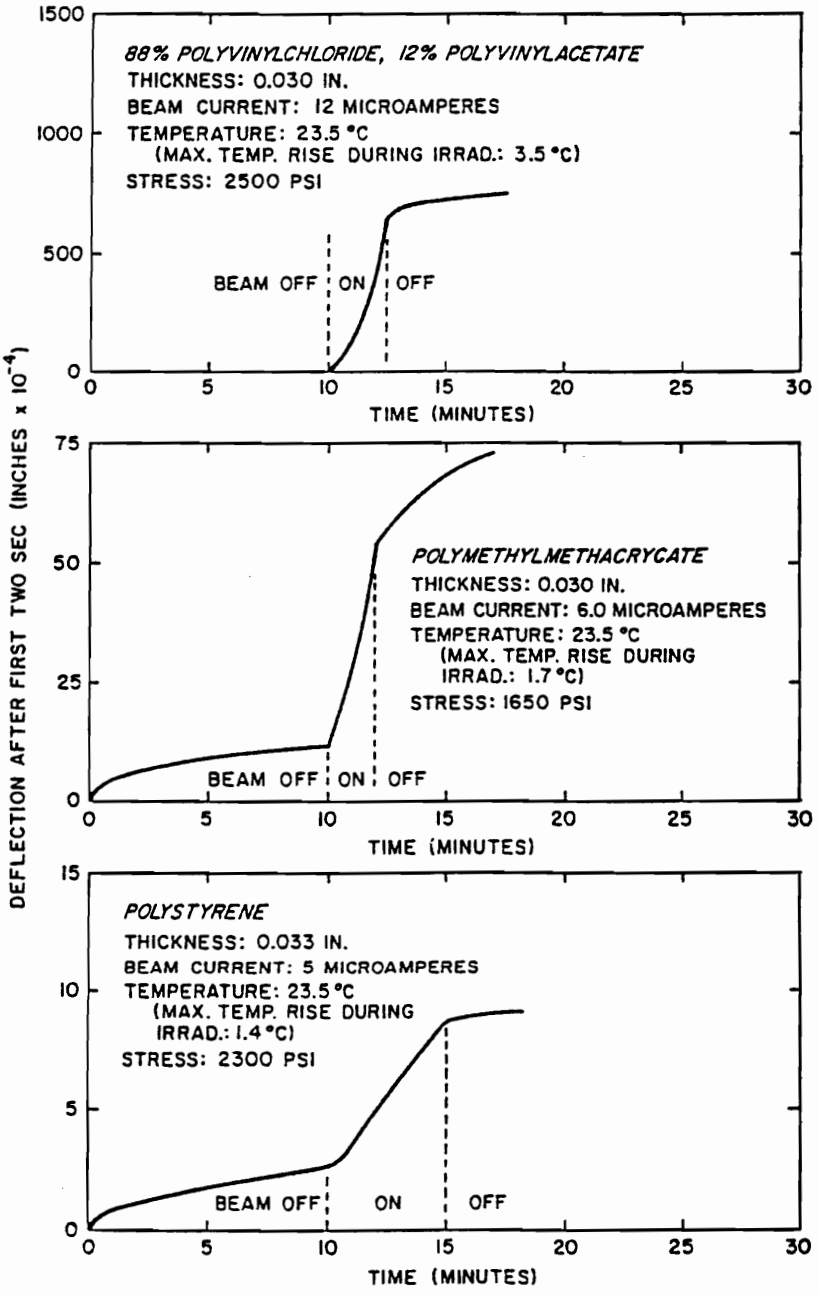

Figure 2-19. Relative creep of polystyrene, poly(methyl methacrylate), and poly(vinyl chloride) before, during and after exposure to a 3 MeV electron beam. (ref. 72)

Table 2-6. G- values for gas evolution and relative creep rates for polystyrene, poly(methyl methacrylate) and poly(vinyl chloride). (ref. 72)

Polymer	*Primary Gases Evolved*	*Approximate G Value for Gas Evolution molecules 100 e.v.*	*Ratio of G values*	*Ratio of Creep Rates from Figure 2*[a]
Polystyrene	H_2	0.022	1	1
Poly (methyl methacrylate)	CO, CO_2, H_2, CH_4	1.7	77	10 to 43
Poly (vinyl chloride)	HCl, H_2	7.0	328	100 to 400 (PVC/PV Ac copolymer)

[a] Range of initial to final rates from start to finish of irradiation period.

(a)

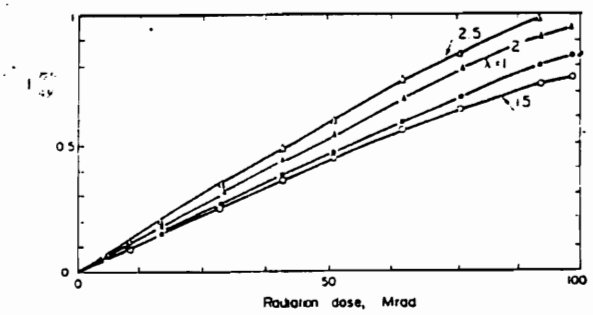

(b)

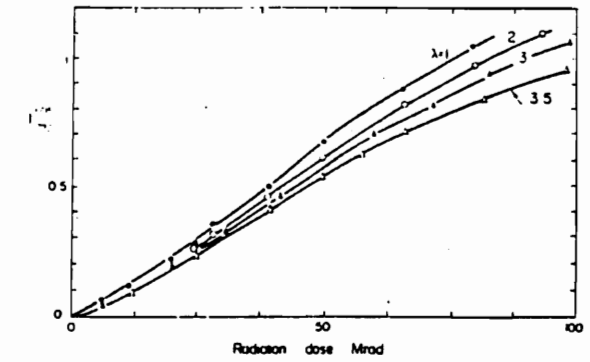

(c)

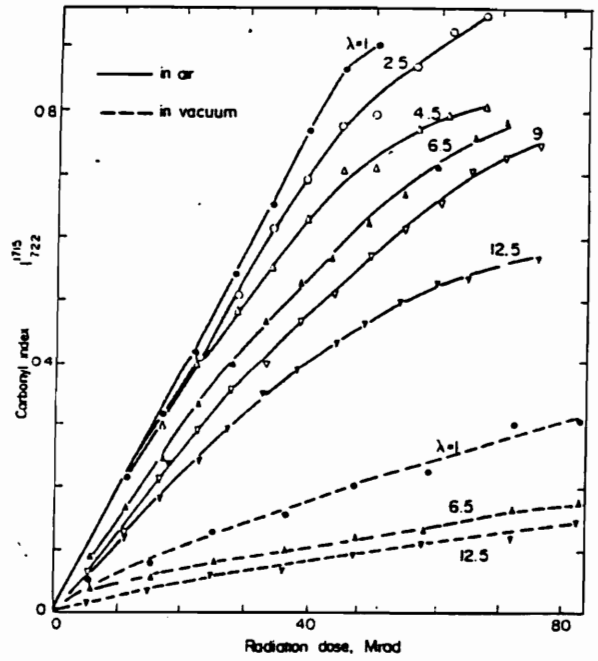

Figure 2-20a-c. Normalized carbonyl peak height versus Dose at various extension ratios (λ) for (a) poly(vinyl chloride), (b) low density polyethylene and (c) high density polyethylene. (ref. 79)

reactions which typically lead to crosslinking and chain scission. The mechanisms discussed earlier for crosslinking and chain scission do not apply when oxygen is present, as well as the classifications made concerning predominately crosslinking and chain scissioning polymers. In general, the presence of oxygen promotes chain scission in irradiated polymers, which has been termed as radiation induced oxidative degradation.

Radiation induced oxidative degradation is thought to be the result of the following free radical reactions (82):

$$R \rightarrow R\cdot \qquad [30]$$

$$R\cdot + 0_2 \rightarrow R0_2^{\cdot} \qquad [31]$$

$$R0_2^{\cdot} + RH \rightarrow R0_2H + R\cdot \qquad [2\text{-}32]$$

$$R0_2H \rightarrow R0\cdot + H0\cdot \qquad [2\text{-}33]$$

$$R0\cdot + RH \rightarrow R0H + R\cdot \qquad [3\text{-}34]$$

$$H0\cdot + RH \rightarrow H_20 + R\cdot \qquad [2\text{-}35]$$

$$R0_2H,\ R0_2^{\cdot},\ R\cdot \rightarrow \textit{scission and crosslinking} \qquad [2\text{-}36]$$

$$2R0_2^{\cdot} \rightarrow R0_2R + 0_2 \qquad [2\text{-}37]$$

Reaction 30 is the radiation induced initiation step, while reactions 31 and 32, 33 - 35, and 37 correspond to propagation, chain branching, and termination steps, respectively. Evidence for these reactions is found by analysis of the reaction products in polymers, which include oxidized structures such as ketones, carbonyl groups, carboxylic acids, peroxide species, and alcohol functionalities. In addition, gaseous products such as $C0_2$, CO, and H_20, are known to be generated, which are not typically formed in the absence of oxygen. Comparison of these reactions with the free radical mechanisms discussed earlier reveals profound differences, which illustrates why the presence of oxygen drastically changes the radiation induced transformations in polymers.

The predominance of chain scission under oxidative conditions is evident in the resulting physical properties of irradiated polymers. For example, consider polystyrene, a polymer which is fairly resistant to radiation and mainly crosslinks under an inert atmosphere. However, when irradiated in the presence of oxygen severe degradation (chain scission) occurs, as illustrated in Figure 2-21. As shown, the tensile strength is dramatically reduced (indicative of extensive chain scission) at an absorbed dose of 10^6 Gy (100 megarads) when irradiated in air, yet the original properties are retained when irradiated under nitrogen to a dose of 10^7 Gy (1000 megarads). Similar effects can be expected to occur in many other polymers, regardless of the physical property under consideration.

For oxygen to impose its detrimental effects on irradiated polymers, it must be present locally within the polymer, where the free radicals are generated and react. Hence, oxygen must be able to diffuse into the material as it is consumed during irradiation in order to alter the chemistry. However, this diffusion process takes time, which gives rise to dose rate effects, which are not present under inert atmospheres. For example, at very low dose rates oxygen will be consumed slowly, and atmospheric oxygen will have sufficient time to diffuse into the irradiated material and replenish the oxygen supply within the sample as it is being consumed. As the dose rate is increased, the rate of oxygen consumption will exceed the rate of diffusion, and the oxygen content within the sample will become depleted. At sufficiently high dose rates, the consumption rate will be so high that oxidation effectively occurs only on the surface, where diffusion rates are extremely fast. This concept is schematically represented in Figure 2-22, which qualitatively shows the effect of dose rate on the half dose value (the dose required to reduce a mechanical property to half its original value) for irradiation in air and inert atmosphere. In addition, experimental observation of dose rate effects are illustrated in Figure 2-23, which shows the effect of dose rate on the relative elongation of poly(vinyl chloride) as reported by Clough and Gillen (85). For a given dose, the relative elongation decreases as the dose rate decreases, indicative of greater extents of chain scission.

When irradiation conditions lie in the sloping region of Figure 2-22 (i.e. where properties are very sensitive to dose rate), heterogenous oxidation occurs. This is a

special case of radiation induced oxidative degradation. In this region there is a gradient in the oxygen content within the sample, which results in a gradient in the extent of oxidative degradation. This is the result of the dose rate being low enough such that oxygen can diffuse part way into the material before it is completely consumed. In this case, the chemistry occurring in the center of the sample may be drastically different from regions closer to the surface. This phenomenon has been extensively studied by Clough et.al. in recent years (86-88). These workers have developed a number of techniques for monitoring heterogeneous oxidation degradation in irradiated polymers (87,88). In one particular study, this phenomenon was analyzed in ethylene - propylene rubber (EPR) formulations by cross sectioning the irradiated material and measuring the relative hardness on each section (86). Relative hardness measurements were made by monitoring the penetration depth of a small, weighted probe into the material. Figure 2-24a&b shows the results of these measurements on the EPR for two different doses and dose rates of gamma radiation at 70°C in air. Irradiation of this material results in hardening, due to crosslinking reactions. However, at a dose rate of 6.7×10^5 rad/hr the relative hardness is quite dependent on the location within the sample. The center of this material has the greatest hardness, where crosslinking reactions can proceed unimpeded in the absence of oxygen. In the outer 20% of the sample, the relative hardness steadily decreases due to an increasing oxygen supply which hinders the crosslinking reactions and promotes a greater extent of chain scission. Decreasing the total dose (compare

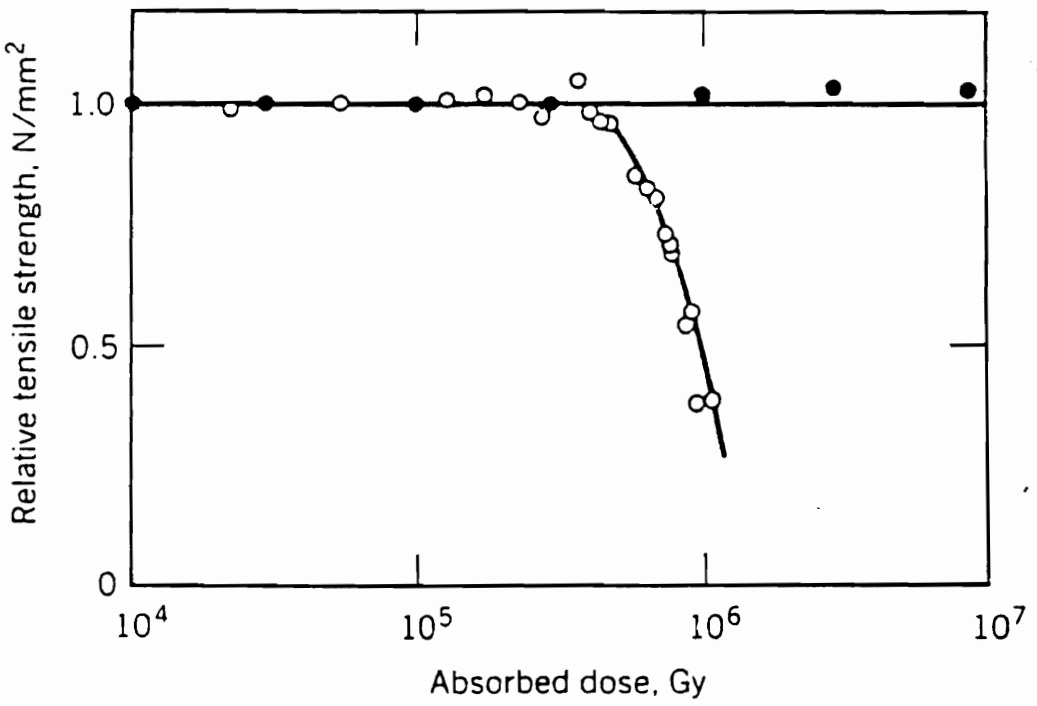

Figure 2-21. Relative tensile strength of polystyrene as a function of absorbed dose for irradiation under nitrogen (●) (4.7 x 10^3 Gy/hr) and under air (○) (13 Gy/hr). (ref. 77)

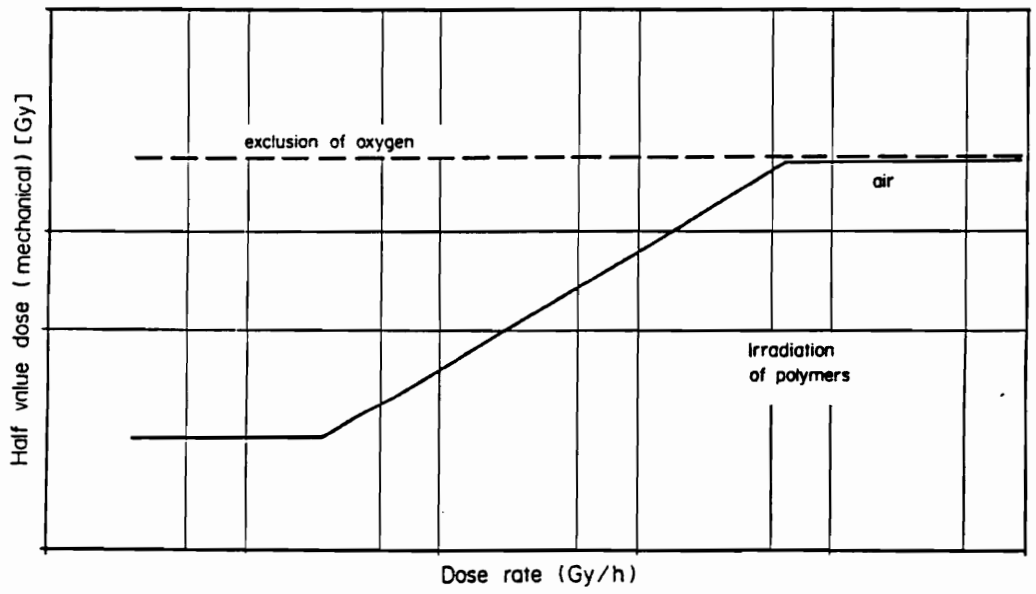

Figure 2-22. Influence of dose rate on the half value dose of polymers for irradiation in air and inert atmosphere. (ref. 78)

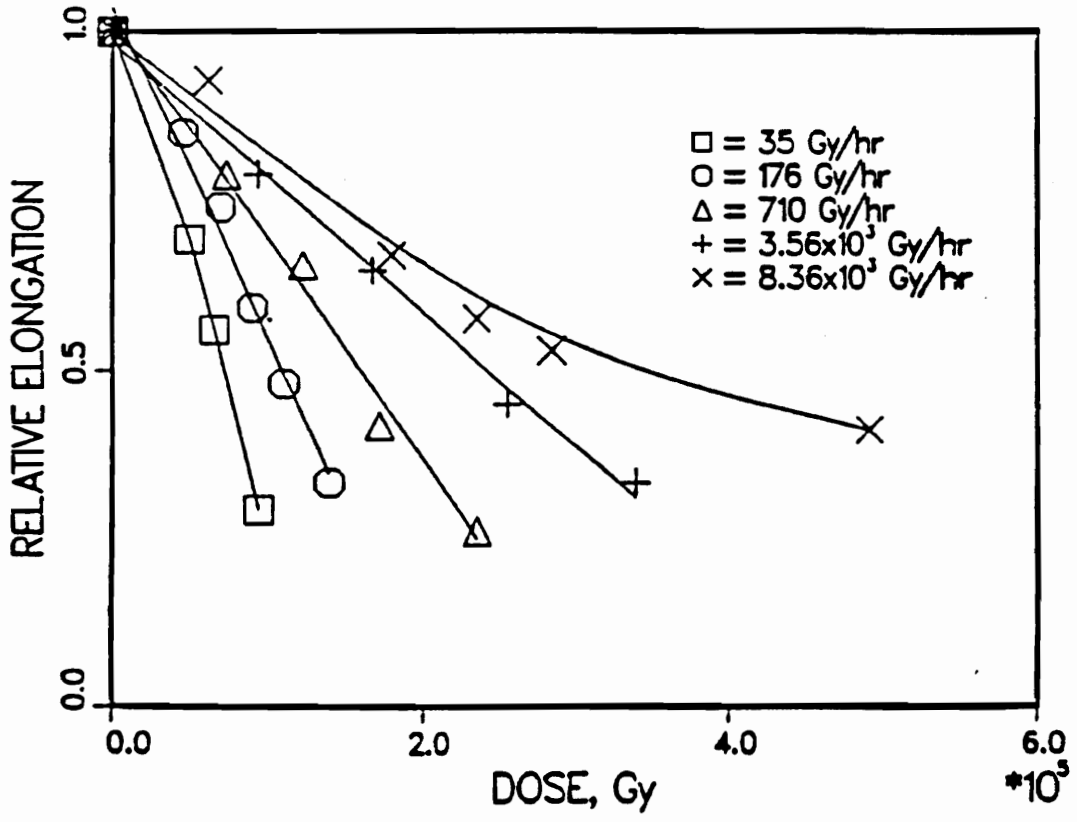

Figure 2-23. Effect of dose rate on the relative elongation of poly(vinyl chloride). (ref. 79)

open circles in Figure 2-24a with open squares in Figure 2-24b) does not affect the hardness of the center of the material or the oxygen penetration distance, but does increase the hardness near the surface. This can be attributed to less oxidative degradation (chain scission) occurring at a lower absorbed dose. Notice that as the dose rate is decreased to $1.1x10^5$ rad/hr the profile reaches a homogenous condition. Apparently at this dose rate the rate of oxygen consumption is low enough such that the oxygen has sufficient time to diffuse to the center of the material before it is completely consumed. Hence, a reduction in dose rate causes the oxygen penetration distance to increase.

The contention that oxygen diffusion effects can alter the relative extents of crosslinking and chain scission across the sample thickness has been convincingly demonstrated by the work of Bowmer et. al. (89). In this particular study the actual G - values were determined (using the GPC method) at various depths in gamma irradiated polystyrene. As shown in Figure 2-25, there is a pronounced decrease in G(S) with increasing sample depth, in addition to a slight increase in G(X). Although this study utilized a different material from that used in Clough's work,it does support the proposed mechanism responsible for the hardness profiles obtained.

It should be apparent now that the occurrence of heterogeneous oxidative degradation is dependent on the relative rates of oxygen consumption and diffusion (i.e. rate of replenishment). Hence it seems likely that the sample thickness will be a determining factor in whether or not heterogeneous oxidative degradation occurs.

(A)

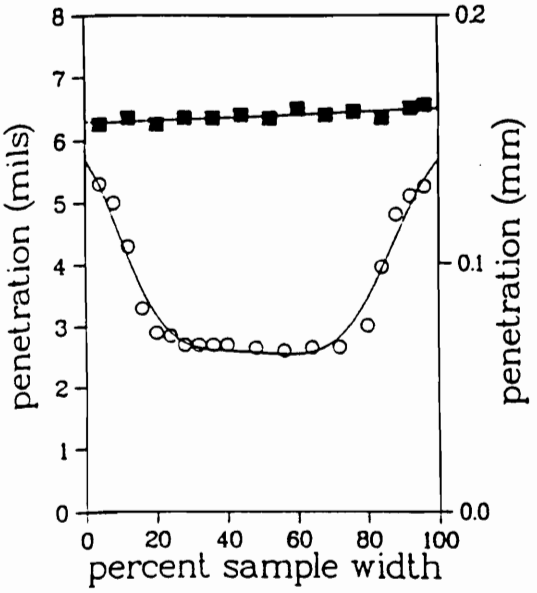

(B)

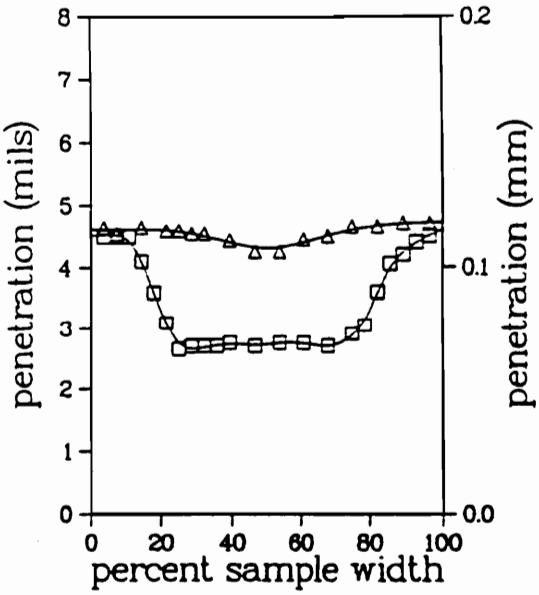

Figure 2-24a&b. Profiles of relative hardness of irradiated EPR. A:(■)- unirradiated material,(o)- 0.67 Mrad/hr(297 Mrads). B:(□)- 0.67 Mrad/hr(165 Mrads),(▵)- 0.11 Mrad/hr(175 Mrads). (ref. 86)

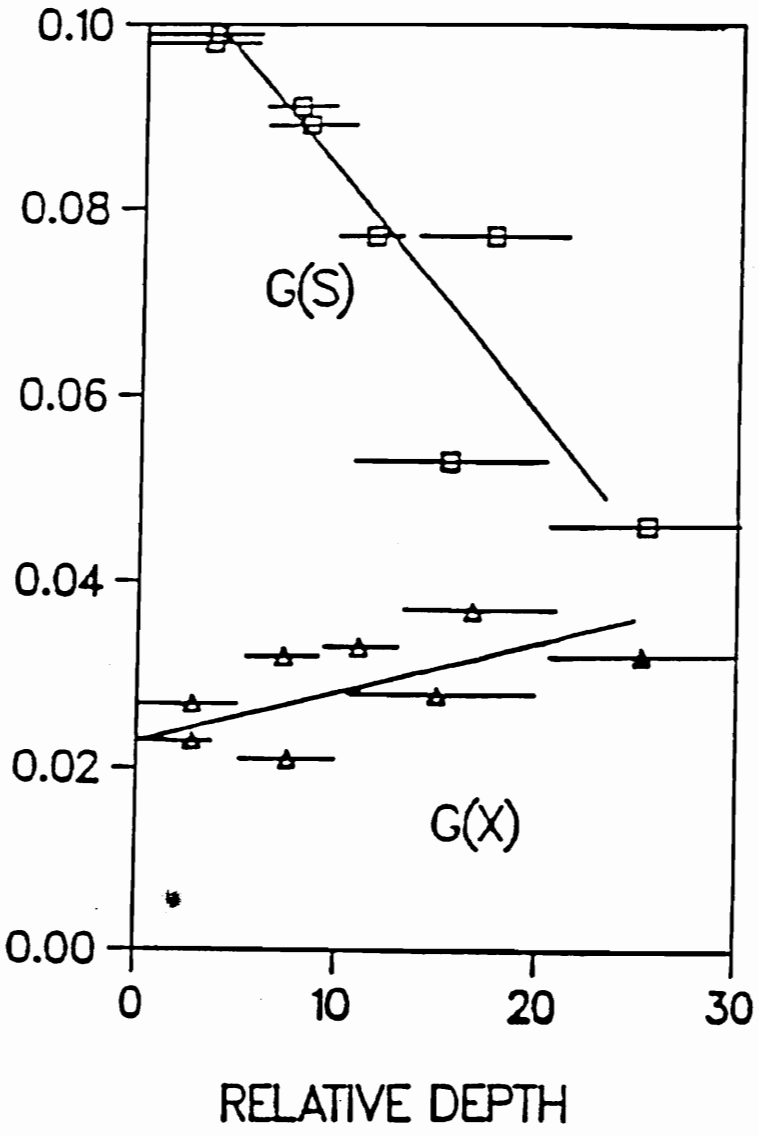

Figure 2-25. G - values for chain scission (G(S)) and crosslinking (G(X)) in polystyrene irradiated in air as a function of sample depth. (ref. 89)

In fact, Cunliffe and Davis (90) have developed a relationship for predicting when heterogeneous oxidative degradation will occur based on sample thickness. In one form, this relationship can be expressed as:

$$L^2 = \frac{8\ p\ P_{ox}}{\phi} \qquad [2\text{-}38]$$

where:

L = maximum sample thickness for which overall sample oxidation is 90% of the oxidation that would occur in the absence of oxygen diffusion effects.
p = oxygen partial pressure in surrounding atmosphere
P_{ox} = oxygen consumption rate
ϕ = oxygen permeation coefficient

This relationship is simply the culmination of the various parameters that will affect the oxygen diffusion and consumption rates. For this equation to be of practical utility, some knowledge of the radiation induced reaction kinetics is necessary, in order to determine the relationship between dose rate and oxygen consumption.

The presence of oxygen can also affect post - irradiation processes in addition to the events that occur during radiation exposure. As mentioned previously, free radicals can become trapped in glassy materials or within crystalline superstructures for long periods of time after irradiation. If the material is exposed to air, oxygen can diffuse into these materials and react with these free radicals, resulting in further degradation. This has been demonstrated in the work of Rijke and Mandelkern,

which has been previously discussed on the effects of irradiation temperature in polyethylene (73). Referring back to Figure 2-18, the effects of post - irradiation treatment on the gel fraction obtained at various irradiation temperatures is illustrated. If polyethylene is heated to 140°C (7°C above the melting point), immediately following irradiation, a significantly higher gel fraction is obtained, compared to aging the sample at room temperature in air for three days. It is likely that heating the sample mobilizes any free radicals trapped in the material, and induces complete reaction of the free radicals. Hence no reactive species are present to react with absorbed oxygen during aging. On the other hand, the material that was not heated prior to aging probably has a number of free radicals present which will react with the absorbed oxygen. This effectively deteriorates the network formed during radiation exposure, as is evident from the low gel fractions obtained. As the irradiation temperature is increased, the effects of post - irradiation treatment are diminished. This is likely due to the increased reactivity and mobility of the free radicals at elevated temperatures, which results in a lower reactivity of the material with oxygen during aging.

In summary, a number of factors exist which can affect the radiation response of polymers. Most of these influences arise due to some type of alteration in the free radical reactions, be it modifications in the spatial distribution of the reaction sites, kinetics, reactivity of the medium, or the actual reactions occurring. It must be stressed that many of the influences discussed can be interrelated. For example,

changes in molecular weight may not only affect the critical gelation dose, but may also affect the crystalline content in semicrystalline polymers, which could have further influences, as discussed. Hence one must be extremely careful when analyzing the effects of radiation on polymers, as slight modifications in the material may impact the response in a number of different ways.

This concludes discussion on the interaction of radiation with polymers. Focus will now turn to some important aspects of radiation induced polymerization, particularly with acrylated materials, in light of the nature of the experimental work that will be presented subsequently.

2.7 RADIATION INDUCED POLYMERIZATION

So far, the majority of this review has been concerned with radiation effects on polymeric systems. As mentioned in the introduction, this topic is one of two active areas of research involving radiation and polymers. Focus will now turn to some important aspects of the other significant research area, namely, radiation induced polymerization of monomeric and oligomeric species. It should be realized however, that much of the earlier discussion on the interaction of radiation with condensed matter and the processes which follow radiation exposure will be pertinent to this subject as well, as will be shown. Radiation induced polymerization involves the creation of linear, branched or network polymers from relatively low molecular weight reactive species exposed to ionizing radiation. Ultra-violet light is also a common source for inducing polymerization, but this will not be covered here, although some aspects to be presented may be relevant to photopolymerizations as well.

2.7.1 Advantages

Radiation initiated polymerizations have several advantages over conventional polymerization schemes, which provide the motivation for developing this type of process (21):

1. No catalyst or initiator is required, which may become incorporated in the polymer as an impurity and may continue to react, possibly accelerating degradation.

2. The initiation rate is independent of temperature. In conventional polymerizations, the temperature condition required for initiation may not be the optimum for chain propagation. In radiation processes, the reaction temperature can be chosen to optimize chain propagation, with no effect on the initiation rate.

3. Radicals can be produced uniformly throughout the system in precise concentrations. Therefore, much closer control of the reaction is possible.

4. No solvents are necessary and solid state polymerizations are possible. This makes radiation processing (especially with electron beams) well suited for applying protective coatings for a variety of applications, which has become a successful industrial process.

Gamma radiation is better suited for initiating bulk polymerizations due to its high penetration capabilities, as compared to electron beams. Since electron beams have limited penetration distances, but high intensities, they are commonly used for curing films.

2.7.2 Mechanisms

It is well known that conventional polymerization of vinyl monomers may proceed via free radical or ionic mechanisms. Therefore, neither mechanism should be ruled out for radiation initiated polymerizations. Ionizing radiation produces ions, free radicals, and excited species in organic systems, but free radicals are thought to be the primary intermediates in most radiation initiated polymerizations. However, depending on the monomer and reaction conditions, ionic reactions may be

prevalent. Table 2-7 shows some monomers and possible reaction mechanisms that they may undergo. As shown, some monomers may react by different mechanisms, indicating that reaction conditions play an important role in determining the reaction pathways. In particular, low reaction temperatures favor ionic reactions, possibly due to the lower reactivity of free radicals and the longer lifetimes of ionic species. In addition, thorough drying promotes ionic reactions, due to the inhibiting effect of water.

Free Radical Mechanism

Radiation initiated free radical polymerizations involve initiation, propagation, and termination steps (as well as possible chain transfer steps). Initiation is the result of the interaction of radiation with the molecular species, which produces free radicals. Propagation involves the addition of monomer to the growing chain, and termination renders the chain ends inactive, either by disproportionation or combination of two active chains, producing a stable polymer. These reactions have already been discussed previously, but are shown here again, along with rate constants, to develop the relationship between dose rate and reaction rate:

$$R \rightsquigarrow R^{\cdot} \qquad \text{initiation } (k_i)$$

$$R^{\cdot} + M \rightarrow RM^{\cdot}$$

$$RM_n^{\cdot} + M \rightarrow RM_{n+1}^{\cdot} \qquad \text{propagation } (k_p)$$

$$2RM_n^{\cdot} \rightarrow P \qquad \text{termination } (k_t)$$

Table 2-7. Possible reaction mechanisms for polymerization of a variety of monomeric species. (ref. 91)

Cationic	Free radical	Anionic
Isobutylene	Vinyl chloride	Nitroethylene
Cyclopentadiene	Vinyl acetate	Vinylidene cyanide
Alkyl vinyl ethers	Acrylonitrile	Acrylonitrile
β-Pinene	Methyl methacrylate	Methyl methacrylate
α-Methylstyrene	Ethylene	α-Methylstyrene
Styrene	Styrene	Styrene
Butadiene	Butadiene	Butadiene

Under steady state conditions, the radical concentration will be constant, and therefore the rate of radical formation (R_i) equals the rate of radical destruction by termination. Assuming termination by combination only,

$$R_i = k_t [RM_n^{\cdot}]^2 \qquad [39]$$

the propagation rate (R_p) is given by:

$$R_p = k_p [RM_n^{\cdot}][M] \qquad [40]$$

substituting,

$$R_p = \frac{k_p}{k_t^{0.5}} R_i^{0.5} [M] \qquad [41]$$

The initiation rate is the rate at which free radicals are produced, and therefore is proportional to the G - value for radical production and the dose rate (i.e. intensity). Hence, for radiation initiated free radical polymerizations,the rate of polymerization is proportional to the square root of the dose rate (for electron beam processes, the dose rate is proportional to the beam current).

Ionic Mechanism

Radiation induced ionic polymerization involves basically the same steps as the free radical polymerization although the species participating in the reactions are quite different. Initiation results in the removal of an electron from a molecule,

producing a cation. This leads to the propagation step, where monomer adds to the growing cation, producing a polymer. Termination is usually caused by reaction of the chain end with an impurity, or possibly with an anion (if present), rendering the chain inactive:

$$R \rightsquigarrow R^+ + e^- \qquad \text{initiation } (k_i)$$

$$R^+ + M \rightarrow RM^+$$

$$RM_n^+ + M \rightarrow RM_{n+1}^+ \qquad \text{propagation } (k_p)$$

$$RM_n^+ + X \rightarrow RM_n + X^+ \qquad \text{termination } (k_t)$$

Assuming steady state conditions, the initiation and termination rates will be equal:

$$R_i = k_t\,[X][M_n^+] \qquad [42]$$

The propagation rate will be:

$$R_p = k_p\,[RM_n^+][M] \qquad [43]$$

substituting,

$$R_p = \frac{k_p}{k_t}\frac{[M]}{[X]}R_i \qquad [44]$$

Hence, for radiation induced ionic polymerizations, the rate of polymerization will be directly proportional to the dose rate. However, for most electron beam applications, the free radical mechanism is predominate, so the rate of polymerization will scale closely to the square root of the beam current (dose rate).

2.7.3 Electron Beam Induced Free Radical Polymerization

As previously mentioned, radiation induced polymerizations have the advantage of being able to control the rate of initiation. This is a simple task with electron beams. Through manipulation of the beam current and accelerating voltage, the generation of free radicals can be systematically controlled. This can be illustrated by referring back to Figure 2-5, which depicts how the track structure (i.e. spatial distribution of free radicals) is influenced by the accelerating voltage (or specific ionization) and beam current. By increasing the beam current or decreasing the accelerating voltage, the concentration of spurs per unit volume is increased. Recall that increasing the beam current increases the incident energy per area and decreasing the accelerating voltage increases the rate of energy dissipation through the sample (i.e. higher stopping power). This increases the concentration of spurs, which results in an increase in the free radical concentration. For monomeric species which form linear species (i.e. bifunctional molecules) an increase in radical concentration results in more polymer chains being produced, but the average molecular weight will decrease. This is illustrated in Figure 2-26, which shows how the rate of polymerization and the molecular weight of polystyrene vary with dose rate. Hence, a higher beam current or lower accelerating voltage (both of which increase the effective dose rate) reduces the molecular weight of the polymer product, assuming a linear topology is generated. However, this relationship does have its limits. For example, a very low accelerating voltage will not produce many spurs (or radicals) due to the low penetration ability of the electrons.

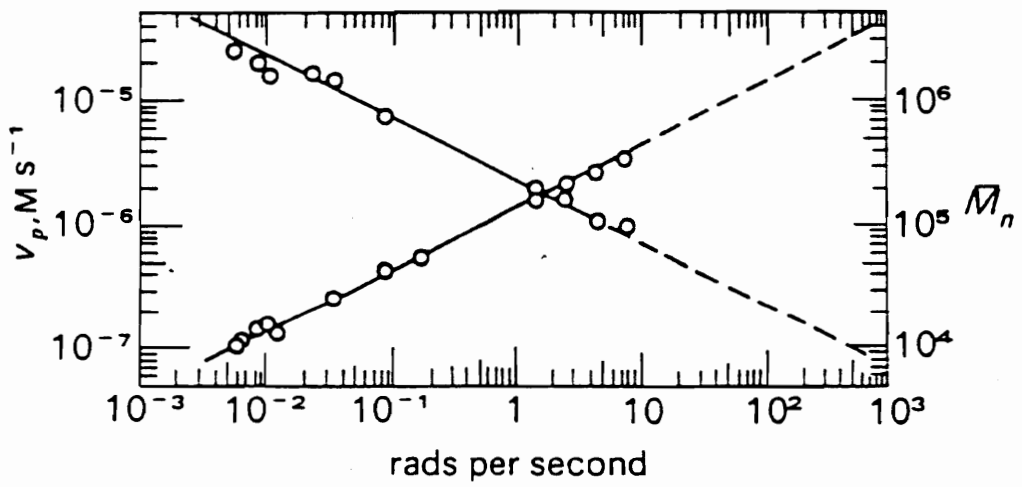

Figure 2-26. Effect of dose rate on the rate of polymerization and molecular weight of the polymer for the radiation initiated free radical polymerization of styrene. (ref. 98)

In most applications of electron beam curing, multifunctional monomers and oligomers are utilized, often with acrylated end groups. The acrylate functional group lends itself well to electron beam processing, due to its high G - value for radical production (i.e. high sensitivity to radiation). In addition, it has a high $k_p/k_t^{0.5}$ ratio, compared to other functional groups, as shown in Table 2-8. Hence it has a high rate of cure and high conversions can be reached, which is desirable. In any case, regardless of the functional end group present, irradiation of multifunctional oligomers results in the eventual formation of a crosslinked network, of infinite molecular weight (mathematically). The considerations of beam current and accelerating voltage on the molecular weight just discussed are not applicable to these systems. However, if the accelerating voltage is extremely high, the electrons may pass through the reactive medium with little interaction (low stopping power) which can result in low conversion of the reactive groups. Obviously, a too low beam current will have the same effect, but for different reasons. In addition, if the accelerating voltage is too low, such that the stopping power is sensitive to sample depth, then the rate of energy dissipation will vary across the sample thickness, resulting in a non-uniform cure.

2.7.4 Network Formation

During the irradiation of multifunctional oligomers, the end groups react with one another with a subsequent increase in the molecular weight of the system. There will be species present with varying molecular weights, with the eventual formation of a

Table 2-8. Rate constants for propagation and termination at 60°C for several monomers. (ref. 92)

Monomer	k_p, Litres/ Mole Second	k_t, Litres/ Mole Second x 10^{-7}	$k_p/k_t^{1/2}$
Vinyl Acetate	2,300	2.9	0.42
Styrene	145	0.130	0.12
Methyl Methacrylate	705	1.8	0.16
Methyl Acrylate	2,090	0.47	0.96
Vinyl Chloride	12,300	2300	0.08
Methacrylonitrile	184	2.3	0.04

gel. Prior to gel formation, the weight average degree of polymerization (DP_w) can be calculated by (93):

$$DP_w = \frac{(1+\alpha)}{1-\alpha(f-1)} \qquad [45]$$

where:

α = fraction of functional groups reacted
f = functionality of the reacting species (i.e. number of reactive groups per molecule prior to irradiation)

The gel point is defined by the condition:

$$\alpha = \frac{1}{f-1} \qquad [46]$$

At this point there is a minute amount of gel present along with the sol (portion of molecules not incorporated into a network). By substituting the gel point condition into the equation for the weight average degree of polymerization, it can be seen that DP_w becomes infinite (in a mathematical sense).

As the reaction proceeds, more gel is formed as the sol is incorporated into the network. Eventually, the increasing amount of gel causes a significant increase in the viscosity of the system. When this occurs, the reaction rate may increase significantly, which is known as the Tromsdorff effect. This is the result of a reduction in termination by combination, since the increased viscosity restricts the mobility of the long chain ends, which effectively reduces the probability of combination between two reactive long chains. However, the sol molecules are relatively small, and the

increased viscosity does not impair mobility as much. Hence, the polymerization can proceed at a much faster rate, due to the increased concentration of free radicals.

2.7.5 TTT and TTE Diagrams

As the reaction proceeds still further, the gel fraction continues to increase and the amount of sol decreases. For systems which form a glass at some point during the reaction, vitrification may occur. Vitrification is essentially the point where a chemically controlled reaction rate becomes diffusion controlled, due to the onset of the glassy state.

As the molecular weight of a polymerizing system increases, the glass transition temperature of the system will increase as well. If the glass transition temperature reaches the reaction temperature before complete conversion, then the reaction rate will become diffusion limited. This has been exemplified by the work of Gillham et. al. (94 - 96), who has proposed the Time - Temperature - Transition (TTT) diagram to illustrate this phenomenon. The TTT diagram is shown in Figure 2-27. This essentially shows the transitions which occur during the course of reaction (log time) at some reaction temperature (T_{cure}). T_{g0} represents the glass transition temperature of the system before any reaction takes place. If the reaction temperature is below T_{g0}, the reaction will proceed very slowly (if at all) and the system will remain an ungelled glass. If the reaction temperature is increased to some point above T_{g0} but below ${}_{gel}T_g$ (glass transition temperature of the system at the gel point) then the reaction will proceed as normal for some time until the glass transition temperature

reaches the reaction temperature. At this point, the reaction rate is drastically reduced and is being controlled by the physical relaxations of the glassy state, which are also extremely slow (95). It is important to realize that the reaction has not completely stopped. In fact, gelation may eventually occur if the system is allowed to react long enough and the reaction temperature is not too far below ${}_{gel}T_g$ (see Figure 2-27). If the reaction temperature is between ${}_{gel}T_g$ and $T_{g\infty}$ (glass transition temperature of the fully cured system) then gelation will occur before vitrification and a gelled glass (with some sol fraction present) will be obtained. However, if the reaction temperature is not too far below $T_{g\infty}$, the system can become fully cured if allowed to react for a sufficient period of time. If the reaction temperature is above $T_{g\infty}$, then vitrification will not occur and a crosslinked rubber will be formed, although there will be some unreacted groups present in the network with very little (if any) sol remaining. This is the most desirable state to achieve, since the presence of a sol fraction can have detrimental effects on the physical properties of polymers.

This concept of vitrification is extremely important in electron beam curing, since reactions are typically carried out at room temperature, making the possibility of vitrification occurring quite high for some systems. In fact, the TTT concept has been modified specifically for electron beam processes by Kim and Wilkes, which has been termed a Time-Temperature-Energy (TTE) diagram (97). The TTE diagram qualitatively illustrates The curing process with the onset of vitrification in terms of the sample temperature increase that can be expected due to radiation heating and

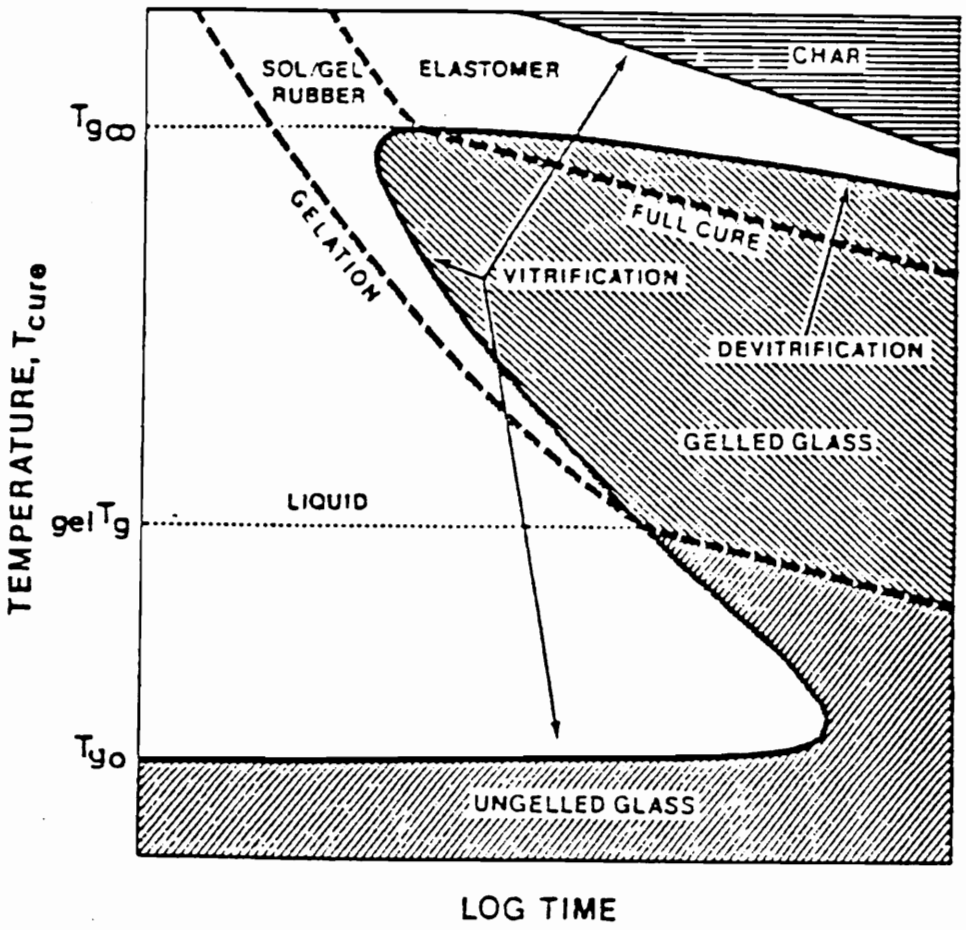

Figure 2-27. Time-Temperature-Transition diagram proposed by Gillham to describe the times to gelation, vitrification, etc. as a function of reaction temperature. (ref. 95)

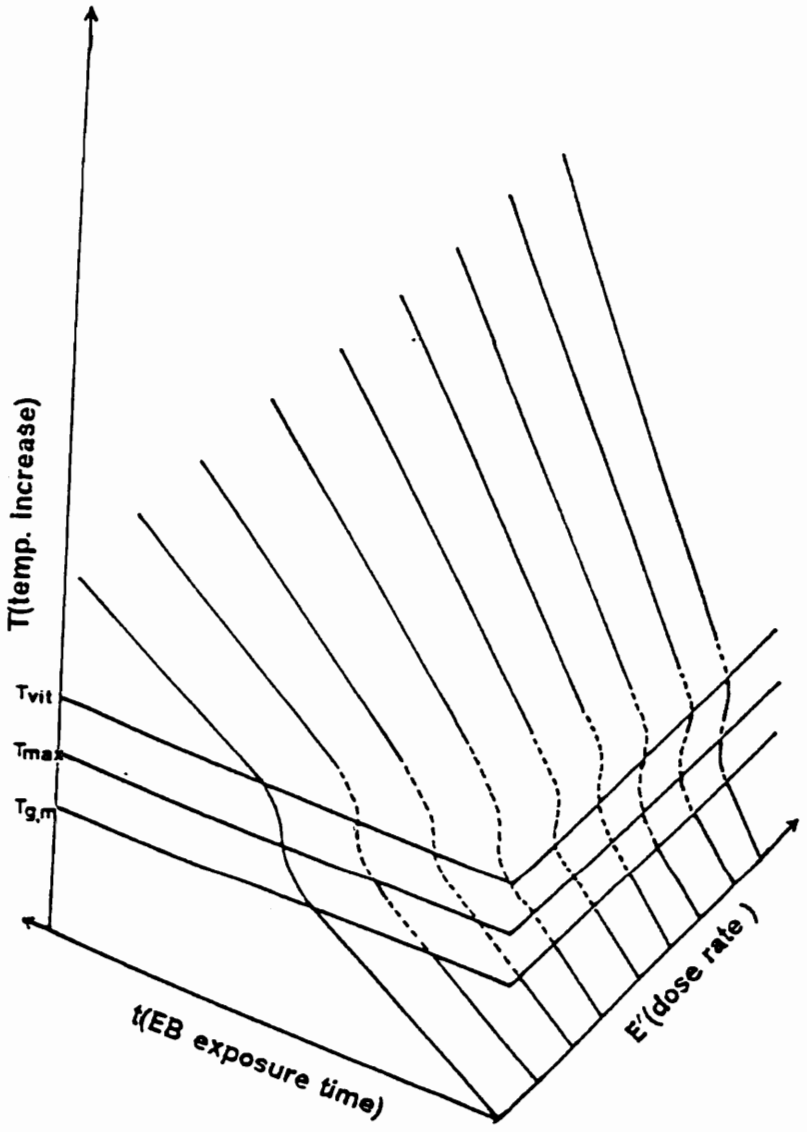

Figure 2-28. Time-Temperature-Energy diagram proposed by Kim and Wilkes to qualitatively describe the temperature increase in an electron beam irradiated reactive system as a function of time and dose rate. (ref. 97)

the reaction exotherm for a stationary, adiabatic system. An example of the TTE diagram is shown in Figure 2-28. This qualitatively illustrates the temperature rise in an irradiated, reactive material for various dose rates as a function of exposure time. As shown, there will be a linear increase in temperature with exposure time until the temperature of the system reaches the glass transition temperature of the monomer ($T_{g,m}$). At this point, there is an exponential increase in the system temperature as the molecular species gain segmental mobility and begin to react, as the viscosity decreases. During this time, the reaction proceeds with the onset of the Tromsdorff effect which further increases the rate of temperature increase. At some point, $T_{g,max}$ is reached which represents the point where the reaction conditions optimize the reaction rate. Past this point, the reaction begins to slow down, due to diffusion limitations, as vitrification sets in. This is evidenced in the lower rate of temperature rise, caused by a lower rate of heat evolution by reaction as the glass transition temperature of the system approaches the reaction temperature (T_{vit}). Past the vitrification point, the temperature increase becomes linear again, since no reaction is occurring and only radiation heating is significant.

This section has described some features pertinent to the application of radiation exposure for inducing chain reactions (polymerizations) to create various types of polymeric systems. Emphasis has been placed on electron beam processing and some important considerations pertaining thereto, which are necessary to obtain desired product properties.

This concludes the literature review section of this dissertation. A variety of topics have been discussed, ranging from fundamental interactions between radiation and condensed organic matter, to the various types of transformations which may result, as well as how these transformations can produce desirable (and not so desirable) changes in the physical properties of polymers. It is intended that this review has provided a sound basis for understanding and discerning the experimental research that will now be presented.

2.9 REFERENCES

1. O'Donnell, J.; Sangster, D. *Principles of Radiation Chemistry*, American Elsevier Publishing Co., New York, NY, 1970.

2. Roentgen, W.C. *Sitzungosberichte der Physikalisch- Medizinischen Gesellschaft zu Wurzburg*, 1895.

3. Becquerel, H. *Compt. rend.*, 1896, **122**, 420.

4. Salmon, G.A. *Polymers for High Technology*, American Chemical Society, Washington, DC, 1987.

5. Coolidge, W.D. *Science*, 1925, **62**, 441.

6. Newton, E.G. U.S.P. 1, 1929, 402 to the B.F. Goodrich Co.

7. Charlesby, A. *Proc. Roy. Soc.* 1952, **A215**, 187.

8. Bovey, F.A. *The Effects of Ionizing Radiation on Natural and Synthetic High Polymers*, Interscience, New York, NY, 1958.

9. Vasilakos, N.P.; Magalhaes, F. J. *Microwave Power*, 1984, **19(2)**, 135.

10. Silinski, B.; Kuzmycz, C.; Gourdenne, A. *Euro. Poly. J.*, 1987, **23(4)**, 273.

11. Raj, R. G. *Polym. Mater. Sci. Eng.*, 1986, **55**, 49.

12. Raj, R. G. *Polym. Mater. Sci. Eng.*, 1987, **57**, 537.

13. Holden, D.A. *Ency. Poly. Sci.*, John Wiley and Sons, New York, NY, 1988, **11**, 127.

14. Hughes, G. *Radiation Chemistry,* Clarendon Press, Oxford, Eng., 1973.

15. Holden, D. A. in *Encyclopedia of Polm. Sci. Eng.*, 2nd edition, John Wiley and Sons, New York, NY, 1988, **11**, 128.

16. Swallow, A. J. *Radiation Chemistry of Organic Compounds*, Pergamon Press, New York, NY, 1960

17. Guillet, J. *Polymer Photophysics and Photochemistry*, Cambridge University Press, New York, NY, 1985.

18. Coyle, J.D. *Introduction to Organic Photochemistry*, John Wiley and Sons, New York, NY, 1986.

19. Chatterjee, A. In *Radiation Chemistry - Principles and Applications*, editors, Farhataziz; Rodgers, M., VCH Publishers, New York, NY, 1987.

20. O'Donnell, J; Sangster, D. *Principles of Radiation Chemistry*, American Elsevier, New York, NY, 1970.

21. Charlesby, A. *Atomic Radiation and Polymers*, Pergamon Press, New York, NY, 1960.

22. Pacansky, J. *Rad. Cur.*, 11/87

23. Pacansky, J. *IBM Research J.* 1983, 3884.

24. Berger, M.J.; Seltzer, S.M. *Table of Energy Losses and Ranges of Electrons and Positrons*, NAS - NRC publication 1133, National Academy of Sciences and National Research Council, Washington, DC, 1964.

25. Grun, A.E. *Z. Naturforch.*, 1957, **12a**, 89.

26. Everhart, T.E.; Hoff, P.H. *J. Applied Physics*, 1971, **42**, .

27. Mozumder, A.; Magee, E. *Radiat. Res.*, 1966, **20**, 203.

28. Mozumder, A; Magee, E. *J. Chem Phys.*, 1966, **45**, 3332.

29. Hirsch, J.; Martin, E. *J. Noncrystallographic Solids,* 1970, **4**, 133.

30. Partridge, R.H. in *The Radiation Chemistry of Macromolecules*, Editor, Dole, M., Academic Press, New York, NY, 1968.

31. Forster, Th. *Ann. Phys.*, 1948, **2**, 55.

32. Bethe, H.A.; *Handb. Phys.*, 1933, **24**, 273.

33. Pacansky, J.; Waltman, R. *Radiat. Phys. Chem.*, 1985, **25**, 625.

34. Spinks, J.W.T.; Woods, R.J. *An Introduction to Radiation Chemistry,* John Wiley and Sons, New York, NY, 1976.

35. Chapiro, A. *Radiation Chemistry of Polymeric Systems,* John Wiley and Sons, New York, NY, 1962.

36. Lewis, F.M.; Walling, C.; Cummings, W.; Briggs, E.R.; Mayo, F.R. *J. Am. Chem. Soc.,* 1948, **70**, 1519.

37. Seitzer, W.H.; Goeckermann, R.H.; Tobolsky, A.V. *J. Am. Chem. Soc.,* 1953, **75**, 755.

38. Sun, K.H. *Modern Plast.,* 1954, **32**, 141.

39. Swallow, A.J. *Radiation Chemistry,* Longman, Great Britian, 1973.

40. Miller, A.A.; Lawton, E.J. Balwit, J.S. *J. Polm. Sci.,* 1954, **14**, 503.

41. Charlesby, A. *Proc. Roy. Soc.,* 1952, **A215**, 187.

42. Lawton, E.J.; Bueche, A.M.; Balwit, J.S. *Nature (London),* 1953, **172**, 76.

43. Charlesby, A. *Adv. Chem. Ser.,* 1967, **66**, 1.

44. Charlesby, A. *Proc. Roy. Soc. (London),* 1954, **A222**, 60.

45. Dole, M.; Keeling, C.D.; Rose, D.G. *J. Am. Chem. Soc.,* 1954, **76**, 4304.

46. Miller, A.A.; Lawton, E.J.; Balwit, J.S. *J. Phys. Chem.,* 1956, **60**, 599.

47. Dole, M.; Keeling, C.D. *J. Am. Chem. Soc.,* 1953, **75**, 6082.

48. Pearson, R.W., *Chem Ind.,* 1956, 903.

49. Waterman, D.C.; Dole, M.J. *J. Phys. Chem.,* 1970, **74**, 1913.

50. Seguchi, T.; Tamura, N.J. *J. Phys. Chem.,* 1973, **77**, 40.

51. Alexander, P.; Black, R.M.; Charlesby, A. *Proc. Roy. Soc. (London),* 1955, **A232**, 31.

52. Madorsky, S.L.; Straus, S.; Thompson, D.; Williamson, L. *J. Polym. Sci.,* 1949, **4**, 639.

53. Shultz, A.R. *J. Polym. Sci.,* 1959, **35**, 369.

54. Turner, D.T. *J. Polym. Sci.,* 1964, **A2**, 1699.

55. Alexander, P.; Charlesby, A.; Ross, M. *Proc. Roy. Soc. (London),* 1954, **223**, 392.

56. Charlesby, A; Pinner, S.H. *Proc. Roy. Soc.,* 1959, **A244,** 367.

57. Pacansky, J.; Waltman R.J. *J. Rad. Cur.*, 10/88, 12.

58. O'Donnell, J.H.; Winzor, C.; Winzor, *Macromolecules,* 1990, **23**, 167.

59. Ross, M.; Charlesby, A. *Atomics,* 1953, **4**, 189.

60. Kisbenyi, M.; Hedvig, P. *Eur. Polym. J. Suppl.,* 1969, 291.

61. Fowler, J.F.; Farmer, F.T. *Nature (London),* 1953, **171**, 1020.

62. Fowler, J.F.; Farmer, F.T. *Nature (London),* 1954, **173**, 317.

63. Fowler, J.F.; Farmer, F.T. *Nature (London),* 1954, **174**, 136, 800.

64. Fowler, J.F.; Farmer, F.T. *Nature (London),* 1955, **175**, 516, 590, 648.

65. Bhateja, S.K.; Young, R.J. *J. Polym. Sci.,* 1983, **23**, 523.

66. Bhateja, S.K.; Andrews, E.H. *J. Mat. Sci.,* 1985, **20**, 2839.

67. Aslanian, V.M.; Vardanian, V.I.; Avetisian, M.H.; Felekian, S.S.; Ayvasian, S.R. *Polymer,* 1987, **28**, 755.

68. Ellison, M.S.; Zeronian, S.H.; Qinghua, X. *Tex. Res. J.,* 1989, **59**, 657.

69. Birkinshaw, C.; Buggy, M.; Daly, S.; White, J.J. *Thermochimica Acta,* 1987, **117**, 365.

70. Kumar, S.; Adams, W.W. *Polymer,* 1990, **31**, 15.

71. Flory, P.J. *J. Am. Chem. Soc,* 1941, **63**, 3096.

72. Stockmayer, W.H. *J. Chem. Phys.*, 1944, **12**, 125.

73. Rijke, A.M.; Mandelkern, L. *Macormolecules,* 1971, **4**, 594.

74. Dole, M.; Katsuura, K. *J. Polym. Sci.*, 1965, **3B**, 467.

75. Lyons, B.J.; Weir, F.E. in *The Radiation Chemistry of Macromolecules,* Editor, Dole, M., Academic Press, New York, NY, 1973, **2**, 281.

76. Lyons, B.J. Unpublished work by Raychem Corp.

77. Okada, T.; Mandelkern, L.; Glick, R.; *J. Am. Chem. Soc.*, 1967, **89**, 4790.

78. Bell, J.P.; Michaels, A.S.; Hoffman, A.S.; Mason, E.A. in *Irradiation of Polymers,* editor, Gould, R.F., ACS Publications, Washington, D.C., 1967.

79. Akay, G.; Tinçer, T.; Aydin, E. *Euro. Polym. J.,* 1980, **16**, 597.

80. Brady, T.E.;Jabarin, S.A.; Miller, G.W. in *Permability of Plastic Films and Coatings,* editor, Hopfenberg, H., Plenum Press, New York, NY, 1974.

81. Yasuda, H.; Peterlin, A. *J. Appl. Polym. Sci.*, 1974, **18**, 5 .

82. Clough, R.L. in *Encycl. of Polym. Sci. Eng.*, 2nd edition, John Wiley and Sons, New York, NY, 1988, **13**, 667.

83. Wiliski, H. Duch, E.; Leugering, H.; Rosinger, S. *Coll. Polym. Sci.,* 1981, **259**, 818.

84. Wiliski, H. *Rad. Phys. Chem.*, 1987, **29**, 1.

85. Clough, R.L.; Gillen, K.T. *J. Polym. Sci., Chem. Ed.*, 1981, **19**, 2041.

86. Clough, R.L.; Gillen, K.T.; Quintana, C.A. *J. Polym. Sci., Chem. Ed.*, 1985, **23**, 359.

87. Gillen, K.T.; Clough, R.L. in *Handbook of Polym. Sci. Tech.,* editor, Cheremisinoff, N.P., Marcel Dekker, New York, NY, 1989, **2**, 167.

88. Clough, R.L.; Gillen, K.T. *ACS Symp. Ser.,* 1985, **280**, 411.

89. Bowmer, T.N.; Cowen, L.K.; O'Donnell, J.H.; Winzor, D.J. *J. Polym. Sci.*, 1979, **24**, 425.

90. Cunliffe, A.V.; Davis, A. *Polym. Degrad. Stab.,* 1982, **4**, 17.

91. Schildknecht, C.E. *Polymer Processes,* Interscience, New York, NY, 1956.

92. DeMarteau, W.; Giets, P.; Loutz, J.M. *Rad. Cur.*, 1984, **2**, 12.

93. Stockmayer, J. *Chem. Phys.*, 1943, **11**, 45.

94. Gillham, J. K. *Polym. Eng. Sci.*, 1979, **19(10)**, 676.

95. Peng, X.; Gillham, J.K. *J. Appl. Polym. Sci.*, 1985, **30**, 4685.

96. Gillham, J.K. in *Developments in Polymer Characterization - 3*, editor, Dawkins, J.V., Applied Science, London, Eng., 1982.

97. Kim, H.C.; Wilkes, G.L. *Rad. Cur.,* 1989, **2**, 8.

98. Chapiro, A.; Wahl, P. *Compt. Rend.*, 1954, **238**, 1803.

CHAPTER III

3.0 FORMATION OF POLYMERIC MICROSPHERES USING ELECTRON BEAM RADIATION

3.1 INTRODUCTION

Polymeric microspheres have been produced by a variety of different techniques. Emulsion polymerization of vinyl polymers is probably the most well known process (1). More recently, several investigators have described the formation of polymeric microspheres using radiation processes. Yoshida et. al. (2) have reported on the formation of polymeric microspheres by gamma irradiation of a homogenous solution of diethylene glycol dimethacrylate in methyl orthoformate. Rembaum et. al. (3) also demonstrated the formation of microspheres by a gamma radiation emulsion polymerization technique. The investigation reported in this dissertation illustrates the formation of crosslinked polymeric microspheres utilizing a polyaphron system and electron beam radiation. This method possesses several advantages over past or current techniques that have been reported. The polyaphron system facilitates formation of microspheres in a aqueous medium with monomer concentrations as high as 67 vol %. In addition, electron beam radiation allows for reaction times on the order of seconds, as opposed to gamma radiation, where reaction times are on the order of hours. Hence, electron beam radiation is well suited for continuous web line processing, which would be easily adapted to this application for polymeric microsphere production.

At the onset of this work, the formation of polymeric particulates was attempted using trimethylolpropane propoxylate triacrylate (a radiation curable monomer) in an emulsion system coupled with electron beam radiation. This scheme posed numerous processing difficulties and the resulting product was quite disperse in size. In order to circumvent these problems, an attempt was made to incorporate the monomer into a polyaphron system, which, as will be shown in this paper, is a successful approach.

Polyaphrons were discovered by Sebba, who also developed all of the current theory for these systems and coined the term "aphron" from the Greek word for foam. In addition, he invented a continuous polyaphron generator, which may make it possible to design a continuous process for the formation of solid polymeric microspheres, although this scheme has yet to be reduced to practice. Sebba's work deals with strictly liquid systems, although he does mention the possibility of making polymerizable aphrons, which is the focus of this work.

According to Sebba, an aphron is a phase that is encapsulated in a thin soapy film (4). Polyaphrons (a collection of a large number of aphrons) are similar to foams in that they consist of a continuous aqueous phase with a second phase (of greater volume) dispersed throughout the aqueous matrix. Instead of a gas being dispersed, as with a foam, an immiscible liquid constitutes the dispersed phase. Each droplet of this immiscible liquid is encapsulated in a thin soapy film which imparts extremely high stability to the system. This stability allows for the existence of high

concentrations of the dispersed phase with no coalescence or need for agitation. Obviously, aphrons are structurally very different from emulsion droplets. Emulsion systems consist of two distinct phases with an electrical double layer at the interphase, which stabilizes the droplets. On the other hand, aphron systems contain three distinct phases (continuous, dispersed, and encapsulating phases), where the third encapsulating film phase imparts some unique and desirable characteristics to the system (see Figure 3-1).

The mechanism of aphron formation requires the ability of each phase to spread on the other. This is achieved through the presence of a surfactant in both phases. In order for an aphron to form, the liquid to be dispersed must spread on an aqueous surface. A large aqueous surface area can be obtained by foaming the water prior to contact with this second phase. This large surface area allows the liquid to spread into a very thin film on the aqueous interface. As the film becomes very thin, and the contact angle becomes low enough, the aqueous phase spreads over this liquid film. As the film spreads, local disturbances eventually cause the film to break up into tiny globules and these globules become encapsulated by the aqueous phase. Hence, each thin film forms a single layer of aphrons (4).

As is evident from the proposed aphron formation mechanism, the creation and resulting size distribution of a system of polyaphrons will be strongly dependent on the spreading phenomena that occurs when two immiscible phases come in contact with each other. Aphron formation requires the ability of each phase to spread on

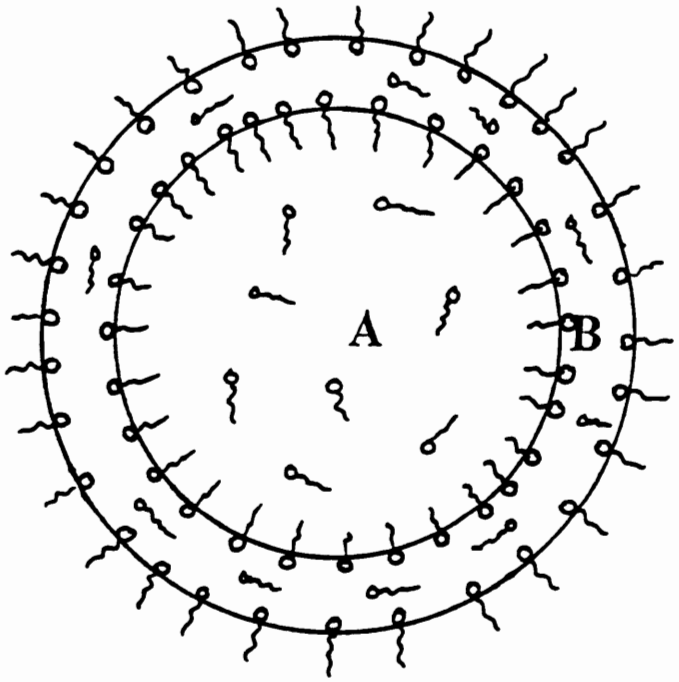

Figure 3-1. Physical structure of an aphron. It is comprised of (A) the core phase which contains the monomer solution, and (B) the aqueous shell which encapsulates and stabilizes the core, preventing coalescence.

the other, as previously mentioned. Thus, the surfactant concentration in both phases should be sufficient such that the resulting spreading coefficients (or surface pressures) are approximately equal. If the coefficients are substantially different, one of the phases will have difficultly spreading on the other, resulting in inefficient (or total lack of) aphron formation. If the nonpolar phase has a significantly higher spreading coefficient than the water phase, it will be able to spread easily on the water surface. However, the water will not be able to spread over the top of this phase as easily, which is necessary for aphron formation. On the other hand, if the spreading coefficient of the water phase is significantly higher than the nonpolar phase, there will be a large aqueous surface area, but the nonpolar phase will have difficulty spreading on it, due to the high surface pressure (compared to its own surface pressure.)

The above discussion suggests many factors that will affect the formation of aphrons and the underlying spreading phenomena that is occurring, some of which include (4): (a) nature and concentration of the water soluble surfactant, (b) nature and concentration of the nonpolar phase soluble surfactant, (c) equilibrium surface pressure on the water surface (related to (a) above), (d) preparation temperature, and (e) viscosity of the phases. While this list is by no means a complete listing of all the factors affecting spreading, it does provide a basis for this study.

This paper addresses the effects of the aqueous surfactant type, monomer and aqueous phase surfactant concentration, and the formation temperature on a

polyaphron system containing a radiation sensitive monomer as the dispersed liquid phase which is subject to electron beam radiation to form crosslinked polymeric microspheres. Obviously, due to the nature of the aphron formation process, a distribution of aphron sizes will be produced. The objective of studying these variables is to determine what conditions influence the size distribution of polymeric microspheres, with an attempt to produce small microspheres with as narrow a size distribution as possible. In addition to this size distribution study, the ability to modify the surface characteristics (i.e. wettability) of the microspheres is illustrated through use of a polymerizable surfactant (a fluorinated acrylate) in the monomer phase.

3.2 EXPERIMENTAL

3.2.1 Materials

1. Distilled water

2. Trimethylolpropane propoxylate triacrylate (TMPPTA)(Henkel Corp.) (see Figure 3-2)

3. Sodium dodecyl benzene sulphonate (NaDBS) water soluble anionic surfactant (Tennessee Chemical Co.)

4. Sodium didodecyl disulfonated diphenyloxide (Dowfax 2Al) water soluble anionic surfactant (Dow Chemical Corp.)

5. Alkyloxypolyethyleneoxyethanol (Tergitol 15-S-3) oil soluble surfactant (Union Carbide Corp.)

6. 2-(N-ethylperfluorooctane-sulfonamido) ethyl acrylate (FX-13 Fluororad) fluorochemical acrylate (3M Corp.)

3.2.2 Aphron Formation

A specified amount of aqueous surfactant solution is placed in a closed vessel and shaken vigorously to create a foam. Several drops of the monomer (with the specified amount of surfactant) is added to the foam and shaken vigorously for approximately 20 seconds. This facilitates the spreading and breakup of the monomer film with subsequent aphron formation. This process is repeated until the desired concentration of monomer is obtained. During this process, the solution slowly transforms from a conventional foam (only gas is dispersed in the aqueous

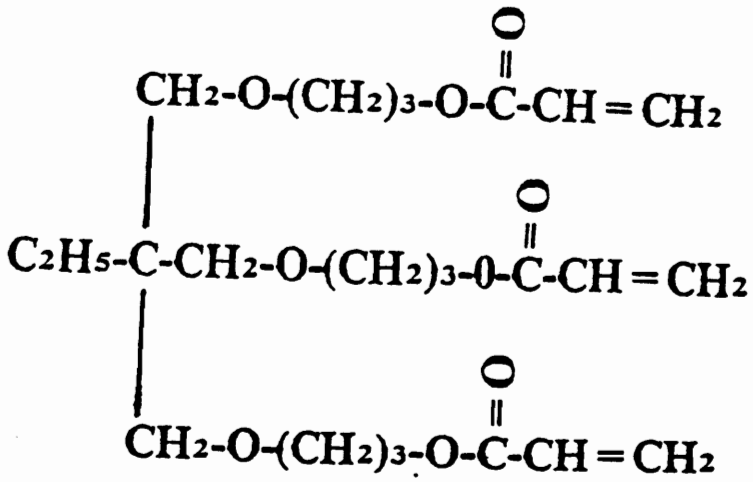

Figure 3-2. Molecular structure of trimethylolpropane propoxylate triacrylate.

solution) to a biliquid foam (only the monomer is dispersed in the aqueous matrix). After several milliliters of monomer has been added, it is possible to add increasing amounts of monomer in a single step. Aphron formation requires the presence of a large aqueous surface area. However, the surface of an aphron works just as well as an aqueous film in this respect. Therefore, once a significant number of aphrons have been produced, increasing amounts of monomer may be added at one time. For reasons to be discussed, the final concentration of monomer dispersed in the aqueous solution was 67 vol % for most samples prepared in this study. In order to gain an understanding of how various factors affect the particulate formation, several variables were systematically manipulated to determine their influence on the final product. The following variables were considered:

a. Monomer Phase Concentration. Four aphron samples were prepared with a 1.0% NaDBS aqueous solution and 0.4% Tergitol 15-S-3 in TMPPTA in a monomer to water ratio of 1:1, 2:1, 3:1, and 9:1 to determine the effect of monomer concentration on the resulting product.

b. Monomer Phase Surfactant Concentration. Surfactant concentrations of 0.04, 0.07, 0.4, 0.8 and 1.0 volume % of Tergitol 15-S-3 in TMPPTA were used with various aqueous solutions to determine the effect of the monomer phase surfactant concentration on the final product.

c. Aqueous Phase Surfactant Type and Concentration. Aqueous solutions containing 0.5% and 1.0% of NaDBS or Dowfax 2A1 were prepared for use as the

continuous phase of the aphron systems to determine what effect this has on the final product.

d. Temperature. Various aphron samples containing different combinations of the specified aqueous and monomer solutions were prepared at 25°C and 75°C to determine the effect of formation temperature on the final product since the viscosity and surface tension of the phases are dependent on this parameter.

3.2.3 Surface Modification

Alteration of the wettability of polymeric microspheres has been considered by substituting the fluorinated acrylate surfactant, FX-13, for the nonionic surfactant, Tergitol 15-S-3, in the monomer phase. In addition to preparing microspheres containing this compound, thin films were made with varying concentrations of FX-13 to facilitate contact angle measurements on this material, which complements the wettability measurements made on the microspheres. The wettability of the microspheres was determined by placing 15 milligrams of the particles on the surface of a series of solutions containing increasing amounts of isopropanol in water and visually observing when the particles sank into solution. Contact angle measurements were made on thin films using small droplets of deionized distilled water and measuring the advancing contact angle at ambient conditions.

3.2.4 Radiation Curing

The aphron samples were cured to form crosslinked polymeric microspheres under the following conditions. A small amount of biliquid foam was placed on an inert

semicrystalline polyester substrate, PET, and spread to a thickness of 5 mil (maximum thickness allowed to ensure uniform radiation dosage) using a wet film applicator. Samples that had been made more than a day or two prior to curing tended to settle out, forming a clear aqueous layer on the surface of the polyaphron phase. This aging posed no problem; the liquid was simply shaken to restore homogeneity and ensure a representative sampling. All wet film samples were cured at ambient temperatures under a nitrogen atmosphere with electron beam radiation. The electron beam source utilized was an Energy Sciences Inc. CB150 Electrocurtain operating at 175 kV, with a beam current of 2.4 milliamps and a conveyor speed of 40 ft/min (see Appendix for complete description of this equipment). This resulted in a total radiation dose of ca. 4 megarads. This dosage is slightly above the manufacturer's recommended dose for film curing (3 megarads). After curing, the particles were washed in acetone, filtered, washed in water, filtered, then washed in acetone and filtered again, then placed under vacuum for at least 24 hours prior to analysis.

3.2.5 Analysis

Particle analysis was performed using a Cambridge Instruments Stereoscan 2000 scanning electron microscope and a Shimadzu SA-CP3 centrifugal particle size analyzer to obtain information on the size, shape, and size distribution of the crosslinked microspheres. The particle size analyzer is based on the sedimentation method for particle size determination and measures the particle concentration

photometrically. Accelerated sedimentation of small particles is facilitated by a rotating sample holder which exerts a centrifugal force on the colloid solution. All distributions shown represent an average of three runs made on the analyzer, which were performed using a 30 vol % solution of glycerol in distilled water with Dowfax 2A1 as a dispersant. To obtain an indication of the error associated with these distributions, three solutions of one polyaphron sample were prepared and analyzed. In addition, three polyaphron samples of the same composition were prepared and analyzed. This allowed the error associated with the aphron preparation and the particle analysis to be qualitatively separated.

In order to obtain information on the mechanical properties and degree of cure of these particles, thin films were formed from the monomer under the same radiation conditions and analyzed using dynamic mechanical analysis (Automated Vibron - Toyo Baldwin Inc.) at a frequency of 11 Hz and differential scanning calorimetry (Seiko Instruments Inc.). FT-IR spectroscopy was attempted on the particles, but this did not produce a good quality spectra with the apparatus available, due to the low transmittance (large degree of scatter) of the IR beam. This same method was applied to the thin films with success, since the smooth surface of film did not scatter the beam as the particles did.

Surface tension values were measured using the Du Nouy ring method of surface tension determination. In order to obtain a quantitative measurement of the relative foam stability of the aqueous surfactant solutions, 10 milliliters of each solution was

placed in a capped 100 ml graduated cylinder and shaken vigorously to create a foam. The foam was allowed to sit for twenty seconds and the volume of drained water was measured as a qualitative indication of this property.

3.3 RESULTS AND DISCUSSION

3.3.1 Effects of Process Variables

As previously mentioned, the formation of polymeric particulates was first attempted by introducing TMPPTA into an emulsion with glycerol, water, and Dowfax 2A1 constituting the continuous phase. The emulsion was subjected to electron beam radiation to form solid polymeric microspheres. This system required extensive stirring prior to processing to sufficiently disperse the monomer phase and the monomer concentrations had to be kept fairly low (about 5 vol %). The resulting product was quite disperse in size (see Figure 3-3) and required extensive purification, which resulted in the production of a large amount of by-product (i.e. the reaction medium). As mentioned earlier, these difficulties were eliminated by developing a polyaphron system with TMPPTA incorporated into the dispersed phase.

Electron beam irradiation of the polyaphron samples did result in the creation of polymeric microspheres, but their formation was strongly dependent on the monomer concentration. Figure 3-4a-d illustrate the effect of monomer concentration on the formation of microspheres. At monomer concentrations of 50 and 67 vol %, polymeric microspheres are produced with very little (if any) production of other geometric structures (see Figure 3-4a&b). In addition, there does not appear to be any difference in the size distribution of particles between these two concentrations. However, as the monomer concentration is increased to 75 vol %, the production of

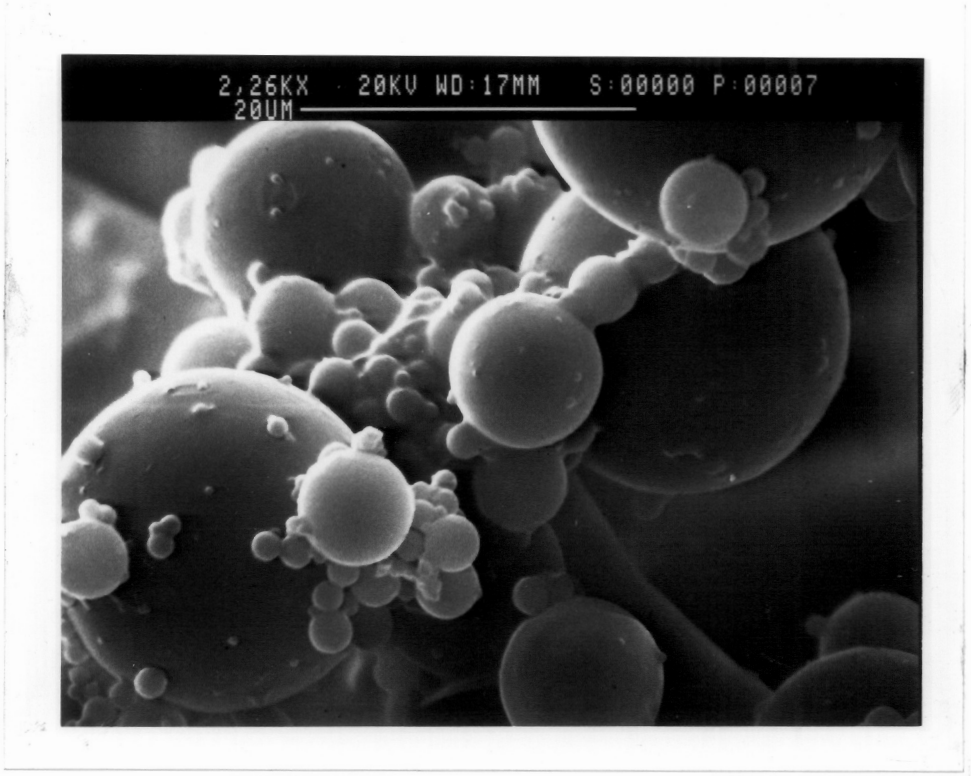

Figure 3-3. Polymeric microspheres formed via irradiation of an emulsion system containing TMPPTA

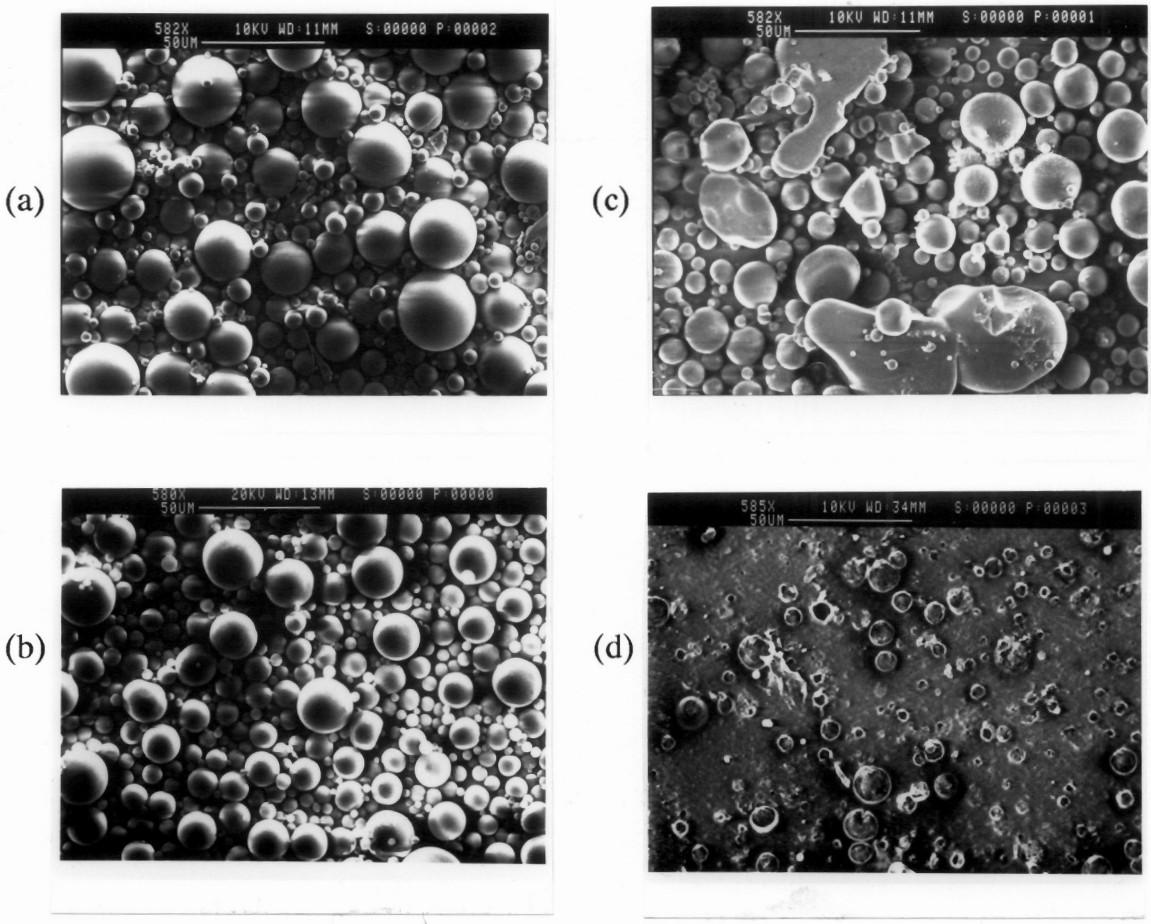

Figure 3-4a-d. Polymeric microspheres obtained by irradiation of a polyaphron system containing (a) 50%, (b) 67%, (c) 75%, and (d) 90% TMPPTA dispersed in an aqueous matrix.

irregular fragments (in addition to microspheres) becomes significant (Figure 3-4c). In fact, at a monomer concentration of 90 vol %, irradiation of the sample results in the formation of a continuous film (Figure 3-4d). Apparently, as the monomer concentration approaches 75 vol % or higher, the aphrons become so close to one another that the encapsulating soap film around the individual aphrons does not prevent monomer in one aphron from coalescing with monomer in neighboring aphrons, under the reaction conditions specified in this study. It should be noted that at a concentration of approximately 75 vol % of the dispersed phase, Sebba (5). has reported that liquid aphrons begin to lose their spherical character and take on a polyhedral structure due to the close packing of aphrons. In light of this, the production of irregular fragments at a monomer concentration of 75 vol % should become evident. Due to the lower yield of microspheres and an increase of undesirable structures created at this monomer concentration, all subsequent aphron samples to be discussed were produced using a monomer concentration of 67 vol %.

By varying the concentration of the monomer phase surfactant, it is possible to change the size distribution of the resulting microspheres. Although the end points of the size distribution (i.e. the largest and smallest spheres produced) are not dramatically affected by the monomer phase surfactant concentration, the relative distribution of particle sizes between the end points is significantly dependent on this variable (see Figure 3-5). It should be noted that an error analysis was performed on the sample containing 1.0 vol % Tergitol 15-S-3 in TMPPTA. The results show

an overall average error of ± 14% for all data points greater than 10 cumulative % (see Figure 3-6a). Below this value the percent error was somewhat greater, due to the small average value used in the calculations. This represents the error associated with both the aphron preparation and the size analysis. The average error associated with the size analysis alone was determined to be ± 12% (see Figure 3-6b). This suggests that the procedure used to produce the aphron samples gives fairly consistent results in terms of the size distribution of the final polyaphron system. Although this error analysis was performed on only one composition, it is indicative of the error associated with all the distributions shown.

As illustrated in Figure 3-5, varying the monomer phase surfactant concentration from 0.04 to 1.0 vol % results in a minimum average particle size at 0.4 vol %. Increasing the surfactant concentration in the monomer phase from 0.04 to 0.4 vol % results in a significant decrease in the average particle size, which may be attributed to the Gibbs effect. The Gibbs effect applies to thin films or small volumes which contain a surfactant, and can be described as follows. If a fixed volume of a liquid contains a surfactant and the surface area is increased (as in spreading), then surfactant molecules will move to the surface in accordance with the Gibbs adsorption isotherm and reduce the surface tension of this new surface. However, if the surfactant concentration becomes so low that the liquid surface already contains a significant portion of the total amount of surfactant, then there may not be enough surfactant available to reduce the surface tension of this new

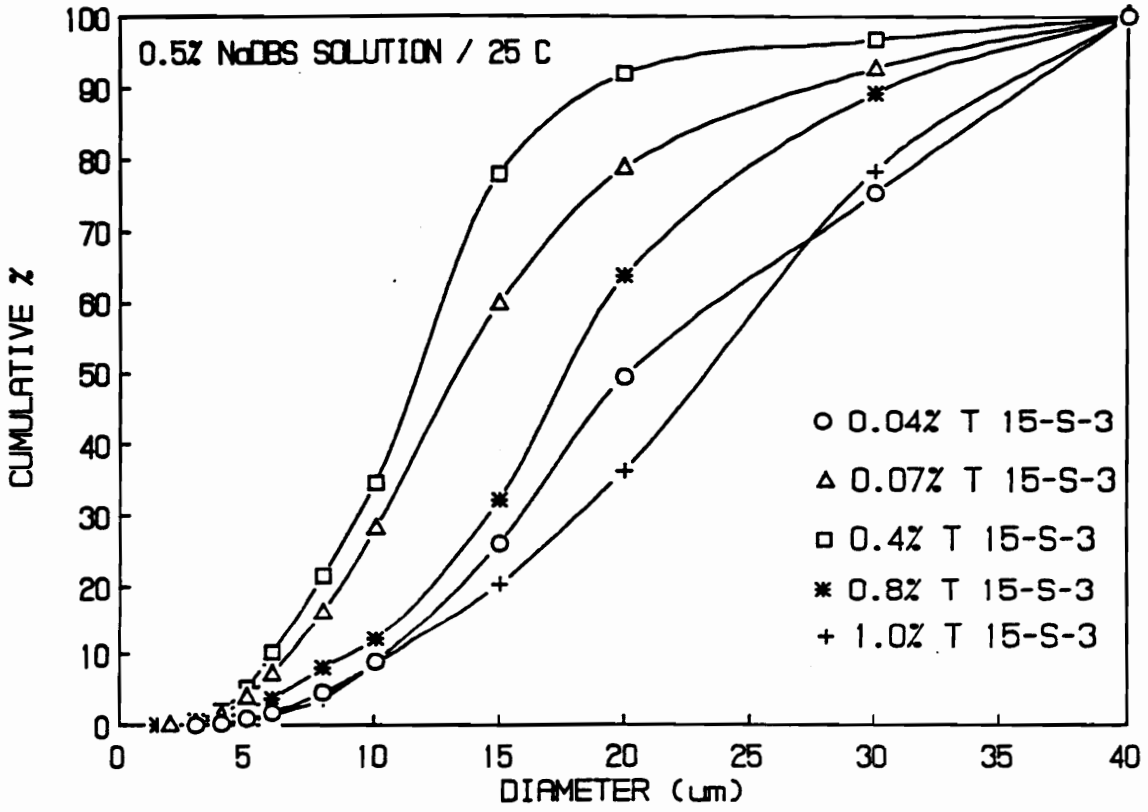

Figure 3-5. Effect of Tergitol 15-S-3 concentration in TMPPTA on the particle size distribution of microspheres formed at 25°C with a continuous phase of 0.5% NaDBS aqueous solution.

(a)

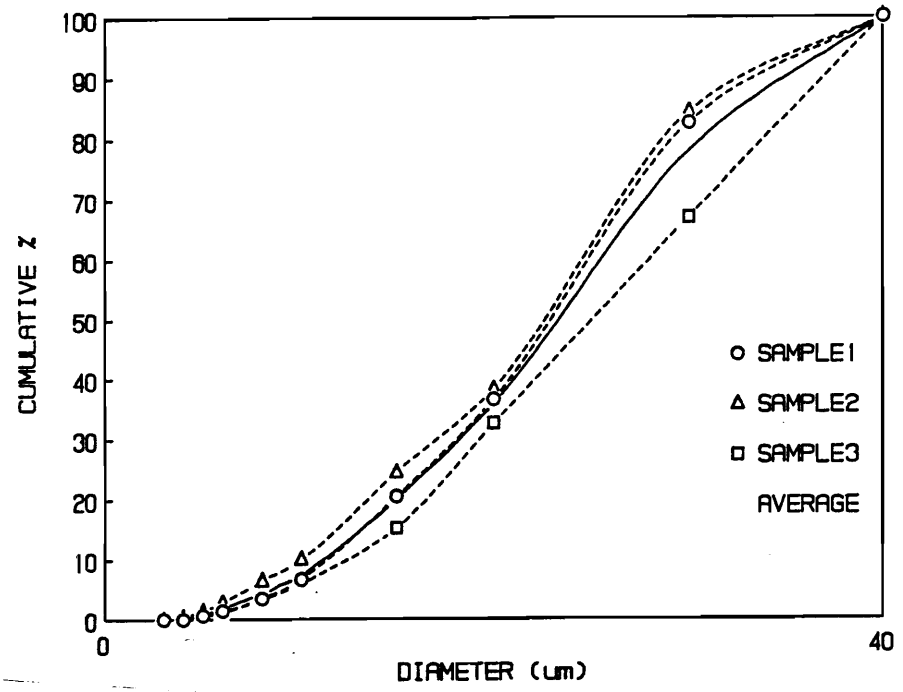

(b)

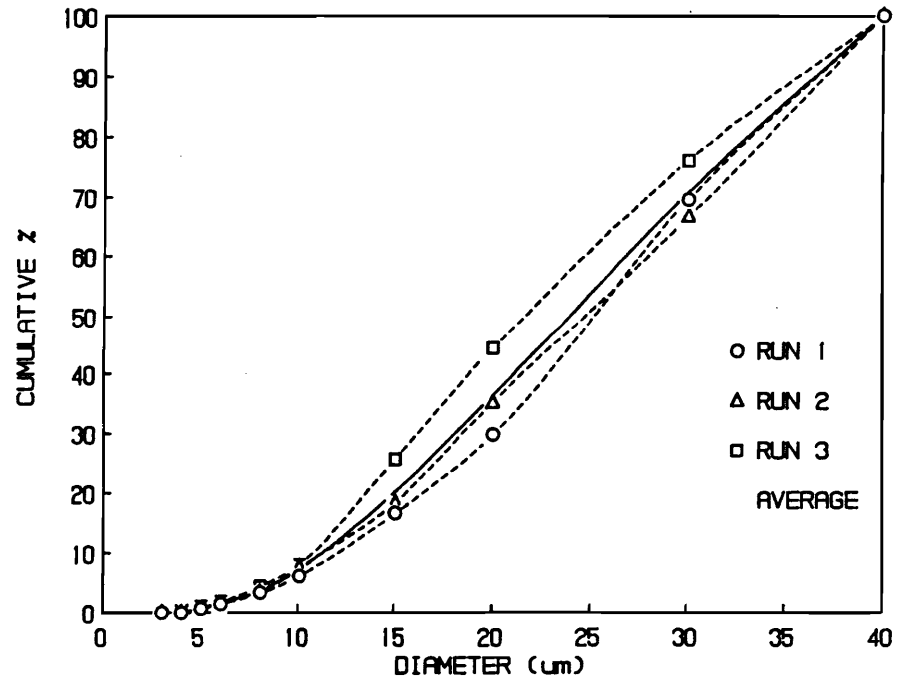

Figure 3-6a&b. Error analysis on the size distributions of the microspheres produced in this study.

surface. The net effect is to produce a restoring force which resists further thinning of the liquid surface. Hence, as the surfactant concentration is increased, the monomer phase can form thinner films prior to breaking up and being encapsulated in the soap film, thus forming smaller aphrons. However, as the surfactant concentration is increased further (to 0.8 and 1.0 vol %), the average particle size increases.

The increase in average particle size at the higher monomer phase surfactant concentrations may have several origins. One possibility is that at high concentrations, the surfactant may be forming complex micellar structures in the monomer phase which may be very stable and not break down readily as the surface area is increased. Thus, the surfactant molecules may not be able to diffuse to the surface, allowing the Gibbs effect to occur. A second possible explanation is related to the Marangoni effect. This effect is similar to the Gibbs effect except that it is not restricted to thin films. If a liquid contains a surfactant and its surface area is increased, this new surface area will have a greater surface tension than the surface which was already present. This is a non-equilibrium condition because the Gibbs adsorption isotherm requires that surfactant molecules must diffuse to the surface from the bulk to reduce the surface tension to its equilibrium value. Although this diffusion time is very small, the momentary increase in surface tension produces a restoring force preventing the extension of the surface, thus causing a surface elasticity. If the concentration of the surfactant is very high, this diffusion time will

be very small. Hence, the surface will have minimal elasticity, and the film may become unstable. This instability could cause the monomer film to break up and become encapsulated by the soap film before it is able to thin sufficiently, thus producing larger aphrons. A third possibility is that the high surfactant concentration produces a spreading coefficient that is substantially "out of balance" (as discussed earlier) with the spreading coefficient of the aqueous phase thus causing inefficient formation of aphrons due to the hindered ability of the aqueous phase to spread over the monomer phase.

Figure 3-7a illustrates the variation of the particle size distribution with monomer phase surfactant concentration for a series of polyaphrons formed using the Dowfax 2A1 aqueous surfactant. Note that there is no apparent trend here with respect to particle size distribution and the monomer phase surfactant concentration (as was discussed previously for the polyaphron systems utilizing the NaDBS aqueous surfactant). This indicates that other factors may be present here which essentially override the ability of the monomer phase surfactant concentration to control the resulting particle size distribution. The reduced foamability of the Dowfax solution (compared to the NaDBS solution - see Table 3-1) may account for this apparent lack of control. The Dowfax solution produces less aqueous surface area for the monomer to spread on which may affect the aphron formation process. However, if the preparation temperature is increased to 75°C, the trends discussed with the systems containing the NaDBS solution is established (see Figure 3-7b). Table 3-1

(a)

(b)

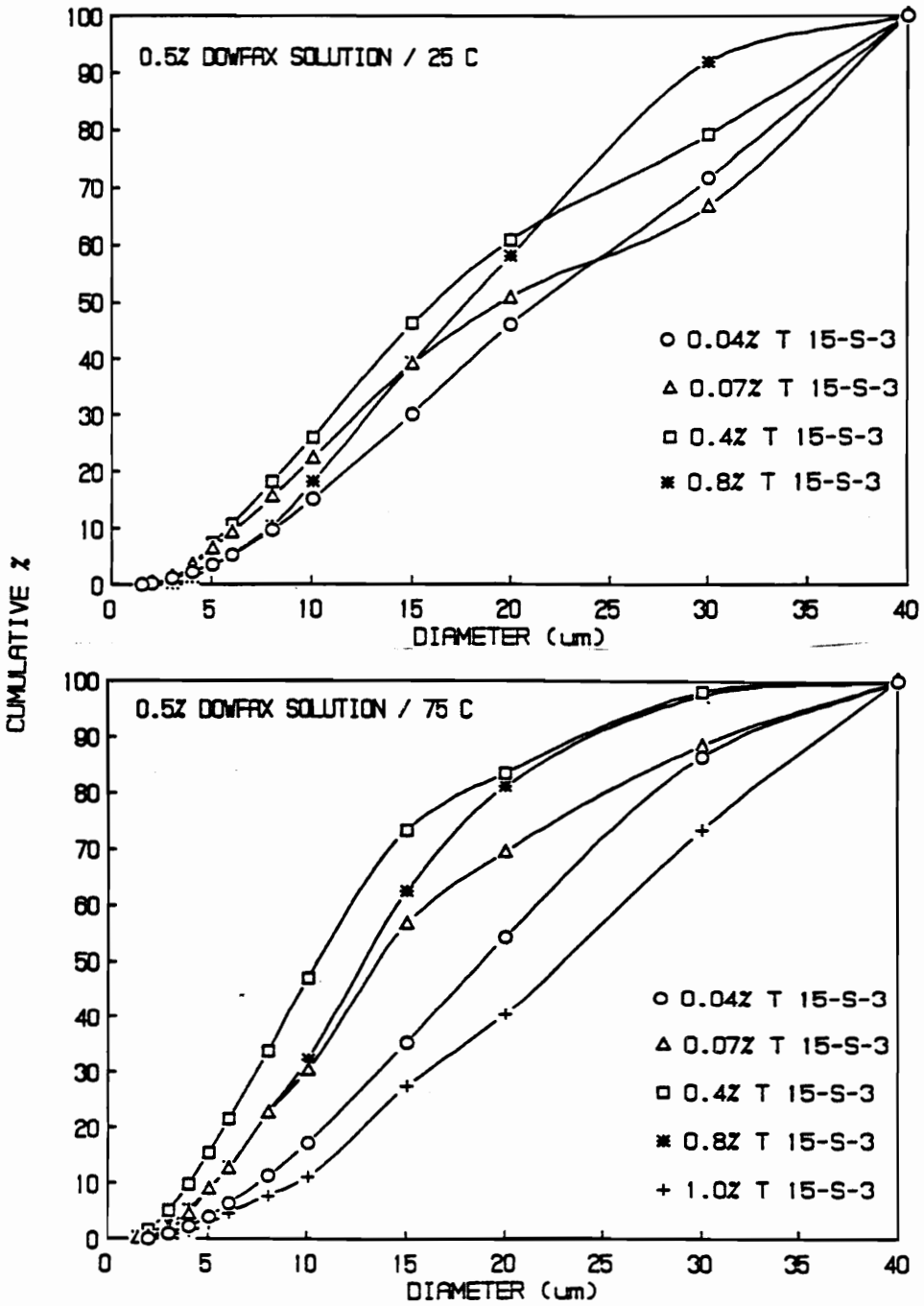

Figure 3-7a&b. Effect of Tergitol 15-S-3 concentration in TMPPTA on the size distribution of microspheres formed at (a) 25°C and (b) 75°C with a 0.5% Dowfax 2A1 solution as the continuous phase.

Table 3-1. Some physical properties of the surfactant solutions used in this study and their temperature dependence.

MATERIAL	APPARENT SURFACE TENSION (dyne/cm)***	VISCOSITY (CPS)**	FOAM STABILITY (vol%)*
TMPPTA (all T-15-S-3 concentrations)	25°C 75°C 37 32	25°C 75°C 140 32	--
0.5% NaDBS solution	33 32	-- --	25
0.5% Dowfax 2A1 solution	33 32	-- --	50

* Vol % of water drained in 20 seconds after foaming solution
** Brookfield viscosity
*** Determined by DuNouy Ring Method

shows that the main effect of the temperature increase is to reduce the viscosity and surface tension of the monomer phase. Both of these physical property changes will improve the ability of the monomer to spread, so the surface area produced with the Dowfax solution may now be sufficient for the Gibbs effect (or other effects previously discussed) to govern the aphron formation process.

These points lead one to consider the effects of the aqueous phase surfactant type and concentration on particulate formation and properties. Figure 3-8a illustrates these effects on the particle size distribution for a series of aphron systems formed at 75°C with a Tergitol 15-S-3 concentration of 0.07 vol % in the monomer phase. An increase in the aqueous surfactant concentration increased the average particle size for both NaDBS and Dowfax 2A1 surfactants. Increasing the surfactant concentration produces a higher surface pressure on the aqueous film, which increases the resistance to spreading of the monomer film. This will produce a thicker monomer film, which will lead to the formation of larger aphrons when the film breaks up and becomes encapsulated in a thin soapy film. However, if the Tergitol 15-S-3 concentration is increased to 1.0 vol %, the average particle size decreases with increasing aqueous phase surfactant (NaDBS) concentration (see Figure 3-8b). This trend reversal at high monomer phase surfactant concentrations strongly supports the fact that a "balance" between the spreading coefficients (or spreading pressures) is necessary for the efficient production of small aphrons.

SEM analysis of the crosslinked particles has shown some differences among the shape of various microspheres that appears to be related to the aqueous phase surfactant type. It should be noted that SEM sample preparation was facilitated by using double sided adhesive tape to secure the specimen to the SEM stub. Some microspheres may appear to be semicircular, where actually they are imbedded in the adhesive layer. Figure 3-9a&b shows SEM micrographs of polymeric microspheres formed with 0.5 vol % Dowfax 2A1 and 0.5 wt % NaDBS solutions respectively, with equal concentrations of Tergitol 15-S-3 in the monomer phase. The micrographs show the presence of some indentations on the surface of the larger microspheres formed with the NaDBS solution. These distortions were not found on all the samples prepared from the NaDBS solution, but they were present to a much larger extent than the microspheres produced with the Dowfax 2A1 solution. Sebba has reported that increasing the ionic strength of the encapsulating film (i.e. by increasing the surfactant concentration or strength) increases the attractive forces between aphrons and the smaller aphrons will tend to adhere to the surface of larger aphrons and distort their sphericity. This is a likely cause of the surface distortions seen on the microspheres formed with the NaDBS solution. However, it is expected that some shrinkage of the monomer phase occurs during curing as a result of the polymerization through double bond moieties. This shrinkage can induce stresses which may affect the curvature of the larger microspheres to a greater extent, due to the larger volume, but this does not account for the apparent surfactant type

(a)

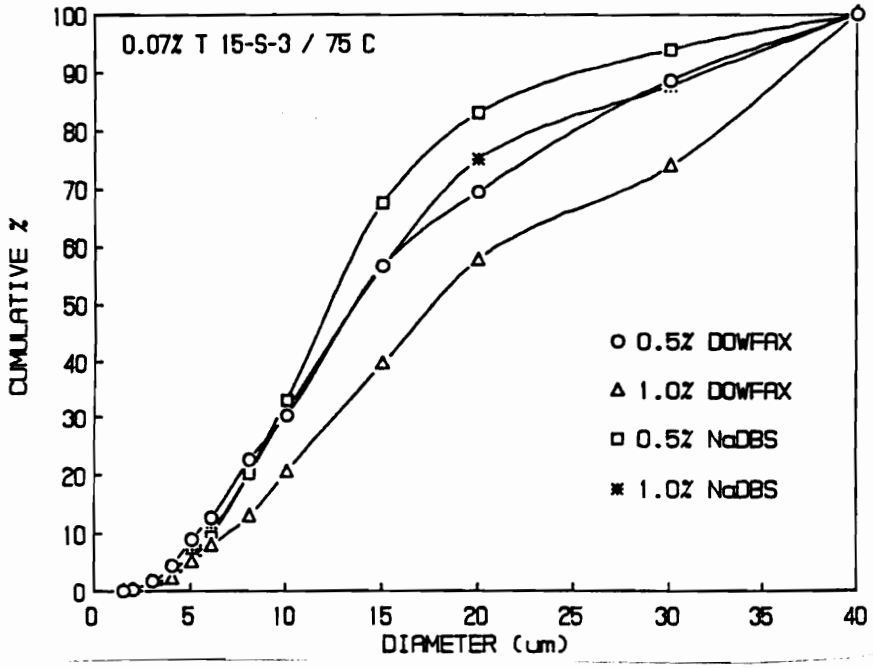

(b)

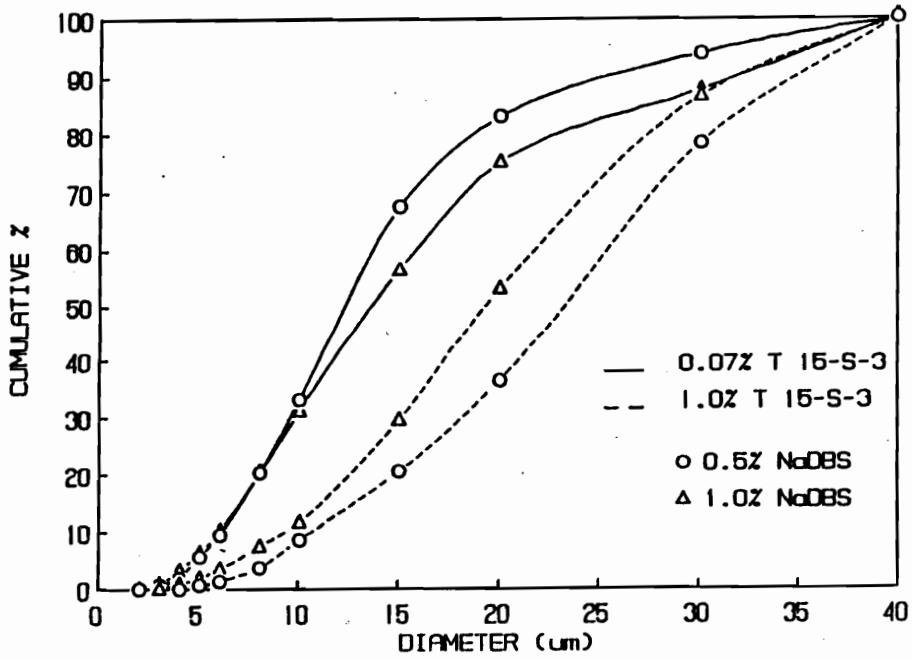

Figure 3-8a&b. Effect of the (a) aqueous phase surfactant type and (b) concentration on the size distribution of microspheres formed at 25°C with 0.07% and 1.0% Tergitol 15-S-3 in TMPPTA.

(a)

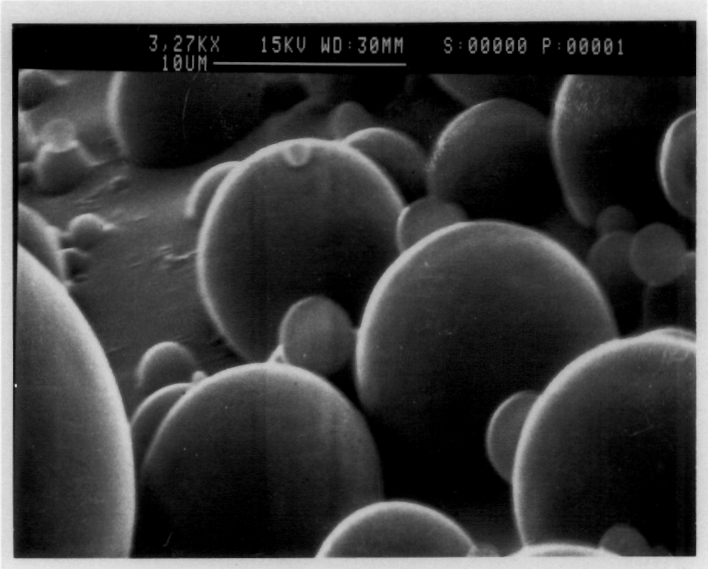

(b)

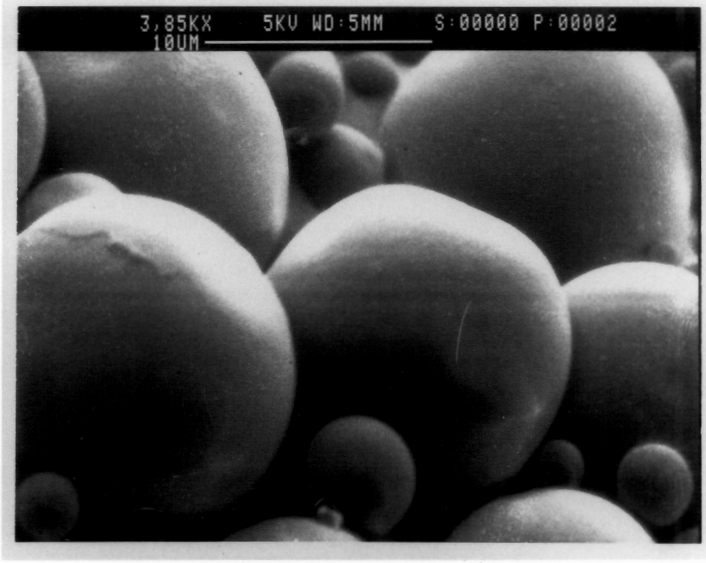

Figure 3-9a&b. SEM micrographs depicting the effect of the aqueous phase surfactant type on the shape of the resulting microspheres - (a) Dowfax 2A1, and (b) NaDBS.

dependence. Hence, we discount this latter explanation as the cause for the lack of particle sphericity.

As previously discussed, increasing the aphron preparation temperature produces a significant decrease in the monomer viscosity and surface tension, as well as a slight decrease in the surface tension of the aqueous solution. As illustrated in Figure 3-10, this temperature increase causes a decrease in the average particle size over the entire range of monomer phase surfactant concentrations studied. The reasons for this should be obvious. A reduction in the monomer surface tension will promote more spreading since the surface energy is lower. The same holds true for the aqueous phase, but to a much lesser extent. A reduction in the monomer viscosity obviously promotes better spreading, but this will also reduce the diffusion time of the surfactant molecules to the surface as spreading occurs. This may cause the monomer film to become stable for a longer period of time (allowing for more film thinning) as the surfactant molecules become depleted from the bulk and the diffusion paths (or diffusion times) become longer. It should be noted from Figure 3-10 that the reduction in particle size with increasing temperature appears to be dependent on the monomer phase surfactant concentration. The reasons for this are not entirely clear, but it may be related to the relative balance of spreading coefficients that exists in each system and the extent to which temperature may affect this condition.

Since the objective of this investigation has been to gain an understanding of the conditions which promote the production of small polymeric microspheres with a narrow size distribution, it is worthy to highlight the best and worst cases found in this respect. Figure 3-11 shows the SEM micrograph and particle size distribution for the smallest polymeric microspheres obtained in this study. The average particle size is approximately 7 microns with 90% of the particles between 3 and 18 microns. Although this is not an extremely narrow size distribution, it is a significant improvement over many of the samples obtained in this study and it does illustrate which conditions decrease the dispersity of the size distribution. These microspheres were produced using 0.4 vol % Tergitol 15-S-3 in TMPPTA and a 0.5 wt % NaDBS aqueous solution prepared at 75°C. Figure 3-12 depicts one of the worst cases. The microspheres in Figure 3-12 have an average particle size of 24 microns with 90% of the particles between 5 and 38 microns. These particles were formed at 25°C with 0.04 vol % Tergitol 15-S-3 in TMPPTA and the 0.5 vol % Dowfax 2A1 aqueous solution. In contrast, a similar "worst case" was obtained by forming microspheres at 25°C with 1.0 vol % Tergitol 15-S-3 in TMPPTA and a 0.5 wt % NaDBS aqueous solution. The average size of these microspheres was 23 microns with 90% of the particles between 7 and 40 microns. These best and worst cases illustrate some of the conditions that will promote (and hinder) the production of polymeric microspheres with a narrow size distribution. The best case illustrates that a higher preparation temperature facilitates a narrower distribution. The two worst cases

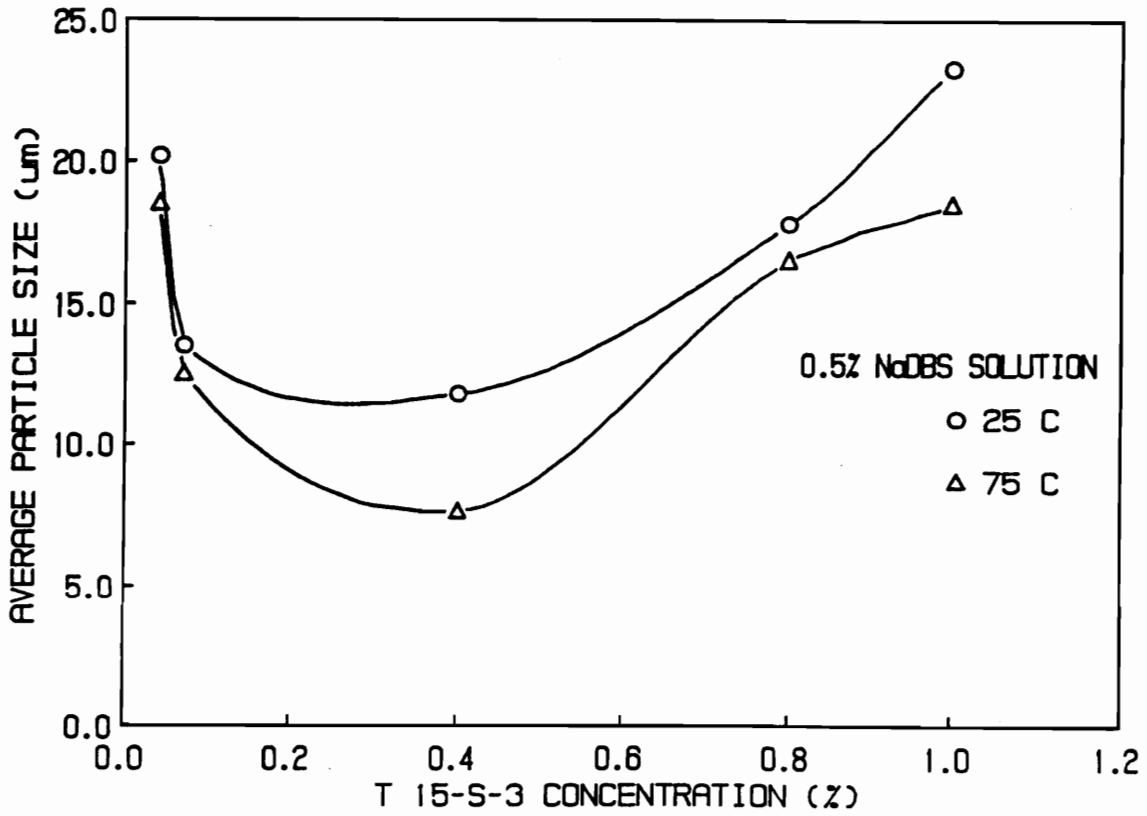

Figure 3-10. Effect of the aphron formation temperature on the average particle size of microspheres formed with varying amounts of Tergitol 15-S-3 in TMPPTA.

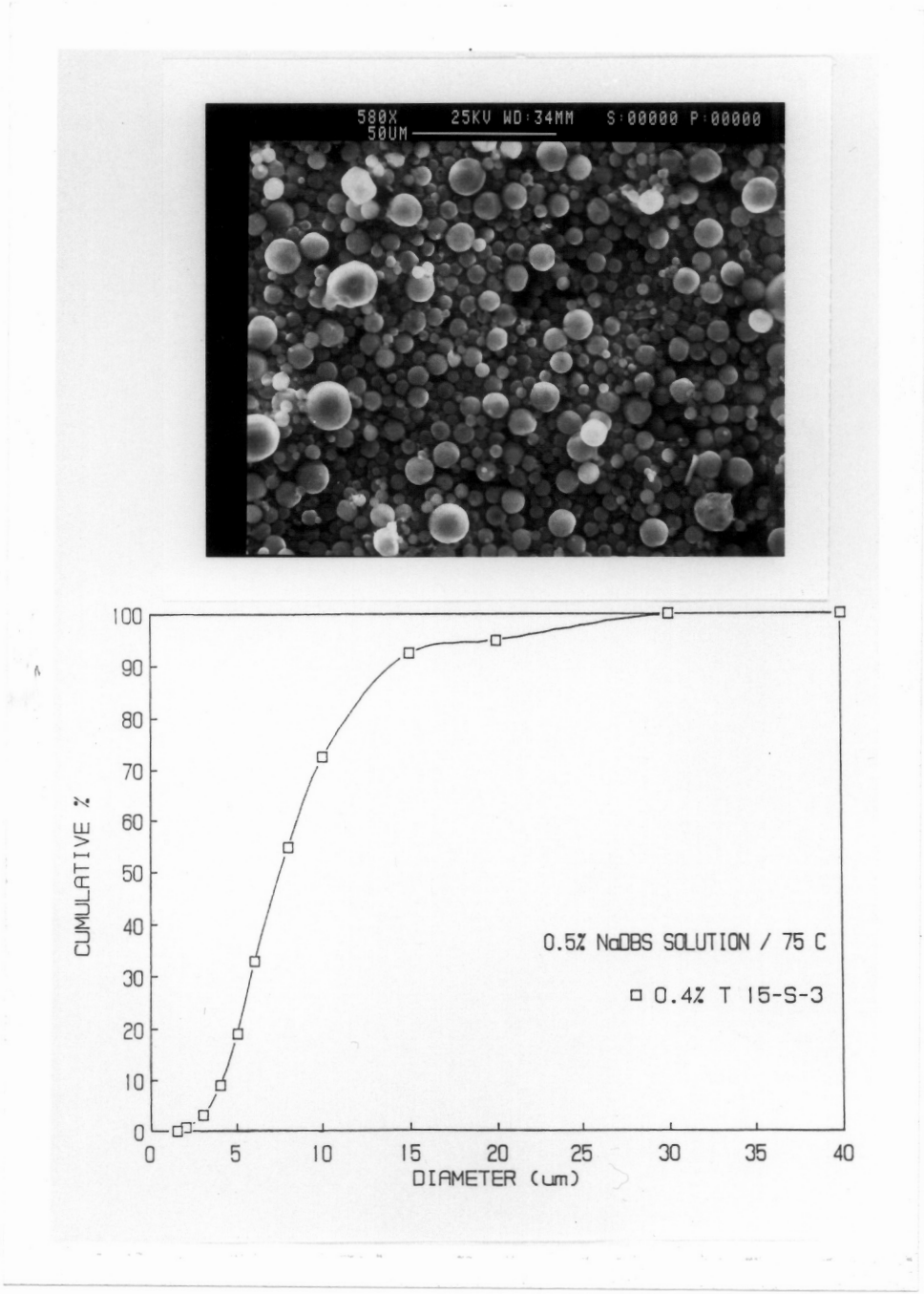

Figure 3-11. SEM micrograph and size distribution of microspheres obtained by irradiation of a polyaphron system formed at 75°C with 0.4% Tergitol 15-S-3 and 0.5% NaDBS (a "best case").

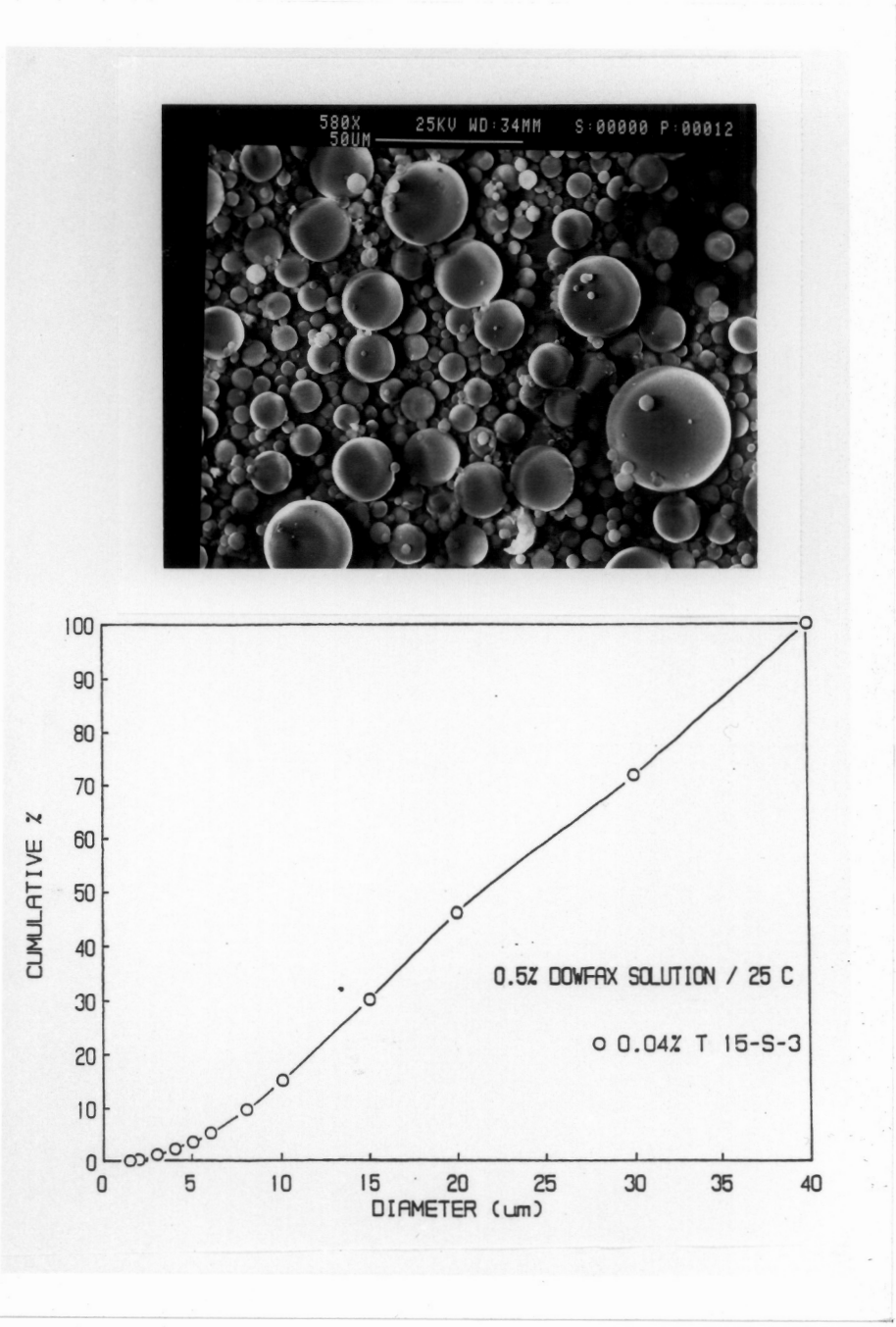

Figure 3-12. SEM micrograph and size distribution of microspheres obtained by irradiation of a polyaphron system formed at 25°C with 0.04% Tergitol 15-S-3 and 0.5% Dowfax 2A1 (a "worst case").

further support the need for a delicate balance between the surfactant concentrations in both phases; either too much or too little surfactant in the monomer phase can have a detrimental effect on the production of small microspheres with a narrow size distribution.

3.3.2 Surface Modification

The process scheme that has been discussed here has also been modified to produce microspheres with reduced wettability. The only change necessary is the substitution of FX-13 for Tergitol 15-S-3 in the monomer phase. Figure 3-13 shows the resulting product with 5.0 vol % FX-13 in TMPPTA with a 0.5 wt % NaDBS solution as the continuous phase that was prepared at 75°C. It was possible however, to produce microspheres with as little as 0.5 vol % FX-13 in the monomer phase. In order to analyze the relative wettability of these particles, a series of isopropanol - water solutions were prepared to determine the maximum liquid surface tension that would wet the particles (see experimental section for details). As illustrated in Figure 3-14, increasing the FX-13 concentration in TMPPTA results in a decrease in the surface energy of the microspheres as evidenced by the increasing isopropanol concentration necessary to wet the particles. The particles containing the Tergitol 15-S-3 surfactant sank into a solution of pure water; the particles produced with 5.0% FX-13 remained on a water surface for several days. A solution of 12 vol % isopropanol in water was needed for these particles to sink into the mixture and become wetted (see Figure 3-14).

As a supplement to the wettability study on the microspheres, thin films were prepared with concentrations of FX-13 ranging from 0 to 10 vol % in TMPPTA for contact angle measurements. Figure 3-15a&b shows the effect of FX-13 concentration on the advancing contact angle of distilled, deionized water on the TMPPTA film. Results for both the TMPPTA - air and TMPPTA - substrate (PET) interfacial surfaces (during curing) both before (Figure 3-15a) and after washing (Figure 3-15b) in acetone are given. The trend shows increasing contact angle with increasing FX-13 concentration, however, there are some differences between the two surfaces. First, the side of the film exposed to the atmosphere during curing has a higher contact angle than the side exposed to the PET substrate. This is in accord with the results obtained by Torstensson et al (6) who reported information regarding various thin films modified with fluorinated acrylate surfactants. Torstensson et al. proposed that this is due to the preferential adsorption of the surfactant towards the less polar phase (i.e. air) since this is more energetically favorable than adsorption toward the PET surface. Also note at a concentration of 0.5%, FX-13 has no effect on the contact angle at the PET - exposed surface. This also was reported by Torstensson et al., which indicates that at low concentrations, the hydrophobic moiety of FX-13 is even less compatible with the PET substrate than the bulk TMPPTA, thus preferentially desorbing at the PET - TMPPTA interface. Another interesting point is the effect of the acetone wash, which seems to cause an increase in the advancing contact angle, even when no FX-13 is present. This may suggest that the

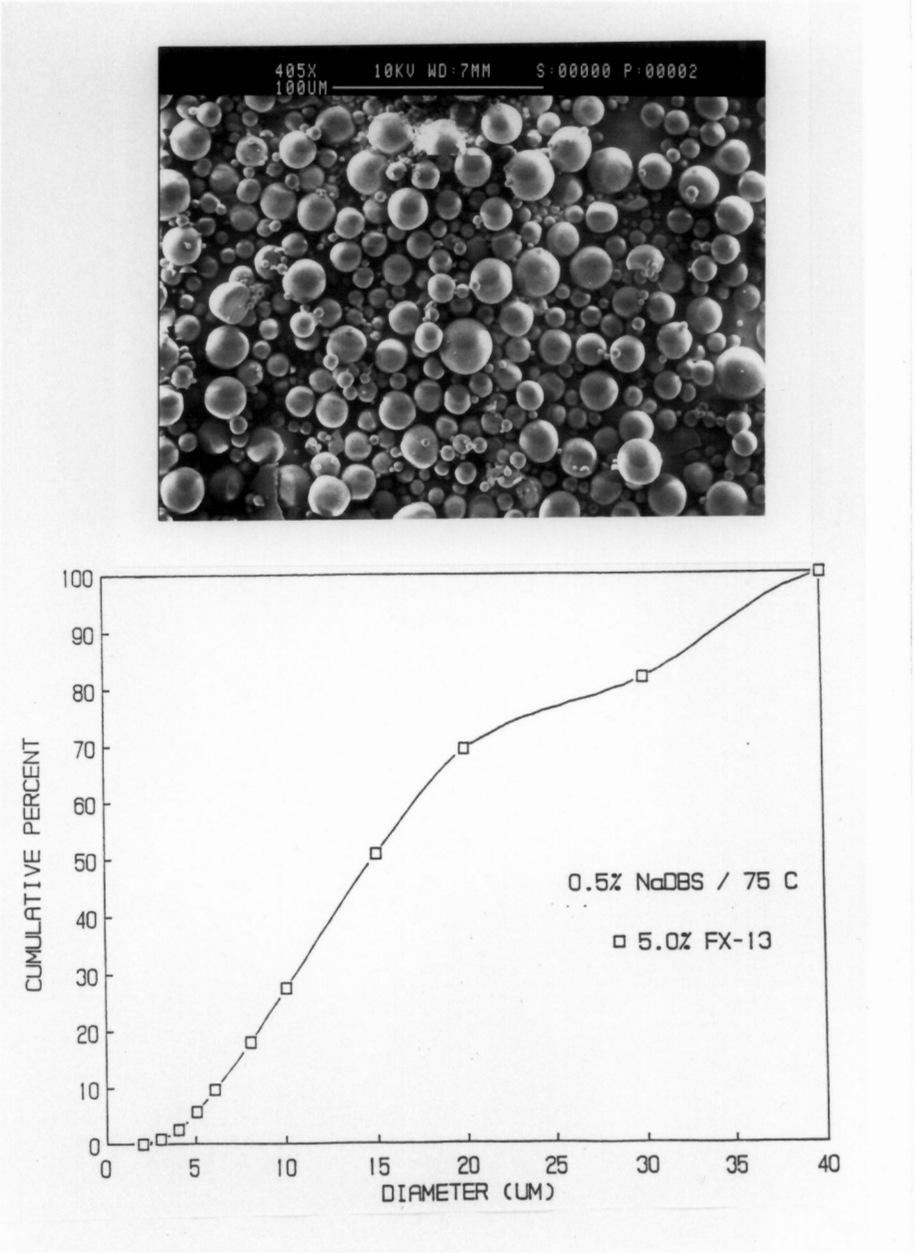

Figure 3-13. SEM micrograph and corresponding particle size distribution of microspheres formed by irradiation of a polyaphron system formed at 75°C with a 0.5% NaDBS solution and 5.0% FX-13 in TMPPTA.

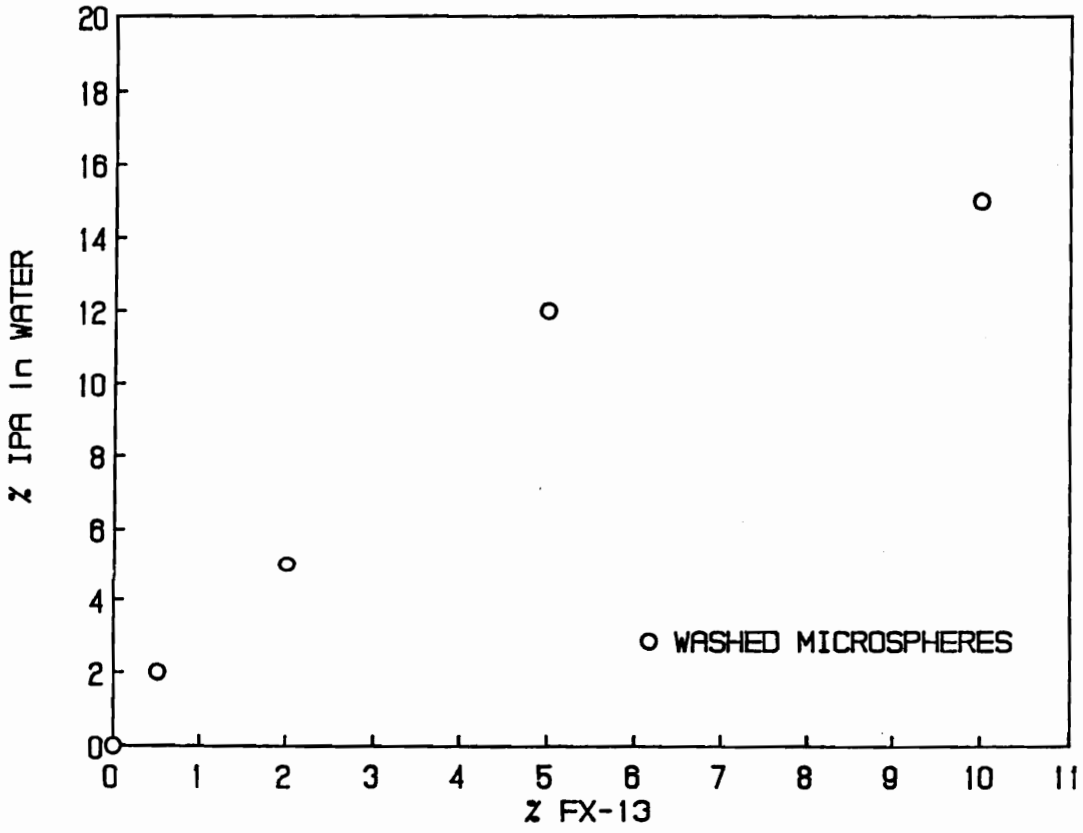

Figure 3-14. Effect of the FX-13 concentration in TMPPTA on the weight percent of isopropanol in water necessary to cause wetting of cured microspheres placed on the surface of the mixture.

(a)

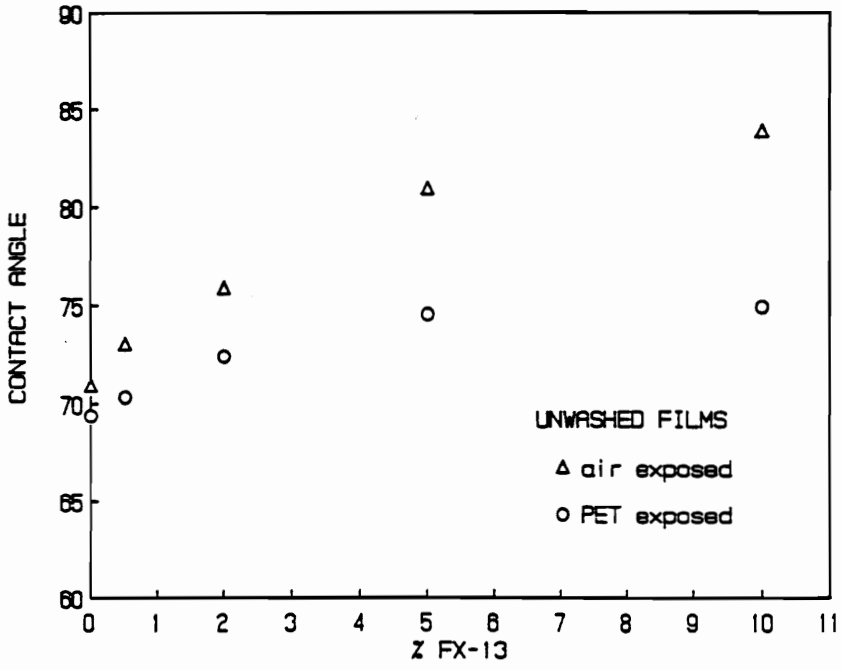

(b)

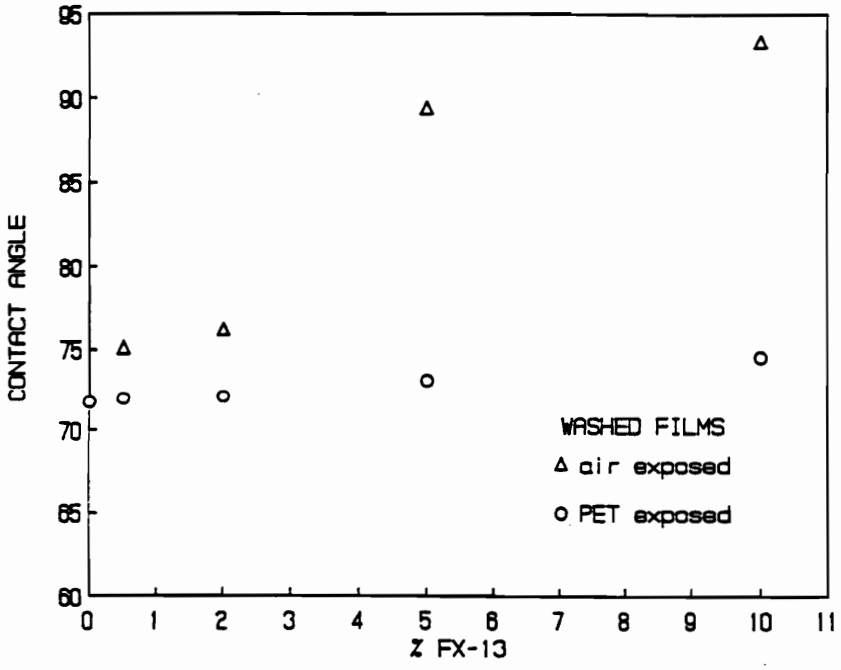

Figure 3-15a&b. Effect of FX-13 concentration on the advancing contact angle of distilled, deionized water on cured TMPPTA films (a) before and (b) after washing in acetone.

acetone wash causes a reduction in the surface energy of the film, thus increasing the contact angle.

3.3.3 Physical Properties

Several techniques were utilized to obtain information on the modulus, glass transition behavior, and extent of cure of the irradiated material: differential scanning calorimetry (DSC), dynamic mechanical analysis (DMA) and FT-IR spectroscopy. These analyses was done at least a week after curing to reduce the possibility of trapped free radicals reacting as the sample is heated, which can cause a broadening of the glass transition range (7,8). The results from DSC for both the films and particulates of TMPPTA cured at room temperature show similar behavior, although the glass transition appears to be slightly higher for the films (see Figure 3-16). This is to be expected since the microspheres were cured in the presence of water, which will absorb some of the electron beam energy and result in a lower effective dose for the microspheres as compared to the films. However, both scans show a wide glass transition range somewhat above room temperature. A glass transition beginning slightly above room temperature may indicate that vitrification occurred in this system during curing. As a network is formed by crosslinking reactions, in this case, principally through the polymerization of double bonds, the glass transition temperature of the material increases as a result of an increase in the crosslink density. If the glass transition temperature reaches the reaction temperature, the polymerizable units lose mobility and are unable to react due to this

restriction. If this occurs before the reaction has reached completion, a certain amount of sol fraction will be left in the network, which can be detrimental to the physical properties of the material. If the material formed is a rubbery network, this is of no concern since the glass transition temperature will not ever reach the reaction temperature. However, TMPPTA forms a glassy network, so there is a strong possibility that vitrification will occur. Although the material was cured at room temperature, heat effects from the electron beam radiation will heat the reaction medium, which accounts for a glass transition somewhat above room temperature. Gillham et al. (9,10) have described this phenomena in terms of a time - temperature - transformation (TTT) diagram which graphically illustrates the physical state of a reactive polymeric medium as a function of time and reaction temperature. More recently, Kim and Wilkes (11) extended this treatment for electron beam initiated systems in terms of a time - temperature - energy (TTE) diagram. The TTE diagram describes the physical state of a crosslinking network in terms of the reaction temperature, time, and the energy imparted to the system from the electron beam radiation. Graphical interpretation of these diagrams show that vitrification will indeed occur if the reaction temperature is below the glass transition temperature associated with the completely reacted system, as previously discussed.

The DMA results on the cured films show the onset of the glass transition at approximately 40°C (see Figure 3-17) which is in reasonable agreement with the DSC results. However, the DMA results indicate a broader transition, with a maximum

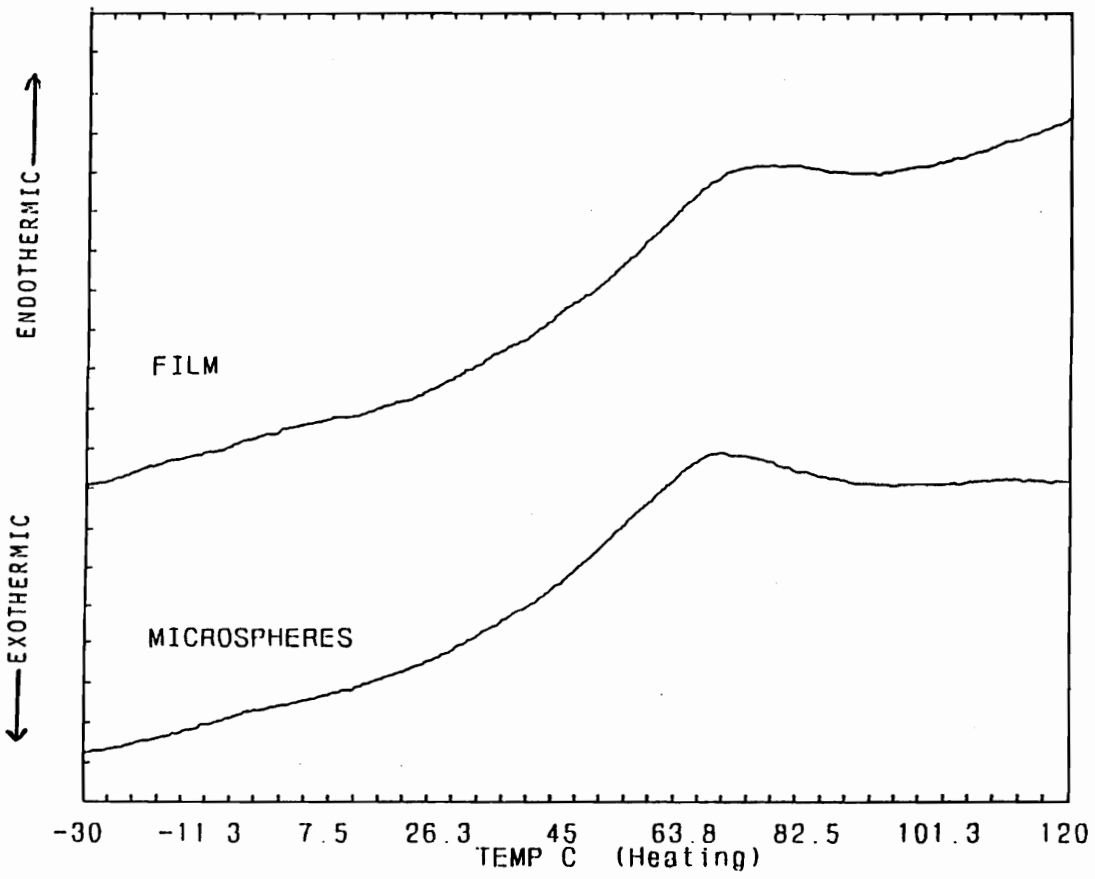

Figure 3-16. DSC scans of TMPPTA films and microspheres cured at room temperature. (DSC heating rate of 15°C/min).

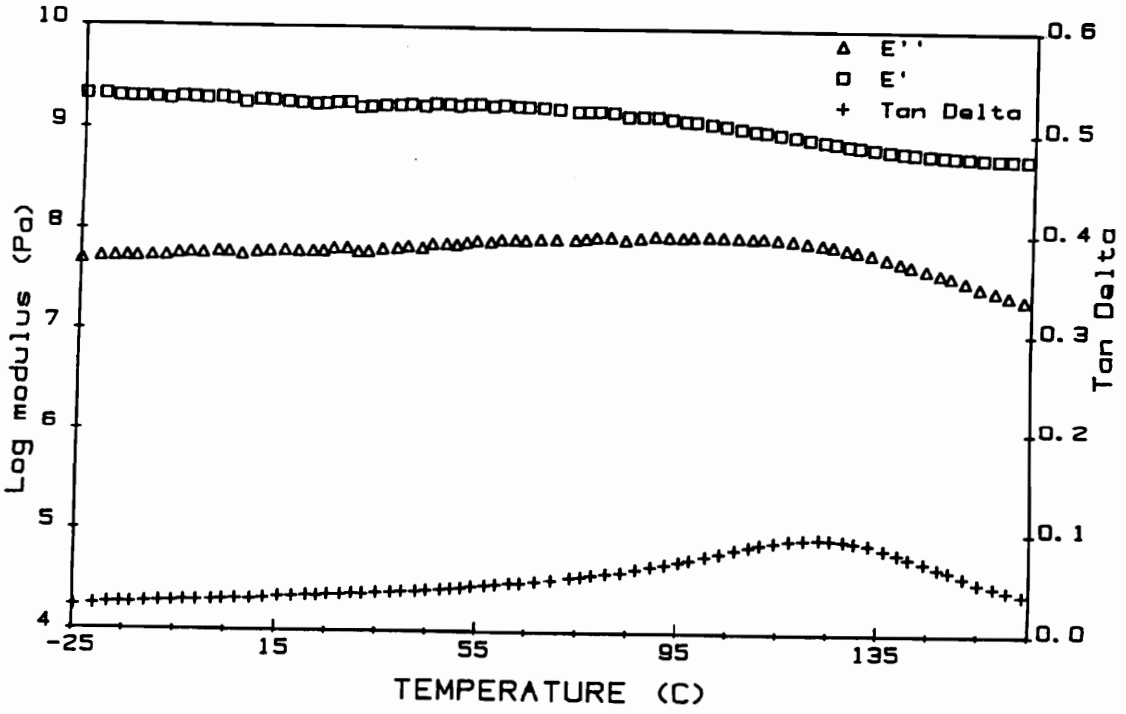

Figure 3-17. DMA of TMPPTA film (cured at room temperature) with a frequency of 11 Hz and a heating rate of 2°C/min.

(a)

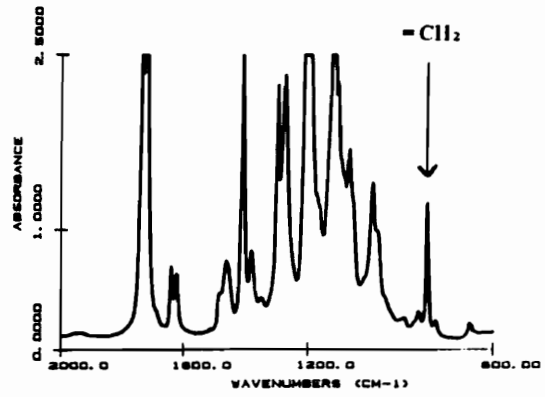

(b)

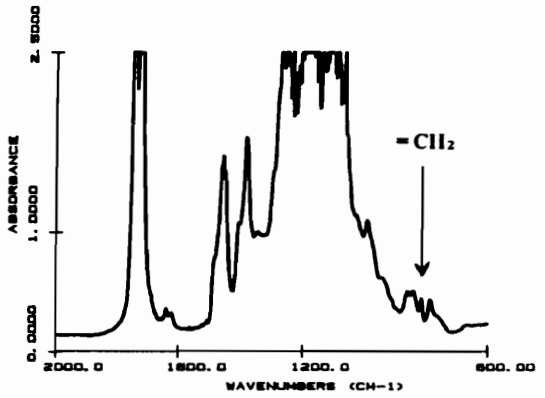

(c)

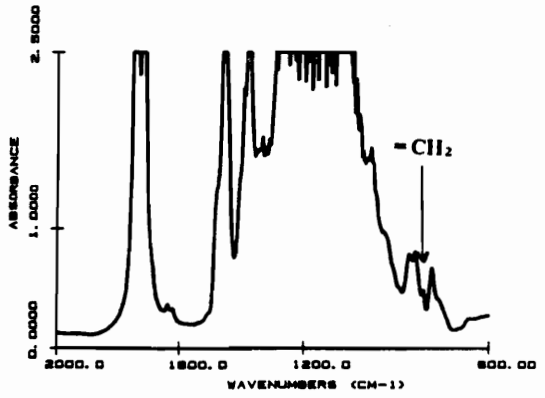

Figure 3-18a-c. FT-IR spectra of TMPPTA (a) monomer, (b) film cured at 25°C, and (c) film cured at 50°C with a 4 megarad dose.

in the tan δ peak at about 125°C. The modulus decreases slightly over this temperature range, from about 2.00 GPa to about 0.63 GPa, which is to be expected for a highly crosslinked material.

To confirm the possibility of vitrification occurring, FT-IR spectroscopy was used to determine the residual double bond content (see Figure 3-18). Comparison of the normalized double bonded methylene peak at 810 cm^{-1} (normalized against the peak at 3550 cm^{-1}, which remained unchanged during irradiation) between the monomer and the film irradiated at 25°C show a residual double bond content of approximately 15% (see Figure 3-18a&b). This gives further evidence that vitrification did indeed occur. To ensure that this was not simply the minimum attainable residual double bond content, FT-IR was carried out on a thin film irradiated at 50°C. (see Figure 3-18c). The residual double bond content for this sample was approximately 9%, indicating that vitrification did occur in the sample cured at room temperature. However, no sol percentage could be extracted from the irradiated material, so it is likely that the residual double bonds are only present as dangling ends in the crosslinked network.

3.4 CONCLUSIONS

This work has illustrated the successful incorporation of TMPPTA into a polyaphron system for the production of crosslinked polymeric microspheres using electron beam radiation. Spherical particulate formation is facilitated at a solids content as high as 67 vol %, with complete conversion and no agitation necessary. There are several parameters that affect the particle size distribution which include: preparation temperature, the relative concentrations of the monomer and aqueous phase surfactants, and the aqueous phase surfactant type. It is also possible to form polymeric particulates with reduced wettability by utilizing a polymerizable surfactant in the monomer phase. These microspheres are glassy materials at room temperature which contain a small amount of unreacted double bonds, due to vitrification occurring during the curing process. However, there is no soluble fraction that can be extracted from the irradiated material, indicating that conversion is nearly complete.

3.5 REFERENCES

1. Piirma, I. *Emulsion Polymerization*, Academic Press, New York, 1982.

2. Yoshida, M.; Asano, M.; Kactsu, J.; Morita, Y. *Radiation Physical Chemistry*, 1987, **30**, 39.

3. Rembaum, A.; Yen, R.C.K.; Kempner, D.H.; Ugelstad, J. *Journal of Immunological Methods,* 1982, **52**, 341.

4. Sebba, F. *"Foams and Biliquid Foams-Aphrons"* John Wiley and Sons, New York, 1987.

5. Sebba, F. *Chemistry and Industry*, 1984, **10**, 367.

6. Torstensson, M.; Ranby, B.; Hult, A. *Macromolecules*, 1990, **23**, 126.

7. Thompson, D.; Song, J.H.; Wilkes, G.L. *Journal of Applied Polymer Science*, 1987, **34**, 1063.

8. Kim, H.-C., PhD. Dissertation, Virginia Polytechnic Institute and State University, Department of Chemical Engineering, 1989.

9. Peng, X.; Gillham, J.K. *Journal of Applied Polymer Science*, 1985, **30**, 4685.

10. Chan, C.C.; Gillham, J.K. *Journal of Applied Polymer Science*, 1984, **29**, 3307.

11. Kim, H.C.; Wilkes, G.L. *Polymer Preprints*, 1989, **30**, 250.

CHAPTER IV

4.0 DSC ANALYSIS OF ELECTRON BEAM IRRADIATED LARC-CPI

4.1 INTRODUCTION

LARC-CPI is a relatively new aromatic polyimide that has been developed by the NASA Langley Research Center. Although the majority of polyimides currently in use are amorphous polymers, LARC-CPI displays a crystalline superstructure. In general, it is well recognized that the presence of crystallinity in any polymer typically offers enhanced resistance to solvents (as compared to the amorphous analog) as well as an enhanced modulus, especially above the glass transition temperature. Hence, the crystallizability of high T_g polyimides would suggest considerable potential for their use as a structural matrix resin or adhesive with desirable properties and reasonable processing requirements. In fact, Hergenrother et. al. (1) have indicated that LARC-CPI may have utility for applications in aerospace vehicles. This suggests that the response of LARC-CPI to ionizing radiation under an inert atmosphere is of practical interest. However, no previous work has been done to determine the effects of ionizing radiation on this relatively new LARC-CPI material, which is the subject of this chapter.

Radiation effects on polymers can be quantified by a number of techniques, since numerous changes in properties result from radiation exposure, usually due to changes in molecular weight. Some of these changes include modifications in mechanical properties (tensile strength, elongation, modulus), solubility, intrinsic

viscosity, infrared absorption spectra, crystallinity, and thermal properties. The amount of pertinent information obtained by monitoring these changes will be dependent on the particular characteristics of the polymer in question. For example, monitoring mechanical property changes in semi-crystalline polymers is somewhat limited since the effects of crosslinking and chain scission reactions may be masked due to the dominance of the crystalline phase on the mechanical properties. On the other hand, an amorphous elastomer lends itself more readily to this type of analysis since the mechanical properties would be very sensitive to changes in crosslink density and molecular weight.

Some limited irradiation studies of polyimides have been previously carried out by various investigators (2-4). However, most of these studies focused on the changes in mechanical properties. This is not surprising, since polyimides are typically amorphous polymers and as such, a thermal analysis, for example, may not be as productive. This present study, on the other hand, focuses on the thermal behavior and crystallinity changes of LARC-CPI induced by electron beam radiation. Changes in these properties have been monitored using differential scanning calorimetry (DSC) with some limited use of x-ray scattering. Due to the strong solvent resistance of LARC-CPI and the presence of crystallinity, analysis based on specific molecular changes was not employed.

Radiation effects on crystallinity and thermal properties have been presented in the literature for a variety of polymers. Kumar and Adams (5) have reported on

electron beam induced changes in unit cell dimensions for a number of high temperature semicrystalline polymers. Their results illustrated a strong correlation between the critical dose required for damage to unit cell dimensions and the melt temperature of the polymer. In addition, numerous studies utilizing differential scanning calorimetry have been made, particularly on polyethylene, polypropylene, and nylon (6-12). A variety of effects have been observed. Birkinshaw et. al. (9) showed that electron beam radiation causes a reduction in the α_1 melting peak of nylon 66, while the α_2 peak remains unaffected. Studies on polyethylene have shown that radiation does not reduce the level of crystallinity during exposure, but upon subsequent heating and cooling, a reduction in crystallinity was observed (10). This was attributed to the presence of crosslinks, which hindered the ability of the chains to recrystallize. However, Bhajeta et. al. have reported that the initial level of crystallinity present in polyethylene can increase as a result of irradiation, likely due to chain scission of tie molecules between crystalline lamella with subsequent reorganization of the crystalline phase (11). Other studies on polyethylene have shown a dependence of the extent of crosslinking on the amount of crystallinity present in the sample. It has been postulated that the superstructure may also affect the relative extent of crosslinking and chain scission (12). However, at least in the case of polyethylene, the influence of crystallinity on the extent of crosslinking is believed to be partially due to the increased concentration of unsaturated ends groups in the amorphous phase, which are excluded from the crystalline lamella (13).

This results in an increased crosslink density in the amorphous regions, due to the higher concentration of reactive end groups. Although these studies involve polymers that have very different structures than LARC-CPI, it does provide some basis for developing an understanding and discerning the radiation effects on LARC-CPI that will be presented here.

4.2 EXPERIMENTAL

4.2.1 Materials and Sample Preparation

The structure of the material studied in this work, LARC-CPI, is shown in Figure 4-1. It is a semi-crystalline polyimide developed by the NASA Langley Research Center. Synthesis of this polymer has been described previously by Hergenrother et. al. (1,14). This polymer was obtained in the form of thin, semicrystalline films with a thickness of ca. 3.5 mils. The films were prepared from a solution of precursor poly(amic acid) in N,N-dimethyl acetamide which was centrifuged and cast onto a glass plate. The precursor poly(amic acid) in a 0.5% solution of N,N-dimethyl acetamide at 25°C has a inherent viscosity of 0.69 dl/gr. This corresponds to a molecular weight of 15,000 to 20,000 gr/mol, based on measurements of similar materials with known molecular weight (1,14). The films were converted to the polyimide by heating in air step wise at 100°C, 200°C, and 300°C for 1 hour (1). These films were thermally treated several different ways prior to irradiation as follows: (1) as received, with no further treatment (denoted as CRY-LARC-CPI), (2) heated to 375°C (slightly above the melting point of ca. 365°C) and held for 10 minutes, followed by quenching in ice water (denoted as Q-LARC-CPI), and (3) heated to 375°C and held for 10 minutes, cooled to 300°C and held for 45 minutes, followed by quenching in ice water (denoted as RECRY-LARC-CPI). Heating was performed by suspending samples in a test tube, which were then placed in a thermal chamber at 375°C for 10 minutes. Quenching was performed by quickly

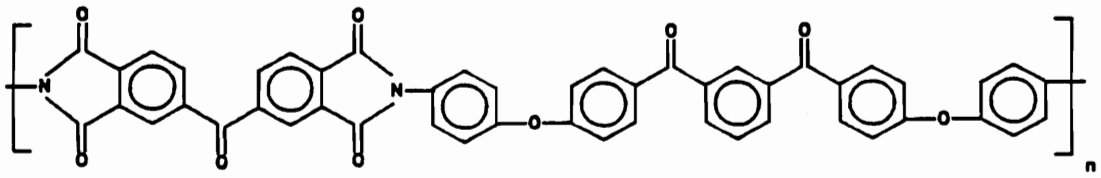

Figure 4-1. Molecular structure of LARC-CPI.

removing the test tube from the chamber and placing it in ice water. Some films were also fast quenched by removing the samples from the test tubes and placing them directly into ice water to eliminate heat transfer effects (denoted as FQ-LARC-CPI). This was done to determine the efficiency of the quenching procedure, and whether the amount of residual crystallinity could be altered by the quenching procedure used, but these samples were not irradiated. Preparation of the Q-LARC-CPI and RECRY-LARC-CPI samples was done to allow comparison between amorphous and semicrystalline samples with similar thermal histories. In summary, four different types of LARC-CPI samples were prepared, but only three were actually irradiated (CRY-LARC-CPI, Q-LARC-CPI, AND RECRY-LARC-CPI).

4.2.2 Radiation Exposure

Electron beam radiation exposure of the LARC-CPI samples was carried out using an Energy Sciences CB150 Electrocurtain operating with a 175 Kv accelerating voltage, a beam current of 4.7 milliamps, and a conveyor speed of 20 ft/min (see Appendix for complete description of this equipment). Irradiation was performed under a nitrogen atmosphere which had an oxygen content of 250-300 ppm. Under these conditions, 15 megarad dosages were deposited in a sample in a single pass. In addition, the film thickness (ca. 3.5 mils) is thin enough to ensure a reasonably uniform depth-dose profile. Samples were exposed to doses of 50, 100, 500 and 1000 megarads by making multiple passes until the desired dose level was achieved. It should be noted here that although the radiation exposure was done under a purged

nitrogen atmosphere, the samples were exposed to air between each pass. Furthermore, several samples were irradiated under air to determine if the presence of oxygen during irradiation has any effect on the subsequent melting and recrystallization behavior for the processing condition employed in this study. Results illustrated that the DSC behavior was not affected, likely due to the high dose rate employed which will minimize any oxidative degradation. Hence, the effects of oxygen during processing were not pursued, and will not be considered hereafter.

4.2.3 Thermal Analysis

Differential scanning calorimetry was performed using a Seiko I differential scanning calorimeter. The samples were sealed in aluminum pans and scans were made from 80°C to 390°C at a rate of 10°C/min under a nitrogen purge. After the first scan was completed, the samples were quickly removed from the chamber and quenched to room temperature. A second scan was then made under the same conditions as the initial scan. This procedure is necessary to evaluate the melting and recrystallization behavior of LARC-CPI regardless of the initial morphological state of the samples.

4.2.4 X-ray Scattering

Both small angle x-ray scattering (SAXS) and wide angle x-ray scattering (WAXS) were carried out on the as-received films (CRY-LARC-CPI) irradiated to low and high doses (50 and 1000 megarads). SAXS was performed using a Siemens Kratky

camera equipped with a M. Braun position sensitive detector from Innovative Technology Inc. to determine the angular intensity dependence. A Philips PW 1729 table top x-ray generator was used operating at 40 Kv and 20 Ma. The radiation source was CuK_{∞}, with a wavelength of 1.54 Å. Lead stearate was used to calibrate the SAXS angular measurements. Lupolen® polyethylene was used for absolute intensity measurements. The sample to detector distance was 30.5 cm. Data was slit-smeared; a computer program developed by Vonk (19) was used to desmear the data.

WAXS was performed using a Siemens model I1 transmission x-ray diffractometer operating at 40 kV and 30 mA. CuK_{∞} was used as the radiation source, with graphite as the monochromator. The goniometer was calibrated with a silicon standard having a characteristic peak maxima at 3.14 Å, 1.926 Å, and 1.64 Å. Constant time measurements of 20 to 60 seconds (depending on sample thickness) were made at 2θ intervals of 0.1°. Samples were scanned through an angular range of 10° - 35°. Thin films were stacked and mounted in a flat film holder which was rotated at a constant rate during scanning to eliminate any possible orientation effects resulting from the casting process.

4.3 RESULTS AND DISCUSSION

4.3.1 DSC Behavior of Quenched LARC-CPI

Figure 4-2 depicts the initial and second DSC scans for the quenched LARC-CPI material (Q-LARC-CPI) prior to any radiation exposure. Inspection of the DSC scan for the non-irradiated material shows the following behavior. Upon heating, the material goes through the glass transition at ca. 220°C. Above the glass transition, the molecular chains gain sufficient mobility such that crystallization takes place, which is apparent by the presence of an exothermic crystallization peak at 306°C. Following crystallization, the melting of the crystals occurs at about 369°C, as characterized by the endothermic peak. Note that there is a 2.6 mJ/mg difference between the integrated area under the melting and crystallizing peaks. This indicates that there may be a small amount of initial crystallinity in the quenched samples. To determine if this is a result of the quenching procedure, a more efficient quench was performed on the material (see experimental sections for details). Figure 4-3 depicts the initial DSC scan for this sample, which shows a difference of 3.3 mJ/mg between the integrated areas under the melting and crystallization peaks. This suggests that the quenching procedure utilized in this study is as efficient as possible. However, there may still be a small amount of crystallinity or partial order present in the quenched samples. This may be due to the relatively short time period that the polymer is held above the melt temperature (i.e. 10 minutes), which may be insufficient to completely disorder the crystalline phase. Longer melting times were

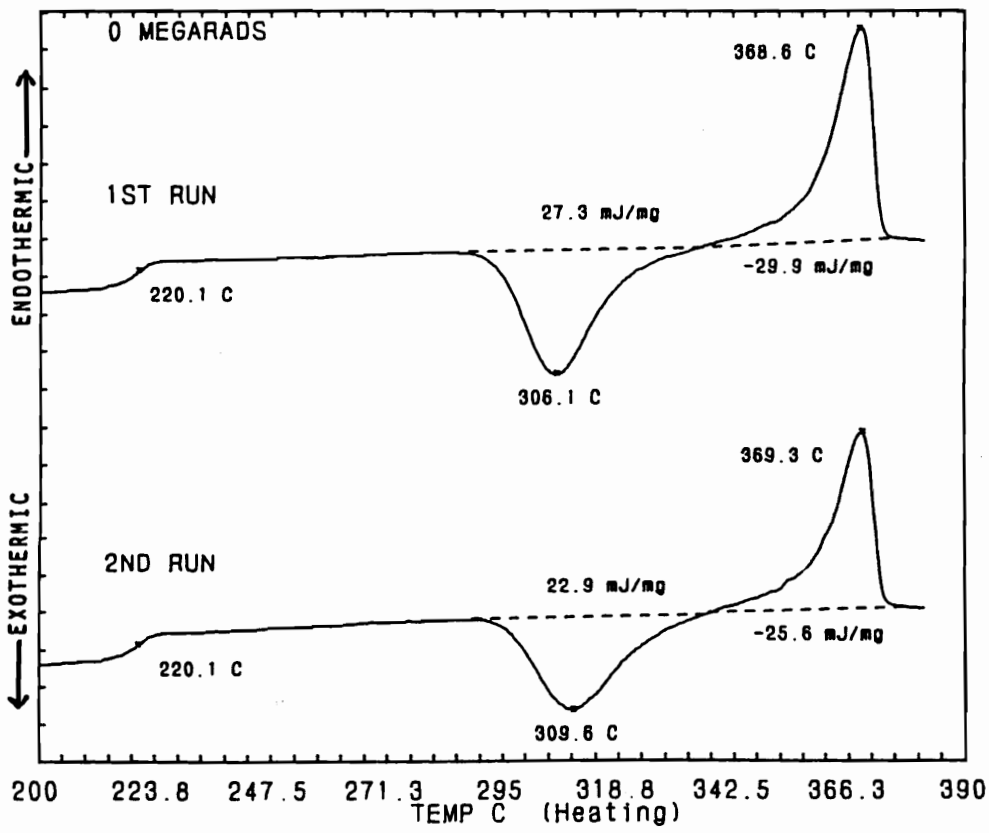

Figure 4-2. First and second run DSC scans for Q-LARC-CPI prior to irradiation.

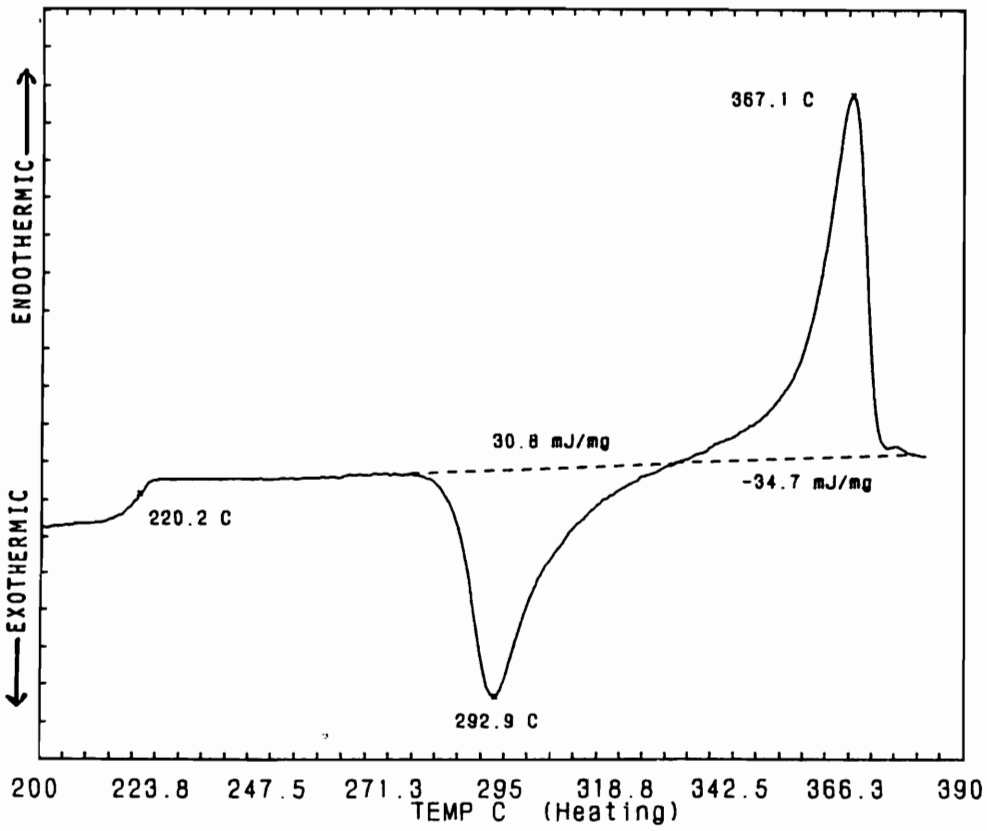

Figure 4-3. First run DSC scan for the FQ-LARC-CPI.

not employed due to the possibility of thermal degradation occurring. In any case, the possibility that a small amount of crystallinity is present in the Q-LARC-CPI samples may explain some interesting behavior that will be subsequently discussed.

Comparison of the initial and second DSC scans of Q-LARC-CPI unveils differences in the crystallization behavior upon successive heating cycles (see Figure 4-2). In particular, the amount of crystallization occurring during heating decreases by ca. 4.4 mJ/mg. This also produces a decrease in the size of the melting peak of the same magnitude, although the difference between the melting and crystallization peaks in the second scan remains relatively unchanged. In addition, the crystallization peak is about 4°C higher in the second scan compared to the first scan. Since the DSC behavior is the criteria used for evaluating the radiation response of LARC-CPI, it is important to realize how this behavior is affected by thermal cycling; otherwise, the influence of thermal history may be confused with the changes induced by irradiation which would result in an incorrect analysis.

Figure 4-4 and Figure 4-5 illustrate the first and second run DSC thermal behavior (respectively) of the Q-LARC-CPI samples irradiated with doses of 50, 100, 500, and 1000 megarads. Comparison of these DSC scans with the unirradiated material shows no observable radiation effects on the initial scan up to a dose of 100 megarads. It should be realized that this is a considerable dose, especially when compared to a dose of 2.5 megarads, which is typically used for radiation sterilization. Inspection of the second run DSC scan on these materials shows a slight decrease

(about 2.7 mJ/mg) in the extent of crystallization for the sample exposed to 100 megarads, as compared to the second scan of the unirradiated sample, and hence is not very significant. However, above 100 megarads, the effects of electron beam radiation exposure on the thermal behavior become evident in both runs of the DSC analysis.

Inspection of Figure 4-4 and Figure 4-5 reveals the effect of radiation dose on the total heat evolved during crystallization upon heating. As the dosage is increased to 500 and 1000 megarads, there is a steady decrease in the amount of crystallization occurring during thermal cycling. The difference in the amount of crystallization between the first and second runs for each dose remains relatively constant (about 5 mJ/mg), hence this is not likely to be a result of the radiation exposure. However, the total amount of crystallization occurring does decrease with increasing dose, indicating that radiation exposure is hindering the crystallization process. This claim is further supported by the behavior of the peak crystallization temperature, T_c, with respect to the radiation dose. As illustrated in Figure 4-6, the peak crystallization temperature significantly increases at dosages above 100 megarads. This indicates that either more thermal energy is required to initiate crystallization or the crystallization kinetics is slowed as a result of irradiation. Both of these possibilities suggest that the crystallization process is being suppressed to a certain extent and kinetically decreased. The crystallization peak temperature increases further during the second run DSC scan, but this increase is fairly constant regardless of dose,

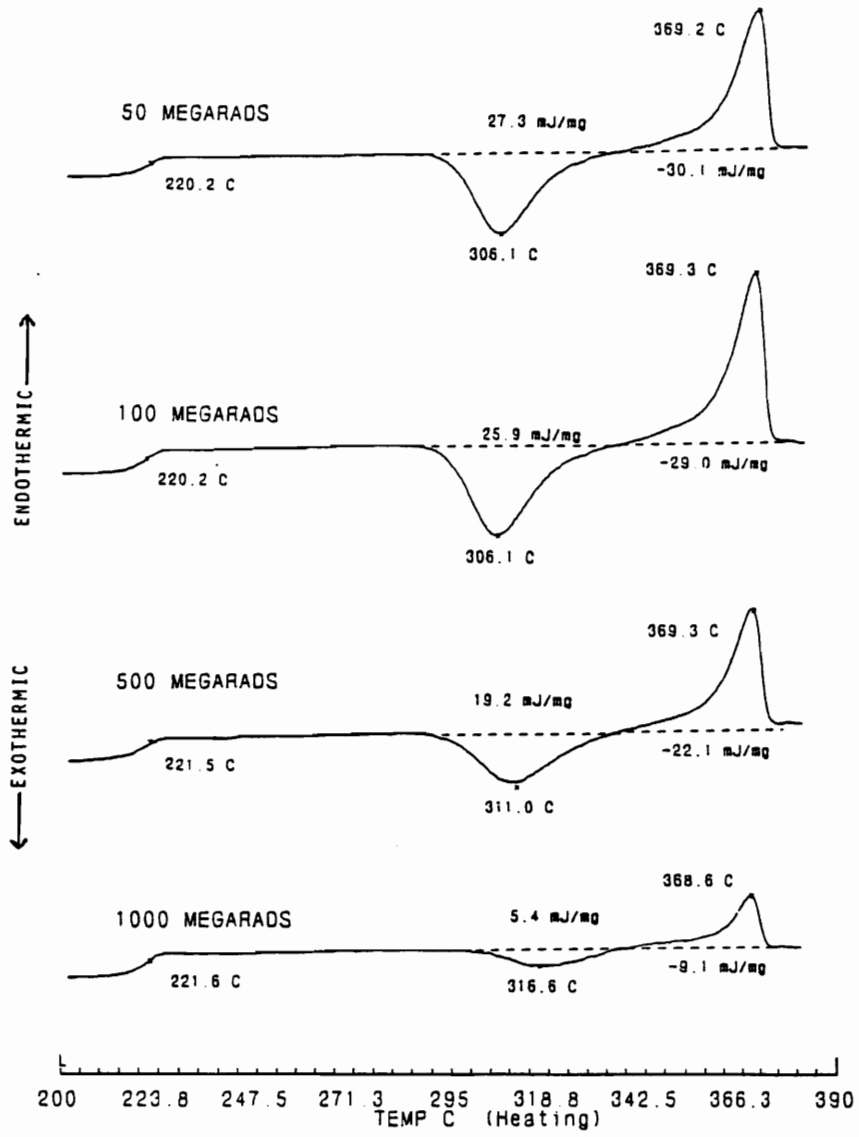

Figure 4-4. First run DSC scans for the Q-LARC-CPI irradiated with doses of 50, 100, 500, and 1000 megarads.

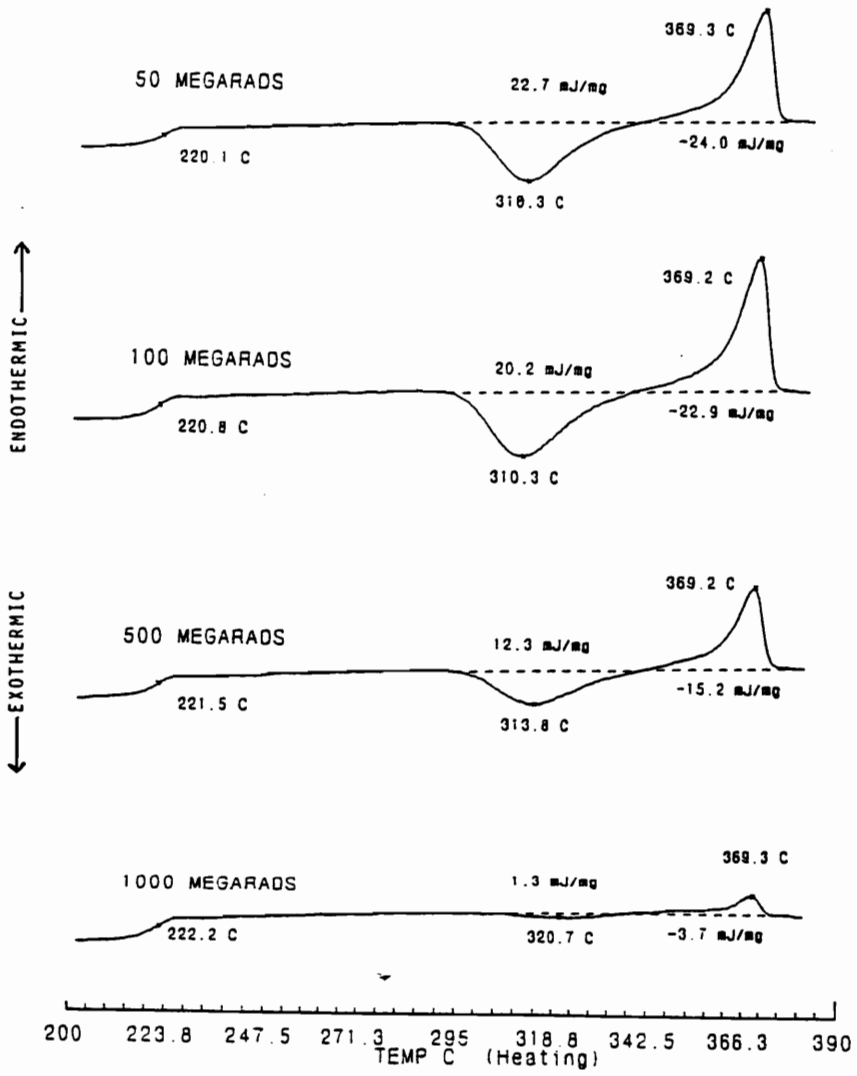

Figure 4-5. Second run DSC scan for Q-LARC-CPI irradiated with doses of 50, 100, 500, and 1000 megarads.

indicating that this is not a result of electron beam exposure. These observations of decreasing heat of crystallization and increasing crystallization temperature with increasing dose is likely the result of crosslinking processes which would restrict chain mobility. However, this is a speculation since neither a swelling nor extraction analysis is feasible on this polyimide since it is insoluble in virtually all solvents.

The melting behavior of Q-LARC-CPI appears to be influenced only by the corresponding crystallization behavior with no direct effect from the electron beam (see Figure 4-4 and Figure 4-5). The total heat absorbed during the melting process does decrease with increasing radiation exposure, but this is simply due to the lower extent of crystallization occurring during heating. In addition, the melting temperature remains unaffected by the radiation dose or the heating cycle (i.e. the initial or second run DSC scan). This suggests that only the extent of crystallization is affected by irradiation, while the crystalline phase that develops upon subsequent heating remains unaltered.

An interesting point to note is that the small difference between the heat of crystallization and the heat of melting during the initial run DSC scan (as previously discussed) remains relatively unchanged with respect to radiation dose (see Figure 4-4 and Figure 4-5). This suggests that there is indeed a small amount of crystallinity present during radiation exposure, and it does not seem to be affected by irradiation. In fact, for the 1000 megarad exposed sample, the difference between the heat of crystallization and the heat of melting (3.5 mJ/mg) corresponds exactly

to the total amount of melting occurring during the second run DSC scan. This suggests that only the chain segments that were originally present in the crystal lattice are able to recrystallize after exposure to 1000 megarads of electron beam radiation and one DSC heating cycle. Hence, the entire initial amorphous phase may have been sufficiently chemically altered such that crystallization is no longer possible, while the initial crystalline phase remains relatively unchanged. This is likely the result of crosslinking reactions selectively occurring in the amorphous phase, which would restrict the mobility of the polymer chains and explain this observed behavior. Crosslinking would also explain why recrystallization of the small fraction of initial crystalline phase occurs. The presence of crosslinks in the surrounding amorphous regions would restrict the mobility of the lattice chains and therefore be able to undergo reordering quite readily. However, this would not necessarily hold true at higher levels of crystallinity since there may not be sufficient crosslinks in close proximity to all the lattice chains to restrict mobility and promote reordering. This point should be kept in mind during the subsequent discussion of the irradiation effects on the semicrystalline "as received" LARC-CPI.

One other effect that can be observed from Figure 4-4 and Figure 4-5 is the effect of radiation on the glass transition temperature of the LARC-CPI. As shown in Figure 4-7, the glass transition temperature begins to increase very slightly at doses above 100 megarads. At a dose of 1000 megarads, there is a 2°C increase in the glass transition temperature. Although the glass transition temperature is generally

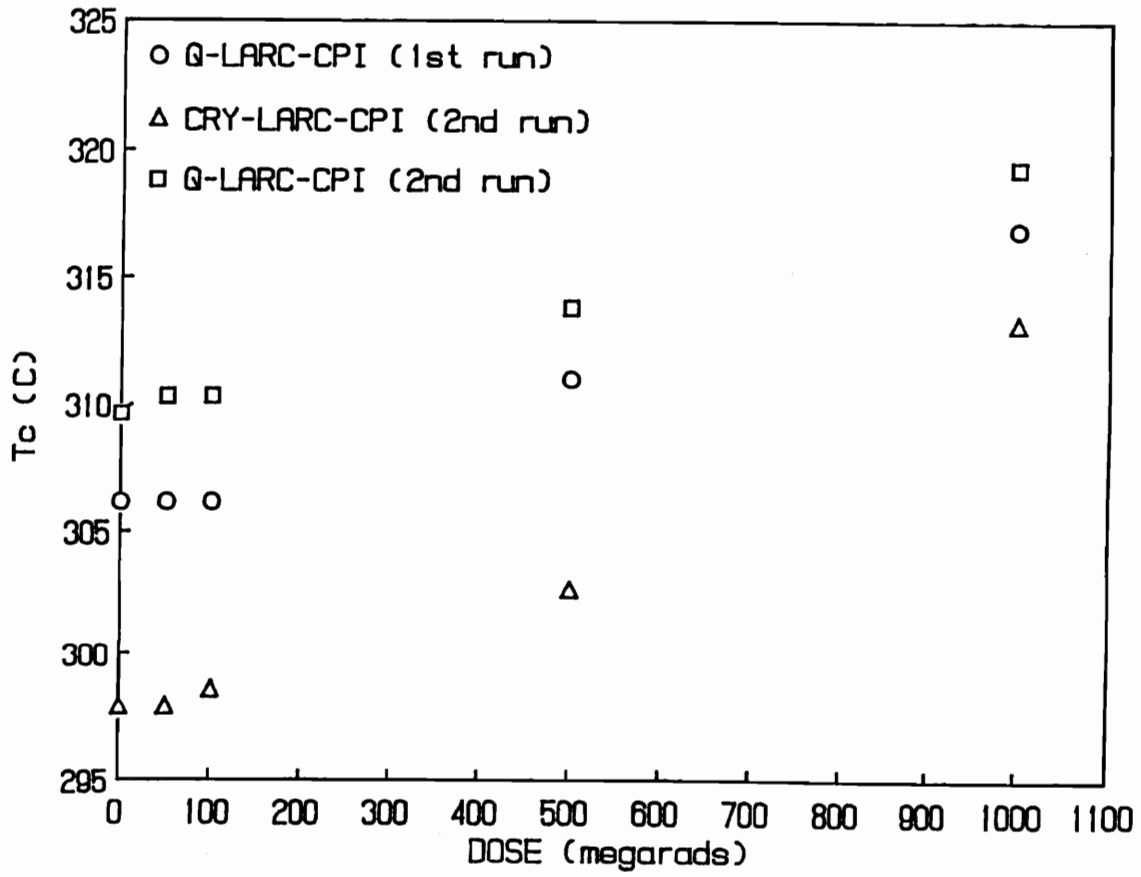

Figure 4-6. Effect of irradiation dose on the crystallization temperature (T_c) of Q-LARC-CPI and CRY-LARC-CPI as determined by the second run DSC scan.

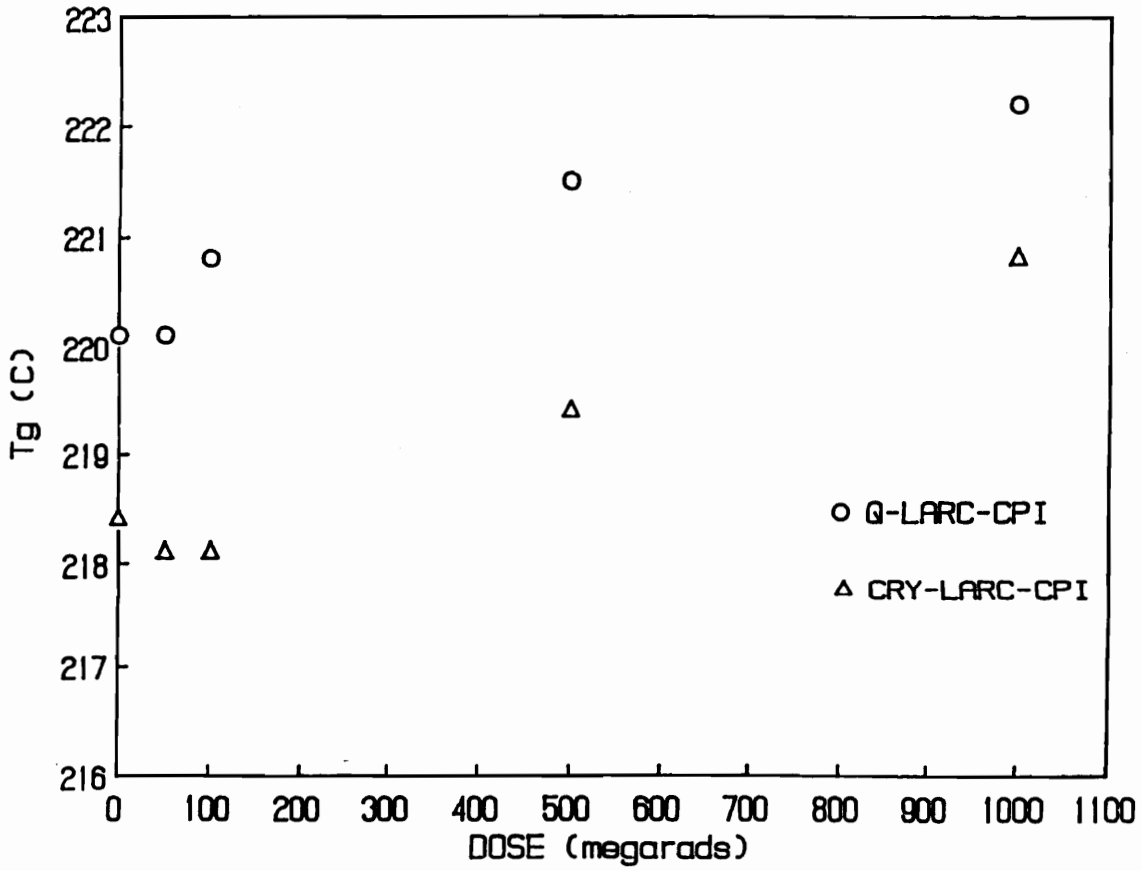

Figure 4-7. Effect of radiation dose on the glass transition temperature (T_g) of Q-LARC-CPI and CRY-LARC-CPI as determined by the second run DSC scan.

insensitive to changes in molecular weight of high molecular weight polymers, the initial molecular weight of the LARC-CPI is low enough such that molecular weight changes may well influence the glass transition. Although no quantitative analysis has been made to determine the absolute molecular weight of this polymer, it is believed that the molecular weight is in the range of 15,000 to 20,000 gm/mole. This molecular weight range is based on viscosity measurements of the soluble poly(amic acid) precursor made by NASA, which were compared with viscosity measurements of similar materials of known molecular weight (1,14). This slight (but reproducible) increase in the glass transition at high doses suggests that the molecular weight is increasing, likely due to crosslinking reactions. This would certainly explain the changes occurring in the thermal behavior of the LARC-CPI. As discussed, the extent of crystallization taking place during heating decreases with increasing dose while the crystallization temperature increases. Both of these observations could be attributed to a decrease in chain mobility as a result of branching or crosslinking, with a corresponding increase in molecular weight.

4.3.2 DSC Behavior of Semicrystalline LARC-CPI

Irradiation of the "as received" semicrystalline LARC-CPI material (CRY-LARC-CPI) was performed to determine if the presence of a crystalline phase affects the radiation response of this polymer. To this point, discussion has predominately focused on amorphous LARC-CPI (Q-LARC-CPI) that may have had a very small amount of crystallinity present (as previously described). In contrast, CRY-

LARC-CPI has a crystalline content of ca. 30%, as reported by Hergenrother and Havens (14). Figure 4-8 shows the initial run DSC scan of CRY-LARC-CPI at the various dosages indicated. Notice that the heat of fusion during this initial run remains relatively unaffected by the dose level. This further supports the claim made that there is no direct major alteration of the crystalline phase present during the radiation exposure. However, as illustrated in Figure 4-9, the ability of the polymer chains to recrystallize after melting is strongly affected by the dose level. Figure 4.7b shows the second run DSC scans for the CRY-LARC-CPI samples. Up to 100 megarads, there is no significant change in the extent of crystallization during heating. In fact, at a 500 megarad dose, the heat of crystallization decreases by only about 4 mJ/mg. However, the heat of crystallization becomes significantly reduced at a dose of 1000 megarads. At this dose, the heat of crystallization decreases from about 33 mJ/mg (0 megarads) to about 19 mJ/mg (1000 megarads). However, this is a significantly higher extent of crystallization than was present in the predominately amorphous sample (Q-LARC-CPI) irradiated with a 1000 megarad dose, as previously discussed (see Figure 4-4 and Figure 4-5). It should be realized, however, that this difference is partly due to the additional thermal cycle that the amorphous samples were subject to prior to irradiation. The effect of this additional thermal cycle can be qualitatively eliminated by comparing the relative decreases in extent of crystallization occurring in both the Q-LARC-CPI and CRY-LARC-CPI samples. For the initial DSC scan of the Q-LARC-CPI sample, a 1000 megarad dose results

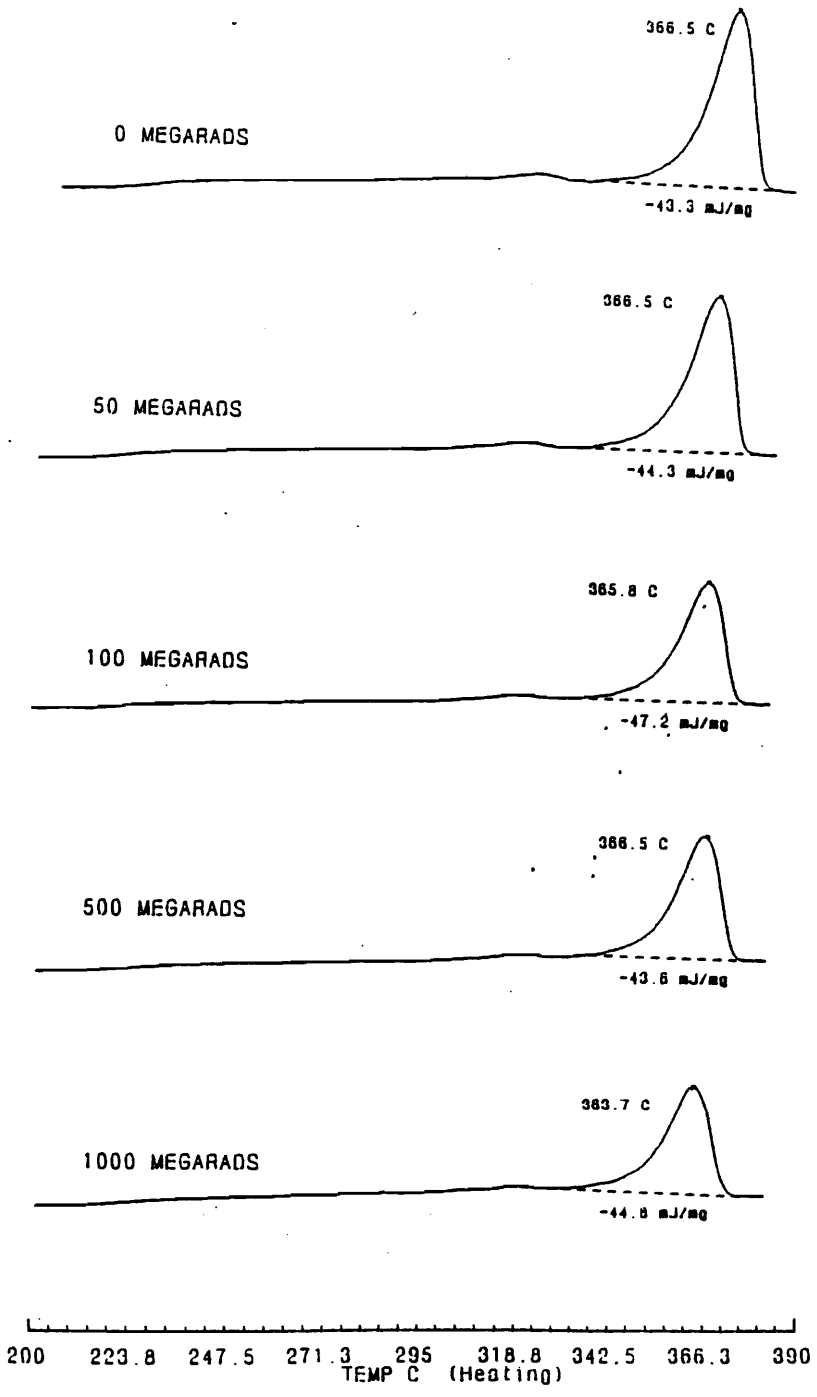

Figure 4-8. First run DSC scans for the CRY-LARC-CPI irradiated with doses of 0, 50, 100, 500, and 1000 megarads.

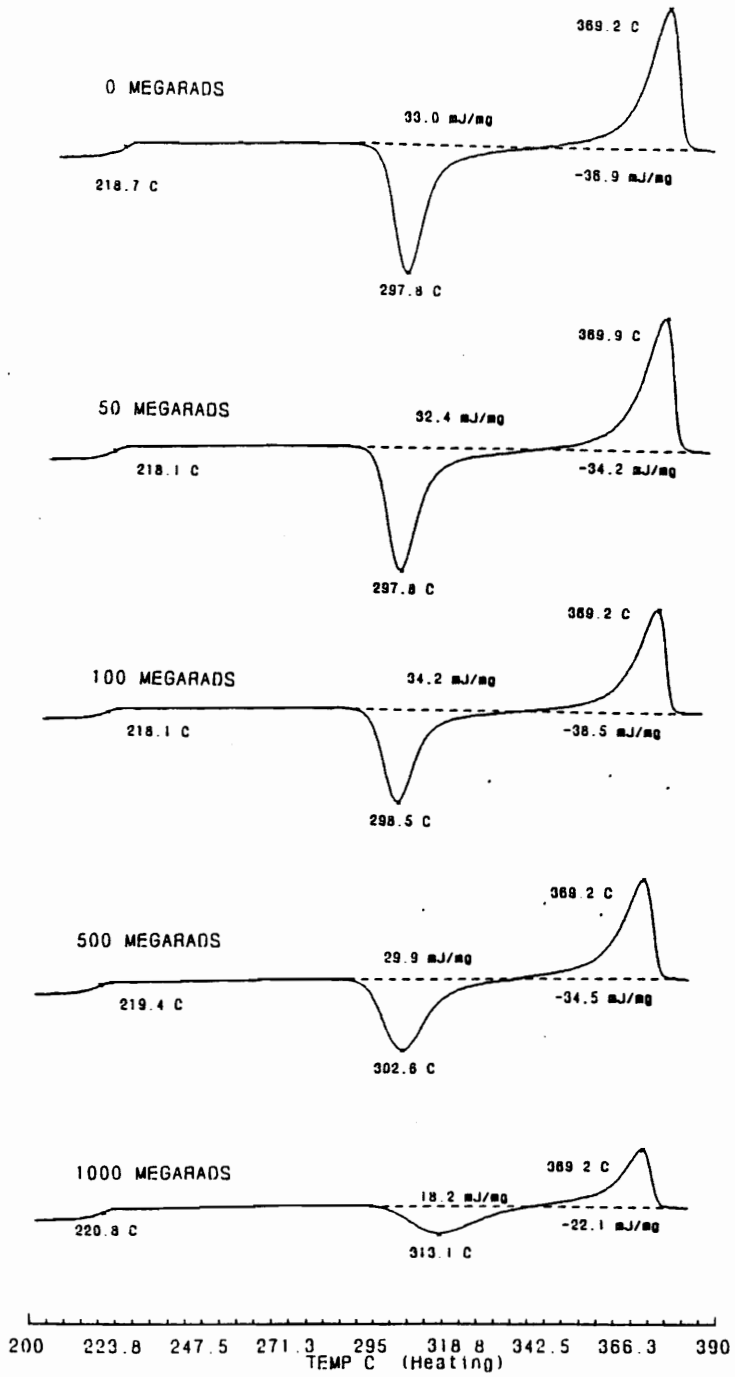

Figure 4-9. Second run DSC scans for the CRY-LARC-CPI irradiated with doses of 0, 50, 100, 500, and 1000 megarads.

in a 70% decrease in the heat absorbed upon melting, while a 43% decrease occurs in the CRY-LARC-CPI sample. This strongly indicates that some radiation protection is afforded to this material by increasing the crystallinity content. This is believed to be due to the increased probability of free radical recombination in the crystal lattice relative to the amorphous regions. The crystal lattice imposes a certain degree of order and reduced mobility to the molecular chains, which can promote the recombination of a free radical pair produced by the electron beam. In the amorphous phase there is more free volume and no order, and hence a free radical pair may be more prone to "lose each other" and react with other chains promoting crosslinking reactions instead of recombining (15,16).

Although it is likely that the presence of crystallinity in LARC-CPI provides some radiation protection, this is difficult to precisely quantify due to the effects of the additional thermal cycle imposed on the amorphous samples, as previously mentioned. Recall that Figure 4-6 and Figure 4-7 illustrated that the crystallization temperature and glass transition temperature (respectively) are dependent on the thermal history of the sample. This is evidenced by the values obtained for these characteristic temperatures on the unirradiated amorphous and semicrystalline samples. Figure 4-6 and Figure 4-7 also showed that the crystallization and glass transition temperatures are slightly higher for the irradiated amorphous material than the irradiated crystalline material, which suggests that more chain restriction is present in the amorphous samples. However, the values for these parameters are

also higher for the unirradiated samples. Hence these differences may be the result of thermal treatment rather than morphological influences on the radiation response of this polymer. In order to resolve this uncertainty, a third LARC-CPI sample was prepared (RECRY-LARC-CPI). This sample was treated identically as the amorphous samples, except that it was allowed to recrystallize during cooling rather than quenched directly to the amorphous state (see experimental section). This should eliminate some of the differences imposed by the different thermal histories of the amorphous and crystalline materials (discussed to this point) as well as some of the ambiguity in the above comparison. Figure 4-10 shows the first and second run DSC scans for the RECRY-LARC-CPI. Comparison of the second run DSC scan for this sample with the second run scan of the Q-LARC-CPI (see Figure 4-2) shows good agreement, the only significant difference being the crystallization temperature -- the amorphous LARC-CPI (Q-LARC-CPI) has a crystallization temperature that is 5°C higher than the recrystallized sample (RECRY-LARC-CPI).

Figure 4-11 shows the DSC scans for the RECRY-LARC-CPI exposed to a 1000 megarad dose. Comparison of the first run scans in Figure 4-10 and Figure 4-11 shows that irradiation results in a decrease in the original level of crystallinity present in this sample. For the 1000 megarad dose, there is almost a 6 mJ/mg decrease in the heat of melting, which was not observed in the CRY-LARC-CPI samples. Notice the presence of a "shoulder" on the melting endotherm of the RECRY-LARC-CPI (see Figure 4-10), which seems to be altered by the electron beam (see Figure 4-11).

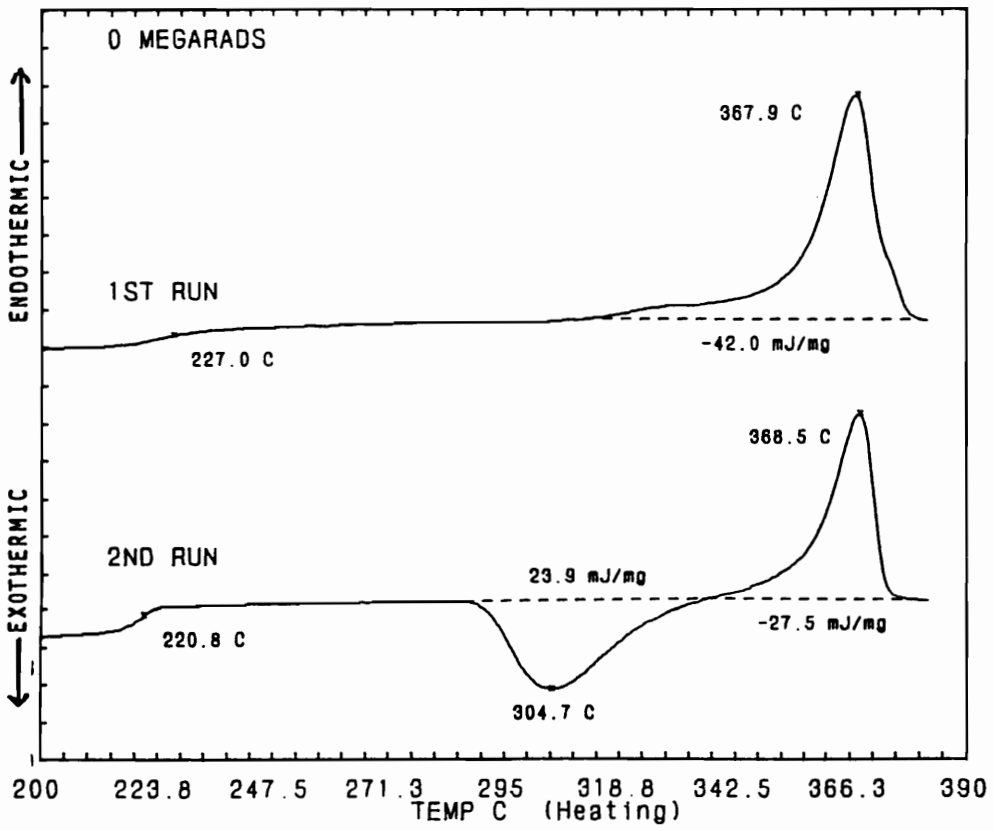

Figure 4-10. First and second run DSC scans for the RECRY-LARC-CPI prior to irradiation.

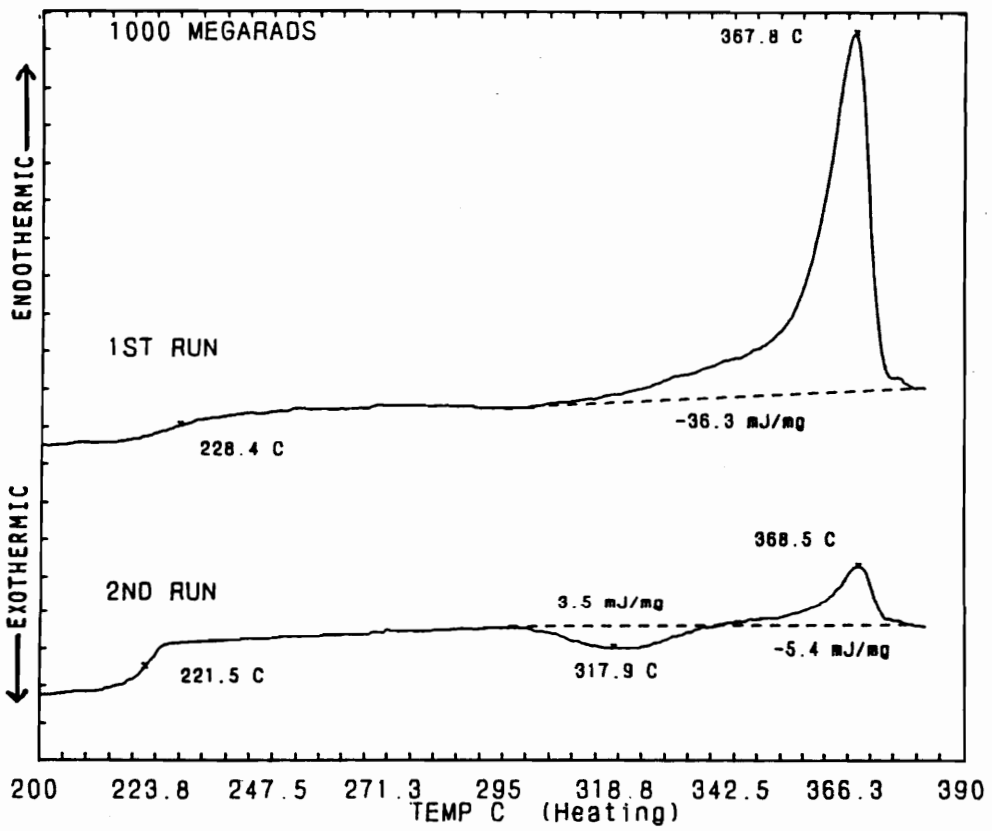

Figure 4-11. First and second run DSC scans for the RECRY-LARC-CPI exposed to 1000 megarads.

The crystals corresponding to this shoulder have a lower melting point and hence are less stable than the predominant crystals present. It has been shown in other high temperature polymers that the minimum dose required for damage to the crystal unit cell correlates well with the melting temperature (5). This may explain why this shoulder is altered and the crystallinity decreases as a result of electron beam exposure. Hence, recrystallizing the LARC-CPI films may alter the fine structure of the crystalline phase such that it has less resistance to electron beam radiation than the crystalline phase present in the as received (CRY-LARC-CPI) samples. In fact, differences in the long spacing of the crystalline lamellae (as determined by small angle x-ray scattering) have been detected between the as received (CRY-LARC-CPI) and recrystallized (RECRY-LARC-CPI) films (17). In addition, changes in the crystalline superstructure resulting from recrystallization of the "as received" LARC-CPI films has also been observed from SEM and STEM analyses as reported by Muellerleile et. al. (18).

Comparison of the second run DSC scans for the unirradiated and irradiated RECRY-LARC-CPI shows similar behavior to the other LARC-CPI samples (see Figure 4-10 and Figure 4-11). For instance, there is an increase in the glass transition and crystallization temperatures, a decrease in the extent of crystallization (during the second run) as a result of electron beam exposure, while there appears to be no effect on the melting behavior.

Comparison of the second run DSC scan for the irradiated RECRY-LARC-CPI (Figure 4-11) with the second run DSC scan for the Q-LARC-CPI (Figure 4-5) irradiated to the same dose level (i.e. 1000 megarads) shows the differences in the radiation response arising from a variation in the sample morphology (i.e. mainly amorphous versus semicrystalline states). However, both of these samples have been thermally cycled to 375°C prior to irradiation, so this comparison may give a better indication of the influence of morphology on the radiation response of LARC-CPI than the comparison of Q-LARC-CPI and CRY-LARC-CPI (CRY-LARC-CPI was not heated prior to irradiation). The recrystallized sample (RECRY-LARC-CPI) has a higher extent of crystallization upon heating (3.5 mJ/mg) than the quenched (Q-LARC-CPI) sample (1.3 mJ/mg). In addition, the glass transition and crystallization temperatures are slightly lower for the recrystallized sample. This suggests that some radiation resistance is indeed afforded by the presence of a crystalline phase during irradiation. However, this effect is not large, and is certainly much less than would be indicated by a comparison of the thermal behavior of the Q-LARC-CPI and CRY-LARC-CPI samples.

Before concluding, it should be stressed that the radiation dosages necessary to alter the DSC behavior of LARC-CPI are quite high. Consider for example, that the typical dose used for radiation sterilization is 2.5 megarads, while a dose exceeding 100 megarads is necessary to effect any change in the DSC behavior of LARC-CPI. Furthermore, doses approaching 1000 megarads are necessary to strongly influence

the extent of crystallization that occurs during the subsequent DSC analysis. However, even at this extremely high dose there are no observable changes in the creasability of the films, color, or other qualitative properties. In addition, the presence of oxygen during irradiation to a dose of 1000 megarads had no effect on the DSC behavior of this polyimide when compared to samples irradiated under nitrogen. This should not be surprising considering that a quite high dose rate was employed, thus limiting the possibility of oxidative degradation occurring.

4.3.3 X-ray Scattering Analysis

As a supplement to the DSC analysis, both SAXS and WAXS experiments were carried out on the as-received films (CRY-LARC-CPI) irradiated to 50 megarads and 1000 megarads to determine if any differences in the scattering profiles were arising from radiation exposure. As illustrated in Figure 4-12a&b, there appears to be no significant differences in the SAXS profiles of these two samples. This suggests that irradiation to high doses does not alter the long range crystalline order present in the films. However, differences do exist in the WAXS profiles of these two samples (see Figure 4-13) , indicating that there are radiation induced changes in the short range crystalline order (i.e. on the order of unit cell dimensions). The decrease in the scattering intensity at 1000 megarads suggests that the crystalline content has decreased, possibly due to radiation induced defects and distortions in the unit cells of the crystal lattice resulting from crosslinking reactions and gas evolution. In fact, the crystalline content of these two samples was determined from the WAXS profiles,

(a)

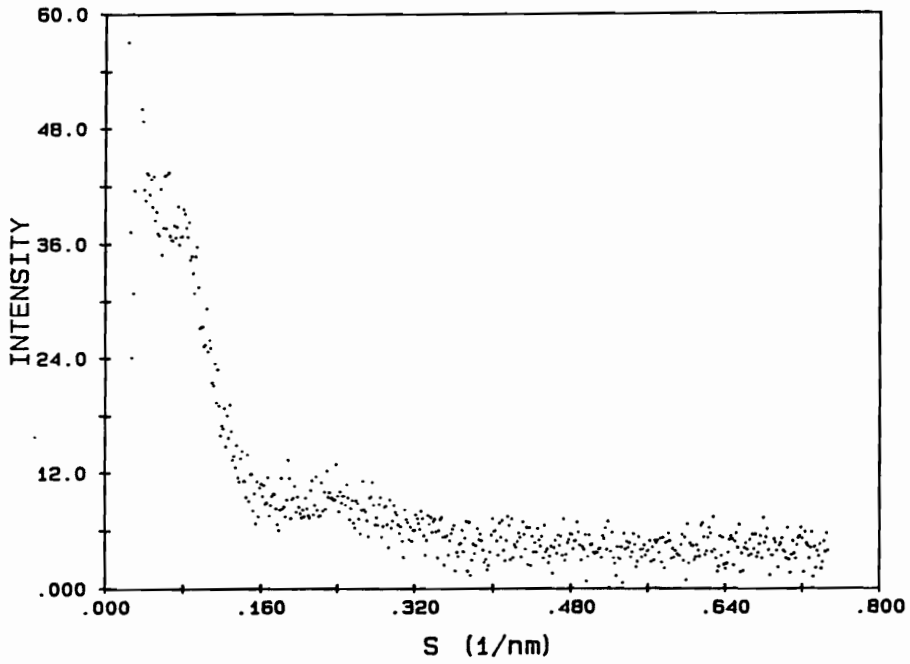

(b)

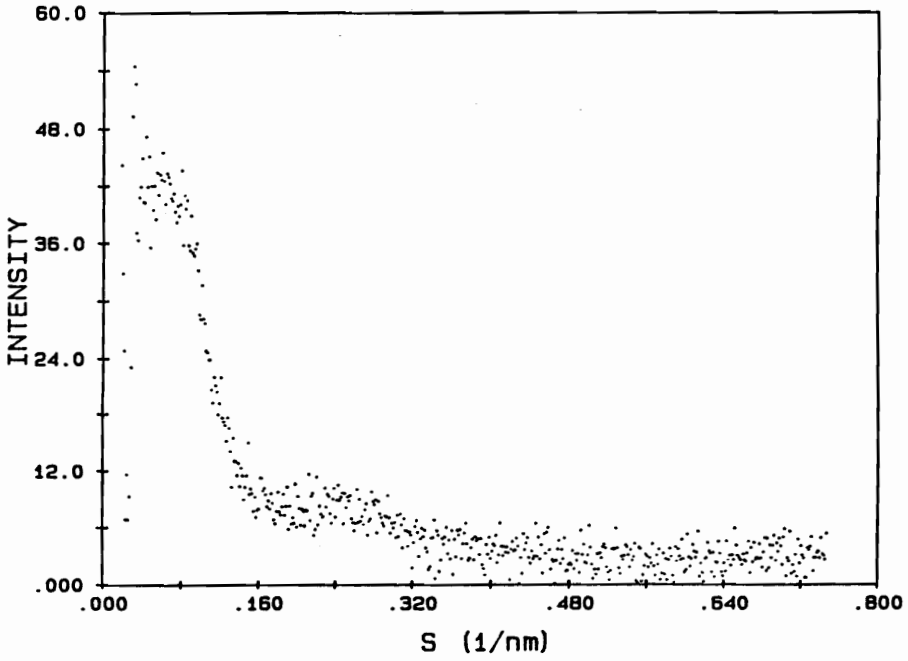

Figure 4-12a&b. SAXS profiles of (a) CRY-LARC-CPI exposed to 50 megarads and (b) CRY-LARC-CPI exposed to 1000 megarads.

(a)

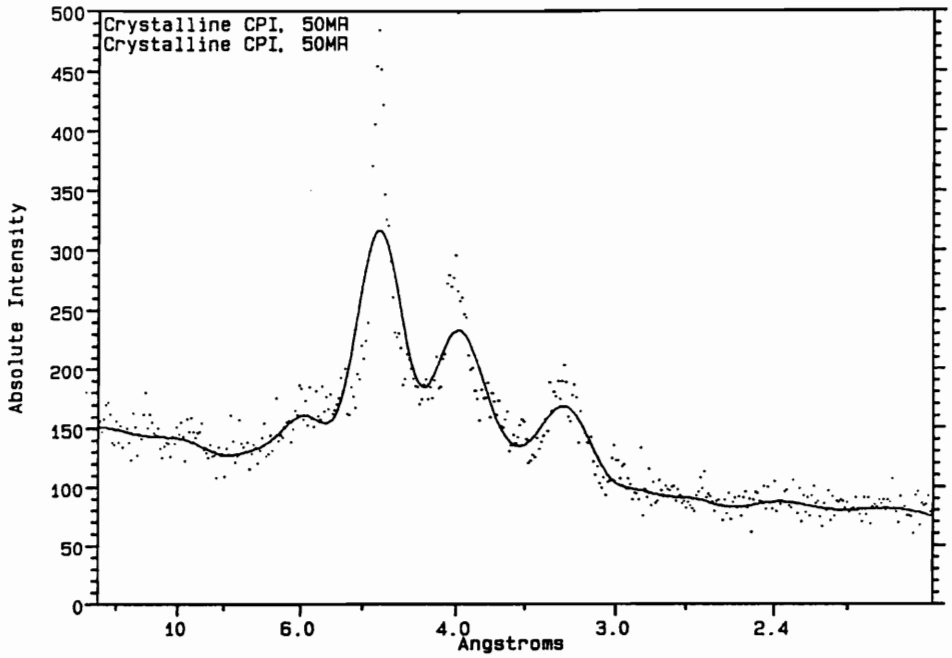

(b)

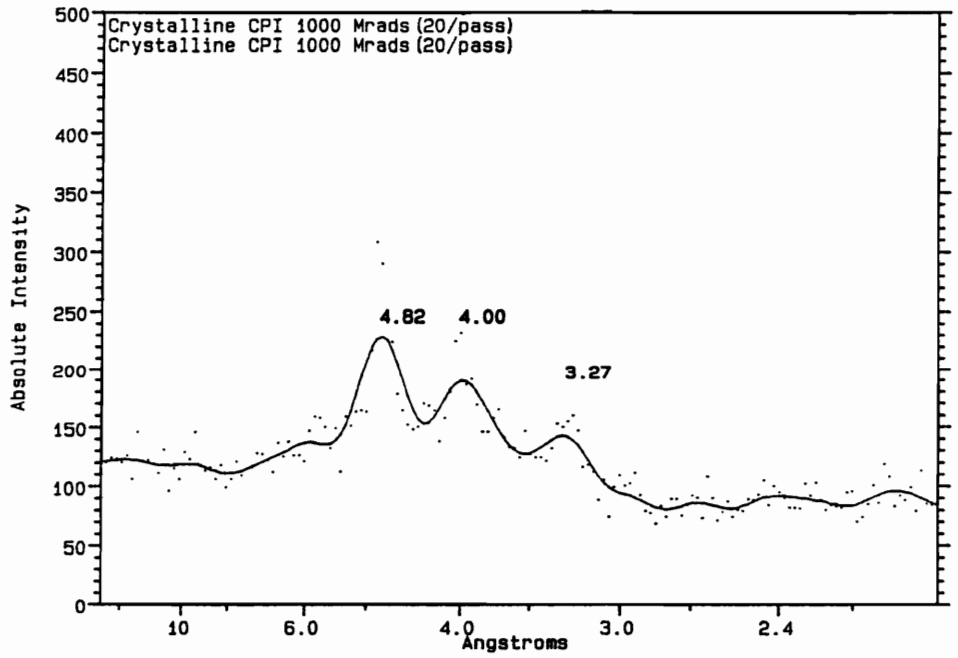

Figure 4-13a&b. WAXS profiles of (a) CRY-LARC-CPI exposed to 50 megarads (crystalline content - ca. 38%) and (b) CRY-LARC-CPI exposed to 1000 megarads (crystalline content - ca. 30%).

following the procedure of Herman and Weidinger (20). The crystalline content of the 50 and 1000 megarad CRY-LARC-CPI was determined to be 38% and 30% (± 2%), respectively. This corresponds to a ca. 21% reduction in the crystalline content of CRY-LARC-CPI after exposure to 1000 megarads. This compares with a 35% decrease in the heat absorbed during melting in the *second run* DSC scan of the same samples (see Figure 4-9). These numbers are in good agreement, since one would expect a greater decrease in crystalline content after melting and recrystallizing a sample which has undergone prior crosslinking. Due to the hindered mobility of the chain segments in close proximity to the crosslinks, crystallization would be suppressed in these regions, which may have not been initially distorted or contributing to the reduced scattering intensity.

It is interesting to note that there is no corresponding decrease in the heat absorbed during melting of the 1000 megarad CRY-LARC-CPI during the *first run* DSC scan (see Figure 4-8). This suggests that crystalline phase is not being destroyed (i.e. transformed into amorphous regions) such that the internal energy (and corresponding thermal behavior) is being altered, but sufficiently distorted to reduce the x-ray scattering intensity. The presence of defects or distortions in the crystalline phase after irradiation is supported by the fact that there is a 3°C decrease in the melting peak temperature (see Figure 4-8), which is indicative of a decrease in the stability of the crystalline phase. However, there is no longer a melting point depression after melting and recrystallizing the CRY-LARC-CPI exposed to 1000

megarads (see Figure 4-9). This seems reasonable, since it is likely that any radiation induced defects in the crystal lattice would be excluded during recrystallization and hence no depression in the melting point would occur.

4.4 CONCLUSIONS

This study has illustrated how electron beam radiation affects the DSC behavior of LARC-CPI. Although the DSC behavior of this polymer is sensitive to its thermal history, which has indeed complicated the analysis of morphological influences on the radiation response, several features of the radiation induced changes in LARC-CPI have been elucidated. In particular, it has been shown that high doses of electron beam radiation are necessary to produce changes in the DSC behavior. In fact, doses up to 100 megarads have negligible effects in this respect. Above this dose level, the heat of crystallization for a quenched, amorphous specimen decreases with increasing dose, while the temperature of crystallization as well as the glass transition temperature increases. This suggests that the polymer chains are being restricted as a result of irradiation, which has been speculated to be due to crosslinking. This has been shown to be true regardless of the crystallinity content during exposure. However, the effects of the presence of a crystalline phase on the extent of these radiation induced changes is somewhat obscured by the dependence of the thermal behavior on the thermal history.

An attempt was made to eliminate thermal history influences on the DSC behavior by recrystallizing LARC-CPI prior to irradiation so that the amorphous and crystalline samples had similar thermal histories. The results indicate that the presence of crystals in the polymer may lessen the effects of irradiation, although there is not a large difference in the resulting DSC behavior. There are only slight

differences in the transition temperatures, but the heat of crystallization in the recrystallized sample is more than twice that of the quenched sample. Finally, it has been shown that the thermal history may also influence whether or not irradiation alters the crystalline phase. In particular, the results have indicated that recrystallized LARC-CPI may have a somewhat lower resistance to electron beam irradiation. It has been proposed that this may be due to thermally induced changes in the character of the crystals, which reduces the radiation resistance of the polymer.

4.5 REFERENCES

1. Hergenrother, P.M.; Wakelyn, N.T.; Havens, S.J. *J. Polm. Sci. Part A,* 1987, **25**, 1093.

2. Sasuga, T.; Hayakawa, N.; Yoshida, K.; Hagiwara, M. *Polymer*, 1985, **26**, 1039.

3. Hanks, L.L.; Hamman, D.J. *"Radiation Effects Design Handbook"*, section 3, NASA - CR 1787 (1971).

4. Sasuga, T. *Polymer*, 1988, **29**, 15.

5. Kumar, S.; Adams, W.W. *Polymer*, 1990, **31**, 15.

6. Minkova, L.; Lefterova, E.; Koleva, Ts.; Nedkov, E.; Nikolova, M. *Coll. Polym. Sci.*, 1988, **266**, 898.

7. Minkova, L. *Coll. Polym. Sci.*, 1988, **266**, 6.

8. Yoshii, F.; Makuuchi, K.; Ishigaki, I. *Angew. Makromol. Chemie,* 1986, **143**, 75.

9. Birkinshaw, C.; Buggy, M.; Daly, S.; White, J.J. *Thermochimica Acta,* 1987, **117**, 365.

10. Williams, T.F.; Matsuo, H.; Dole, M. *J. Amer. Chem. Soc.*, 1958, **80**, 2595.

11. Bhajeta, S.K.; Andrews, E.H.; Young, R.J. *J. Polym. Sci., Polym. Phys. Ed.*, 1983, **21**, 523.

12. Dole, M; Katsuura, K. *J. Polym. Sci.,* 1965, **3B**, 467.

13. Okada, T; Mandelkern, L. *J Polym. Sci.,* 1967, **5 (A-2)**, 239.

14. Hergenrother, P.M.; Havens, S.J.; *J. Polym. Sci. Part A*, 1989, **27**, 1161.

15. Sasuga, T.; Hagiwara, M. *Polymer,* 1986, **27**, 821.

16. Patel, G.F.; Keller, A.J. *J. Polym. Sci., Polym. Phys. Ed.,* 1975, **13**, 303.

17. Muelleriele, J.T.; Wilkes, G.L., to be published, 1991.

18. Muellerliele, J.T.; York, G.A.; Wilkes, G.L. to be published, 1991.

19. Vonk, C.G. *J. Applied Crystallography*, 1971, **4**, 340.

20. Hermans, P.H.; Weidinger, A. *Textile Research Journal*, 1961, **31**, 558.

CHAPTER V
5.0 REVERSAL OF PHYSICAL AGING IN AMORPHOUS GLASSY POLYMERS BY ELECTRON BEAM IRRADIATION

5.1 INTRODUCTION

This chapter illustrates a rather unusual phenomena which has been found to occur in amorphous polymeric glasses that have undergone physical aging and subsequently exposed to electron beam radiation. It will be shown that these materials undergo a partial (or complete) reversal of physical aging ("deaging") when subjected to electron beam radiation. This phenomena occurs in a variety of glassy polymers regardless of the intrinsic response or sensitivity of the polymer to ionizing radiation. Before examining this behavior and detailing the experiments that were performed, some aspects of physical aging and the non-equilibrium behavior of polymeric glasses that are pertinent to later discussion are reviewed.

5.1.1 Origins of Physical Aging

Physical aging is a phenomenon which occurs due to the non-equilibrium nature of the glassy state. Consider an amorphous, linear polymer that is held at some temperature which is above the glass transition temperature (T_g) of the material. Upon cooling, the material begins to solidify and stiffen as the glass transition is approached. During this process, the segmental mobility of the polymer chains decreases, as well as the molar volume of the sample. The rate of this volume decrease will be dependent on the thermal expansion coefficient of the polymer. As the cooling process proceeds, and the glass transition is reached, there will be a sharp

decline in the rate of volume contraction due to the severe restrictions on the segmental mobility of the polymer chains at the onset of the glassy state. This volume relaxation is quite slow, and can never be completed in the time frame of the cooling process, regardless of the cooling rate (unless of course, the cooling rate is infinitesimally small, which is not practical). Hence, with the onset of the glassy state, there will be a certain amount of excess volume that will be "frozen" in the system. This excess volume is known as the free volume (V_f) and is defined by:

$$V_f = V - V_o(T)$$

where:

V = total macroscopic volume

$V_o(T)$ = volume occupied by the molecules

It should be noted that there is an inherent amount of free volume associated with all condensed matter, regardless of whether or not a state of equilibrium exists. The above definition for free volume pertains to both the inherent free volume associated with equilibrium conditions and the excess free volume that is incorporated into the glassy state as a result of the finite cooling rate. Faster cooling rates result in more free volume incorporated into the system. Hence, excess free volume is a result of the inability of the polymer chains to pack themselves into a glassy equilibrium state within the time allowed by the cooling rate to a given temperature below T_g. However, with time, the free volume will decrease as the equilibrium glassy state is approached. This free volume decrease in the glassy state that occurs over time is

known as volume relaxation and is generally viewed as the primary component of physical aging.

It appears that the concept of free volume relaxation in polymers at temperature below T_g is a well established phenomena. Some of the earlier work done in this area was by Kovacs in 1958 (1). In these experiments, dilatometry measurements were carried out on poly(vinyl acetate) to determine the specific volume as a function of temperature. The results on two samples which had been held below T_g for different times are shown in Figure 5-1. This illustrates that the sample which was held below T_g for a longer period of time has a lower specific volume at all temperatures below the glass transition. Once the glass transition is reached, the liquid state sets in and the two specific volume curves coincide. This clearly proves that the free volume of an amorphous polymer decreases with time when stored below the glass transition. Of course, the rate of this volume relaxation will be dependent on the particular polymer and the storage temperature. More recently, Bartos et. al. have reported on the volume relaxation of polycarbonate as determined by dilatometry (2). As shown in Figure 5-2, the volume decreases with aging time and the rate of decrease increases with storage temperature.

5.1.2 Effects of Physical Aging on Material Properties

Thermal Properties. Since enthalpy is volume dependent, the reduction in free volume associated with physical aging must be accompanied by a reduction in enthalpy as well (although changes in enthalpy can occur without changes in volume).

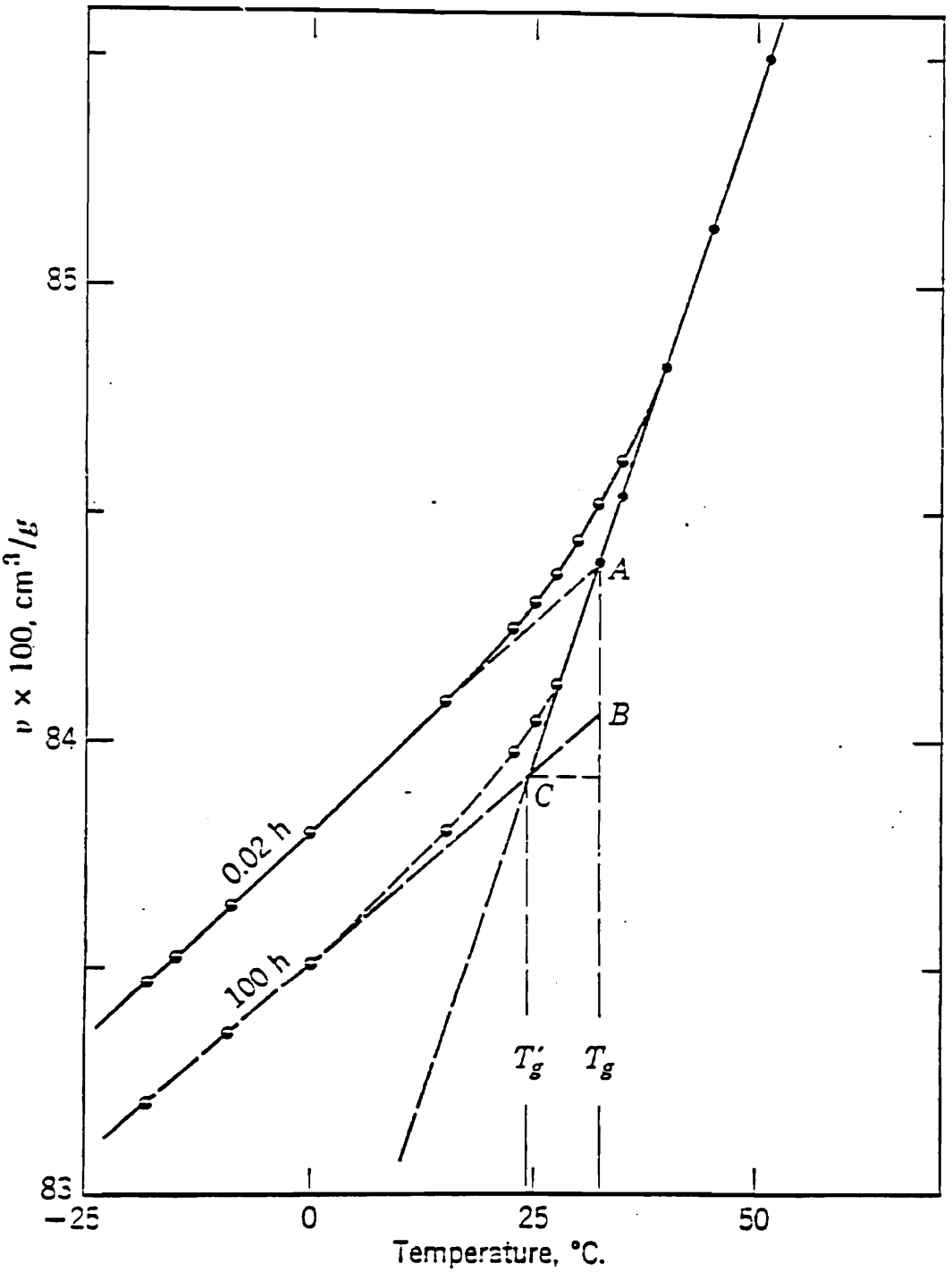

Figure 5-1. Plot of specific volume versus temperature for poly(vinyl acetate) measured at the indicated times after quenching from above the glass transition (ref. 1).

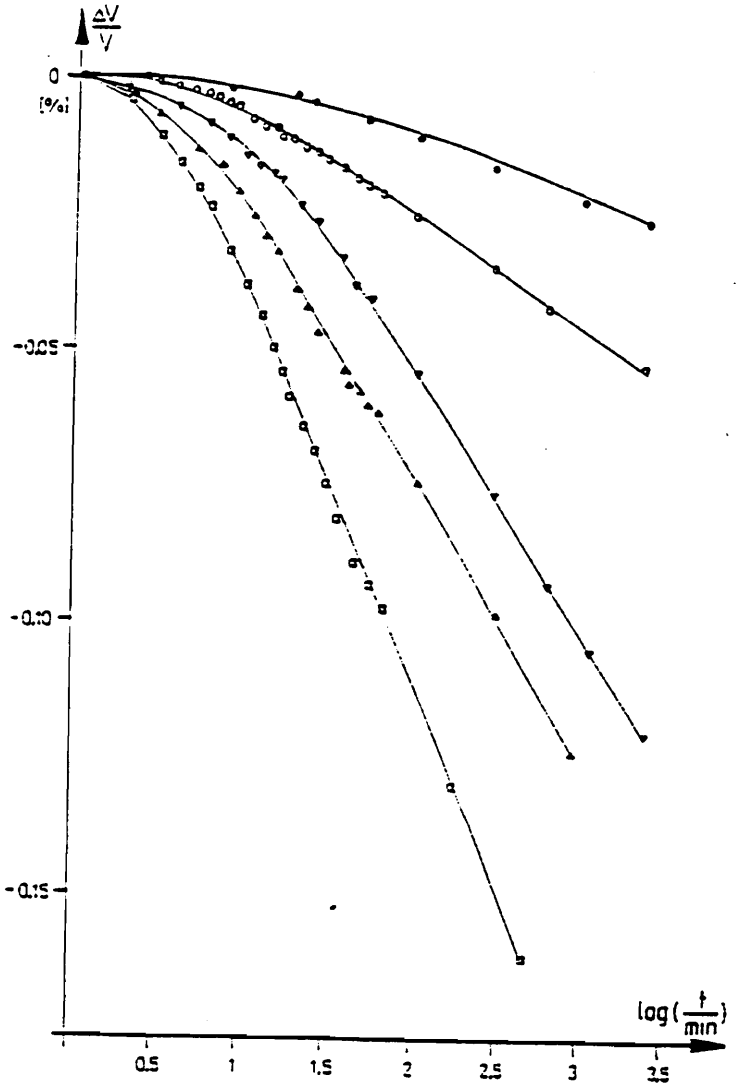

Figure 5-2. Volume versus aging time for polycarbonate at the following aging temperatures: 45°C - ●; 65°C - ○; 70°C - ◇; 100°C - ▽; 110°C - △; 130°C - □. (ref. 2)

Hence, physical aging affects the thermal properties of glassy polymers, especially in the temperature region near the glass transition. To illustrate the effect of aging on thermal properties consider a plot of enthalpy, H, (or volume, V) versus temperature for a glassy polymer as shown in Figure 5-3. Upon quenching from well above the glass transition, the enthalpy of the system follows the solid line in Figure 5-3. After aging at some temperature, T_a, the enthalpy decreases from H_g to some lower value, H_a. Upon subsequent heating, the enthalpy increases and follow as the dotted line in Figure 5-3. However, the enthalpy increase does not follow the line associated with the equilibrium glassy state at T_e. Instead, the enthalpy overshoots the equilibrium curve and there what will be assumed to be a near step increase in enthalpy at T_{g1}. This overshoot is a result of a finite heating rate and the longer relaxation times of the polymeric chains resulting from a reduction in free volume during aging. The extent of overshoot will be dependent on the heating rate and the aging time at T_a and increases as either of these variables are increased. Also note that this overshoot results in a measured T_g that is greater than the equilibrium T_g (T_e) and under some conditions will be higher than the measured glass transition of the quenched glass (i.e. $T_{g2} > T_{g1}$).

The temperature derivatives of these enthalpy curves are shown in Figure 5-4a, which is essentially a DSC curve. As illustrated, the step increase in enthalpy at T_{g1} results in an endothermic peak on the DSC curve. The decrease in enthalpy (and free volume) that occurs during physical aging has been characterized by the area of

this endothermic peak for a variety of polymeric glasses. It should be noted however, that the endotherm area may not always give an accurate value for the true enthalpy decrease that has occurred. If the overshoot that occurs during heating is sufficiently large, then inaccurate values will be obtained by this method. To explain why this occurs, consider the enthalpy - temperature diagram in Figure 5-3. If the overshoot extends to T_{g2}, then the increase in enthalpy which occurs at this temperature is greater than true difference in enthalpy between the quenched and aged states (i.e. path (1) = $(H_g - H_a)$, whereas path (2) > $(H_g - H_a)$). Therefore, the endotherm area in the DSC curve will overestimate the true enthalpy difference between the aged and quenched states. The DSC curves for this situation is shown in Figure 5-4b. As has been suggested by Matsuoka and Bair (4) the true value for the enthalpy difference can be obtained by subtracting area A from area B. This consideration becomes important for large enthalpy differences and fast heating rates, which as previously mentioned, result in an increase in the extent of overshoot.

Mechanical Properties. In addition to thermal properties, physical aging can also greatly influence the mechanical properties of polymeric glasses. This is primarily due to the longer relaxation times of the polymer chains which results from the decrease in free volume during aging. The effect of aging on the yield stress will be of importance in this study, and as shown in Figure 5-5, the yield stress of polycarbonate increases with aging time (5). This behavior is common in most glassy polymers. In addition to increasing yield stress, physical aging generally causes a

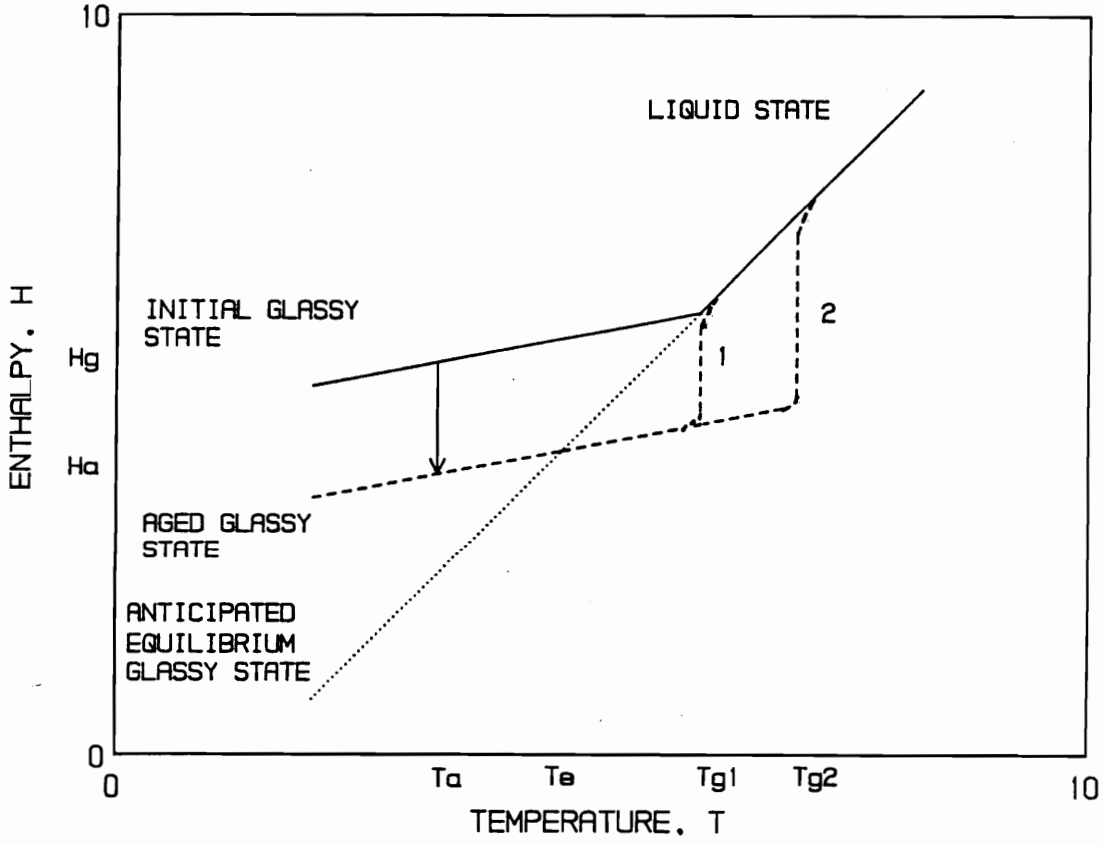

Figure 5-3. Enthalpy - temperature plot of a quenched (-) and aged (--) polymeric glass.

(a)

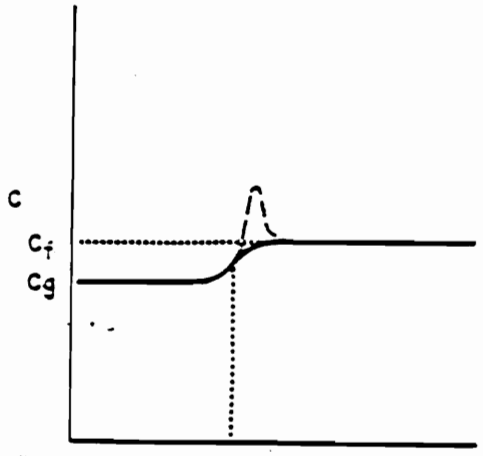

(b)

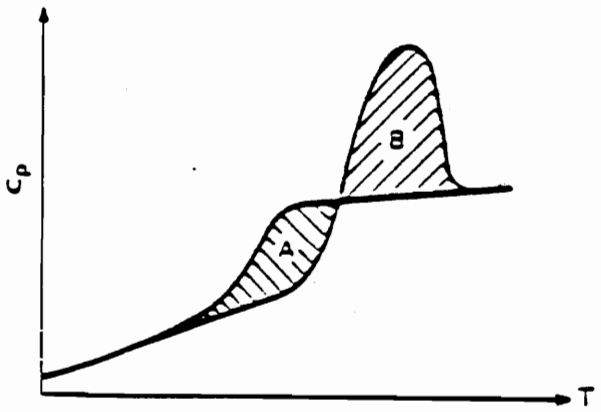

Figure 5-4a&b. Derivatives of the enthalpy plots shown in Figure 5-3, which are DSC plots for (a) aged glass with step increase at T_{g1} and (b) aged glass with step increase at T_{g2}. (refs. 3 & 4)

decrease in creep rate and an increase in the storage modulus (6). Again these changes in properties arise from a decrease in segmental mobility of the polymer chains resulting from the volume relaxation associated with physical aging. Much work has been done on the effects of physical aging on mechanical properties of polymeric glasses and the reader is referred to several reviews and books on the subject for a more detailed treatise on the subject (6-9).

An interesting phenomena which relates to the work in this chapter is the reversal of aging ("deaging") that results from deformation processes in glassy polymers. In recent years, Smith et. al. have reported on this behavior occurring in polycarbonate (10-11) . As shown in Figure 5-6, the storage modulus of aged polycarbonate decreases by ca. 2.5% and 2.0% when a 3.0% extensive or 3.1% compressive strain is applied to the material for 30 seconds, respectively (10). This figure also shows how the storage modulus recovers with time after the initial deformation. These results illustrate that deaging occurs when either an extensive or compressive strain is imposed on the material. Since a compressive strain does not directly result in an increase in free volume per se, a strain induced increase in free volume cannot solely account for this behavior. Struik has suggested that "it is the segmental motion [resulting from deformation] which is related to the increase in free volume, the type of stress field generating this motion being irrelevant" (6). Hence it is thought that the shear component of strain is mainly responsible for this deaging process.

However, the deaging that occurs is greater in tension than compression, indicating that direct increases in free volume also play a significant role.

Permeation of Gases. Since a decrease in free volume is associated with physical aging, this process may affect the permeation of gases in glassy polymers. Lee (12) has shown that the logarithm of the permeability coefficient decreases linearly with the inverse of the specific free volume of glassy polymers (see Figure 5-7). This suggests that a reduction in free volume caused by physical aging may decrease the permeability of polymeric glasses.

Kapur and Rogers have determined the effect of aging on the permeability of polypropylene (13). This work considered the effect of aging (at room temperature) on the permeability of various gases with different molecular weights as well as the effect on the mechanical properties of quenched polypropylene. Although the glass transition of polypropylene is below room temperature and hence the aging cannot be considered to be physical aging per se, the phenomena observed is similar to that of physical aging. For instance, aging of quenched polypropylene produces an increase in yield stress, modulus, and density (with no detectable changes in crystallinity), all of which are observed during physical aging as well. As shown in Figure 5-8, the diffusion coefficients of neon and helium in polypropylene significantly decrease with aging time, while argon remains unaffected. In fact, the effect of aging on diffusivity is shown to decrease with increasing molecular weight of the gas. This observation was attributed to the loss of microvoids in the

amorphous phase which had dimensions large enough to influence the diffusion of helium and neon, but not argon. It will be postulated in this chapter that the radiation induced deaging phenomena observed results from internal gas evolution. Since radiation exposure of organic materials results in the internal production of a variety of different gases, the interrelationships between gas molecule size, diffusivity, and free volume will be of importance in this chapter.

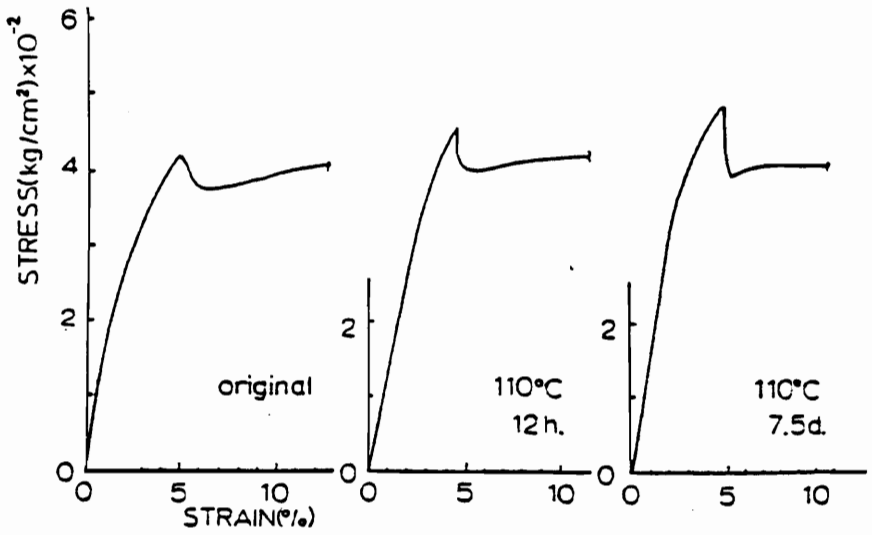

Figure 5-5. Stress - strain curves for PC after storage at the indicated temperature and time. (ref. 5)

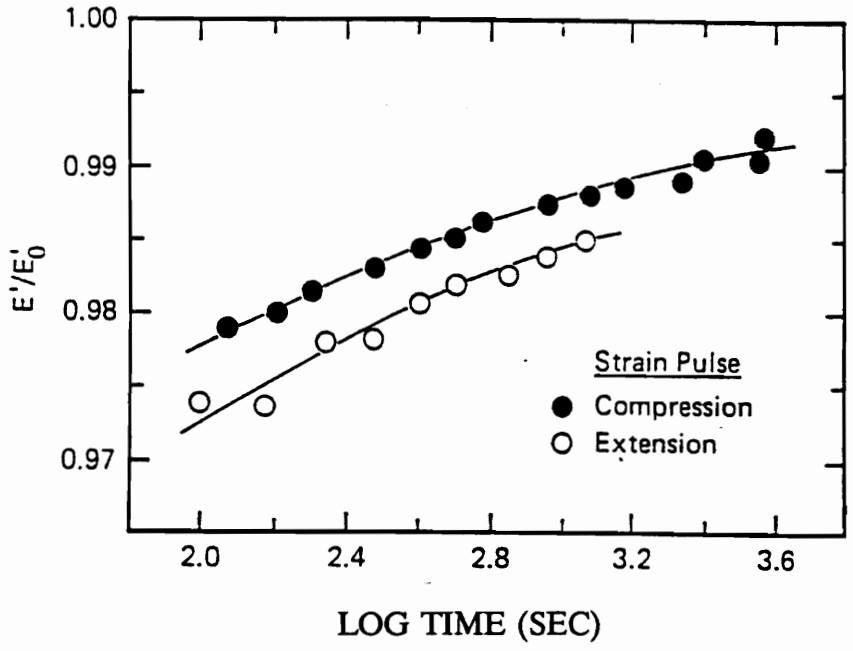

Figure 5-6. Normalized storage modulus (relative to unstressed films) versus time for polycarbonate after imposing a 3.0% (tension) and 3.1% (compression) strain for 30 s. (ref. 10)

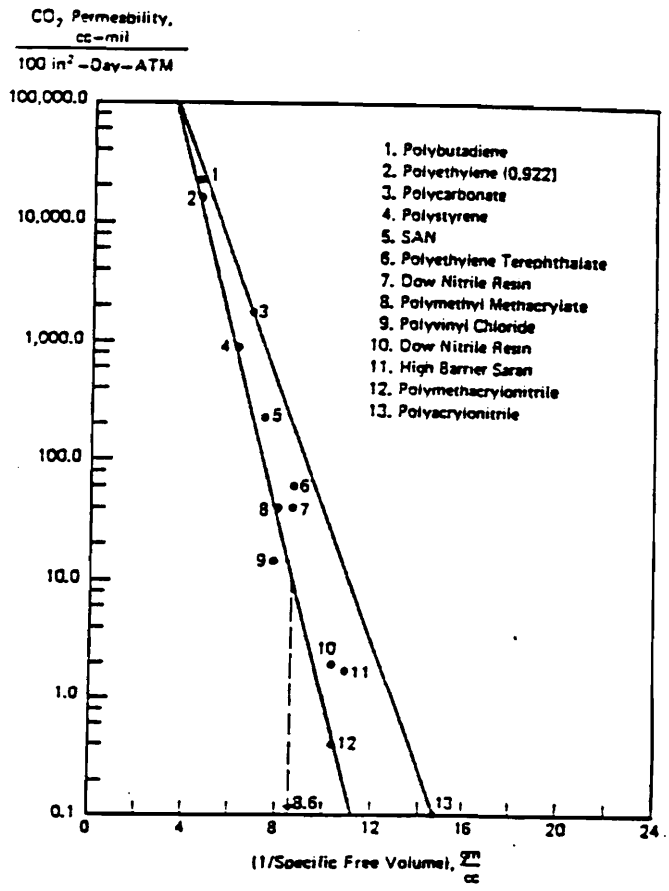

Figure 5-7. Logarithm of permeation coefficients versus the inverse specific free volume for a variety of polymeric glasses. (ref. 12)

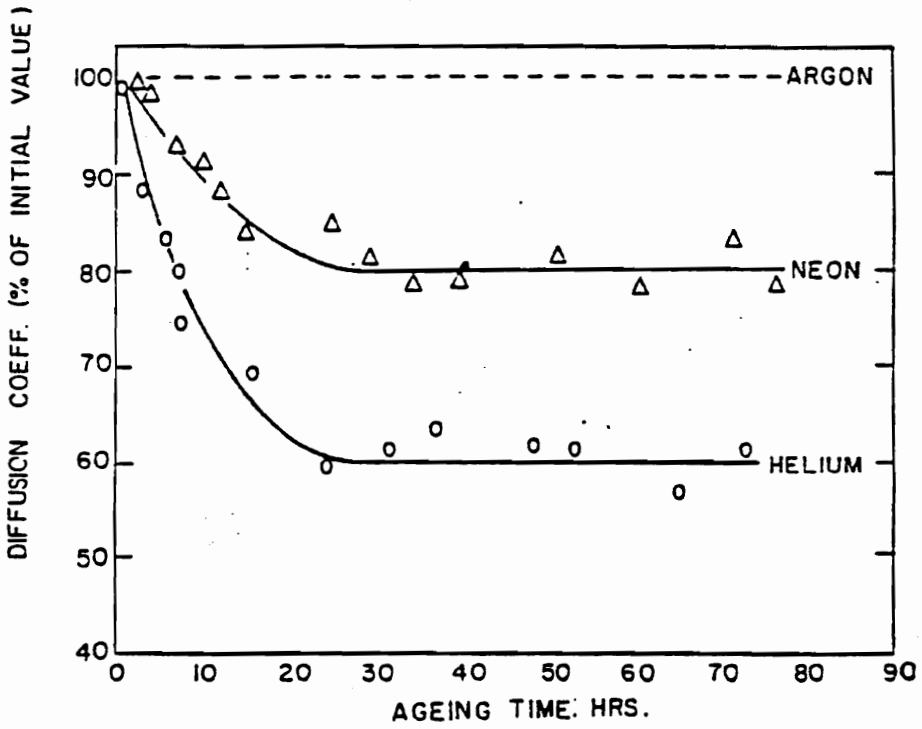

Figure 5-8. Effect of aging time on the diffusion coefficients of various gases in polypropylene. (ref. 13)

5.2 EXPERIMENTAL

5.2.1 Materials and Sample Preparation

The following polymers were used in this study: (1) bisphenol-A polycarbonate (Aldrich Chemical), (2)poly(methyl methacrylate) ( ), and (3) polystyrene (Dow Chemical). Thin films (thickness ca. 3 mils) were obtained by compression molding between teflon sheets at the following temperatures: (1) polycarbonate (PC) - 210°C, and (2) poly(methyl methacrylate) (PMMA) and polystyrene (PS) - 180°C. All samples were quenched to room temperature. Once formed, each film was physically aged at ca. 30°C below its glass transition temperature - 120°C for PC and 80°C for PMMA and PS. Aging was carried out in a vacuum oven for up to one week. At this point, longer aging times resulted in less than a ca. 5 % increase in the glass transition peak area as determined by DSC. It must be stressed however, that this does not imply that aging has ceased. The rate of aging in glassy polymers decreases logarithmically with time, so at some point (depending on the material), further reductions in the enthalpy of the glass may not be observed by DSC.

5.2.2 Radiation Exposure.

All films were irradiated using an Energy Sciences CB150 Electrocurtain as the electron beam radiation source. Details on this equipment and dosimetry are given in the Appendix. Samples were passed under the electron beam in a aluminum tray at speeds of either 20 or 40 ft/min. The beam current was varied up to 6 milliamps. Under these conditions doses ranging from 1 to 20 megarads could be given in a

single pass. All samples were irradiated under a nitrogen purged atmosphere. The oxygen content ranged between 250 - 350 ppm during processing. It should be noted however, that the films were exposed to air between passes when more than one pass was necessary to achieve the required dose and dose rate.

5.2.3 Thermal Analysis.

The aging behavior and extent of enthalpy relaxation of all the polymers was followed by differential scanning calorimetry (DSC) using a Seiko I DSC210 differential scanning calorimeter. The instrument was calibrated using an indium standard. Samples with weights in the range of 7 to 10 mg were sealed in aluminum pans and heated at a rate of 10°C/min. The extent of aging was characterized by the area under the endothermic peak occurring at T_g. The base line was taken by extrapolating the base line established above the glass transition. As noted in the introduction this may result in an inaccurate value for the extent of enthalpy relaxation in the glass. To determine the error associated with this analysis, second run DSC scans were made on some samples after quenching to room temperature and superimposed on the first run scans to determine the net enthalpy difference between the aged and freshly quenched glasses. The results of this error analysis is shown in Figure 5-9. As illustrated, the error associated with this analysis of enthalpy relaxation varies with the particular polymer and the extent of aging in the sample. PS and PC have quite high errors associated with this analysis while the error for PMMA is quite low. This is of little consequence since mainly trends are being

established in this work. However, to be sure that this error is not affecting the trends established, the endothermic peak areas were corrected for PS and PC based on this error analysis. As will be shown in the next section, the error has no significant effects on the trends to be discussed.

5.2.4 Molecular Weight and Gel Fraction Determinations.

Molecular weights given were obtained using a Waters gel permeation chromatography column equipped with an ultra-violet detector (λ = 254 nm). THF was used as the solvent with a flow rate of 1 ml/min. Solutions of 50 wt % polymer were prepared for injection into the column. Only PMMA and PS standards were available, so GPC was not carried out on PC.

Gel fractions on irradiated PS were obtained by extracting the films in THF with a Soxhlet extractor for 24 hours. The insoluble fractions were stored under vacuum (30 in. Hg) at 120°C for at least 16 hours prior to weighing to remove residual solvent. Longer storage times did not result in any significant difference in weight. Gel fractions were obtained by dividing the insoluble weight by the initial weight which was in the range of 80 mg.

5.2.5 Stress - Strain Measurements.

The stress - strain behavior of the PC films were made using a Model 1122 Instron tensile tester interfaced to a computer for data collection and stress calculation. Dogbone samples were cut from films with thicknesses ranging from 3 to 4 mils. The stressed area of the samples were 10 mm long and 3 mm wide. Five

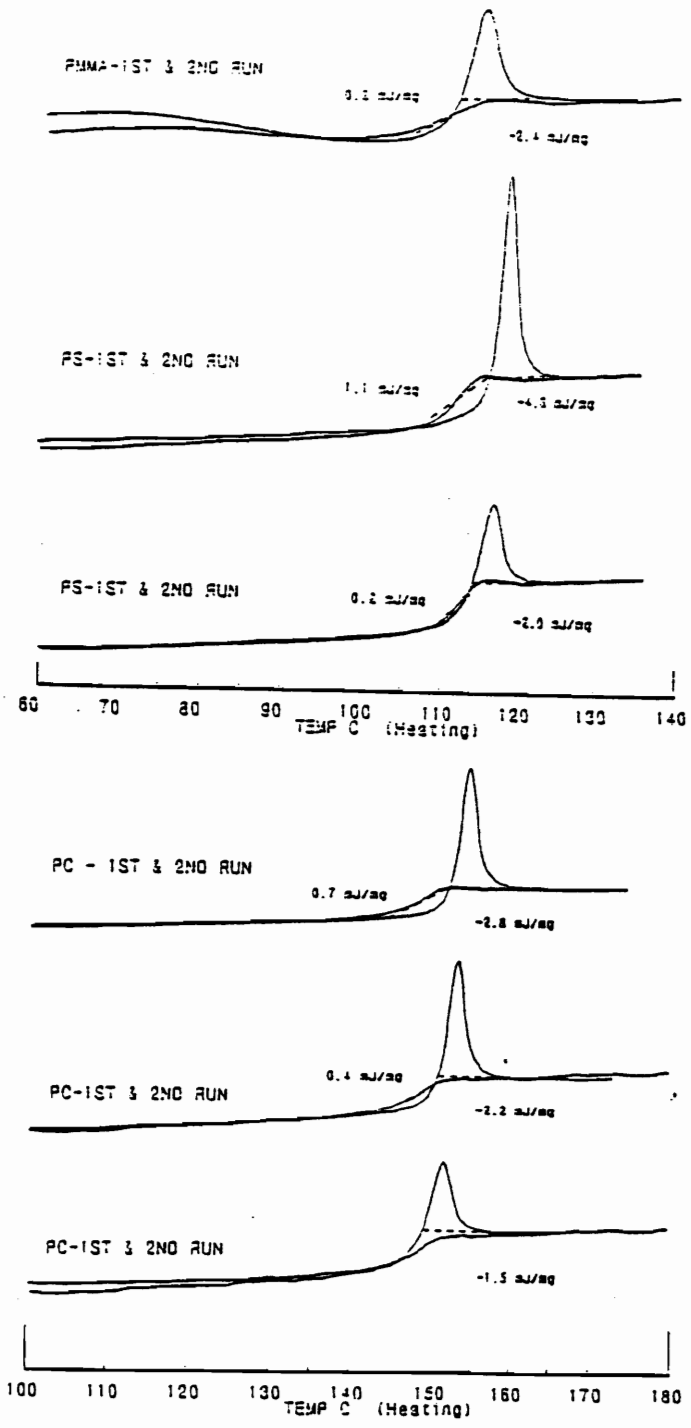

Figure 5-9. Superimposed DSC scans of quenched and aged glasses used in this study.

dogbones of each sample were tested. Values reported for the yield stresses are based on the average of these five tests.

5.3 RESULTS AND DISCUSSION

5.3.1 Effects of Radiation Dose.

As mentioned in the introduction, it has been discovered that electron beam radiation exposure results in "deaging" of glassy polymers. As will be illustrated, this seems to be a general phenomena which occurs in a variety of polymer glasses regardless of the thermal properties or the intrinsic response of the polymer to radiation exposure. This is the first reported observation of a "deaging" phenomena occurring in polymeric glasses that does not involve heating above the glass transition or some sort of deformation process.

Figures 10-12 show the effect of dose on the DSC behavior of PS, PMMA, and PC in the glass transition region, respectively. Prior to irradiation, the former two polymers were stored at 80°C for one week, whereas PC was stored for one week at 120°C. It should be noted that the curvature in the PMMA baselines before the glass transition is due to the desorption of water on the film, but this does not seem to have any effect on the glass transition behavior. The enthalpy values shown on the plots correspond to the area under the endothermic peak using the baselines drawn as shown. In all cases there is a steady decrease in the endothermic peak area and peak temperature with increasing dose. This clearly demonstrates that these polymer glasses are undergoing some form of radiation induced aging reversal process. Furthermore, the extent of this aging reversal is proportional to the total absorbed dose. It should be realized however, that the decrease in peak temperature may be

influenced by radiation degradation as well as a reversal of physical aging. It is important to note that when exposed to ionizing radiation, PS primarily undergoes crosslinking, PMMA undergoes only chain scission, and PC undergoes simultaneous crosslinking and scission with crosslinking predominating at low doses (up to about 5 megarads) and scission predominating at higher doses (14). Hence the occurrence of this "deaging" behavior is not dependent on the specific radiation chemistry taking place or whether crosslinking or scission of the polymeric chains is taking place. Regardless of the specific radiation chemistry, irradiation of polymeric materials results in the internal evolution of gases. It is therefore postulated that this radiation induced "deaging" phenomena is resulting from internal gas evolution which produces an increase in free volume and subsequently causes a reversal of physical aging. Furthermore, it will be clearly shown that this phenomena is not the result of electron beam heating when the effects of dose rate are discussed.

To determine the likelihood of radiation induced gas evolution resulting in "deaging", it is worthy to examine how this aging reversal varies with dose. Figure 5-13a-c shows plots of the normalized endothermic peak area at T^g versus dose for PS, PMMA, and PC, respectively. As discussed in the experimental section, using only the endothermic peak area as a measure of the enthalpy or free volume relaxation associated with physical aging may not always give an accurate value. To ensure that this method of analysis is not affecting the resulting *trends*, the net enthalpy difference between aged and quenched glasses were determined for PS and

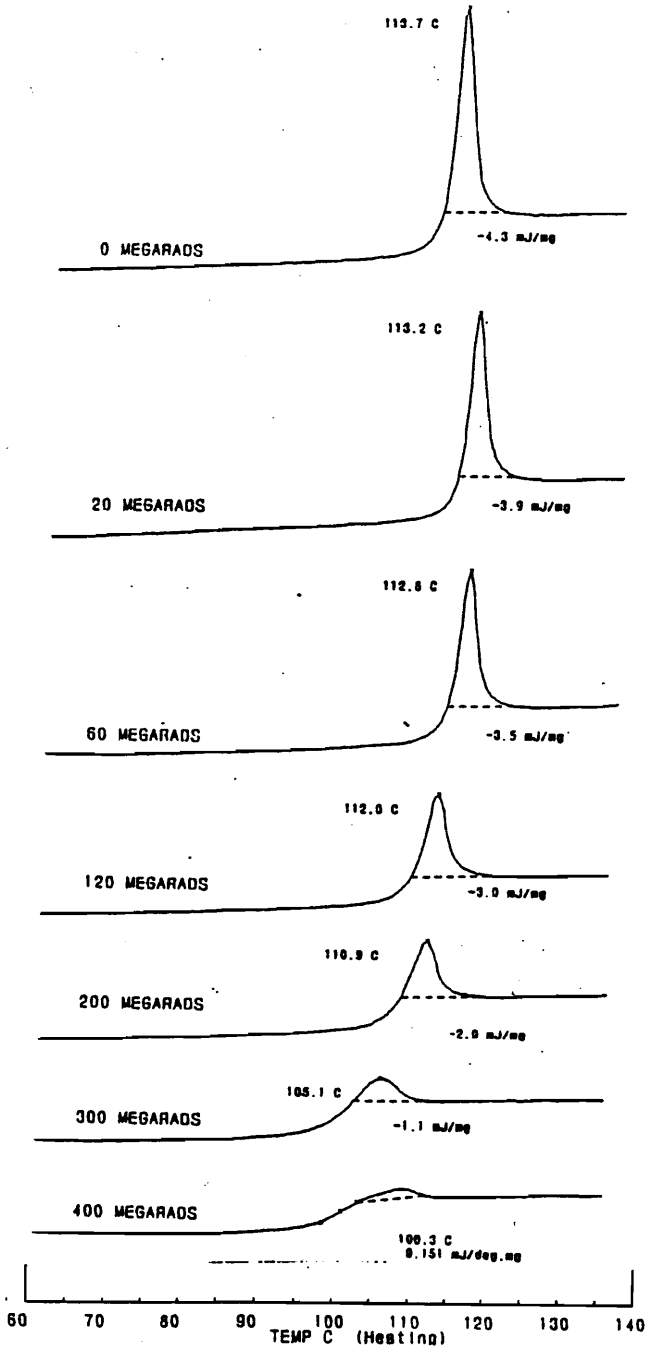

Figure 5-10. DSC scans of aged PS after exposure to the indicated dose.

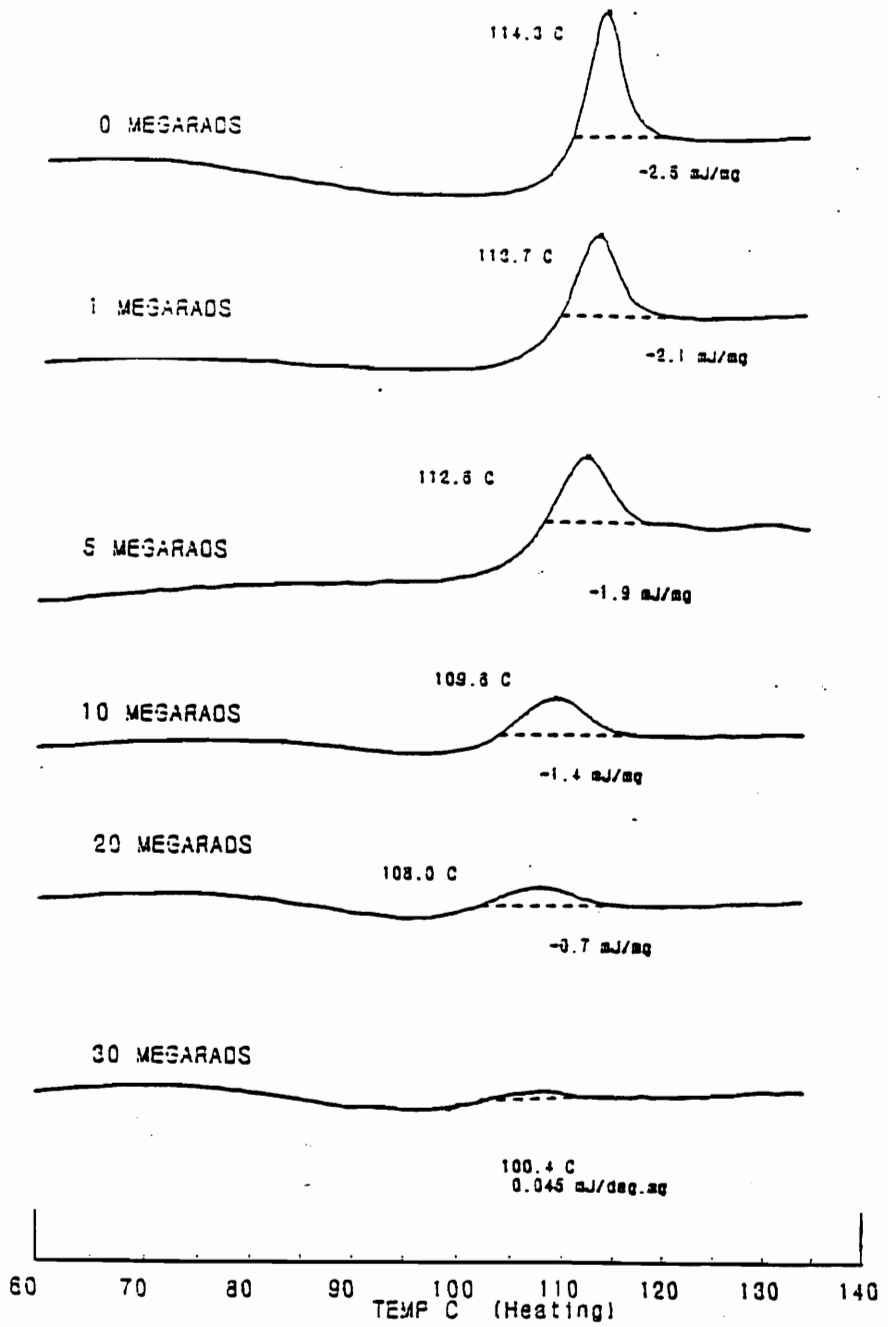

Figure 5-11. DSC scans of aged PMMA after exposure to the indicated dose.

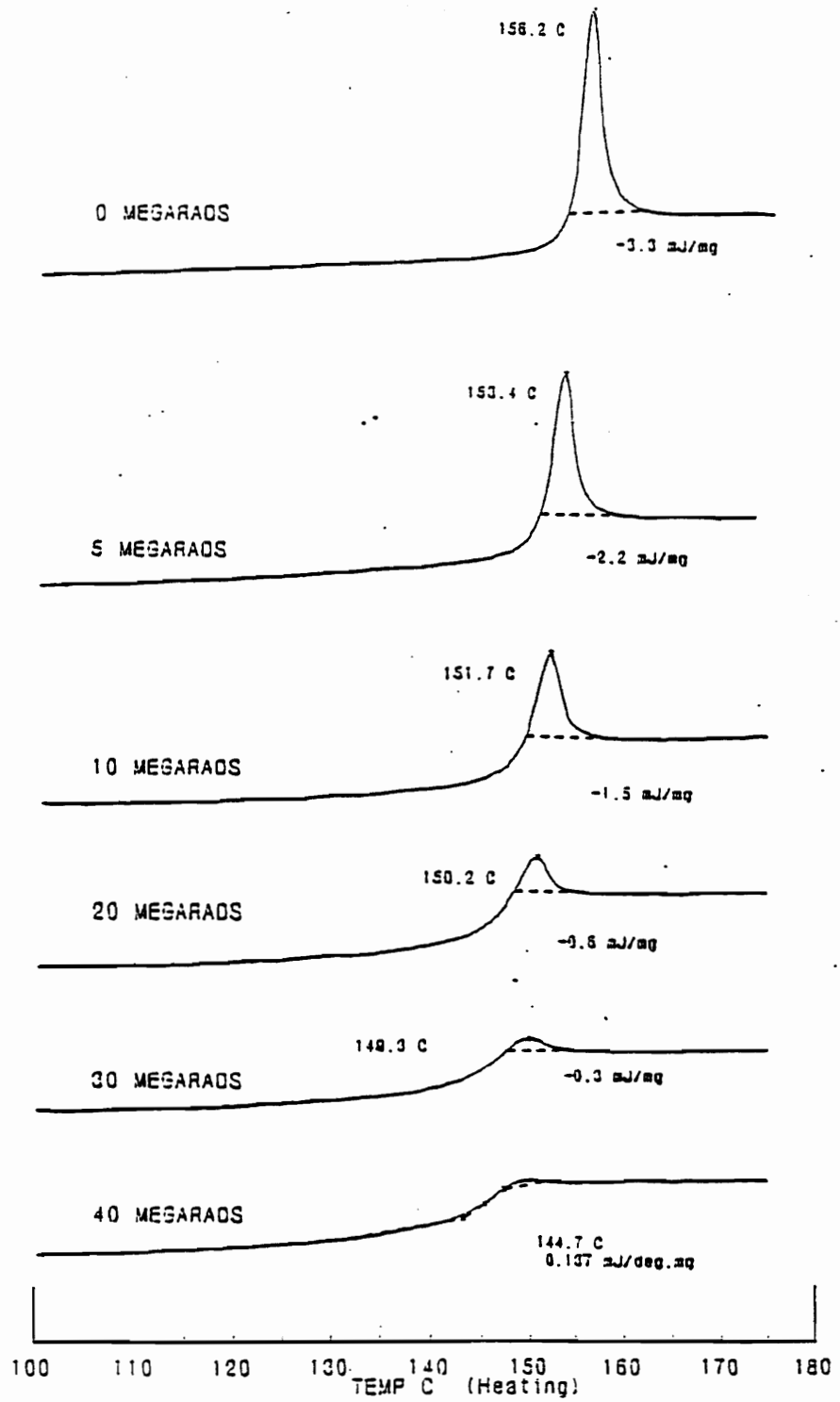

Figure 5-12. DSC scans of aged PC after exposure to the indicated dose.

PC. These values are also plotted in Figure 5-13a&c and as shown, the only resulting difference is a horizontal shift in the enthalpy - dose curve. Hence the use of only the endothermic peak area will provide a sufficient measure of the extent of physical aging for *the purposes of this particular study.* Having addressed this consideration, any error associated with this type of analysis will no longer be considered in this work. Furthermore, when referring to the endothermic peak area at the glass the transition (or simply "peak area") it is implied that this is a reasonable indication of true state of physical aging in the material for *the purposes of this particular study.*

As shown in Figure 5-13a, the endothermic peak area decreases linearly with dose for PS. Assuming that the radiation chemistry does not change with dose (which is a reasonably good assumption for PS since it is quite resistant to radiation induced changes in chemical structure), the amount of gas evolved will also vary linearly with dose. Hence, the results in Figure 5-13a support the postulated mechanism for "deaging".

PMMA also displays a linear relationship between peak area and dose. However, there is a sharp decrease in peak area up to 1 megarad before the linearity is established (see Figure 5-13b). This sharp decrease in peak area between 0 and 1 megarads may be the result of the consumption of highly reactive groups (possibly end groups) at low doses in PMMA which liberate larger amounts of gas than the rest of the polymer. Once these reactive sites are consumed, the radiation chemistry of the system will change. Hence, the G-value for gas evolution may decrease and

(a)

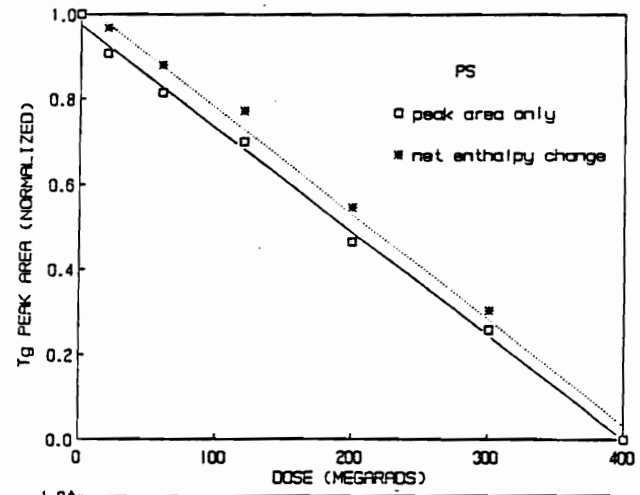

(b)

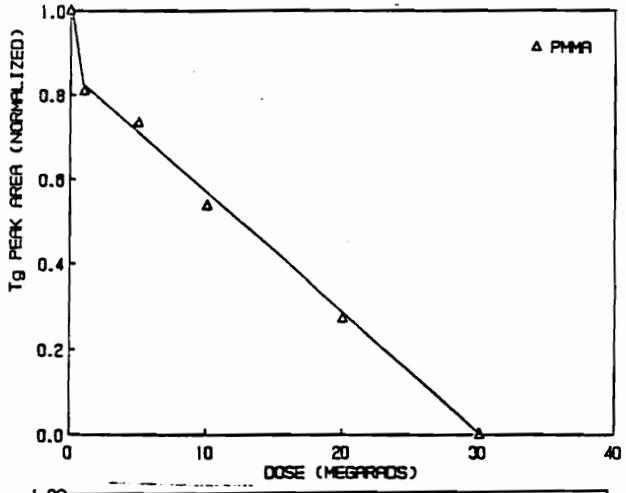

(c)

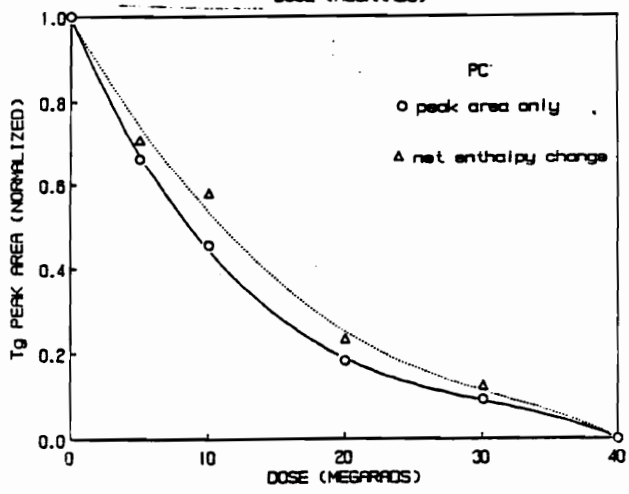

Figure 5-13a-c. Plots of endothermic peak area versus dose for (a) PS, (b) PMMA and (c) PC.

remain constant above a threshold dose (i.e. less than 1 megarad), which is consistent with the behavior displayed in Figure 5-13b. This hypothesis could be verified by comparing the deaging behavior of a series of PMMA with varying molecular weight and corresponding end group concentrations.

PC shows significant non-linearity in the plot of endothermic peak area versus dose (see Figure 5-13c). At low doses (10 megarads or less) the rate of area decrease is much faster than at higher doses. In fact, it appears as if there are two different regimes; a linear region with a high negative slope up to 10 megarads, and another linear region with a much lower slope beginning at 20 megarads. This behavior may have several origins. First, it has been shown (14) that PC undergoes simultaneous crosslinking and chain scission with the former predominating at low doses and the latter predominating at higher doses, which is unique to PC compared to the other polymers studied in this work, as previously mentioned. Hence, the radiation chemistry of PC varies with absorbed dose and therefore it is highly likely that the G-value for gas evolution varies with dose as well. Furthermore, for a particular polymer, it would be expected that more gaseous products would result from crosslinking than chain scission since abstraction of pendant groups (i.e. hydrogen) would be necessary to create a site for crosslinking, as opposed to chain scission. This is a speculation of course, because unfortunately there is relatively very little reported work on the radiation chemistry of polycarbonate. It should be noted

here that this is not the result of dose rate effects, which will be discussed in the next section.

Another possible explanation for the non-linearity in Figure 5-13c is related to gas permeation. It has been shown that physical aging can reduce the permeability of gases in glassy polymers. Hence, as the dose is increased and more "deaging" occurs, the permeability of the gaseous products increases. This could decrease the efficiency of the deaging process since gas could diffuse out of the glass more readily. This would result in a lower internal pressure increase during the evolution of gas which could cause a decrease in the amount of volume expansion. However, the non-linearity displayed in Figure 5-13c is not characteristic of PS or PMMA, and one would expect this proposed phenomena to affect all glasses, although the extent may be material dependent.

An interesting comparison to make in Figure 5-13 is the relative rates of peak area loss with increasing dose. PMMA is the most sensitive (30 megarads to completely reverse the physical aging), PC is slightly less sensitive (40 megarads), and PS is quite resistant to peak area loss (400 megarads). The general radiation resistance of these polymers (which is indicative of the rate of chemical change and hence gas evolution) follows the same trend and relative magnitudes (15). A more quantitative comparison would be to examine the relative differences in slopes in Figure 5-13 and compare them to the G-values for gas evolution of the polymers. Unfortunately, no G(gas) values for PC are available, but this analysis can be made

for PMMA and PS. The G-values that will be used were obtained by gamma irradiation under inert atmosphere at ambient conditions, which closely approximates the radiation conditions in this study. Although this study employs a much greater dose rate, G(gas) values have been shown to be independent of this parameter (17). The ratio of the slopes in Figure 5-13a&b is about 10:1, which corresponds to the ratio of the rate of peak area loss of PMMA to PS. (It is interesting to note that this is about the same ratio obtained for creep rates obtained on these two polymers during irradiation as reviewed in chapter 2 (see page 85). The ratio of G(gas) values for these to polymers is about 19:1 (see Table 5.1 for actual values). While these two ratios are in the same range, the agreement is not that good. However, there are two points which need to be considered. First, as previously discussed, the permeability of the polymer may affect the rate of deaging. However, the permeation coefficients of gases for PMMA in general are much less than for PS (see Table 5-1). If permeation of the material is an important variable in this behavior one would expect the ratio of G-values to be *less than* the ratio of slopes in Figure 5-13 for reasons given earlier. Since this is not the case, it seems that permeability may not be an important issue.

A second point to consider is what gases are being produced during irradiation of PS and PMMA. Irradiation of PS is known to result primarily in the production of hydrogen, while irradiation of PMMA results in the production of a variety of gases including hydrogen, carbon monoxide and dioxide, methane, and other gases.

Table 5-1. Some physical properties of the polymeric glasses used in this study.

POLYMER	WEIGHT AVE. MOLECULAR WEIGHT	PERMEATION COEFFICIENT OF O_2 {cm^2/s cmHg)[16**]	G-VALUES[16*]
PS	300,000 (M_w/M_n = 2.5)	1.9	G(GAS) = 0.08 $G(H_2)$ = 0.033
PMMA	170,000 (M_w/M_n = 2.0)	0.116	G(GAS) = 1.5 $G(H_2)$ = 0.3
PC	45,000 (M_w/M_n = 3.4)	1.05	N/A

* values obtained by gamma irradiation under inert atmosphere at ambient pressure and temperature

** values obtained at 25°C

As reviewed in the introduction, physical aging affects the permeation of lower molecular weight gases more so than higher molecular weight gases. It can therefore be speculated that the production of very low molecular weight gases may affect the "deaging" process more so than the production of higher molecular weight gases. In fact, the ratio of $G(H_2)$ values for PMMA and PS is 10.3:1, which is in excellent agreement with the slope ratios in Figure 5-13 for these two polymers.

5.3.2 Effects of Dose Rate.

To this point, only the effect of total dose on the endothermic peak area at the glass transition has been considered. It has been well established how the peak areas decrease with increasing dose. Furthermore, the behavior displayed by the glassy polymers considered can be explained by the hypothesis relating this "deaging" process to gas evolution. Discussion will now turn to the effects of dose rate at a constant total dose on the peak area loss of PS, PMMA, and PC. Before proceeding, the term dose rate as it will be used in this context should be clarified. As it applies to the electron beam source used in this study, the term dose rate describes the total dose a film is exposed to in a single pass under the electron beam. For example, " X megarads/pass" implies that the sample was exposed to X megarads in a few seconds under a nitrogen atmosphere before being removed from the conveyor system, exposed to air, and returned to the conveyor entrance for the next pass. Up to this point, all glassy films were exposed at a dose rate of 10 megarads/pass for

total doses of 10 megarads or more. For total doses less than 10 megarads, the indicated dose was given in a single pass.

Figure 5-14 illustrates the effect of dose rate on the endothermic peak area at the glass transition of PS for a total dose of 120 megarads. As shown, there is virtually no difference in the DSC behavior for films exposed at 5 megarads/pass and 10 megarads/pass. This is to be expected based on the proposed "deaging" mechanism because it is well known that gas evolution is generally not dose rate dependent. However, at 20 megarads/pass the endothermic peak has completely diminished. It is highly likely that this is due to thermal heating by the electron beam to some temperature above the glass transition. To illustrate this, consider that PS has a heat capacity of 1.2 J/(gr K). It should also be noted that 1 megarad is equivalent to 10 J/gr of energy. If no heat transfer effects are considered, the absorption of 20 megarads in less than several seconds will theoretically result in a temperature increase of 166 K if all of the beam energy is converted into heat. Of course, in a real system, heat transfer effects would be operative and there may not be 100 % conversion of beam energy to heat, so the temperature rise would be less than 166 K. Even so, after six consecutive passes (to achieve a 120 megarad dose) an organic glass such as PS could easily reach a maximum temperature above 105°C (T_g of PS). Hence, it is most probable that the elimination of the endothermic peak at a dose rate of 20 megarads/pass to a dose of 120 megarads is the result of thermal heating above the glass transition of PS.

Figure 5-15 illustrates the effect of dose rate on the peak area of PMMA at a total dose of 20 megarads. This series of DSC scans indicates that there is no effect of dose rate on the extent of deaging in PMMA over the dose rate range considered. Again, this is to be expected based on the postulated deaging mechanism since gas evolution is generally known to be independent of dose rate.

Figure 5-16 depicts a series of DSC scans of aged PC irradiated to 20 megarads for the dose rates indicated. As shown, there does appear to be a substantial influence of dose rate on the extent of peak area loss at this dose. As the dose rate is increased from 2 to 10 megarads/pass the extent of peak area loss increases. There does not seem to be any difference between dose rates of 10 and 20 megarads. This behavior indicates that "deaging" mechanism becomes more efficient as the dose rate increases from 2 to 10 megarads/pass. This behavior can be explained by the following hypothesis, which is consistent with the postulated "deaging" mechanism.

Since PC is fairly permeable (especially compared to PMMA), gases may be diffusing out of the glass between passes at the low dose rates. Hence, the lost gas would have to be replaced by fresh gas before any further increase in free volume could take place. At a relatively high dose rate, the total gas production is almost instantaneous, so there is dramatically less time available for gaseous diffusion out of the film and the free volume increase would be much more efficient.

This consideration may not apply to PMMA since it is much less permeable than PC (see Table 5-1), so there may not be a significant amount of gaseous diffusion out

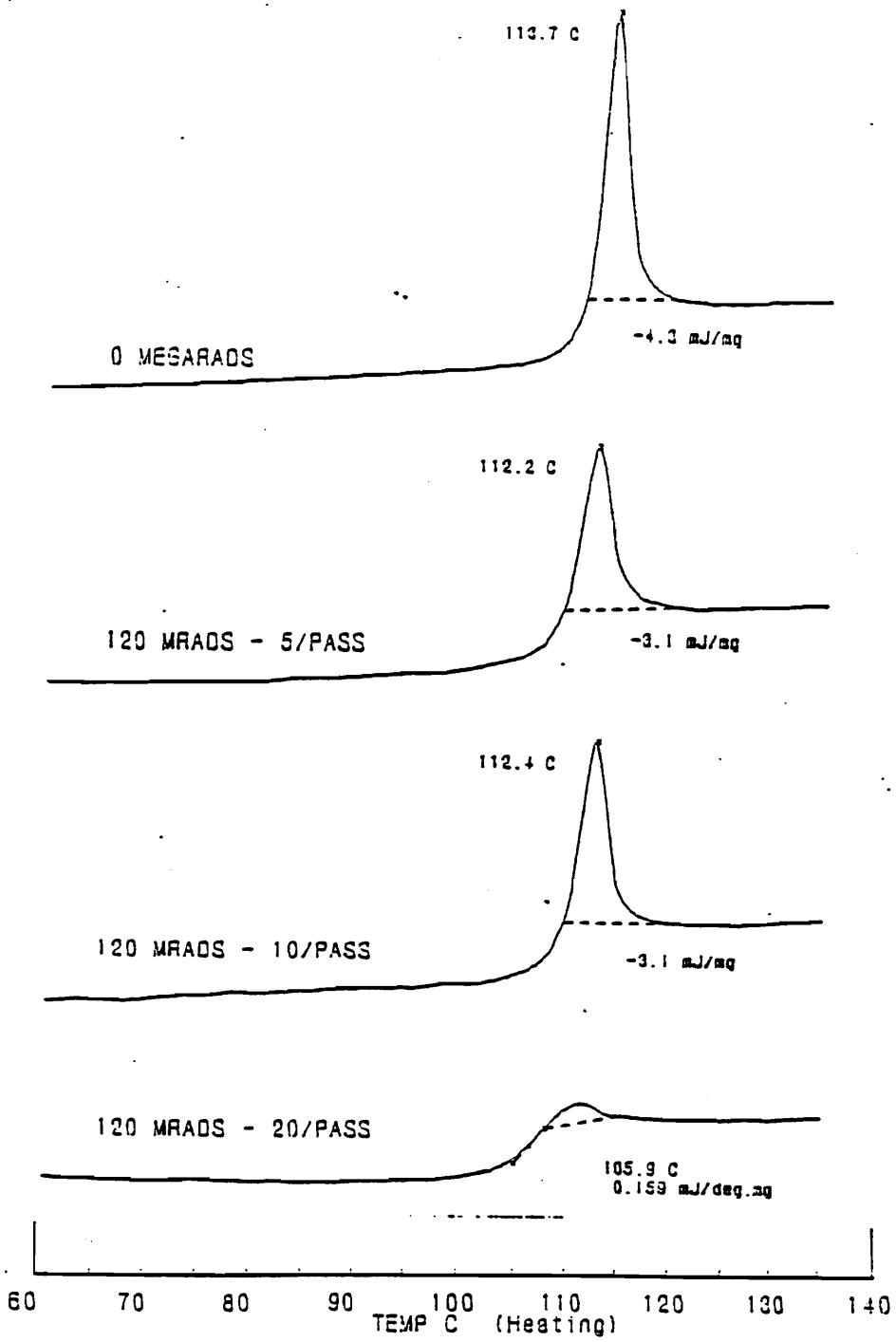

Figure 5-14. Effects of dose rate on the DSC scan of aged PS after exposure to a total dose of 120 megarads.

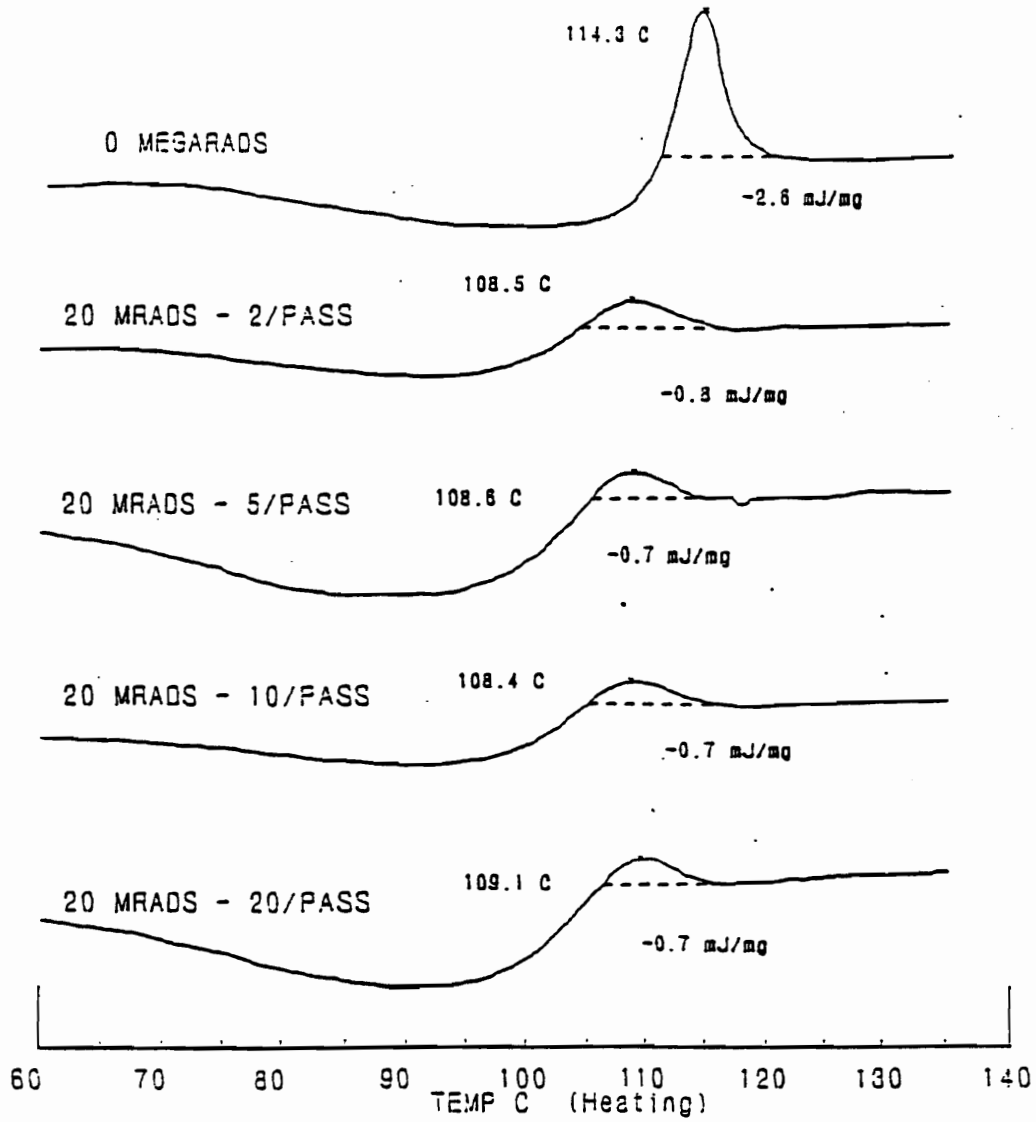

Figure 5-15. Effect of dose rate on the DSC scan of aged PMMA after exposure to the indicated dose/dose rate.

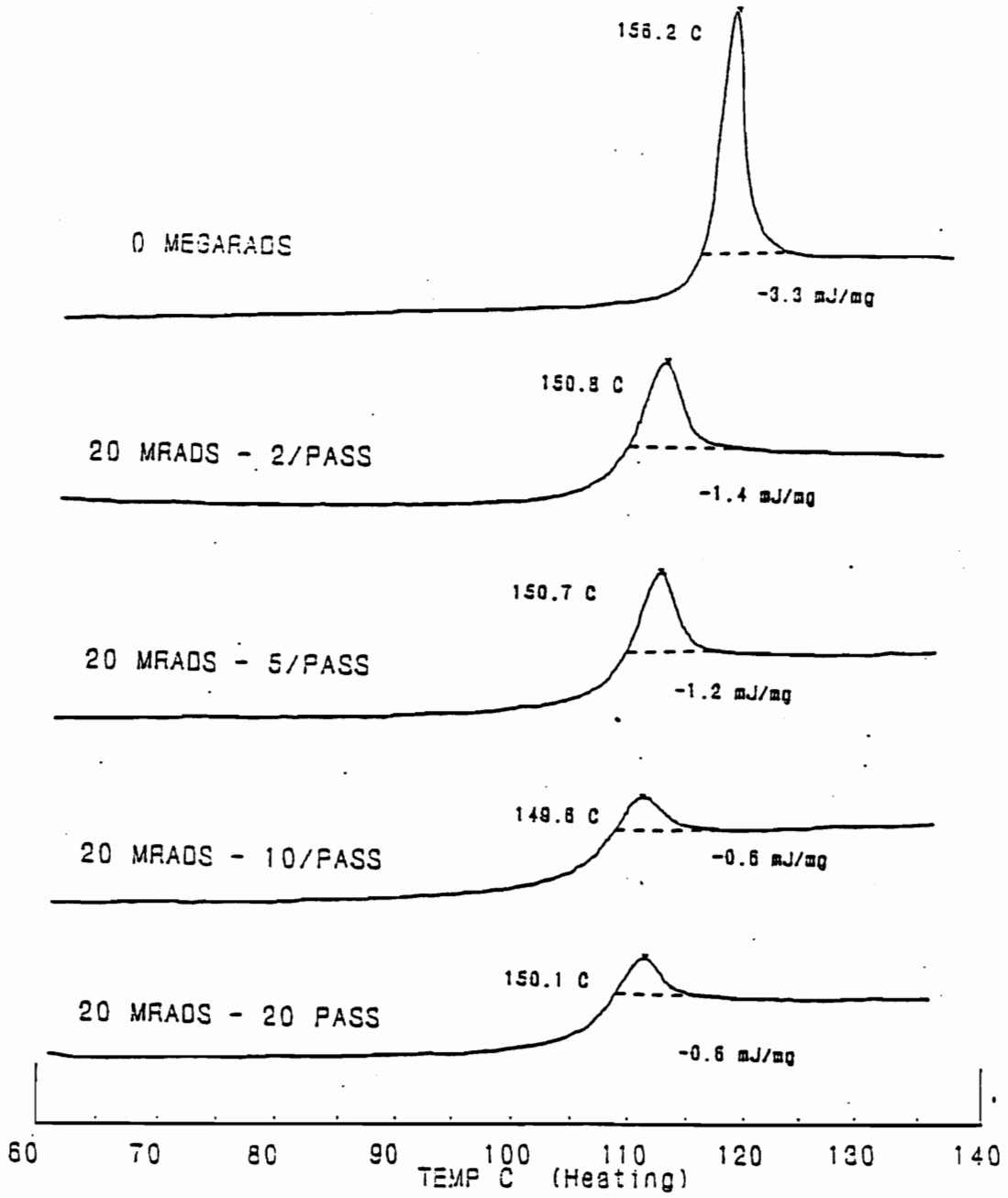

Figure 5-16. Effect of dose rate on the DSC scan of aged PC after exposure to the indicated dose.

of the film in the time frame of the radiation exposure. In, addition this may not apply to PS either, even though the permeability of PS is approximately the same as PC. Recall that PS has a much lower G(gas) value than PC so there will be much less gaseous products building up in the film with each pass. This would result in a much smaller driving force for diffusion of gas out of the film. Although more experiments would be necessary to confirm these arguments, the data shown is supportive and this hypothesis is consistent with the material properties and the overall "deaging" mechanism that has been proposed.

It should also be noted that the dose rate effects evident in PC would not explain the curvature in the peak area - dose plot of this polymer (see Figure 5-13c). Since lower dose rates decrease the extent of peak area loss, one would expect a lower rate of peak area loss at low doses compared to higher doses. However, the converse is displayed in Figure 5-13c, so dose rate effects would not be a important consideration.

The effects of dose rate that have been illustrated also indicate that this radiation induced "deaging" is not the result of thermal heating. Although it has been reported (6) that partial deaging can occur by subsequent heating above the previous aging temperature, this is not the case here. If thermal mechanisms were operative here, there would be a strong influence of dose rate since this parameter determines the temperature rise during irradiation. It should be noted that there are tremendous differences in the temperature rise during processing in the dose rate range of 2

megarads/pass (up to 10°C/pass) to 20 megarads/pass (up to 100 °C/pass). However, there was very little effect of dose rate on PMMA and PS, and one would expect these glasses to be more sensitive than PC to heat effects since they have a much lower glass transition temperature. Furthermore, even though dose rate effects do exist for PC, thermal heating to temperatures above 120°C (aging temperature of PC) are not possible at the dose rates and total dose indicated in Figure 5-16.

5.3.3 Effects on Mechanical Properties.

Since it has been established that irradiation of aged polymeric glasses results in deaging as determined by DSC, it would be worthwhile to establish the occurrence of deaging by another technique. Since it is well known that mechanical properties are influenced by physical aging, the effects of aging and irradiation on the stress - strain behavior of PC have been determined. In fact, mechanical property measurements may give a better indication of physical aging than DSC, since a direct measure of relaxation times in polymeric glasses can be obtained. The yield stress is the most sensitive parameter to physical aging that can be obtained from stress - strain measurements, so an analysis of the effects of aging and irradiation on this variable has been made.

Figure 5-17 and Figure 5-18 illustrate the stress - strain response of quenched and aged PC (respectively) both before and after exposure to 60 megarads. The thermal behavior of the aged PC is shown in Figure 5-12. As shown in Figure 5-12, a 60 megarad dose is sufficient to completely erase the physical aging of PC as determined

(a)

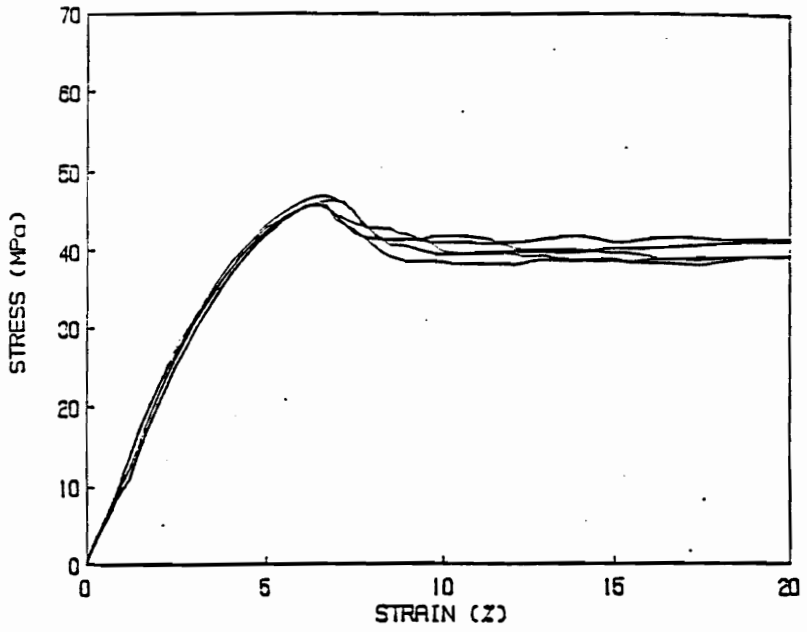

(b)

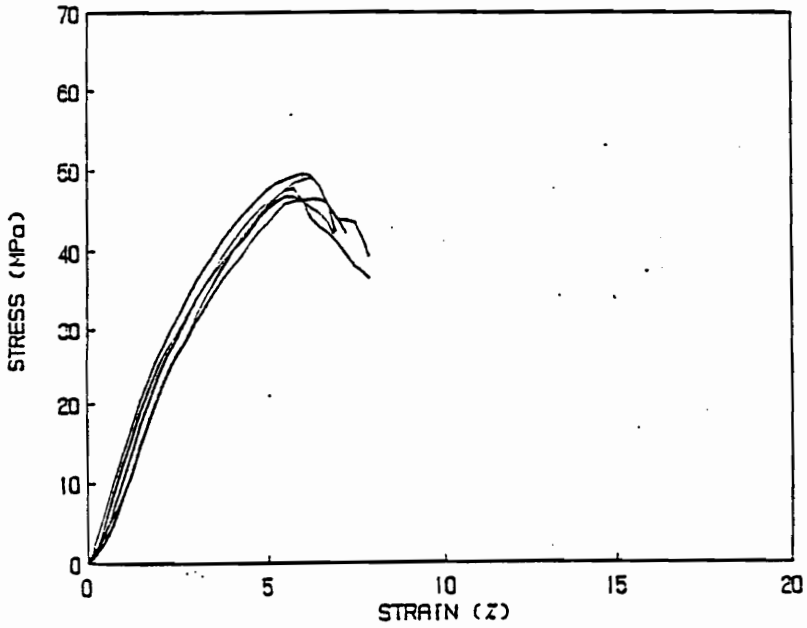

Figure 5-17a&b. Stress strain curves of quenched PC both (a) before and (b) after exposure to 60 megarads.

(a)

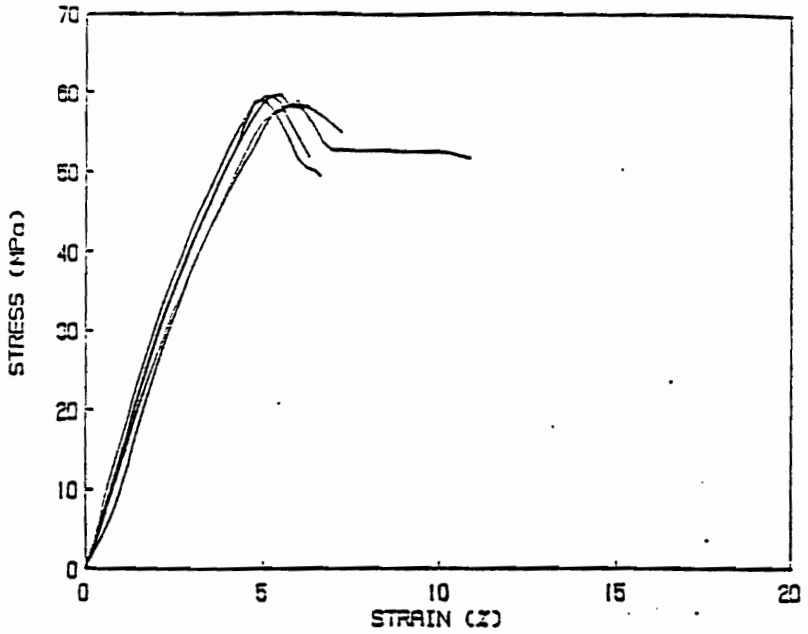

(b)

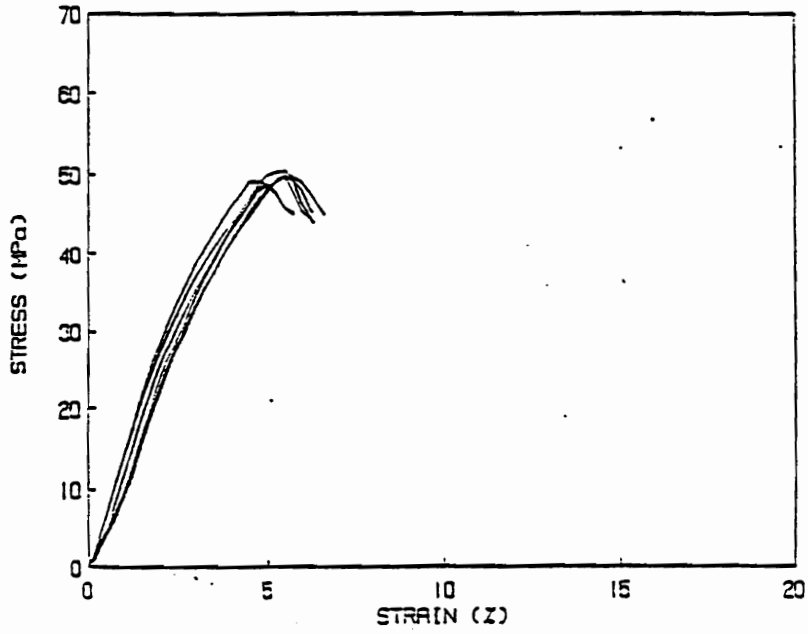

Figure 5-18a&b. Stress - strain curves of aged PC both (a) before and (b) after exposure to 60 megarads.

by the DSC. Figure 5-17 illustrates that exposure of the quenched PC film to 60 megarads results in a significant decrease in the strain at break and a very slight *increase* in the yield stress. These alterations of mechanical response is due to the radiation exposure and changes in molecular weight that result. As shown in Figure 5-18, irradiation of the aged PC film results in a significant *decrease* in the yield stress and very little (if any) change in the strain at break. The radiation induced decrease in the yield stress of only the aged glass indicates that deaging of the glass has indeed occurred. In fact, the stress - strain behavior of the quenched and aged PC films that have been irradiated are indistinguishable, which is consistent with the results obtained by DSC.

5.3.4 Effects of Aging and Irradiation

Up to this point, discussion has focused on establishing the existence of radiation induced "deaging" and some variables which may affect this behavior. The effects of this "deaging" on the subsequent *reaging* of these polymeric glasses will now be considered. In addition, possible effects of aging on the radiation induced changes in glassy polymers will also be briefly explored in this context.

Figures 19 - 21 show a series of DSC scans for various aging times of PS with the following respective histories: (1) quenched, (2) quenched, then exposure to 400 megarads, and (3) aged, then exposure to 400 megarads. As illustrated in these figures, the only noticeable difference among these specimens is the depressed T_g and an increased initial aging rate of sample (3). These differences are not large, but

they are worth noting. The lower T_g of the aged and irradiated specimen (sample (3)) could be due to a greater concentration of low molecular weight products in the glass that were produced during radiation exposure. Since this glass was aged prior to exposure, the lower free volume may have hindered the diffusivity of the low molecular weight products. Furthermore, physical aging has been shown to significantly increase the solubility of gases in glassy polymers (13). Both of these possibilities would result in a higher concentration of low molecular weight products in PS, thereby plasticizing the polymer and lowering the T_g. It should be noted however, that physical aging does not seem to affect the extent of radiation crosslinking in PS. As shown in Table 5-2, the quenched and aged PS have the same gel fraction after exposure to 400 megarads.

Figures 22 - 24 show the same series of DSC scans for PMMA as was just described for PS. Again, the respective sample histories are: (1) quenched, (2) quenched and exposed to 60 megarads, and (3) aged and exposed to 60 megarads. As depicted in these figures, the irradiated PMMA has a much faster aging rate than the unirradiated PMMA and ages to a much greater extent (as characterized by DSC). It is also interesting to note that while the peak area increases with aging time, the there is no upward shift in the peak temperature. As shown, the T_g of the irradiated glasses is more than 10°C lower than the unirradiated glass, which explains the accelerated aging behavior. The depressed T_g of the irradiated glasses is due to the degradation in molecular weight resulting from radiation exposure (see

Table 5-2. Effects of irradiation on the molecular weight of PMMA and the gel fraction of PS.

SAMPLE	M_n	M_w/M_n	GEL %
Quenched PMMA 0 megarads	87,000	2.0	--
Quenched PMMA 60 megarads	run1 15000 run2 20000	2.5 1.8	--
Aged PMMA 60 megarads	run1 18500 run2 23000	2.0 1.6	--
Quenched PS 400 megarads	--	--	64 ± 3
Aged PS 400 megarads	--	--	67 ± 3

Table 5-2). It should also be noted that there may be some small differences between the two irradiated glasses as well. It appears as though the quenched, irradiated PMMA ages slightly faster and has a slightly lower glass transition temperature then the aged, irradiated PMMA. The GPC results are consistent with this behavior as they indicate that the quenched PMMA has a somewhat lower molecular weight. It is also interesting to note that irradiation of this sample resulted in an increase in the polydispersity (M_w/M_n), while the polydispersity of the aged PMMA decreases (as compared to unirradiated PMMA). The reasons for this are not clear based on the data available, but a possible speculation could be that the lower free volume of the aged sample promotes more recombination of the scissioned chains (i.e. enhanced "cage effect") which would result in a higher molecular weight. In any case, the effects of aging on the extent of chain scission are not severe, but further experimentation is certainly warranted to make any firm conclusions and to obtain a better understanding of the role physical aging plays in the radiation induced chain scission of PMMA.

Figures 25 - 27 show similar series of DSC scans for PC as has been discussed for PS and PMMA. The radiation dose used on PC is the same as for PMMA (60 megarads). As shown, the rate of aging is significantly faster for the irradiated samples compared to the unirradiated PC. However, the total extent of aging as characterized by the endothermic peak area is about the same regardless of the history. Most of the aging in the irradiated PC takes place in the first two days while

aging progresses for 7 days in the unirradiated PC. It should be noted however, that aging likely continues for some time in both of these samples, but at a substantially slow rate (due to logarithmic dependence of aging with time) that it may not be observed by DSC in the time frame of this experiment. However, unlike PMMA, there appears to be little difference in the aging behavior of the quenched and aged PC that has been irradiated. Unfortunately, a molecular weight analysis could not be done on this polymer with the equipment available so any differences in molecular weight resulting from aging prior to irradiation could not be determined.

5.4 CONCLUSIONS

This work has illustrated that "deaging" of polymeric glasses can be facilitated by exposure of the glass to electron beam radiation. The extent of "deaging" is controlled by the exposure dose. Although it has not been definitively proved, all the data reported support the postulated "deaging" mechanism that involves an increase in free volume of the aged glass by radiation induced internal gas evolution. As has been illustrated, the relative rates of radiation induced "deaging" of PS, PC, and PMMA follow the same trends as the radiation sensitivity (and likely G(gas)) of these polymers. It was also shown how the dose rate can affect the deaging behavior. Furthermore, reaging of the deaged glasses was shown to be possible and this subsequent aging behavior was compared to the aging behavior of the unirradiated and irradiated *quenched* glasses. Some differences were found to exist among these various glasses which illustrate that changes in molecular weight and structure (due to radiation exposure) can alter the aging behavior of glasses. In addition, the last section has primarily illustrated that the rate and extent of aging can be significantly influenced by changes in molecular weight and structure. Furthermore, it has indicated that physical aging may influence the radiation induced changes in polymeric glasses, which to date, has not been considered in the literature.

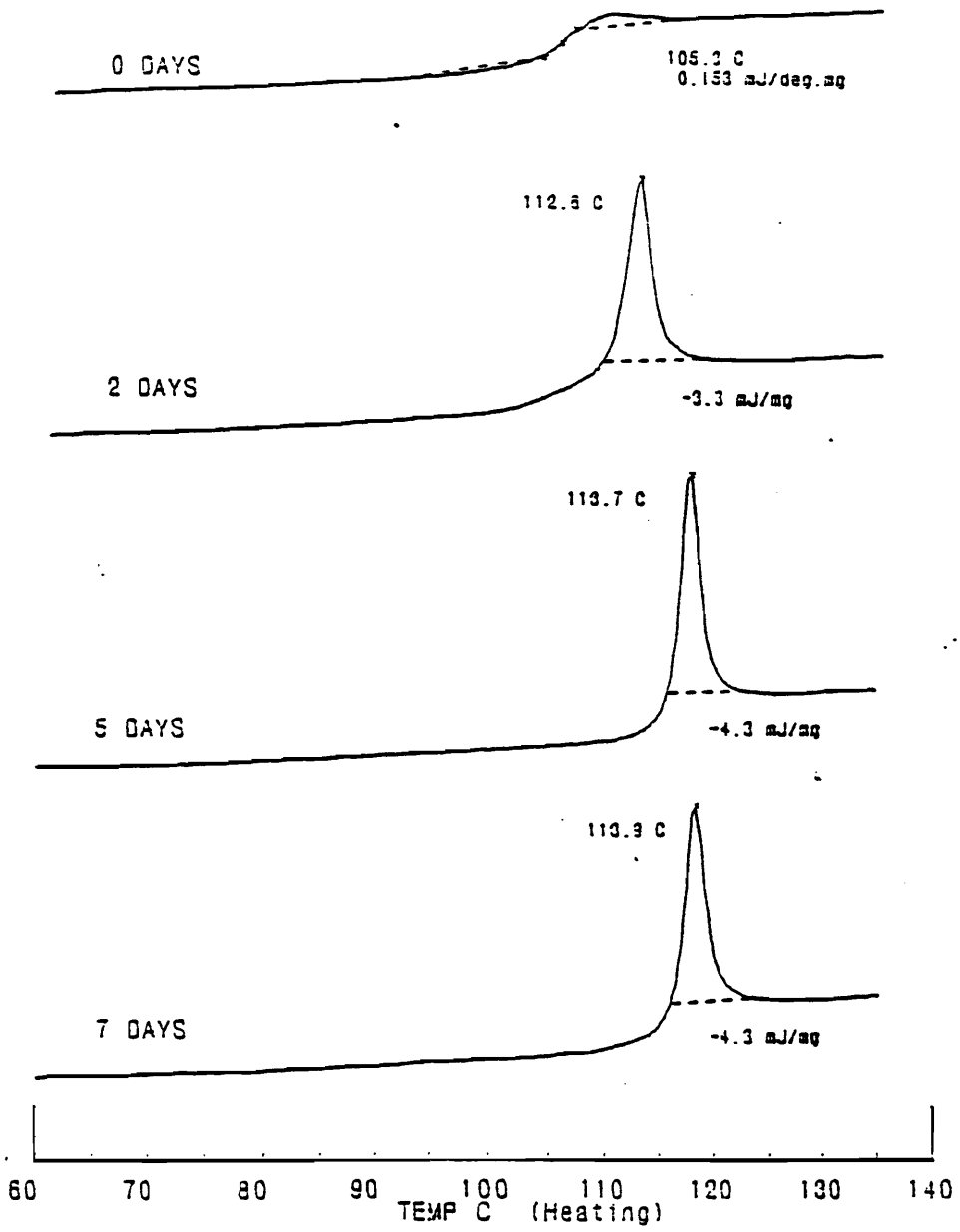

Figure 5-19. DSC scans of quenched PS after the indicated aging times at 80°C.

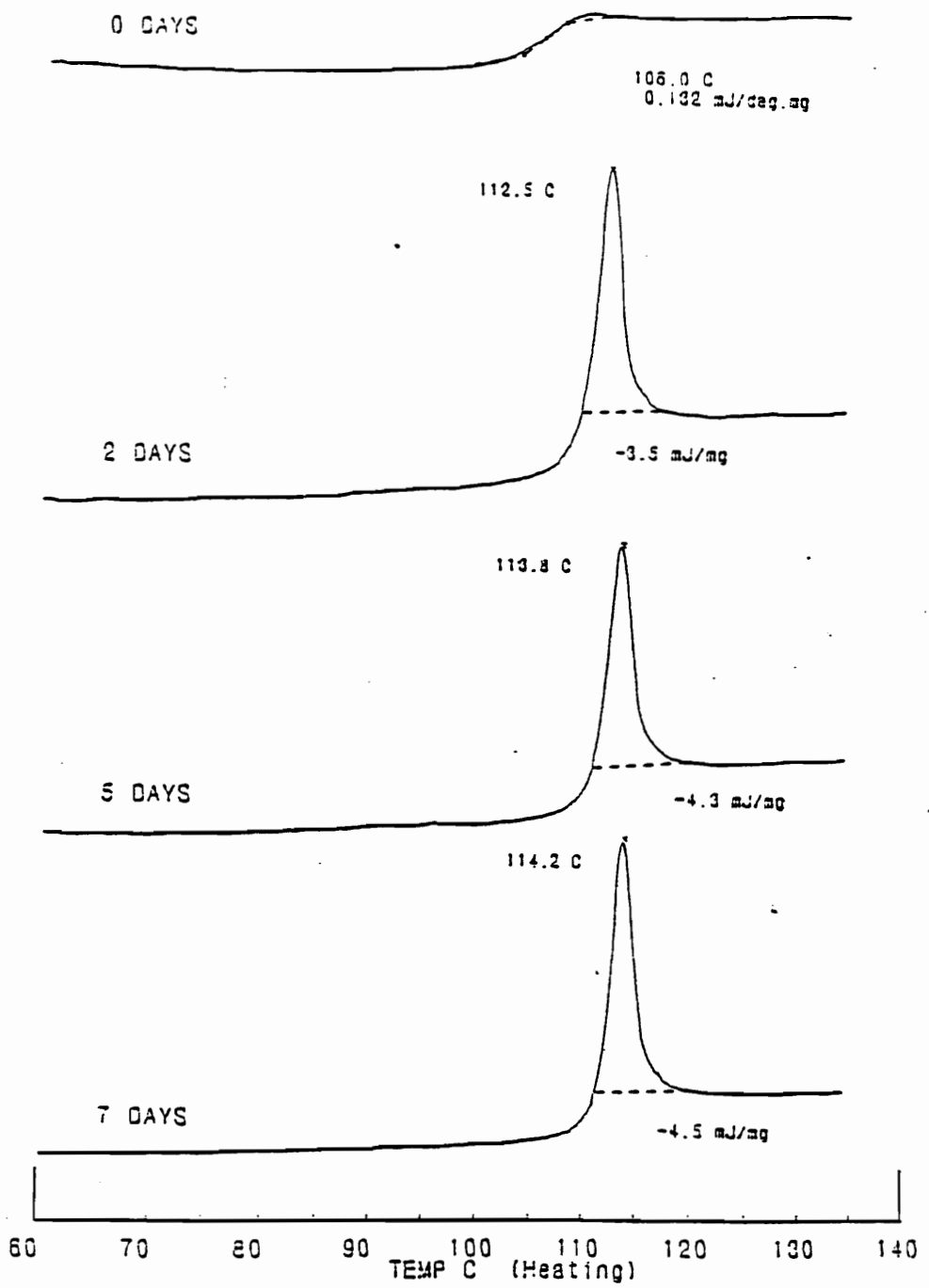

Figure 5-20. DSC scans of quenched PS that has been exposed to 400 megarads after aging for the indicated times at 80°C.

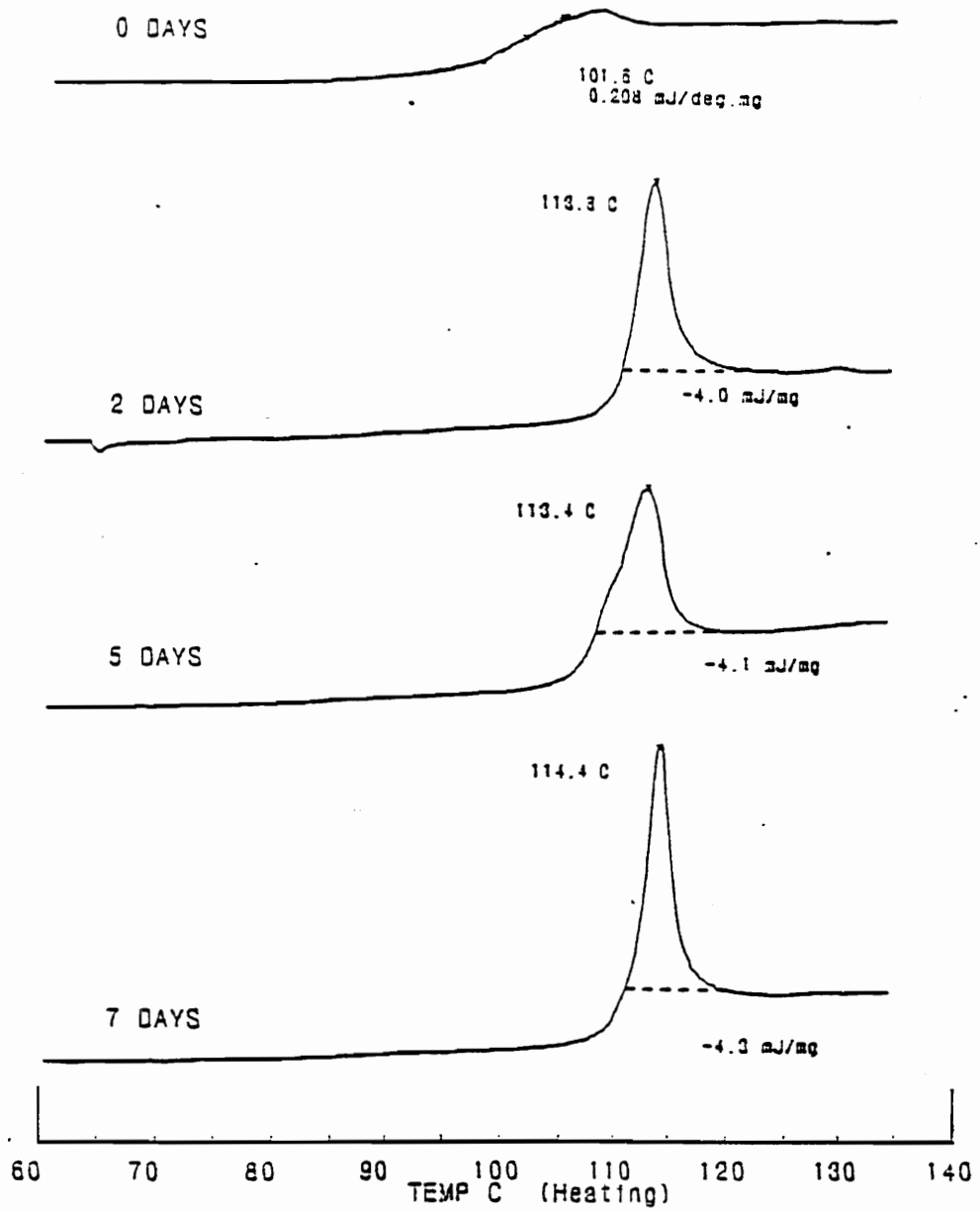

Figure 5-21. DSC scans at various times of aging at 80°C of aged PS that has been exposed to 400 megarads.

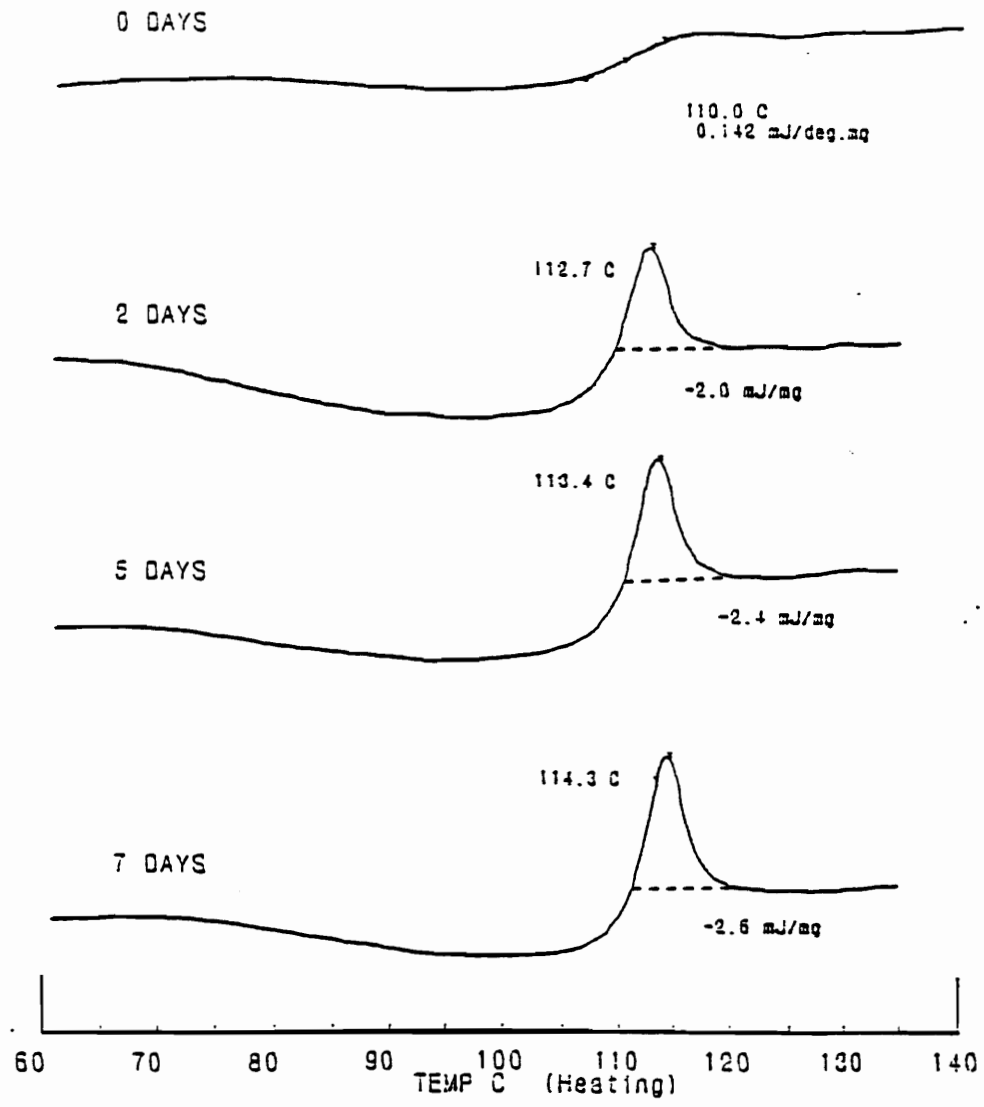

Figure 5-22. DSC scans after aging for the indicated times at 80°C of quenched PMMA.

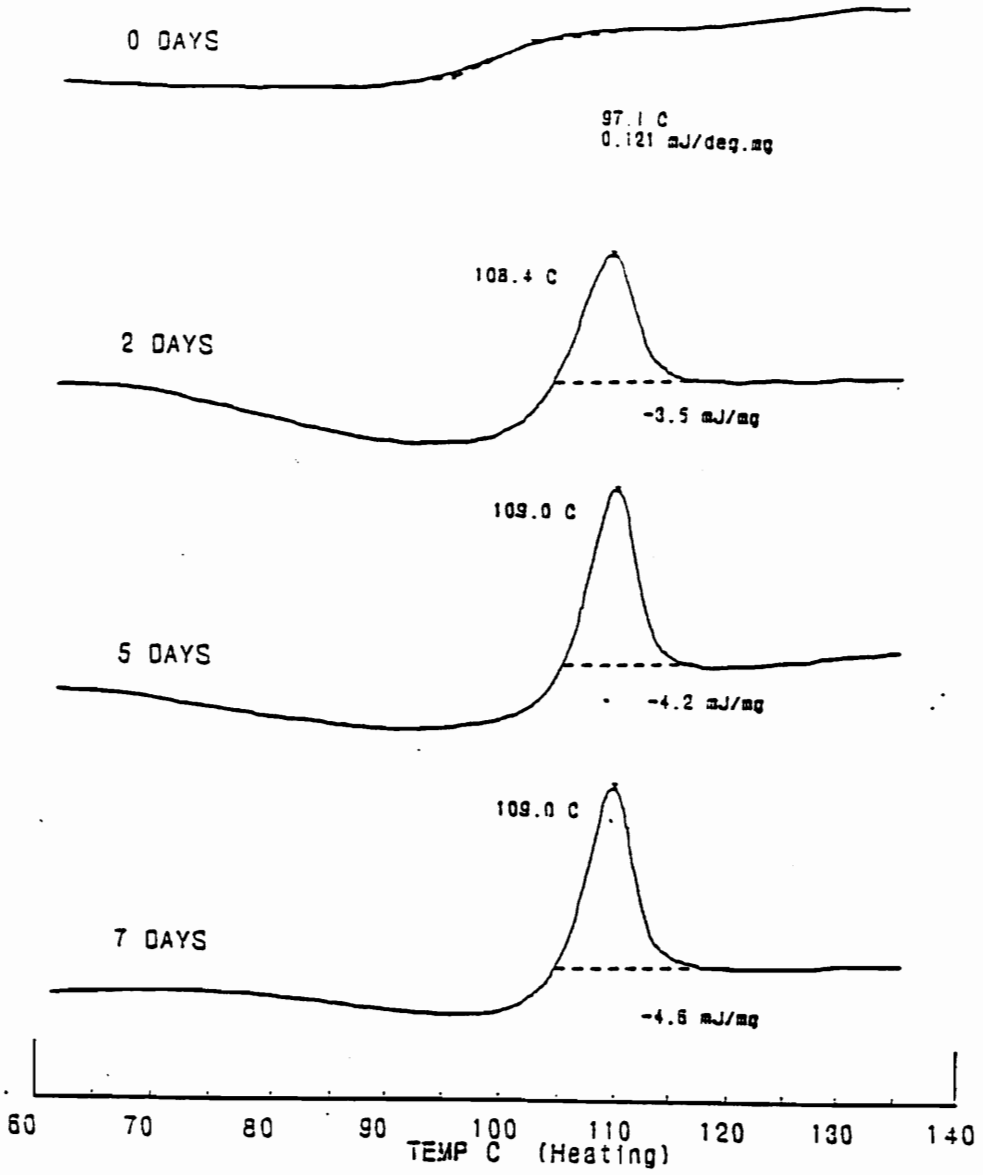

Figure 5-23. DSC scans after various aging times at 80°C of quenched PMMA that has been exposed to 60 megarads.

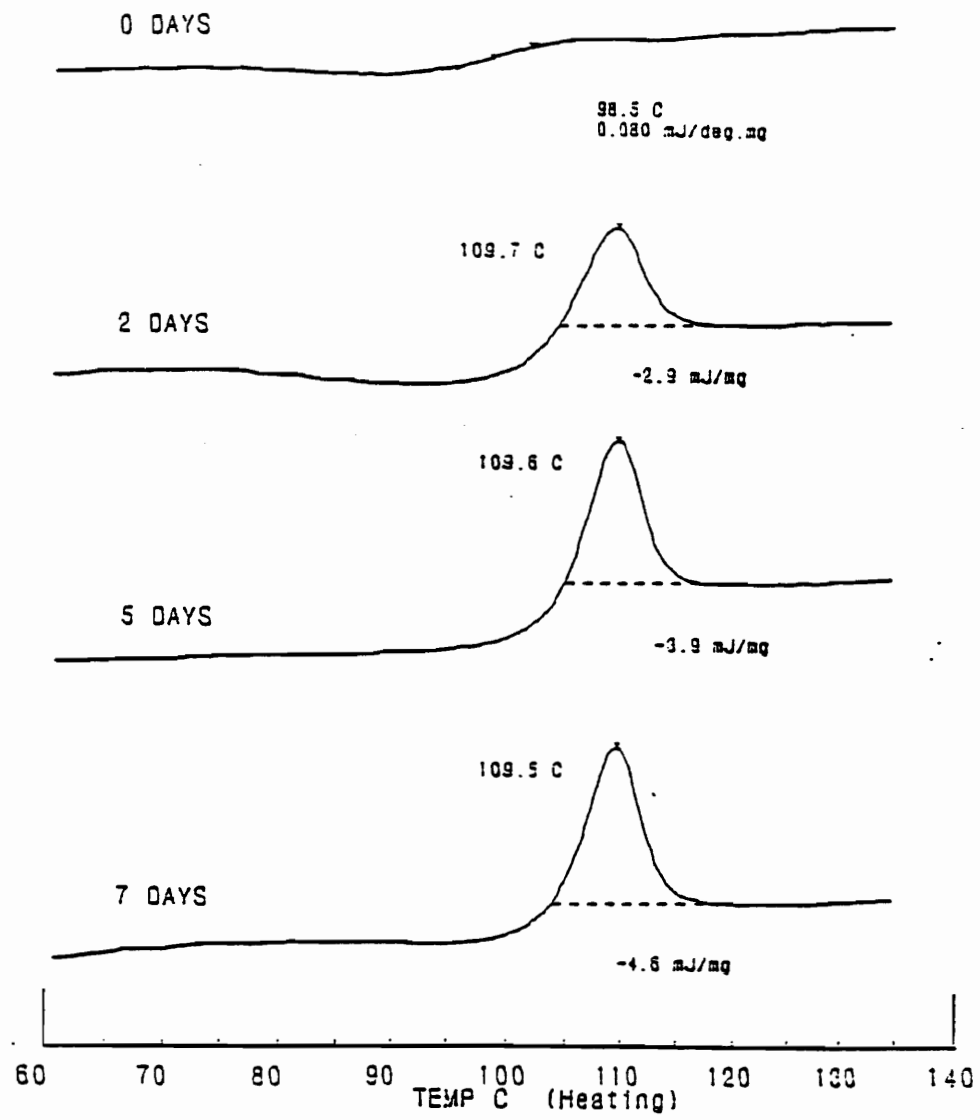

Figure 5-24. DSC scans after various aging times at 80°C of aged PMMA that has been exposed to 60 megarads.

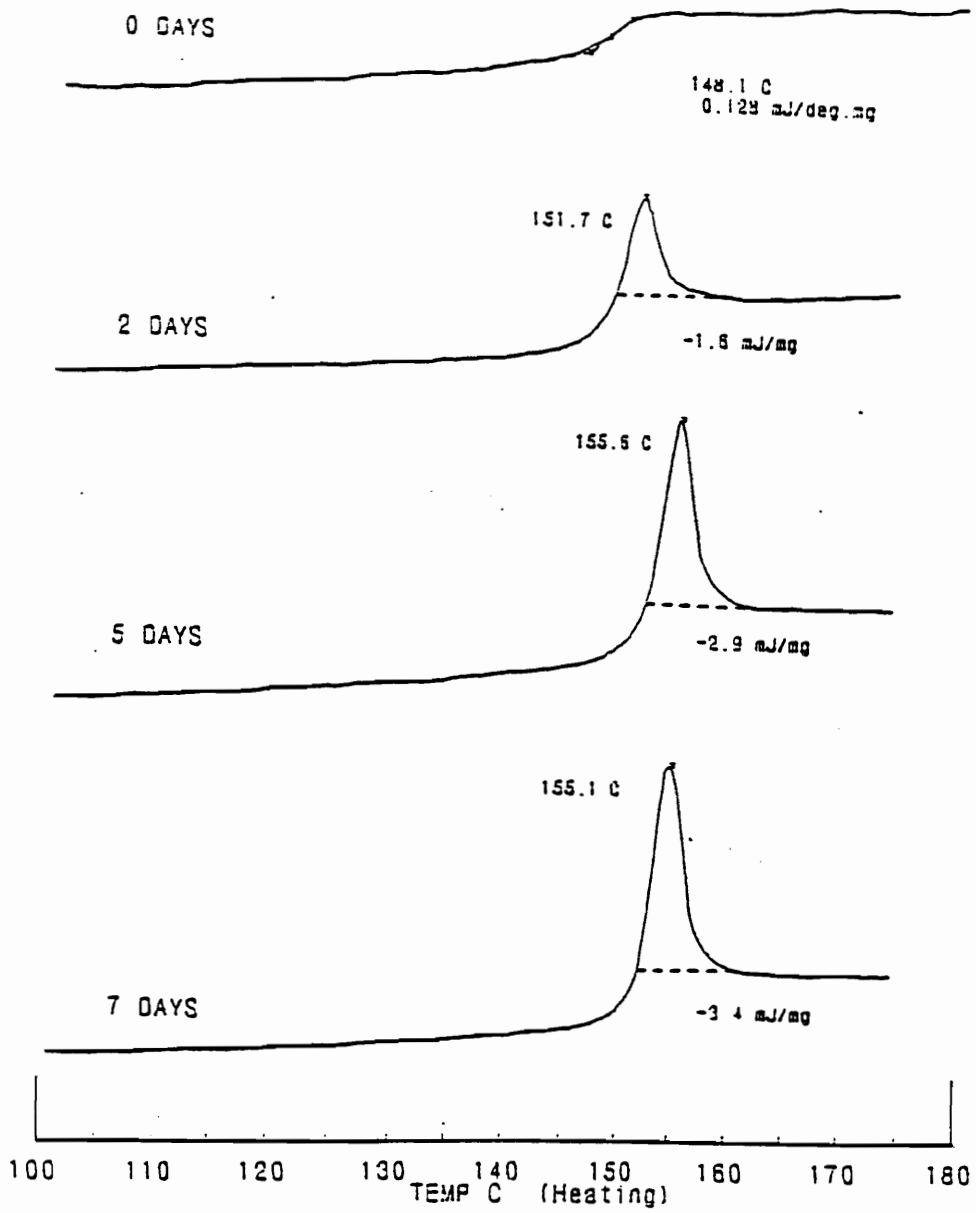

Figure 5-25. DSC scans for various aging times at 120°C of quenched PC.

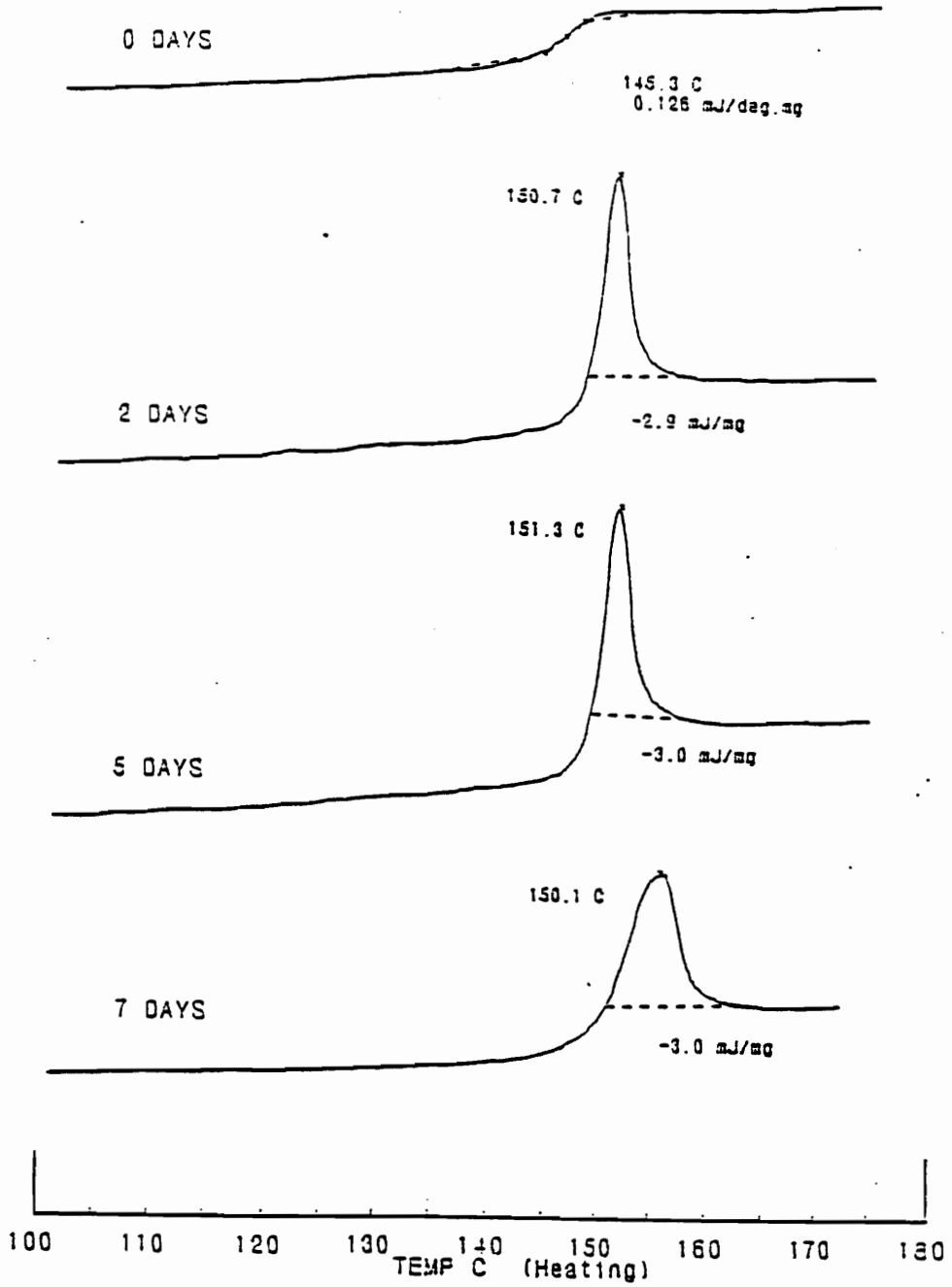

Figure 5-26. DSC scans after various aging times at 120°C of quenched PC that has been exposed to 60 megarads.

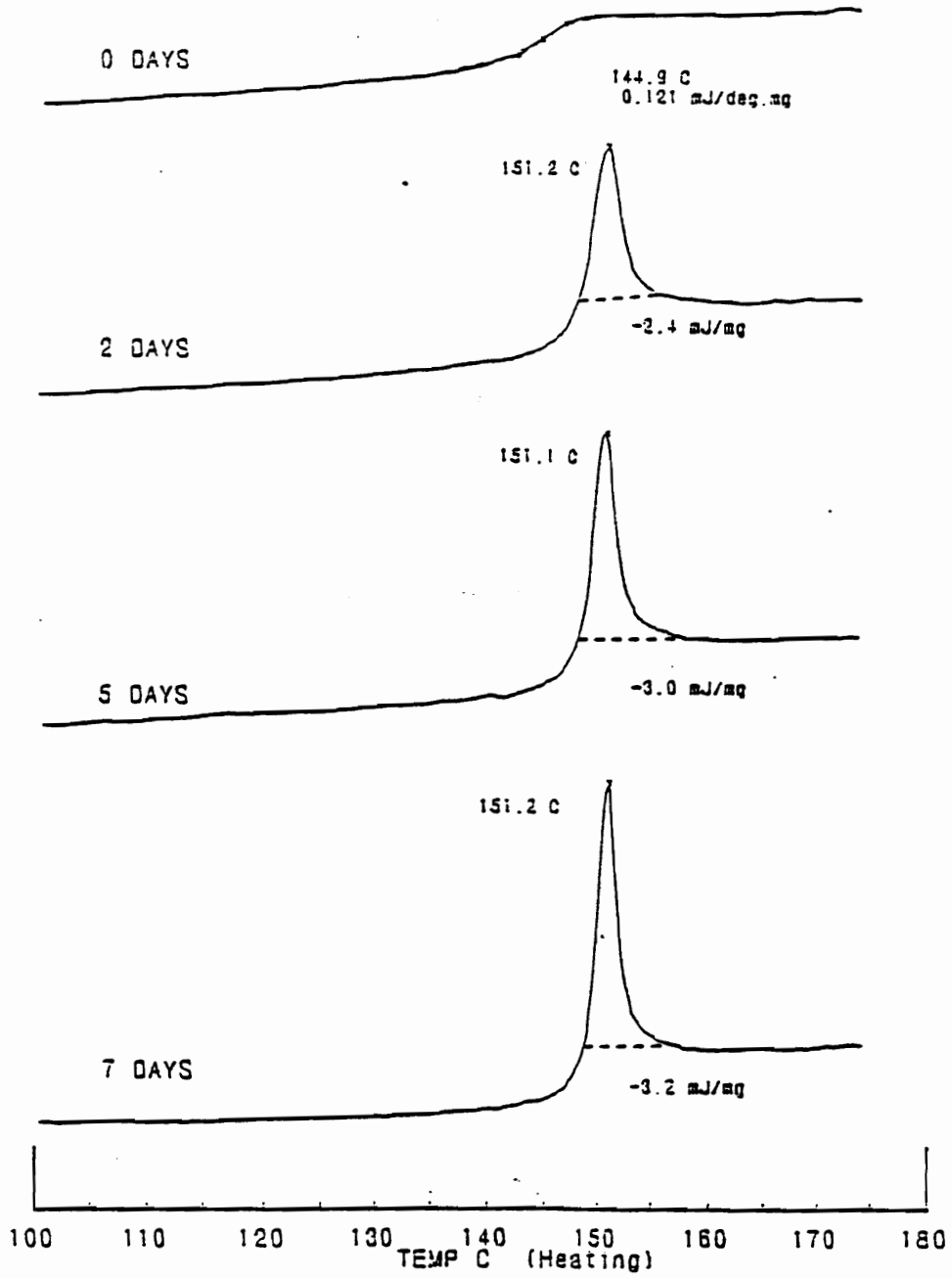

Figure 5-27. DSC scans after various aging times at 120°C of aged PC that has been exposed to 60 megarads.

5.5 REFERENCES

1. Kovacs, A.J. *J. Poly. Sci.,* 1958, **30**, 131.

2. Bartos, J.; Muller, J.; Wendorff, J.A. *Polymer,* 1990, **31**, 1678.

3. Petrie, S.E.B. in *Polymeric Materials,* American Society for Metals, Metals Park, OH, 1975.

4. Matsuoka, S.; Bair, H.E. *J. Appl. Phys.,* 1977, **48,** 4058.

5. Neki, K.; Geil, P.H. *J. Macromol. Sci. - Phys.*, 1973, **B8**, 295.

6. Struik, L.C.E. *Physical Aging in Amorphous Polymers and Other Materials,* Elsevier, New York, NY, 1978.

7. *Physical Structure of the Amorphous State*, Allen, G. and Petrie, S.E.B., editors, Marcel Dekker, New York, NY, 1977.

8. Tant, M.R.; Wilkes, G.L. *Polym. Eng. Sci.,* 1981, **21**, 874.

9. Struik, L.C.E. *Polym. Eng. Sci.,* 1977, **17**, 165.

10. Ricco, T.; Smith, T.L. *Polymer,* 1985, **26**, 1979.

11. Smith, T.L.; Levita, G.; Moonan, W.K. *J. Polym. Sci. Phys. Ed.,* 1988, **26**, 875.

12. Lee, W.M. *Org. Coat. Plast. Chem.,* 1978, **39**, 341.

13. Kapur, S.; Rogers, C.E. *J. Polym. Sci. Phys. Ed.*, 1972, **10,** 2107.

14. Acierno, D.; LaMantia, F.P.; Titomanlio, G. *Rad. Phys. Chem.,* 1980, **16**, 95.

15. Clough, R.L. in *Encycl. Polym. Sci. Eng.,* 2nd Ed., John Wiley and Sons, New York, NY, 1988, **13**, 667.

16. *Polymer Handbook,* 3rd edition, Brandrup, J. and Immergut, E.H., editors, John Wiley and Sons, New York, NY, 1989.

17. Charlesby, A. *Atomic Radiation and Polymers,* Pergamon Press, New York, NY, 1960.

CHAPTER VI

6.0 ELECTRON BEAM IRRADIATION OF POLYSTYRENE - POLY(VINYL METHYL ETHER) BLENDS

6.1 INTRODUCTION

This chapter describes the irradiation and characterization of polystyrene (PS) - poly(vinyl methyl ether) (PVME) blends. This particular polymer blend has been extensively studied and reported on in the literature, however, this chapter will deal with some aspects that have not yet been investigated. In particular, the effects of blend composition and state of miscibility on the radiation response of this system is considered. In addition, some properties of the irradiated blends are presented. Before detailing the experimental methods and results, some pertinent aspects of polymer blends will be discussed, especially with regard to PS-PVME blends. It is intended that this introductory discussion will provide a sufficient basis for understanding basic phase behavior in polymer blends and the experimental results that will be presented. Aspects of radiation chemistry has already been reviewed in chapter II of this dissertation.

PS-PVME blends are unique in that this particular system is among a fairly small group of polymer pairs that are chemically dissimilar yet display compatibility over the entire composition range at room temperature. However, phase separation can result if the temperature of the blend is raised above a critical value, which will depend on the specific characteristics of the blend and the blend components.

Before detailing the specific behavior of this particular system, some general comments on the phase behavior of polymer blends should be made. Discussion will be restricted to binary polymer blends only.

6.1.1 Phase Behavior of Binary Polymer Blends

Phase separation in polymer blends is possible when a reduction in the system free energy can be realized by the formation of two separate phases from a homogeneous single phase state. To illustrate this point, consider the diagrams depicted in Figure 6-1. These diagrams are plots of the change in Gibbs Free Energy of mixing (ΔG_m) as a function of blend composition. The change in Gibbs Free Energy of mixing is simply the free energy of the blend (G) relative to the free energy of the pure components (G°_i) (i.e. $\Delta G_m = G - \Sigma x_i G^\circ_i$). Figure 6-1a illustrates a possible free energy of mixing diagram for a polymer blend that is completely immiscible. From the second law of thermodynamics, it is known that equilibrium exists in a closed system when the total Gibbs Free Energy is at a minimum. Furthermore, for any process to occur spontaneously, the change in Gibbs Free Energy must be negative (i.e. for polymer blends, $d(\Delta G_m) < 0$) and the second partial derivative must be positive (i.e $\partial^2 \Delta G_m / \partial \phi^2 > 0$). The only condition in Figure 6-1a which satisfies the criteria for equilibrium is when both components are completely separated from each other. Any mixing will result in an increase in the free energy of the blend and hence will not occur. Figure 6-1b depicts a free energy of mixing diagram for a completely miscible blend. Demixing at any composition will

result in an increase in the free energy of at least one of the phases and therefore will not occur. Figure 6-1c illustrates a possible free energy of mixing diagram for a polymer blend which can undergo phase separation under proper conditions. In particular, if the blend composition is in the range between points A and B (see Figure 6-1c), then phase separation can occur and will result in the formation of two phases with compositions given by points A and B when the system is at equilibrium. Again, this process can occur because it results in a decrease in the total Gibbs Free Energy of the system. If the blend composition lies outside of the range between points A and B then phase separation cannot occur since it would result in an increase in free energy.

It is important to note that the free energy diagrams shown in Figure 6-1 assume constant pressure and temperature. If one considers how the free energy diagram for a blend system which can phase separate varies with temperature, then a phase diagram can be constructed. In particular, the effect of temperature on the shape of the curve in Figure 6-1c and the location of points A and B will determine the nature of the phase diagram. In fact, the cloud point curve (also known as the binodal line or equilibrium curve) in a phase diagram is a plot of the compositions corresponding to the minima points (i.e. A and B in Figure 6-1c) as a function of temperature. An example of a phase diagram is illustrated in Figure 6-2. Notice that two behaviors can exist: (1) phase separation is promoted by increasing the system temperature and (2) phase separation is promoted by decreasing the system

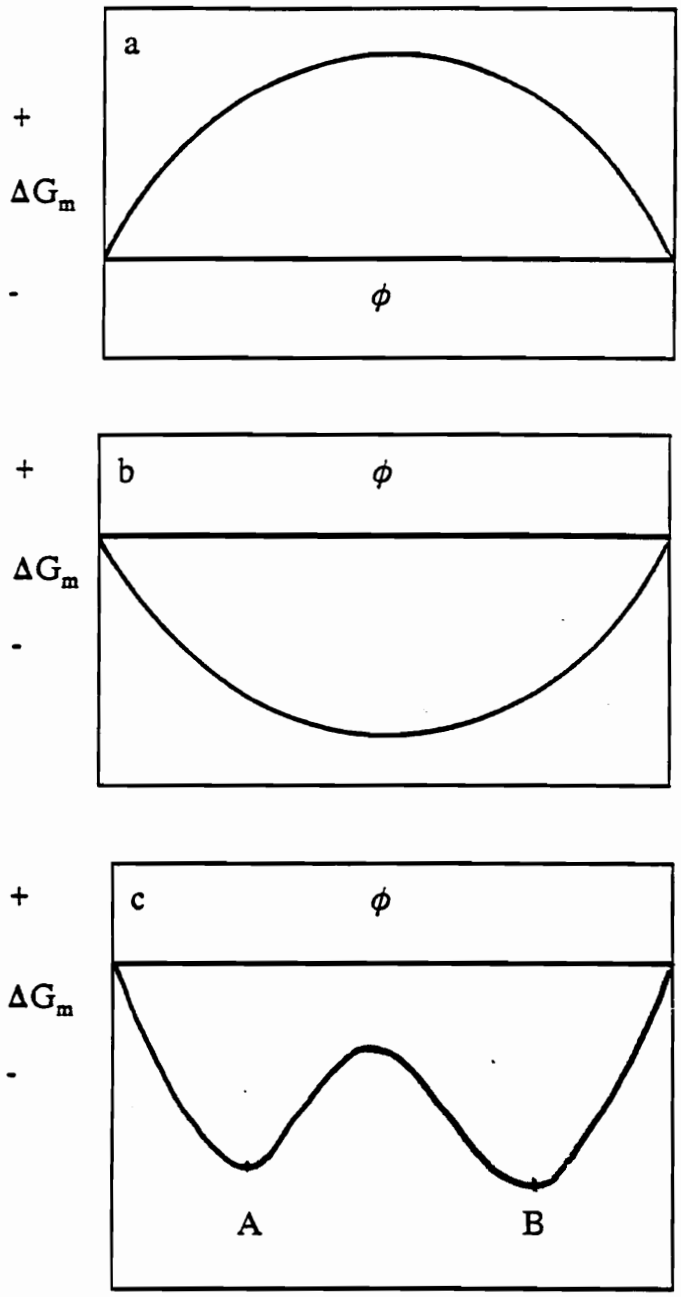

Figure 6-1a-c. Free energy diagrams of the partial molar change in free energy (ΔG_m) as a function of blend composition, ϕ, for (a) completely immiscible, (b) completely miscible, and (c) partly miscible polymer blends.

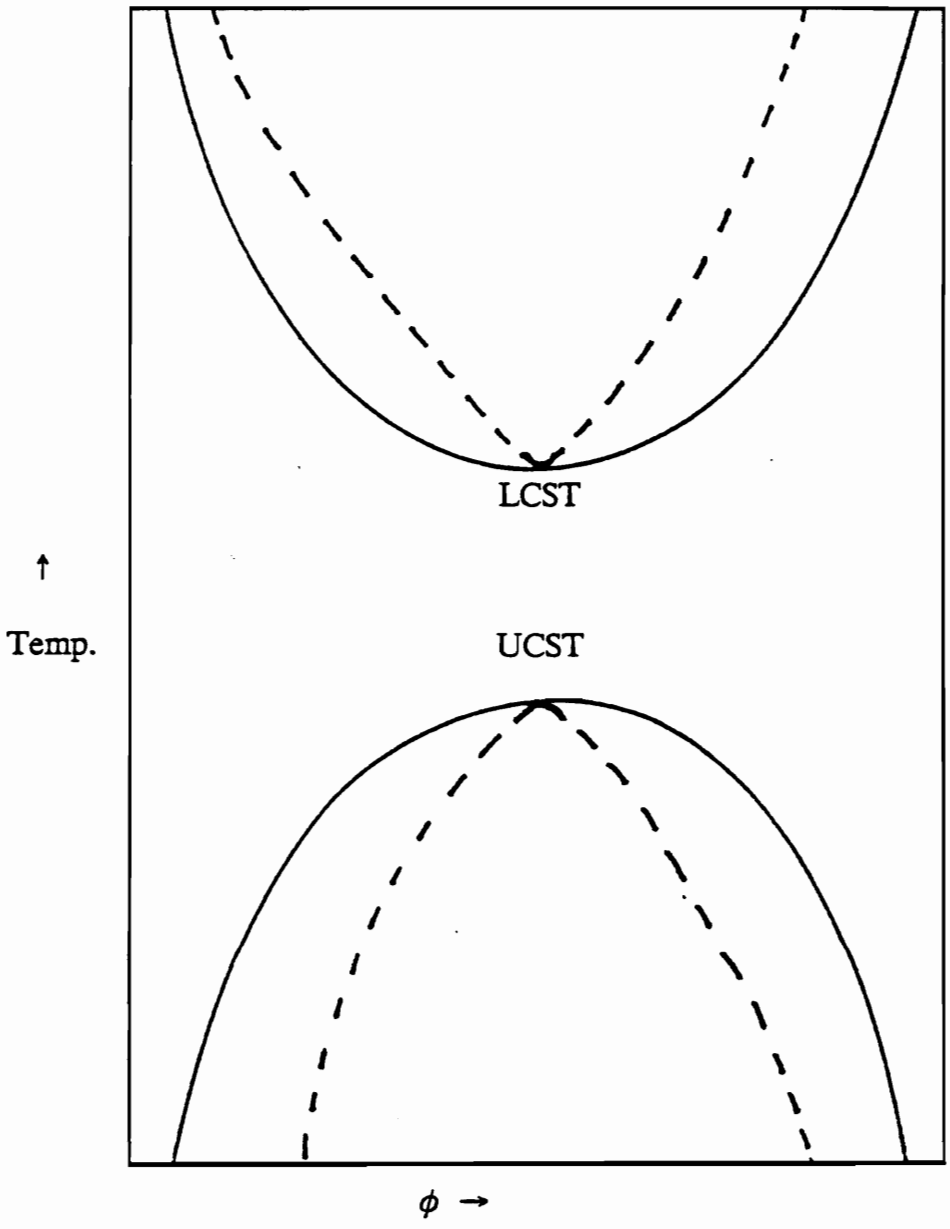

Figure 6-2. Example of a phase diagram for polymer blends which illustrates both LCST and UCST behavior. (-) - binodal line, and (--) - spinodal line.

temperature. These two possibilities have been termed lower critical solution temperature (LCST) and upper critical solution temperature (UCST) behavior, respectively. The occurrence of one behavior or the other (or both) depends on how the free energy diagram varies with temperature. If the shape of the free energy diagram depicted in Figure 6-1c changes toward the shape of the curve in Figure 6-1b with increasing temperature then UCST behavior will result. If increasing temperature results in the shape of the curve changing from Figure 6-1c to Figure 6-1a, then LCST behavior will result. It is important to realize however, that *both* behaviors can occur in one polymer-polymer system.

The dashed lines in Figure 6-2 represent the compositions corresponding to the inflection points between the two minima in Figure 6-1c as a function of temperature. The dashed lines are termed the spinodal lines and the solid lines are termed the binodal lines. These distinctions are important in that the binodal and spinodal lines represent boundaries between the stable and metastable states, and the metastable and unstable states, respectively. The region between the binodal and spinodal lines is termed the metastable region because the system must overcome a free energy barrier in order for phase separation to occur (see Figure 6-1c). No free energy barrier exists in the spinodal (unstable) region, and hence phase separation will occur spontaneously. Furthermore, the state of the blend system will determine the mode of phase separation. If the temperature and composition of the blend corresponds to the existence of a metastable state (i.e. a point between the binodal and spinodal

lines) then phase separation will proceed by a nucleation and growth mechanism. If the system is in a unstable state (i.e. a point within the spinodal lines) then phase separation will proceed by spinodal decomposition. The microstructures that develop as a result of these two phase separation mechanisms are contrasted in Figure 6-3. Nucleation and growth is characterized by the formation of a second phase that grows with time with no change in composition. On the other hand, spinodal decomposition proceeds by the spontaneous formation of two co-continuous phases which coarsen with time and is accompanied by changes in composition of the phases. This type of microstructure associated with spinodal decomposition has also been termed an interpentrating network (IPN). The initial size of periodicity, d (see Figure 6-3), of the spinodal structure is determined by the temperature at which phase separation occurs. As the system temperature becomes farther removed from the spinodal line temperature (at some given system composition), d decreases. Coarsening occurs over time because this minimizes the interfacial surface tension between the two phases through a reduction in interfacial area.

Much of the phenomena that has been discussed can be predicted from theory using the Flory-Huggins Model or the more recent Flory Equation of State Thermodynamic Model. Although both of these theories are based on the lattice model for solutions, the predictions of the Flory-Huggins model are somewhat limited as compared to the Equation of State Model, as will be discussed. Details of the theoretical developments will not be presented here, and the reader is referred

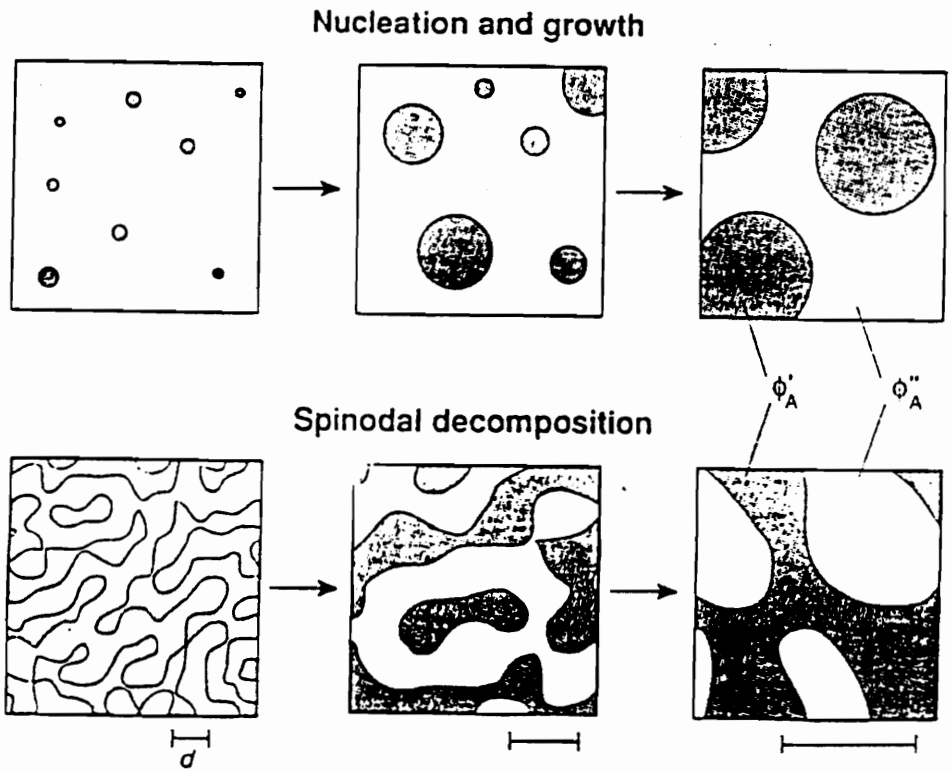

Figure 6-3. Diagram illustrating the microstructures developed during phase separation by (1) nucleation and growth and (2) spinodal decomposition mechanisms. (ref. 1)

to several books and papers on the subject (2-4). The development of the Flory-Huggins theory gives the following result for ΔG_m:

$$\begin{aligned} \Delta G_m &= \Delta H_m - T\Delta S_m \\ &= RT(N\phi_1\phi_2\chi_{12} + (x_1 \ln\phi_1 + x_2 \ln\phi_2)) \end{aligned} \qquad [47]$$

where:

R = gas constant
T = temperature
N = # of lattice sites in system
ϕ_i = volume fraction of species i
x_i = mole fraction of species i
χ_{12} = interaction parameter

The first term on the right hand side of eq. (1) is the contribution from the enthalpy of mixing and it can be positive or negative. The log terms in parenthesis is the contribution from the entropy of mixing and it is always negative (the log of a fraction always yields a negative number). Hence, entropy changes on mixing always favor miscibility in polymer blends. Therefore, in a given system, it is the effect of temperature on the enthalpy of mixing that plays the biggest role in determining the phase behavior. In the Flory-Huggins theory the interaction parameter is an empirical value that is concentration and temperature dependent. Hence, this theory provides little explanation on how (and why) ΔH_m and the corresponding phase behavior varies with temperature. However, the newer Flory Equation of State Thermodynamic Model does give some fundamental explanation of the temperature dependence of ΔH_m. In fact, it has been illustrated that this model predicts the

preferential existence of LCST behavior (although a UCST is not discounted), and that it is a manifestation of differences in the thermal expansion coefficients of the blend components (5). The Flory-Huggins theory on the other hand, predicts the existence of UCST behavior only.

This concludes discussion on the general phase behavior of polymer blends. This brief review is intended to provide a basic understanding of polymer - polymer phase behavior in order to discern aspects of this experimental work that will deal with this subject. In light of the experimental work that will be presented in this chapter, focus will now turn to the specific phase behavior of PS-PVME blends, and a subsequent review of some studies involving the crosslinking of polymer blends.

6.1.2 Phase Behavior of PS-PVME Blends

A phase diagram that has been experimentally determined for a PS-PVME blend with PS and PVME weight average molecular weights of 210,000 and 51,500 (respectively) is shown in Figure 6-4. This diagram was constructed from microscopic observation of the mode of phase separation as well as from thermochromatic properties of the blend (i.e. by monitoring the transmitted light intensity through the blend as a function of temperature). As illustrated, this blend system displays LCST behavior and has a critical point at a composition and temperature of ca. 20 vol % PS and 85°C, respectively. It must be stressed however, that this phase diagram applies only to this particular blend. The specific phase behavior of polymer blends is strongly influenced by the characteristics of the components. The most influential

parameter with respect to the phase diagram of a blend is the molecular weight of the polymeric components. Figure 6-5 illustrates the effects of varying the molecular weight of PVME on the PS-PVME phase diagram. This diagram was developed using the technique of fluorescence emission of anthracene - labeled PS. As shown, increasing the molecular weight of PVME reduces the compatibility of the blend as indicated by a lowering of the critical point temperature. This behavior is predicted by the Flory-Huggins theory and is a result of a smaller contribution to a negative ΔG_m from the entropy of mixing. Increasing the molecular weight of a blend component reduces the mole fraction for a given volume fraction, which results in a smaller negative value for the log terms in eq. (1). Hence, the entropy contribution to a reduction in free energy upon mixing is diminished.

Figure 6-5 also shows that the critical point composition shifts dramatically from ca. 25 wt % PS to 80 wt % PS when the molecular weight of the PVME is raised above the molecular weight of PS. This seems rather striking, and clearly illustrates the molecular weight dependence of the phase diagram. The same trend is established if the PS molecular weight is varied with a constant PVME molecular weight. Figure 6-6 is a plot of the critical point temperature versus the critical point composition for a series of PS-PVME blends with varying PS molecular weight. As shown, as the molecular weight of the PS increases, the critical point temperature and PS wt % decreases.

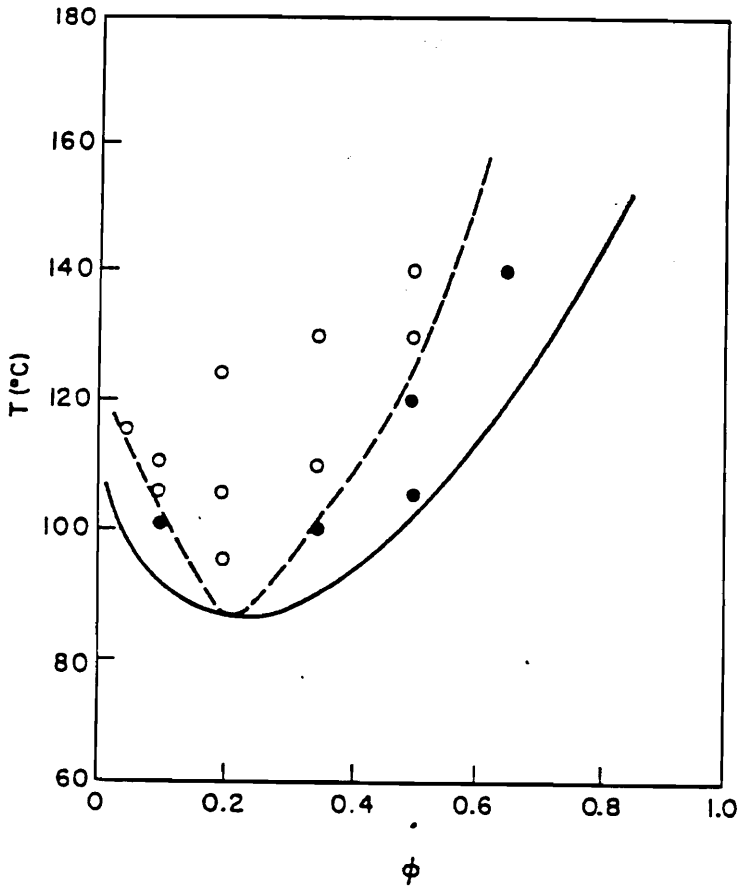

Figure 6-4. Phase diagram for a PS-PVME blend with PS and PVME M_w's of 210,000 and 51,500, respectively. (●) - phase separation by nucleation and growth, (o) - by spinodal decomposition. (ϕ = PS vol fraction) (ref. 6)

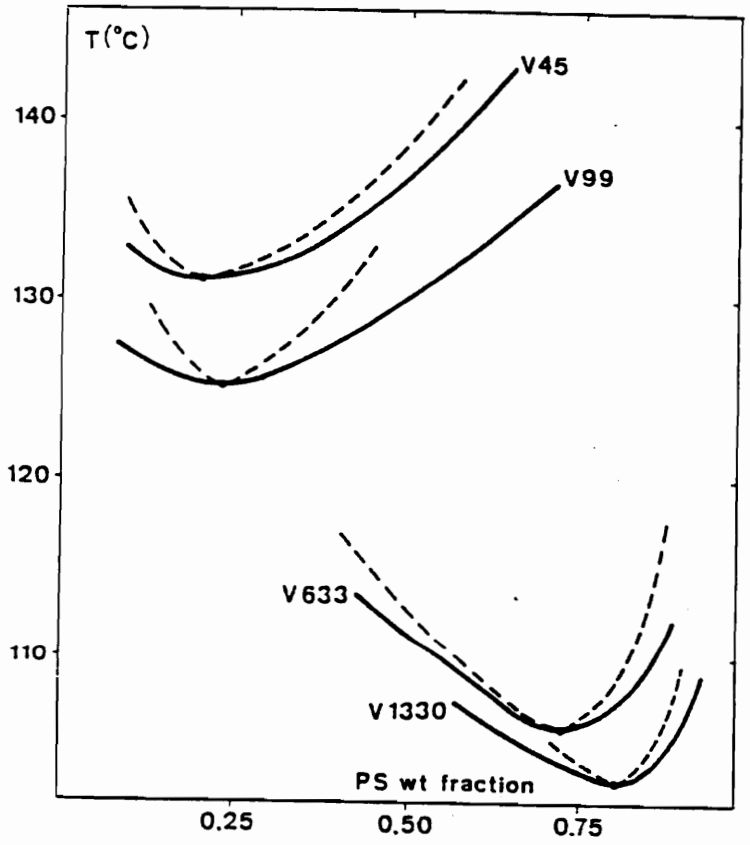

Figure 6-5. Effect of molecular weight of PVME on the phase diagram of a PS-PVME blend. PS M_w = 106,000; the M_w of PVME is given on the phase diagram by V(M_w x 10^{-3}). (ref. 7)

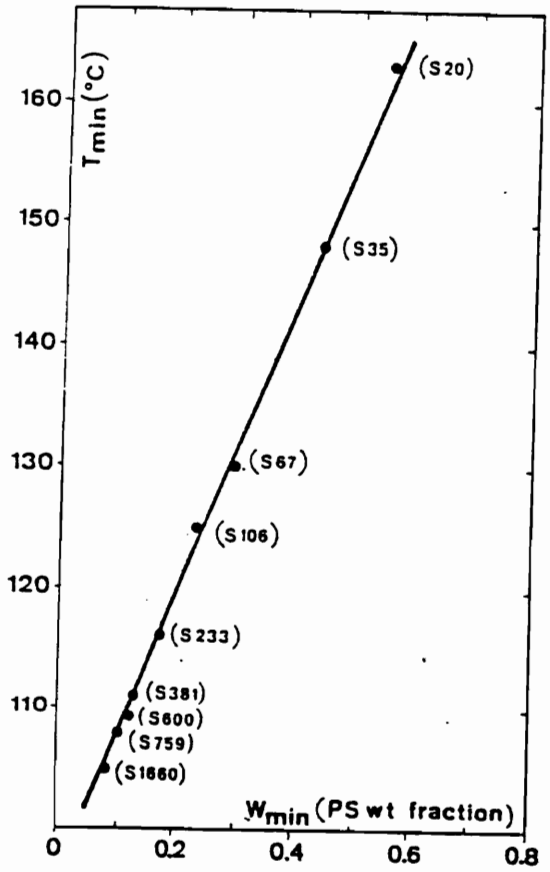

Figure 6-6. Plot of the critical point temperature (T_{min}) versus composition (w_{min}) of a PS-PVME blend series. PVME M_w = 99,000; the PS M_w is given by V(M_w x 10^{-3}). (ref. 7)

6.1.3 Crosslinking of Polymer Blends

Numerous studies have been reported in the literature which involve crosslinking of polymer blends. Several of these studies should be reviewed here to gain a perspective on the work that will be discussed in this chapter.

Briber and Bauer have reported on the effects of crosslinks on the phase behavior of deuterated polystyrene (PSD) - PVME blends (8). It should be noted that this system is not equivalent to a PS-PVME blend in that the binodal curve for the former is ca. 40°C above the latter system. A deuterated PS was used in this study so the phase behavior could be followed by small angle neutron scattering (SANS). Prior to phase separation, the miscible blends (30 wt % PSD) were gamma irradiated with a Co^{60} γ-ray source at 45°C with a dose rate of 1 Mrad/hr. After irradiation, the films were heated to various temperatures to induce phase separation while SANS measurements were made. Figure 6-7 shows the results of these experiments, which are plots of the scattering function, S(q), versus the scattering vector, q ($q = 4\Pi \sin(\Theta)/\lambda$). As shown, the scattering intensity (i.e. S(q)) for this blend system decreases with increasing dose (indicative of a lower extent of phase separation) over the entire dose range and phase separation temperatures. It was concluded that radiation crosslinking of the miscible blend improves the compatibility between the blend components. This is reasonable since some grafting between PSD and PVME was shown to occur, which would obviously hinder the ability of the two components to phase separate.

Other studies have been carried out with the intent to freeze in novel micostructures by crosslinking phase separated blends. Recently, Tran-Cong et. al. have reported on freezing the microstructure developed during the spinodal decomposition of an anthracene labeled polystyrene - poly(2-chlorostyrene) blend (9). Crosslinking was achieved by irradiation with a XeF excimer laser which initiates a intermolecular photodimerization reaction between the anthracene groups attached to the polystyrene chains. Figure 6-8 shows the resulting morphology of the phase separated blends after irradiation during various times of the spinodal decomposition process. Although only one component was crosslinked, the irradiated films showed good thermal stability. As shown in Figure 6-9, the tan δ behavior of the phase separated, irradiated blend does not significantly change after heating the sample to 190°C for 2 hours.

The work that is presented in this chapter involves the electron beam irradiation of a series of PS-PVME blends with varying composition. Both miscible and phase separated morphologies were irradiated and subsequently characterized. Several different analytical techniques were employed to determine the effects of composition and morphology on the extent of crosslinking as well as to determine some of the properties of the irradiated blends. This work has been carried out because it is of interest to examine what type of chemistry and gelation behavior results from blending a radiation sensitive polymer (PVME) with a radiation resistant polymer (PS). Since this blend is comprised of two chemically dissimilar polymers, some sort

of intermolecular energy transfer process is likely to be displayed. This may result in the occurrence of rather interesting radiation chemistry and gelation behavior especially with regard to the influence of blend composition and morphology on these phenomena.

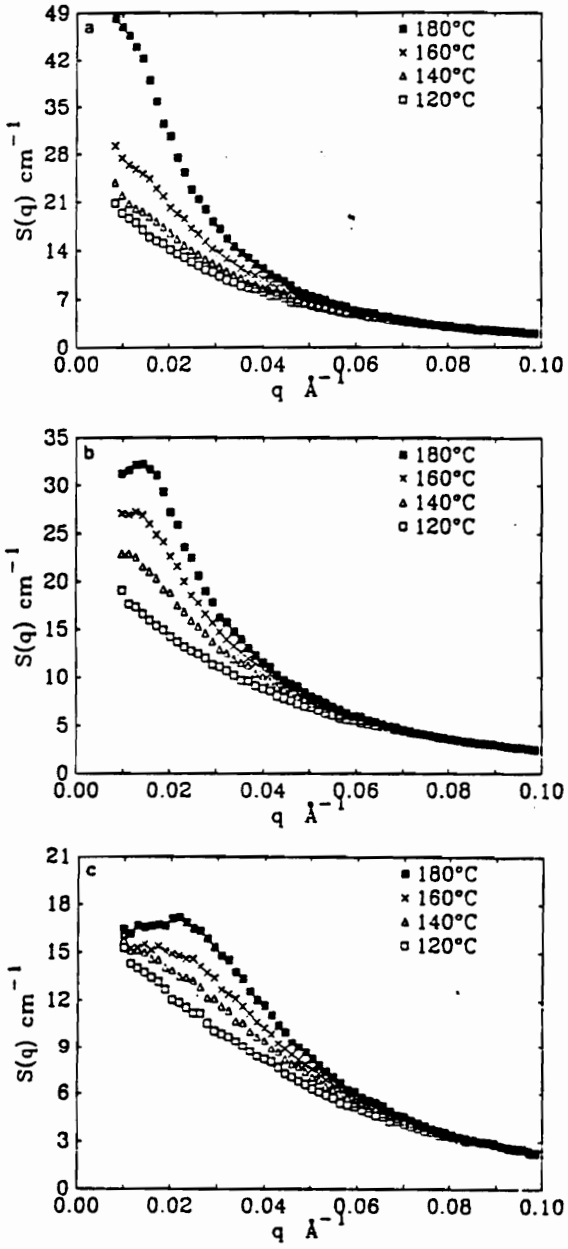

Figure 6-7a-c. Plots of the scattering function (S(q)) versus the scattering vector (q) at various temperatures for PSD-PVME blends exposed to (a) 25, (b) 50, and (c) 125 megarads of gamma irradiation as determined by SANS. (ref. 8)

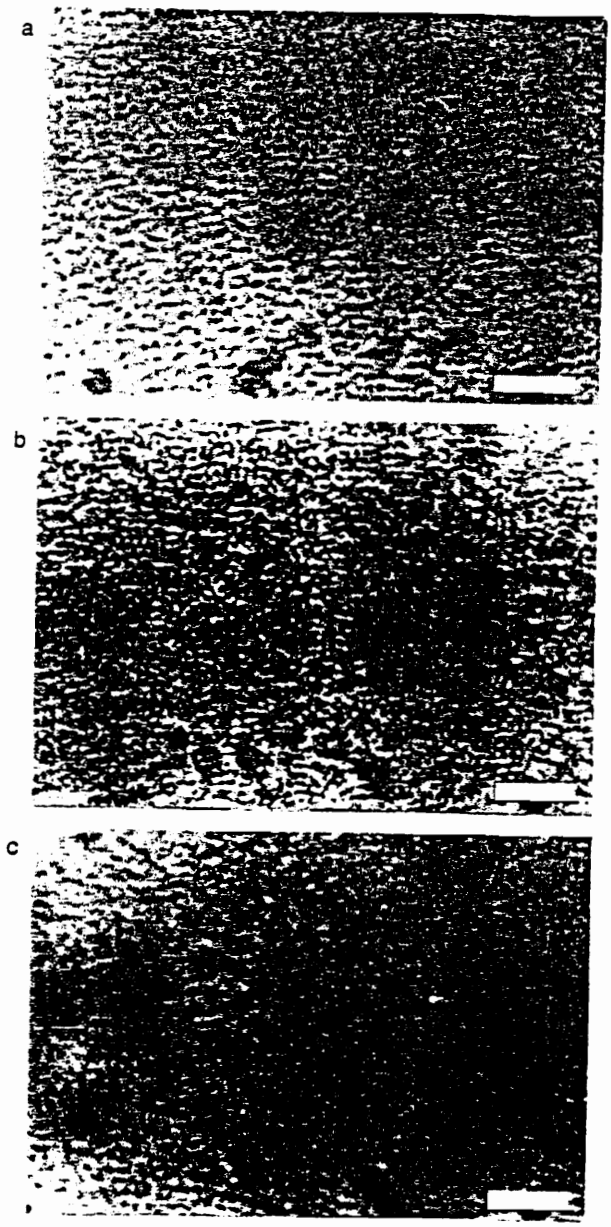

Figure 6-8a-c. Morphology of phase separated PSA-P2CS (40 wt % PSA) blends that have been irradiated by laser radiation after (a) 5, (b) 15, and (c) 25 minutes at 193°C. The scale is 10 microns. (ref. 9)

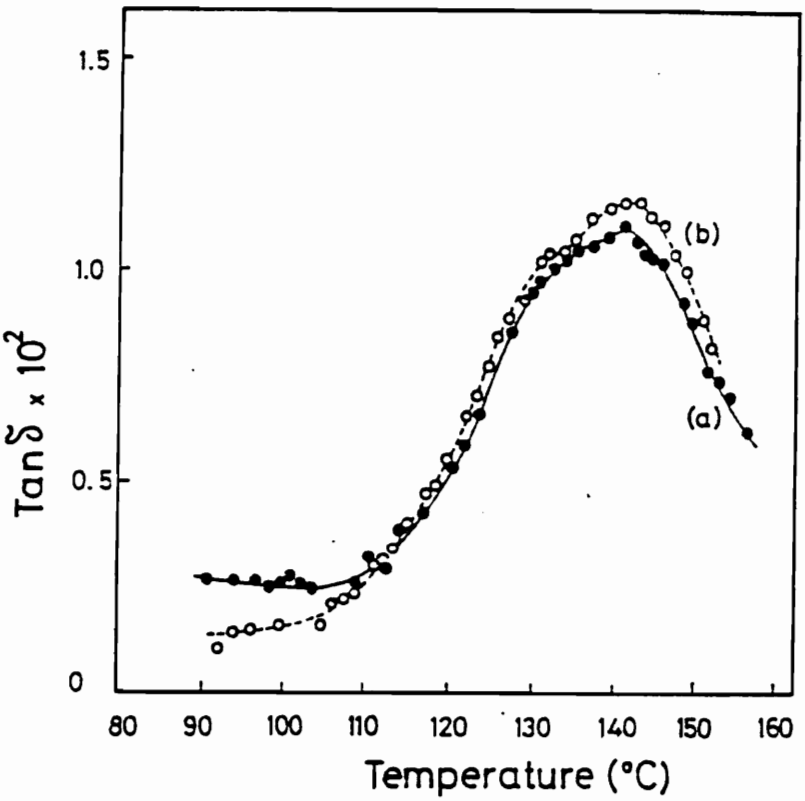

Figure 6-9. Dielectric Tan δ of the blend depicted in Figure 6-8a (a) before and (b) after heating to 190°C for 2 hours. (ref. 9)

6.2 EXPERIMENTAL

6.2.1 Materials and Sample Preparation

Both of the polymers used in this study are commercially available. The polystyrene was obtained from Dow Chemical and has a weight average molecular weight (M_w) of 300,000 and a polydispersity (M_w/M_n) of 2.5. The poly(vinyl methyl ether) was obtained from Dajac Labs and has an unknown molecular weight. However, based on the comparison of the cloud point curve obtained for this blend system (see Results and Discussion) with curves reported on in the literature (7), it is estimated that the M_w of PVME is in the range of 50,000 to 100,000.

Films of the PS-PVME blends were formed by preparing ternary solutions of toluene, PS, and PVME with various polymeric compositions (polymer:solvent = 1:9) which were subsequently cast onto teflon sheets to form transparent films with a thickness of ca. 3 mils. The cast films were dried under ambient conditions for 24 hours and then placed under 25 in. Hg of vacuum at 80°C for at least 48 hours to remove residual solvent. Blends with compositions of 95 % and 100 % PS were stored under vacuum at 120°C to remove residual solvent since these films have glass transitions above 80°C.

All phase separations were carried out isothermally at 160°C for either 30 seconds or two minutes. Two slightly different procedures were employed:

(1) Cast films and the teflon substrate were placed in an oven maintained at 160°C (± 2°C). After phase separation for the specified time, the films were quenched by

holding them directly over a liquid nitrogen bath. Samples handled by this procedure were then quickly prepared and irradiated (see Radiation Exposure) to ensure irradiation of a phase separated morphology.

(2) Cast films were removed from the teflon substrate and sealed in aluminum DSC pans. Phase separation was carried out in a DSC furnace at 160°C (± 0.5°C) for the specified time. Quenching was performed by quickly submerging the sealed aluminum pans in liquid nitrogen. Samples handled by this procedure were then quickly transferred back to the DSC furnace (now at ambient temperature or below) and cooled to -60°C for DSC evaluation (see Thermal Analysis).

6.2.2 Radiation Exposure

All samples were exposed to electron beam radiation with an Energy Sciences CB150 Electrocurtain (see appendix for a detailed description of this equipment). Radiation exposure was carried out under a purged nitrogen atmosphere with a residual oxygen content of 250 - 350 ppm. However, the films were exposed to air between consecutive passes under the electron beam. Samples irradiated to 100 megarads were passed through the electrocurtain five times at a speed of 20 ft/min and received a dose of 20 megarads/pass. Samples irradiated to 50 megarads were passed under the electron beam at a speed of 40 ft/min and received a dose of 10 megarads/pass. All samples were irradiated at ambient temperature, but it should be noted that some sample heating does occur for a short time period (~ 1 sec.) as a result of radiation exposure.

6.2.3 Gel Content Determination

Gel contents of the irradiated blends were determined by extracting weighed samples in tetrahydrofuran (THF) with a Soxhlet extractor for at least 24 hours. After extraction, the insoluble fraction was dried under 25 in. Hg of vacuum at 80°C (120°C for samples with high PS content) for at least 24 hours. Longer extraction or drying times did not result in any further weight reduction. The gel fractions were computed by dividing the weight of the insoluble fraction by the initial weight of the film. All gel fractions reported represent an average of at least two extractions. The error associated with the reported values does not exceed ± 4 gel % for all data points.

6.2.4 Thermal Analysis

All DSC measurements were made with a Seiko DSC 210 differential scanning calorimeter at a heating rate of 10°C/min. Samples were sealed in aluminum pans and cooled in the DSC furnace from room temperature (or below) to the initial scanning temperature. The reported glass transition temperatures were taken as the midpoint between the baselines established before and after the glass transition.

6.2.5 Cloud Point Determination

Cloud point temperatures of the blends were determined by isothermal experiments and visual observation of turbidity in the films. For each composition, toluene solutions of the blend were cast onto glass slides and dried under the same conditions as previously described. A Linkam PR600 hot stage was used for heating

the samples. The following procedure was implemented to determine the cloud point temperature: (1) The glass slide was placed in the hot stage for two minutes at some predetermined temperature. (2) The slide was removed from the hot stage and visually inspected for turbidity in the film. (3) The temperature of the hot stage was increased 5°C and the glass slide was returned to the hot stage for two minutes. This procedure was repeated until the film showed signs of turbidity. At this point, a fresh sample was placed in the hot stage at the highest temperature where turbidity was not observed. The above procedure was repeated except with an incremental temperature increase of 2°C. The cloud point was taken as the average of the temperatures just before and after turbidity was observed. Hence, the cloud point temperatures reported have an associated experimental error of ± 1°C. Repetition showed good reproducibility and was within the stated experimental error.

6.3 RESULTS AND DISCUSSION

6.3.1 Characterization of the Unirradiated PS-PVME Blends

Figure 6-10 depicts the glass transition behavior of the PS-PVME blends under consideration in this study. It is apparent from this series of DSC traces that there is not a linear relationship between the composition (wt % PVME) and the glass transition temperature (T_g) of the blend. Also notice that there is a significant broadening of the glass transition at intermediate compositions. Figure 6-11 illustrates the dependence of the T_g on the blend composition. As shown, the T_g decreases sharply as the PVME content is increased in the PS rich blends whereas the T_g of the PVME rich blends is much less sensitive to composition. This composition dependence of the glass transition behavior is significant in this study because it is of importance to realize the state of each blend during radiation exposure, since this may influence the extent of radiation induced changes in the blends.

The cloud point curve for this series of PS-PVME blends is shown in Figure 6-12. This blend series displays LCST behavior and has an apparent critical point near 115°C and at a composition in the range of 70 to 85 wt % PVME, based on comparison of this curve with those given in the literature (see Figure 6-4). This curve covers compositions ranging from 15 wt % to 85 wt % PVME which is the composition range of the phase separated blends that will be considered in this study.

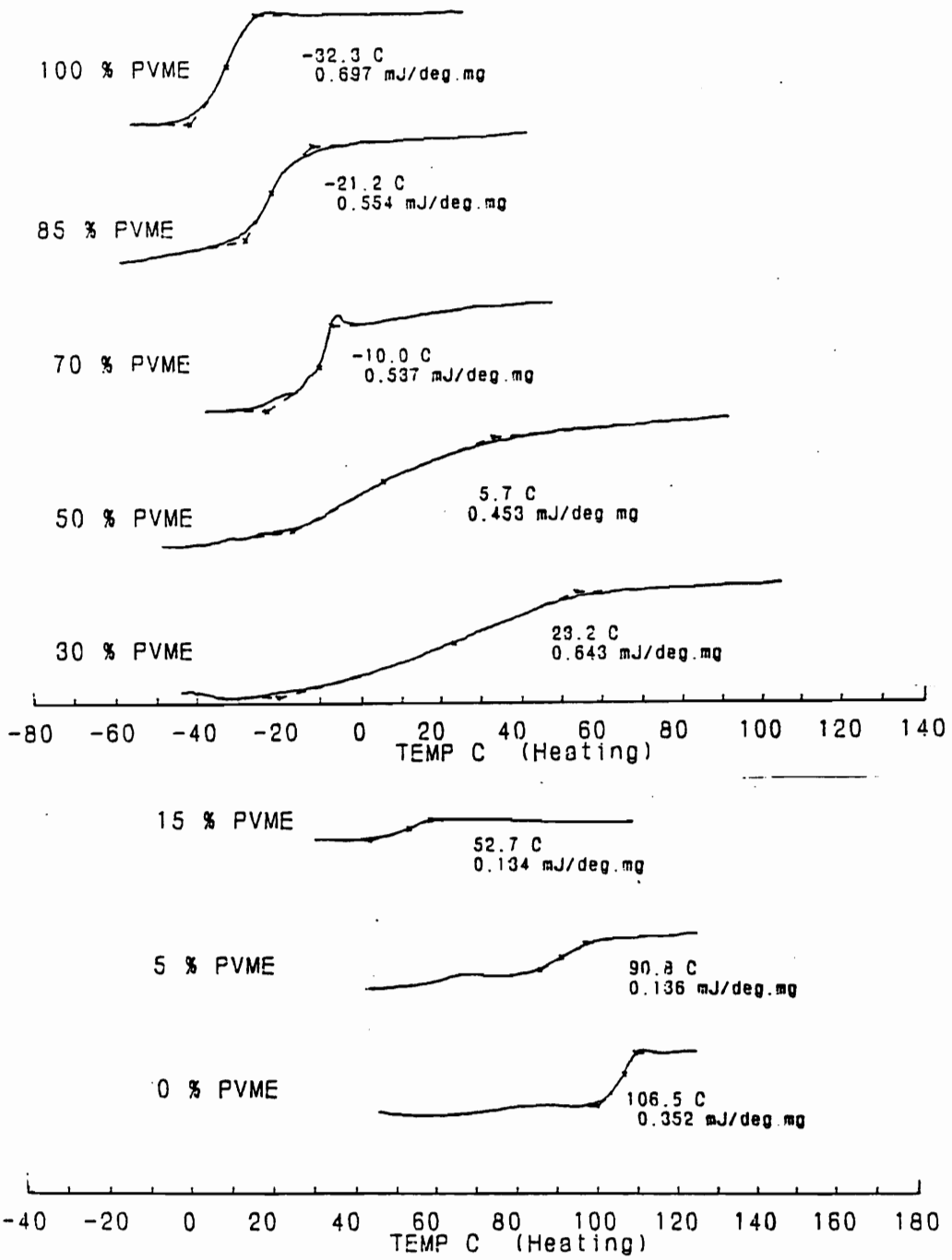

Figure 6-10. DSC scans of the miscible PS-PVME blends used in this study.

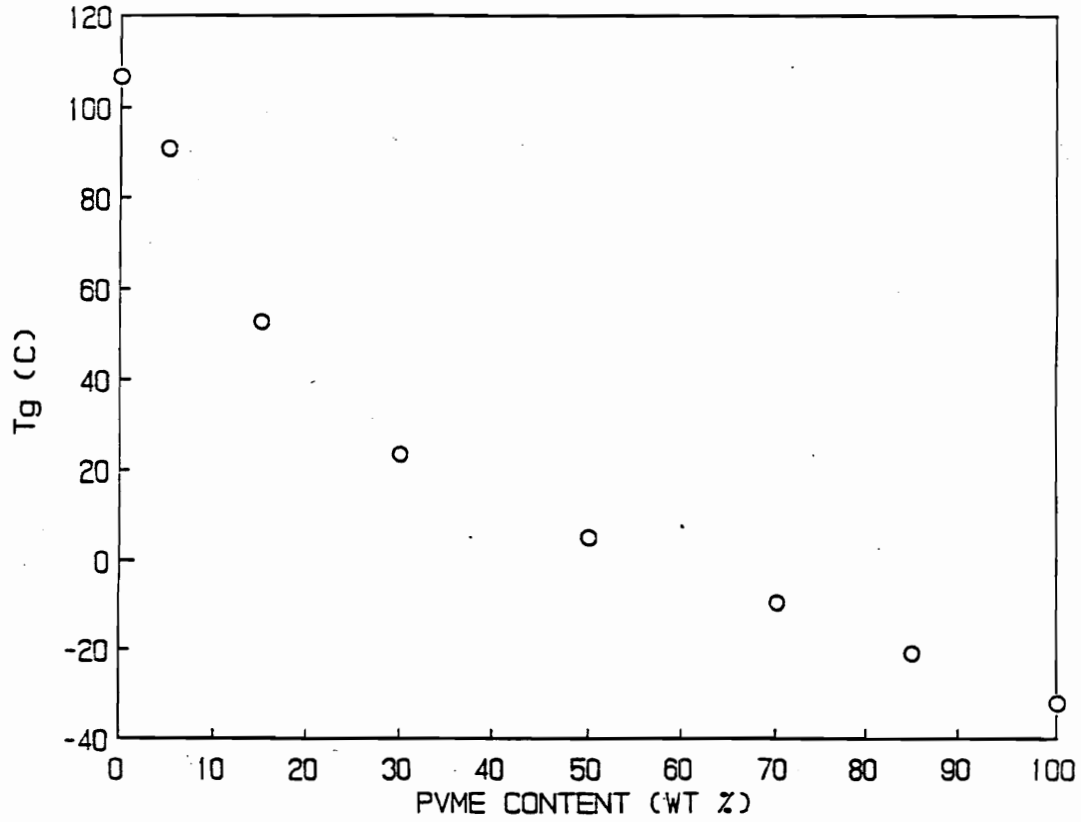

Figure 6-11. Plot of the glass transition temperature (T_g) of PS-PVME blends as a function of blend composition (wt %).

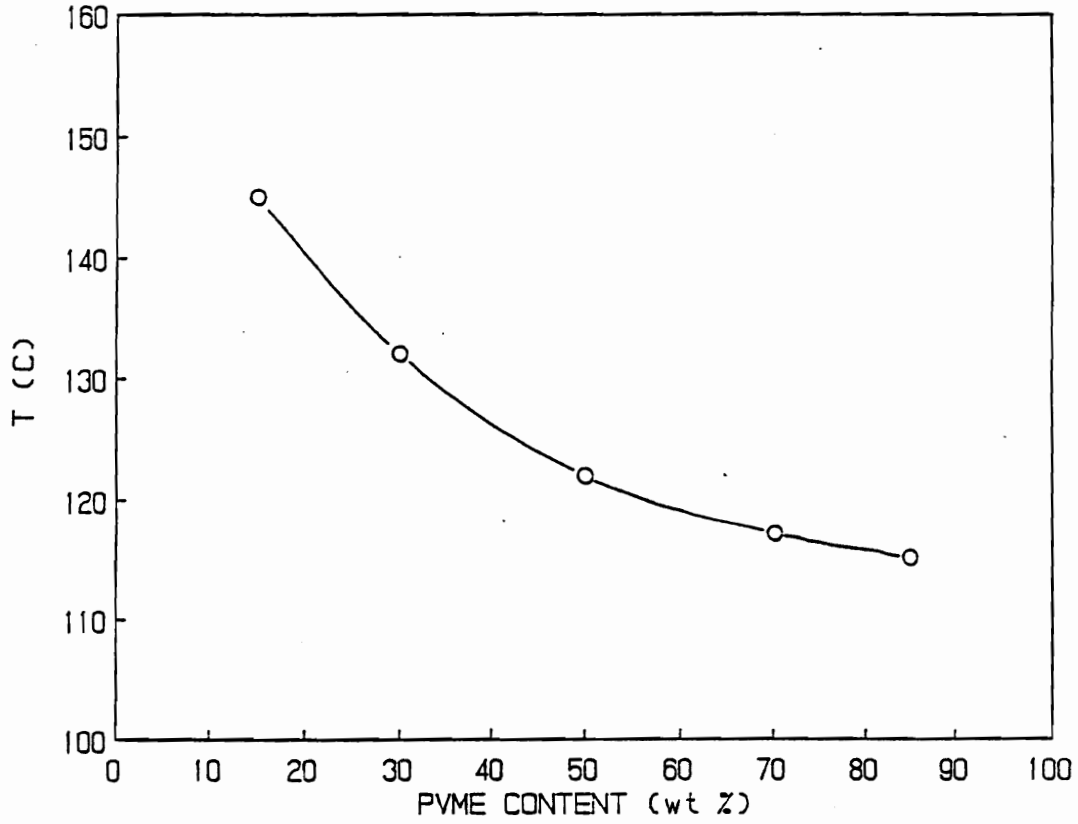

Figure 6-12. Cloud point curve of the PS-PVME blend used in this study.

Figure 6-13 and Figure 6-14 show the DSC behavior of the PS-PVME blends that have been isothermally phase separated at 160°C for 30 seconds and 2 minutes, respectively. As will be shown, phase separation proceeds by spinodal decomposition at 160°C for all the blends under consideration. Although two distinct T_g's are not evident in every sample, comparison of these DSC scans with the DSC scans of the miscible blends (see Figure 6-10) indicates that some phase separation has indeed occurred, as evidenced by shifts in all the glass transitions. For example, the T_g of the 70 wt % PVME blend decreases by ca. 13°C after being held at 160°C for 30 seconds. In fact, after 30 seconds at 160°C, all blends except for 15 wt % PVME display a glass transition at ca. -23°C, indicative of the presence of a PVME-rich phase. The 15 wt % PVME blend also shows signs of phase separation; after 30 seconds at 160°C, there is a 25°C increase in the glass transition, indicative of the development of a PS-rich phase. However, comparison of Figure 6-13 with Figure 6-14 illustrates that phase separation is certainly not complete after 30 seconds at 160°C. After two minutes at 160°C, all blends except the 15 wt% PVME blend display two distinct glass transitions (see Figure 6-14); a lower T_g at ca. - 25°C (indicating the presence of a PVME-rich phase) and a higher T_g at ca. 95°C (indicating the presence of a PS-rich phase). Furthermore, the glass transitions displayed in Figure 6-14 at each composition are more distinct than the glass transitions in Figure 6-13, as evidenced by greater ΔC_p values. It should also be noted that the ΔC_p values in both Figure 6-13 and Figure 6-14 are composition

dependent. As the PVME content decreases, the ΔC_p of the low T_g's steadily decreases while the ΔC_p of the upper T_g's increases. This suggests that the fraction of the PVME-rich phase in the phase separated blend decreases with decreasing PVME content while the PS-rich phase fraction increases, which obviously is expected. Figure 6-14 also illustrates that the compositions of the phases that develop upon phase separation are relatively insensitive to the overall blend composition and to the quench depth, ΔT_q (i.e. the difference between the phase separation temperature and the cloud point temperature). Hence, the only significant difference among the blends depicted in Figure 6-14 that has been detected by DSC is the relative fractions of PVME-rich and PS-rich phases. The one exception to this is the 15 wt % PVME blend. As indicated by the cloud point curve (see Figure 6-12) this particular blend has the smallest quench depth, ΔT_q (~ 15°C). Hence, the rate of phase separation will be the slowest in this blend. Given enough time, the phase separation will likely proceed to the point where the resulting glass transition behavior will be similar to the other blends that have been phase separated for two minutes. This speculation is made because there is experimental evidence that all the blends considered in this study phase separate by spinodal decomposition at 160°C. As previously discussed, spinodal decomposition is characterized by the spontaneous formation of separate phases that undergo changes in composition with time. Figure 6-10, Figure 6-13, and Figure 6-14 illustrate that the observed T_g of the 15 wt % PVME blend steadily increases with phase separation time (i.e. from 53°C

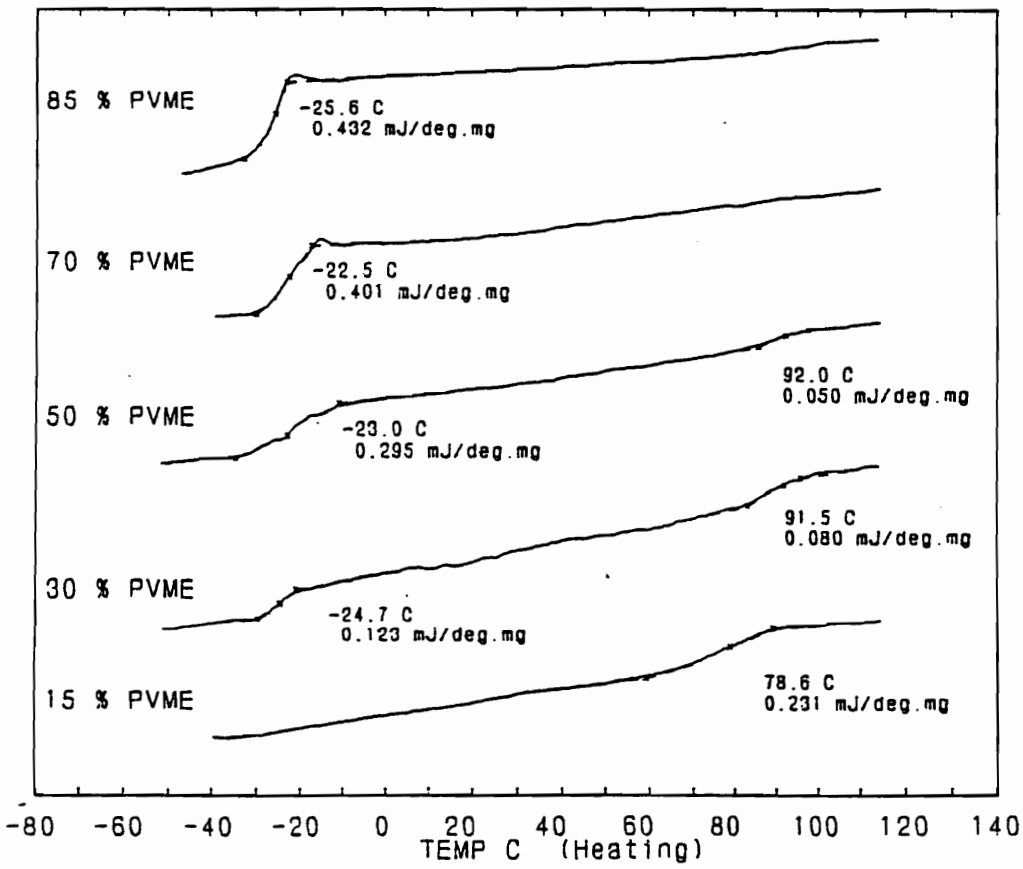

Figure 6-13. DSC scans of PS-PVME blends that have been phase separated at 160°C for 30 seconds.

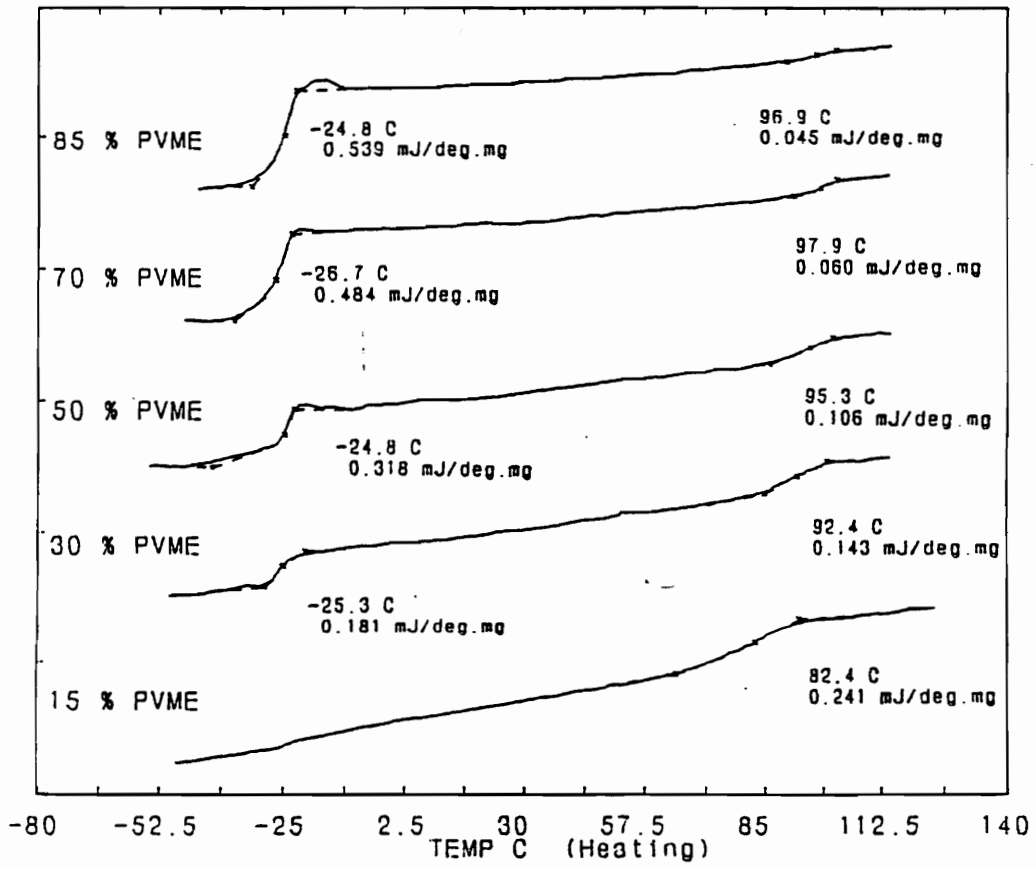

Figure 6-14. DSC scans of PS-PVME blends that have been phase separated at 160°C for 2 minutes.

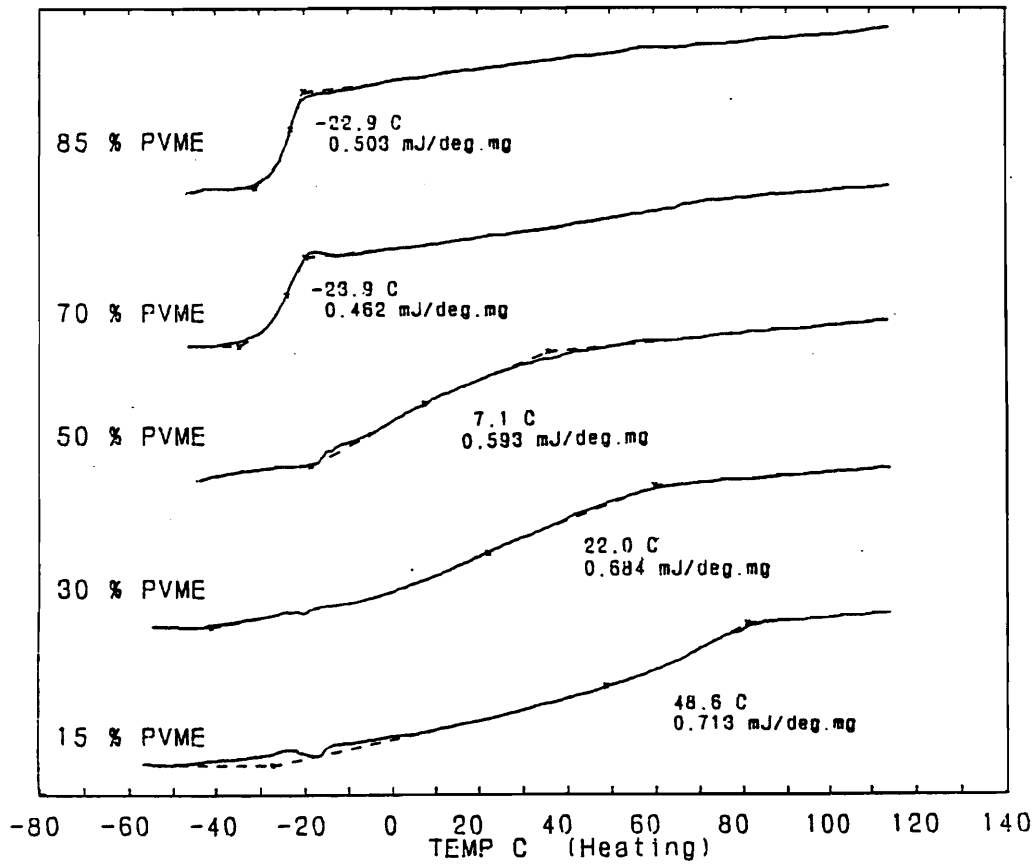

Figure 6-15. DSC scans of PS-PVME blends that have been phase separated at 160°C for two minutes, then held at 100°C for 10 minutes.

to 83°C in two minutes), indicating changes in the composition of the dominant phase, and hence the occurrence of spinodal decomposition. Since this particular blend has the smallest ΔT_q of the blend series, all the other blends must undergo spinodal decomposition at 160°C as well. Notice that there is some change in the T_g's (and hence phase composition) of all the blends with phase separation time, but it is most evident in the 15 wt % PVME blend because the rate of phase separation is slow enough that significant changes can be observed over the time scale between 30 seconds and two minutes.

The thermal stability of the blends phase separated for two minutes has also been considered because a comparison will be made with the thermal stability of these blends after irradiation. Figure 6-15 shows the DSC behavior of the blend series that have been phase separated for two minutes at 160°C, quenched in liquid nitrogen, and then held at 100°C for ten minutes. As illustrated, the thermal behavior of these blends is very similar (if not identical) to the thermal behavior of the miscible blends (compare Figure 6-15 with Figure 6-10), indicating that complete phase dissolution has occurred. The only exception is for the blend with 70 wt % PVME. This particular blend has a T_g of ca. - 24°C, which is characteristic of the phase separated state (see Figure 6-13). Nishi et. al. (6) have reported that the rate of phase dissolution for blends with compositions very near the critical point is clearly much slower than for other blend compositions under the same dissolution conditions. This is likely the cause of the observed thermal behavior of the 70 wt % PVME blend

under consideration here. As previously mentioned, this composition is close to the anticipated critical point as indicated in the cloud point curve shown in Figure 6-12.

6.3.2 Characterization of Irradiated PS-PVME Miscible Blends

Thermal Analysis. Figure 6-16 shows the glass transition behavior of the miscible PS-PVME blends that have been irradiated to 100 megarads. Comparison of these DSC scans with those for the unirradiated blends (Figure 6-10) indicates that the thermal behavior of this blend system is relatively unaffected by a radiation dose of 100 megarads. There is some slight increases in the T_g's after irradiation (less than 5°C), which is likely the result of crosslinking.

Gel Fraction Analysis. Figure 6-17 illustrates the effect of blend composition on the gel fraction present in the blends after irradiation to 50 and 100 megarads. As shown, a small increase in the PVME content of the PS-rich blends results in a drastic increase in the gel content. For instance, at a dose of 100 megarads, the addition of only 5 wt % PVME to pure PS results in a change in gel fraction from ca. 1 % to over 30 %. This clearly indicates that there is a significant amount of radiation grafting occurring between the PS and PVME. Furthermore, at compositions of 50 wt % PVME and greater, there is relatively little change in the gel fraction created by exposure to 100 megarads. This illustrates that there is a significant amount of grafting occurring in the PVME-rich blends as well. This behavior is quite surprising because PS is very resistant to radiation and is often used to afford radiation protection in polymeric materials due to the stabilizing nature of

the aromatic groups (10). It is generally thought that the presence of aromatic groups results in energy transfer to these moieties which act as energy sinks and produce a stabilizing effect. However, this is clearly not the case in this blend system. If PS were providing some radiation protection to these blends, the addition of PS to PVME would result in a significant decrease in the extent of crosslinking, which does not occur.

Since there is a number of different functional groups and hence a number of different excited states after irradiation present in these blends there must be some energy transfer occurring. The transfer of energy in irradiated systems is a downhill process; i.e. energy is transferred from excited states with high energy levels to excited states with low energy levels (see chapter II). Hence, it appears as though the excited state associated with the crosslinking of PVME is at a lower energy level than the excited state of the aromatic groups in PS, which would explain the behavior displayed in Figure 6-17. Another possible explanation for this observed behavior is that the aromatic groups in PS do act as energy traps, but then become active sites for the PVME to react with resulting in radiation grafting between the two polymers. This is purely speculation however, and further experimentation is necessary to understand the radiation chemistry that is occurring in these systems.

It is interesting to note that the T_g of the blend does not appear to strongly influence the extent of crosslinking. For example, a blend with 95 wt % PS has a glass transition of ca. 90°C which is about 15°C below the T_g of pure PS. However,

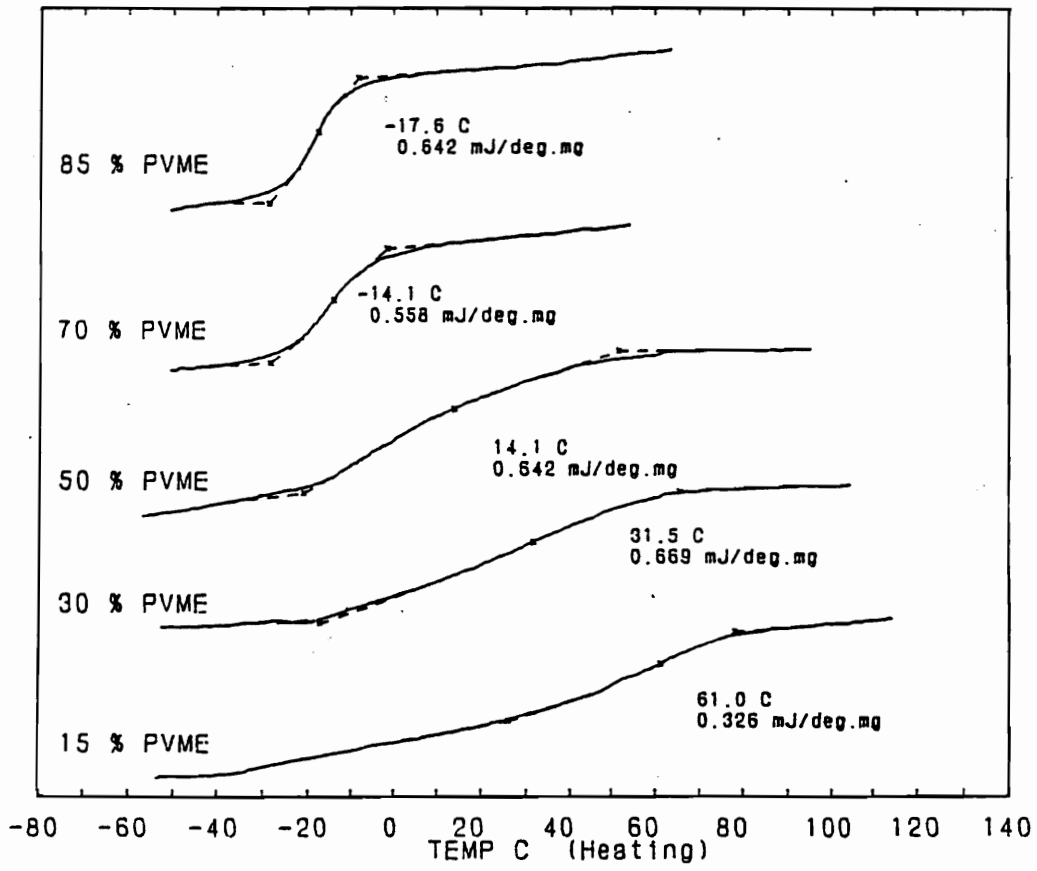

Figure 6-16. DSC scans of miscible PS-PVME blends that have been irradiated to 100 megarads.

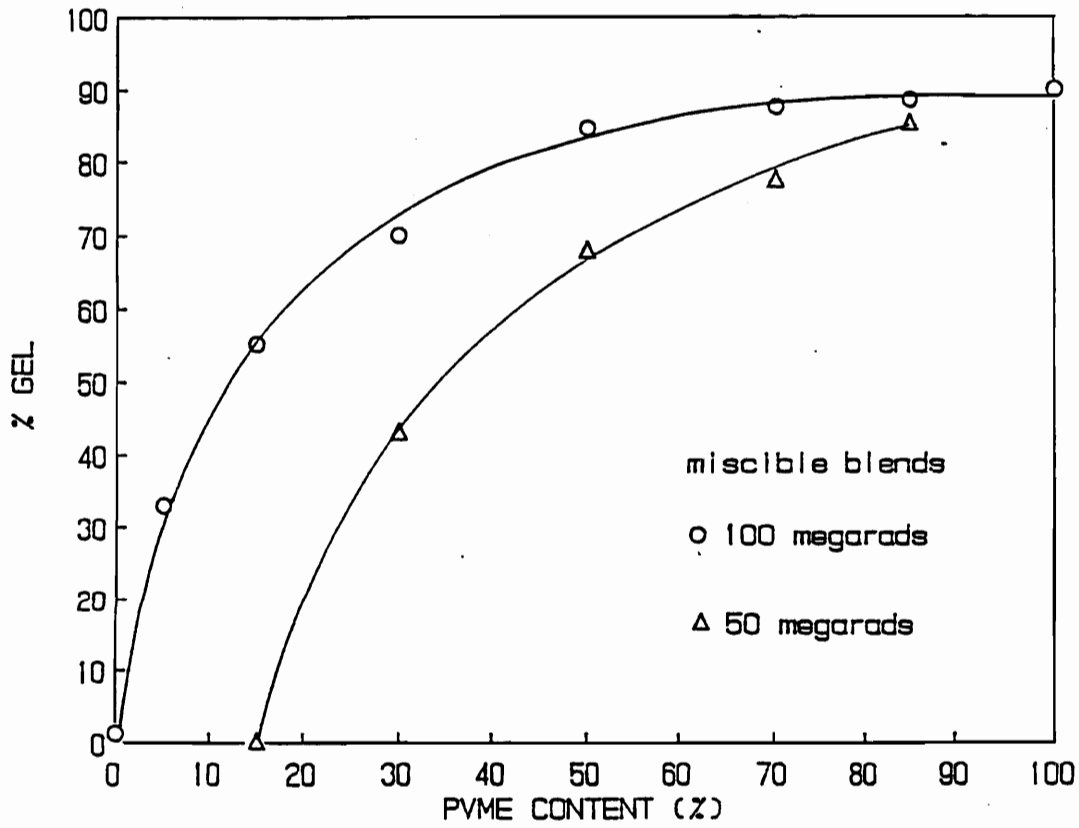

Figure 6-17. Plot of gel fraction versus composition of PS-PVME blends that have been irradiated to the indicated dose.

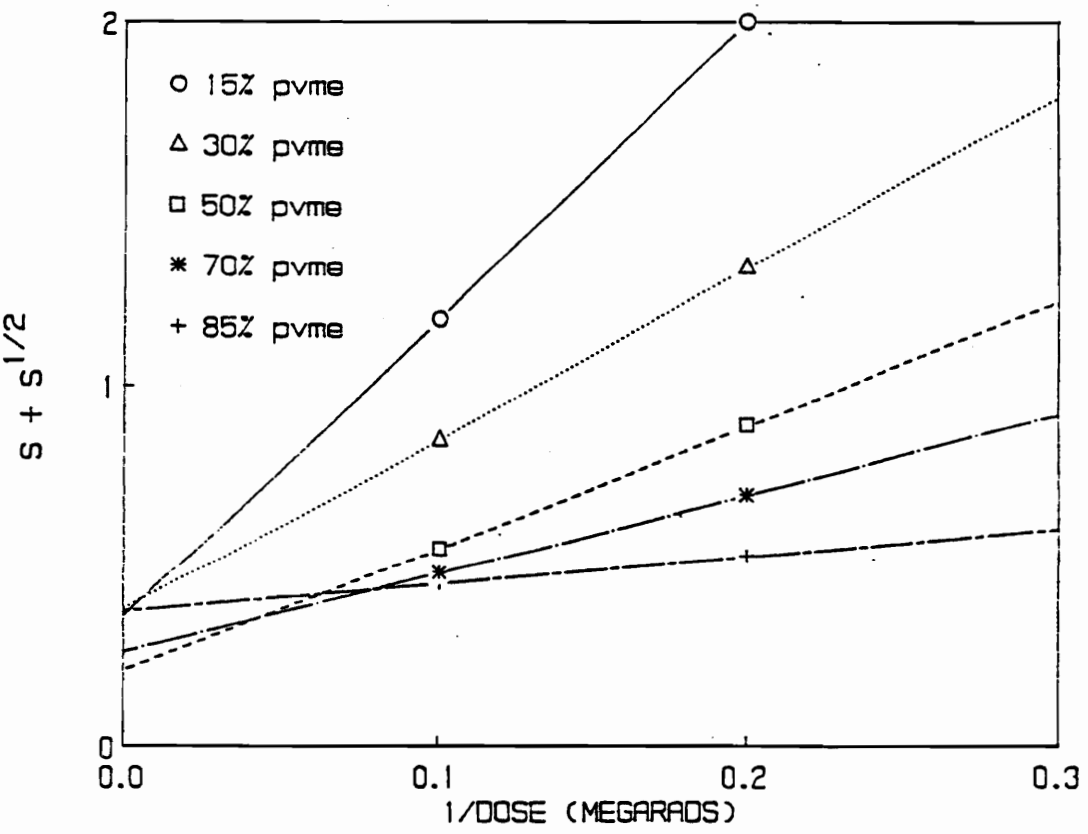

Figure 6-18. Charlesby-Pinner plots for the miscible PS-PVME blends under consideration in this study. (S = soluble fraction)

after irradiation to 100 megarads, the 95 wt % PS blend has a gel content of about 30 %, as compared to 1% for pure PS. Although both blends are clearly in the glassy state, there is a significant difference in the gel content formed upon irradiation to the given dose.

Figure 6-17 also illustrates the effect of dose on the gel fraction formed in these miscible PS-PVME blends. Decreasing the dose from 100 to 50 megarads appears to result in a horizontal shift in the gel - composition curve. Put another way, the change in gel fraction with respect to dose is extremely composition dependent. This suggests that the G-values for crosslinking (G(X)) for this blend series is also composition dependent, which would be expected in a blend with components of very different radiation sensitivity. To illustrate this point, a Charlesby-Pinner plot was made for most blend compositions as illustrated in Figure 6-18. It must be stressed that this is for *illustrative purposes only* as two data points were available for each plot, since only two dose levels were considered. As shown, there is a steady decrease in slope with increasing PVME content in the blend. The slope in this region of the Charlesby-Pinner plot is inversely proportional to G(X) (see chapter II). Therefore, the G(X) values of this blend series does indeed increase with increasing PVME content, as expected.

6.3.3 Characterization of Irradiated PS-PVME Phase Separated Blends

Gel Fraction Analysis. Figure 6-19 illustrates the effect of dose and composition on the gel content in PS-PVME blends that have been phase separated for two minutes

at 160°C prior to radiation exposure. As shown, these blends display a linear dependence of gel content on composition over the range of compositions under consideration. This is in striking contrast to the behavior displayed by the miscible blends. It should be realized however, that this linear behavior cannot be extrapolated to compositions outside of the range under consideration. This linear dependence shows that there is a strictly additive effect of composition on the gel content formed. The reason for this behavior can be related to the morphology that develops in these blends as a result of phase separation. Recall that the thermal behavior of this blend series prior to irradiation suggested that phase separation resulted in the formation of a PVME-rich and a PS-rich phase. Furthermore, the composition of these phases was relatively independent of the overall blend composition and only the relative fractions of these phases varied over the composition range under consideration. In fact, there is a linear dependence of the ΔC_p values at the low temperature glass transitions displayed in Figure 6-14 on the PVME content, as shown in Figure 6-20. This suggests a linear dependence of the PVME-rich phase fraction and the overall blend composition. Hence, the linear increase in gel content with increasing PVME wt % is due to a linear increase in the PVME-rich phase fraction, which will govern gel formation since it is readily crosslinked as compared to the PS-rich phase. It should be stressed again that this is valid only within the composition range under consideration. At PVME contents below the stated range, one would expect to see the gel fraction drop to 0% as the

PVME wt % decreases. On the other hand, at PVME concentrations above the stated range, one would expect the gel fraction to level off at some value as the PVME wt % is increased.

Figure 6-19 also shows the effect of dose on gel content in these phase separated blends. Increasing the dose from 50 to 100 megarads results in an upward shift in the gel - composition curve, as opposed to the horizontal shift that was observed in the miscible blends. Furthermore, the relative change in gel content with dose is relatively independent of composition. This suggests that the rate of crosslinking (i.e. G(X)) is independent of composition as well. To illustrate this point, a Charlesby-Pinner plot was constructed for each composition in the same fashion as was done for the miscible blends described earlier. Again, this is for *illustrative purposes only*, especially in this case since the Charlesby-Pinner analysis was developed for homogeneous, single phase materials. However, the sloping region in the Charlesby-Pinner plot should still give an indication of the relative overall G(X) values in these blends, which is sufficient for comparative purposes. The Charlesby-Pinner plots for this series of phase separated blends is shown in Figure 6-21. As shown, the slopes in this series of plots are relatively constant over the composition range under consideration, indicating that G(X) is indeed independent of composition. Again, this contrasts the behavior of the miscible blends. Since the composition of the highly crosslinkable phase (PVME-rich phase) is independent of overall blend composition, a constant G(X) value for this series should not be surprising.

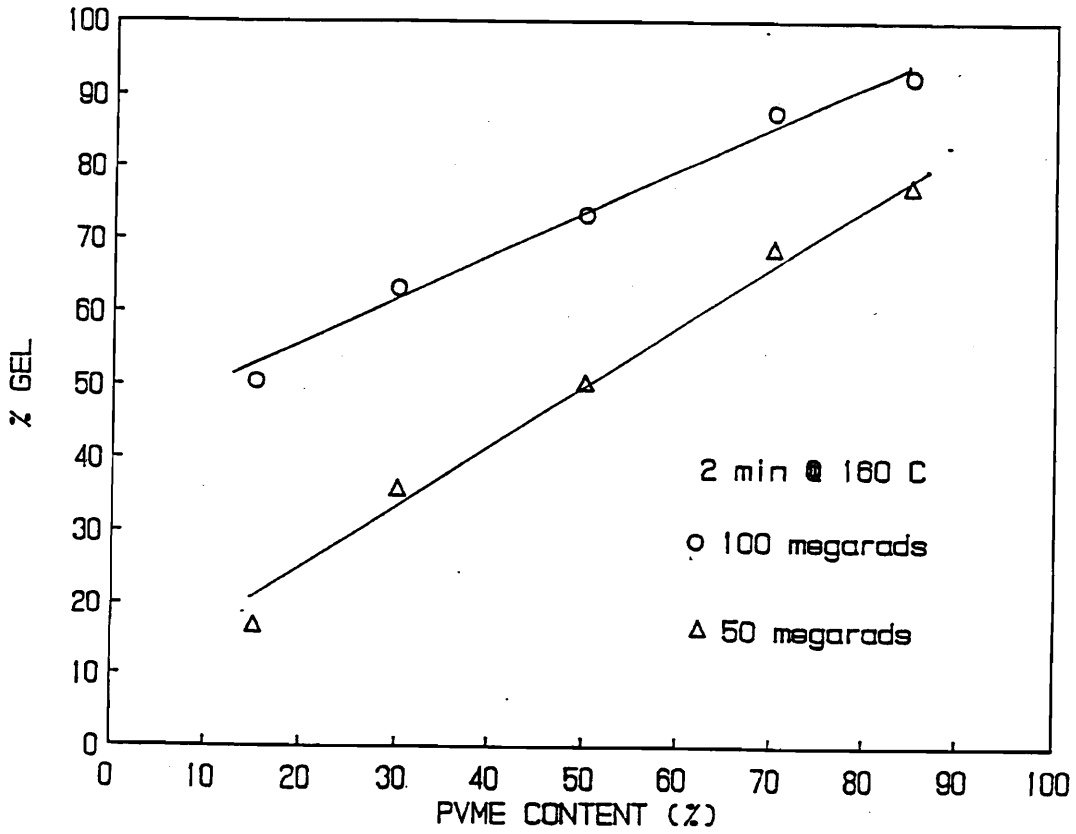

Figure 6-19. Plot of gel fraction versus composition of PS-PVME blends that have been phase separated for 2 minutes at 160°C prior to radiation exposure at the indicated dose.

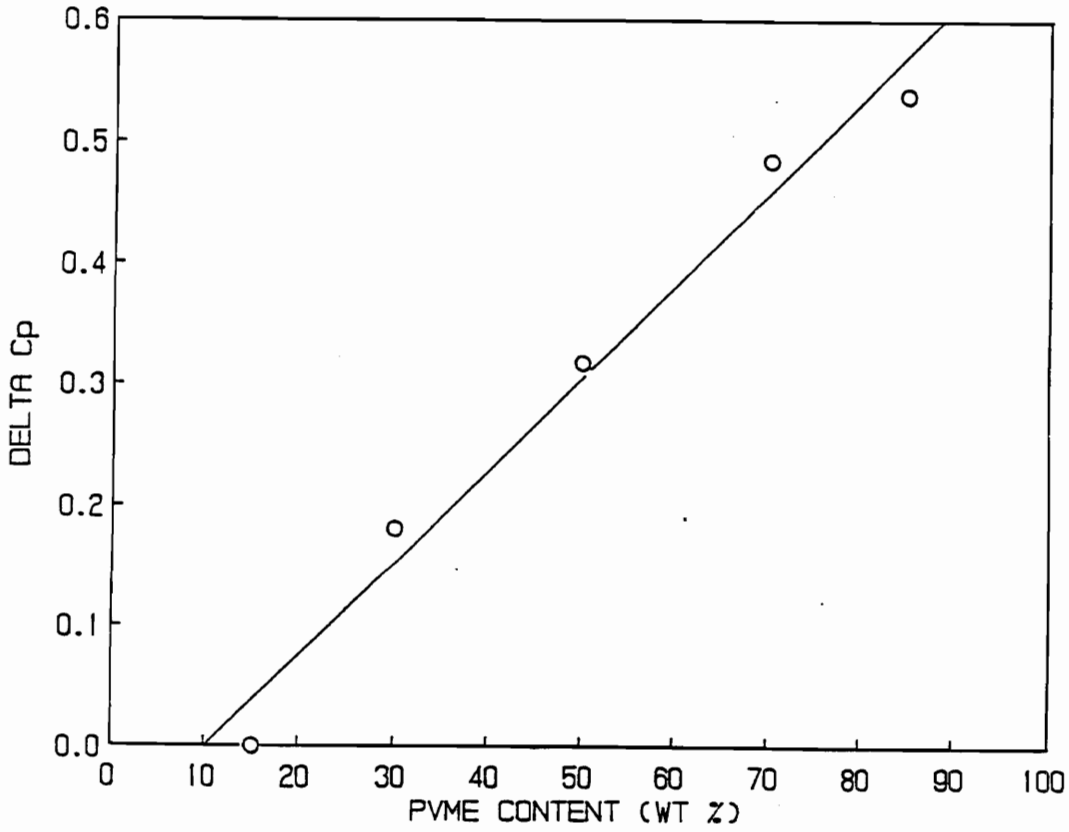

Figure 6-20. Plot of the ΔC_p values versus blend composition for the glass transitions of the PVME-rich phase displayed by the phase separated blends in Figure 6-14.

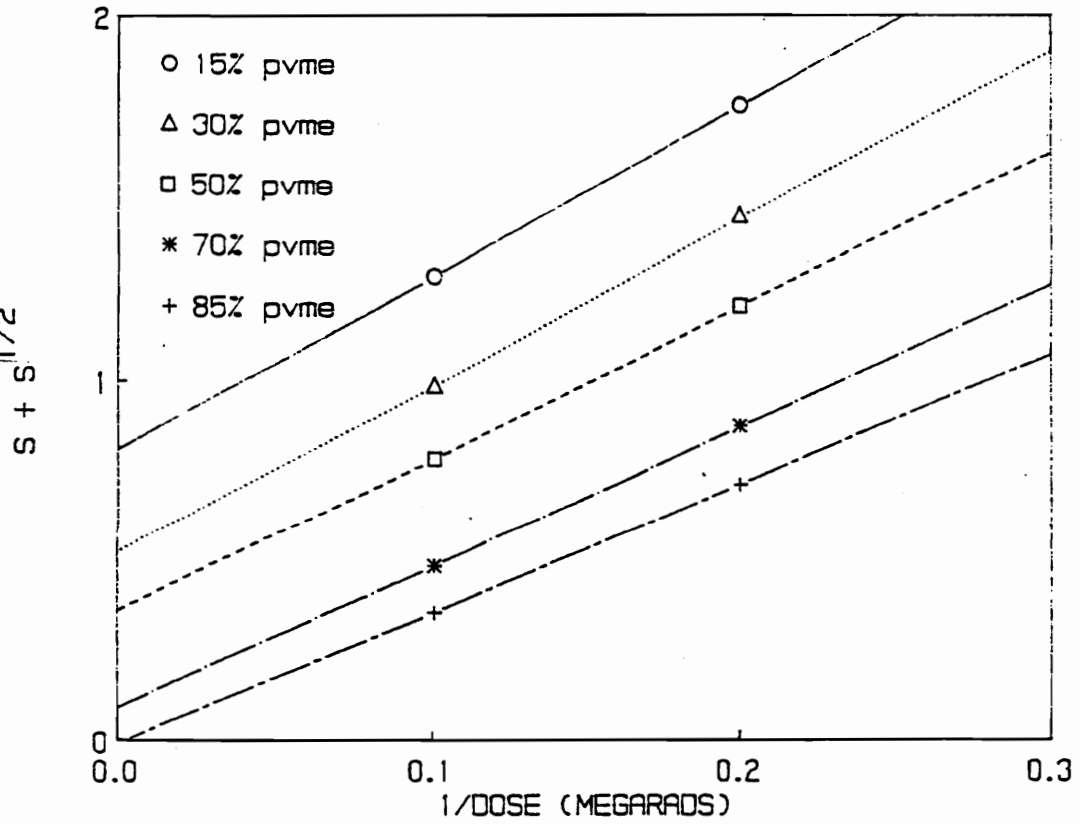

Figure 6-21. Charlesby-Pinner plots of the PS-PVME blends that have been phase separated at 160°C for two minutes.

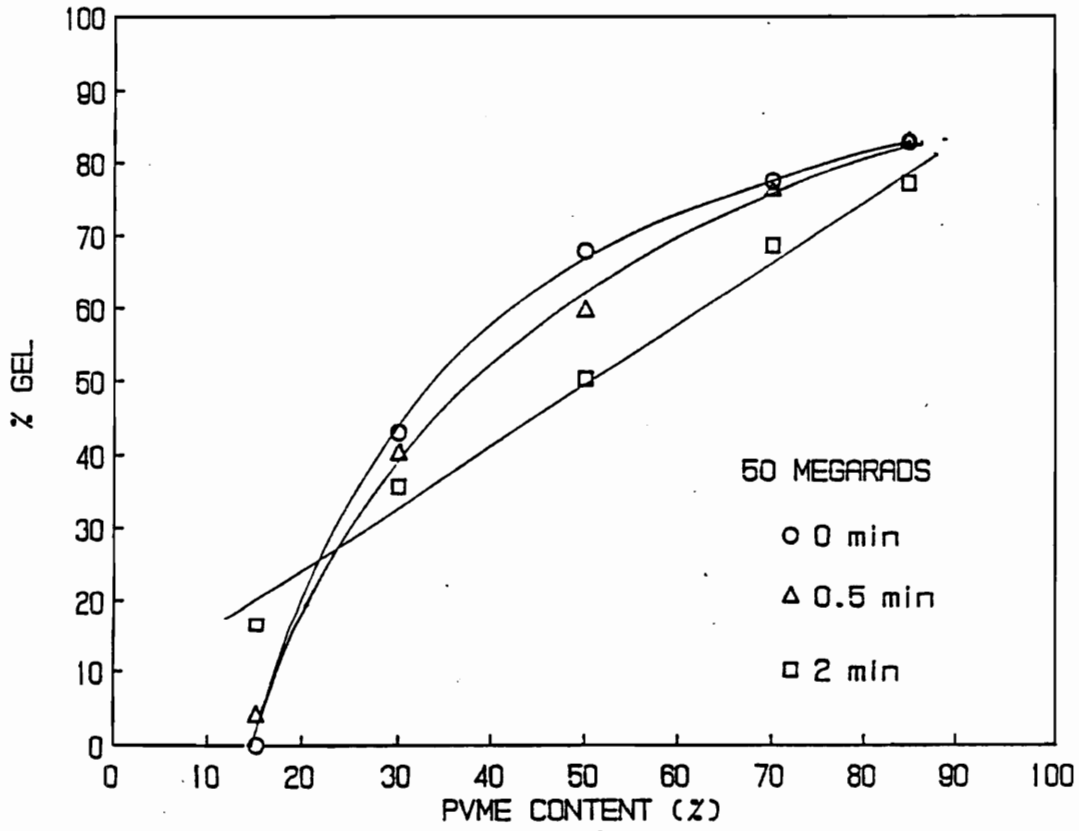

Figure 6-22. Plots of gel fraction versus composition of PS-PVME blends that have been irradiated to 50 megarads after phase separation at 160°C for the indicated times.

Figure 6-22 illustrates the effect of phase separation time on the gel - composition curve for a dose of 50 megarads. As shown, the gel - composition curve is transformed from a non-linear to linear curve as the phase separation time is increased. Furthermore, the change in gel content with phase separation time is composition dependent. At all compositions (except 15 wt % PVME) increasing the phase separation time results in a decrease in gel content, and this decrease is greatest at a blend composition of 50 wt % PVME. This behavior must be related to the relative G(X) values of the miscible blend, the PVME-rich phase, the PS-rich phase, and the relative concentrations of the latter two phases in the phase separated blend. For instance, at a composition of 85 wt % PVME, phase separation results in the formation of one phase with a G(X) value similar to that of the miscible blend and another phase with a relatively small G(X) value. However, the fraction of the low G(X) phase is fairly small, so there is only a small decrease in the gel content relative to the miscible blend. As the PVME content is decreased, the fraction of this low G(X) phase increases, resulting in a larger decrease in gel content as a function of phase separation time. This trend becomes reversed at low PVME concentrations since the G(X) of the miscible blend becomes so small that phase separation results in the development of a phase with a comparatively high G(X), causing an increase in gel content with phase separation time. This behavior is displayed by the 15 wt % PVME blend, where phase separation results in an increase in gel content from 0 to ca. 15 %.

Thermal Analysis. Figure 6-23 shows the DSC behavior of the phase separated blends (for 2 minutes at 160°C) that have been exposed to a 100 megarad dose. Comparison of these DSC scans with those for the unirradiated blends indicate very similar thermal behavior between these two blend series at low temperatures. However, it is evident that the upper glass transitions of the irradiated blends is very broad and not as distinct as the corresponding glass transitions of the unirradiated blends. It should be noted that these two blend series have slightly different thermal histories. The unirradiated blends were quenched from 160°C and immediately placed in the DSC furnace for analysis. The irradiated blends were quenched from 160°C, prepared for radiation exposure at room temperature, which took about five minutes, exposed to the electron beam, and then analyzed by DSC. Hence, the smearing of the upper glass transition could be the result of exposure to room temperature for a period of time or a result of radiation exposure. DSC analysis of the 50 wt% PVME blend just before radiation exposure confirmed the former possibility, as it displayed the exact same thermal behavior after irradiation. This is of little consequence however, since these blends were still phase separated during irradiation, as evidenced by film turbidity and the presence of a low glass transition temperature, even though the presence of a distinct PS-rich phase is not clearly displayed by DSC.

The thermal stability of these irradiated, phase separated blends was analyzed by the same method as described for the unirradiated blends. Recall that this involved

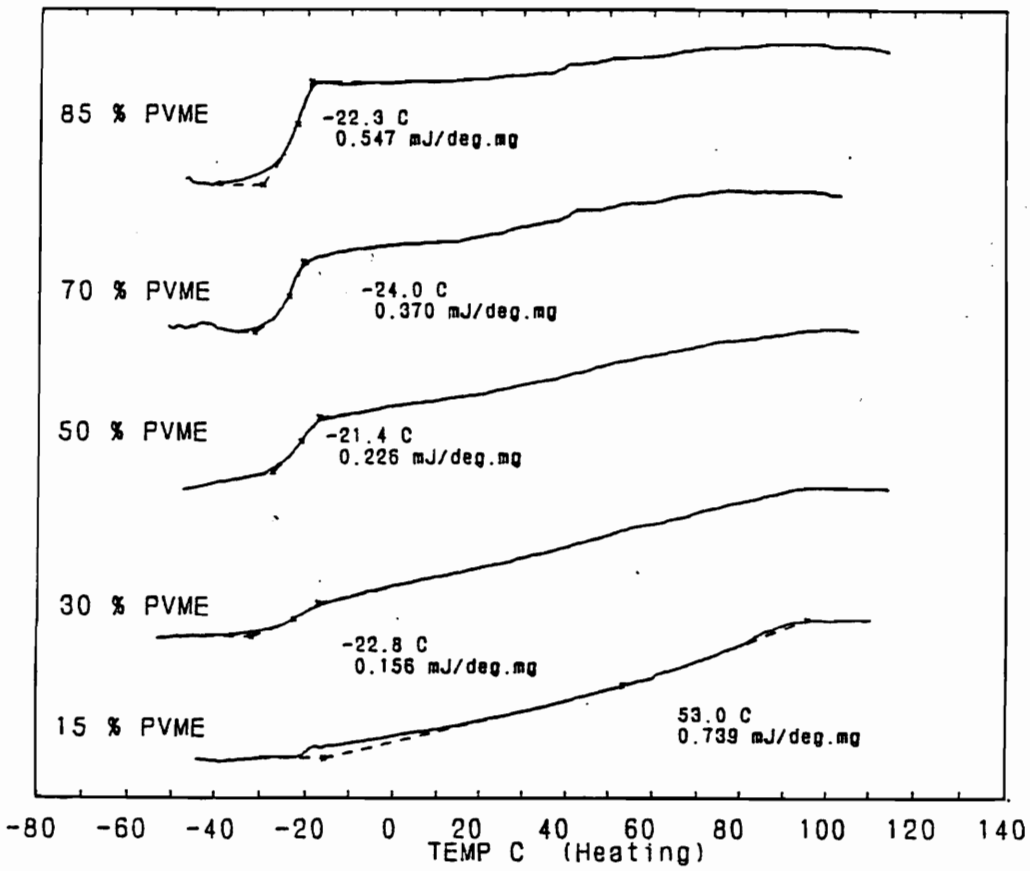

Figure 6-23. DSC scans of PS-PVME blends that have been phase separated at 160°C for two minutes followed by irradiation to 100 megarads.

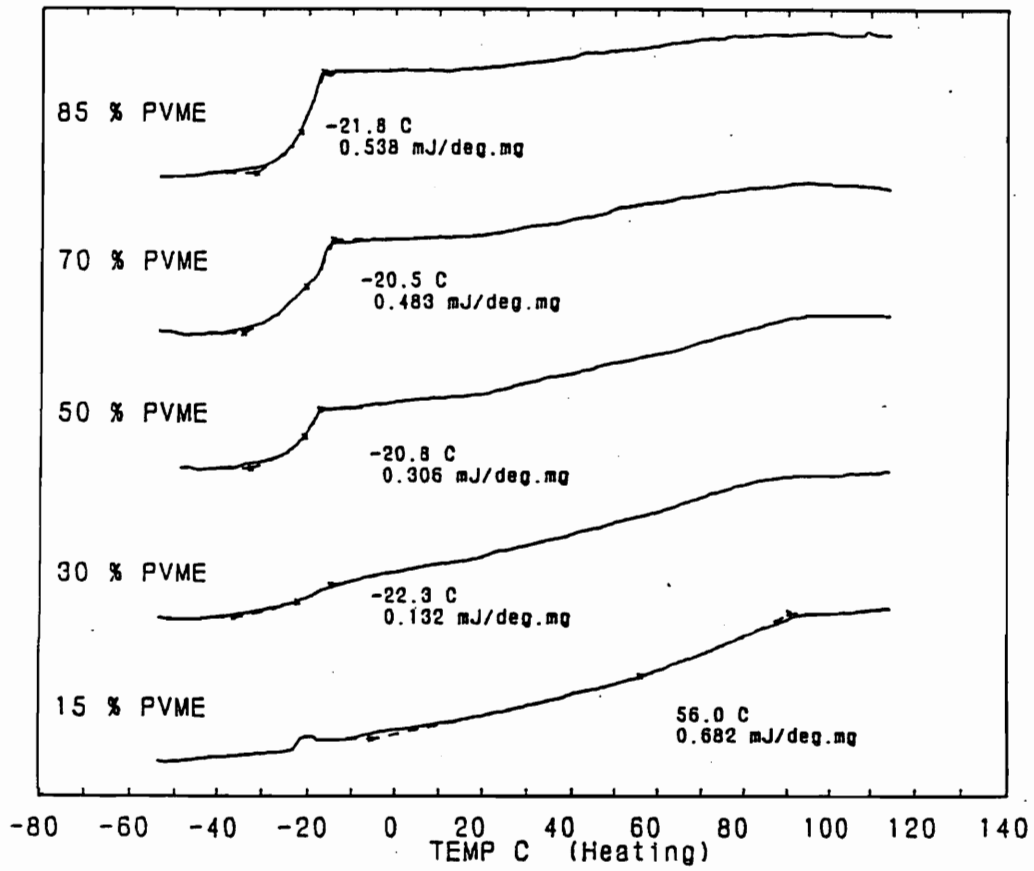

Figure 6-24. DSC scans of PS-PVME blends that have been phase separated at 160°C for two minutes, irradiated to 100 megarads, and then held at 100°C for 10 minutes.

holding the blends at 100°C for ten minutes and then performing the DSC analysis. The results of this experiment for the irradiated blends is shown in Figure 6-24. Comparison of this figure with Figure 6-23 shows no significant differences in the thermal behavior of this blend series, indicating that no phase dissolution occurred in ten minutes at 100°C. Recall that most of the unirradiated blends became completely miscible under these same conditions. Hence, radiation crosslinking of phase separated PS-PVME blends by a 100 megarad dose greatly enhances the thermal stability of this system.

6.4 CONCLUSIONS

This study has illustrated the effects of dose, blend composition, and morphology on the gel content and thermal behavior of a series of PS-PVME blends exposed to electron beam radiation. The extent of phase separation was shown to have a striking effect on response of this blend system to radiation exposure as determined by gel fraction measurements. It was suggested that the extent of phase separation influenced the composition and dose dependence of gel formation through changes in localized composition of the blends. Although exact values were not determined, changes in localized composition obviously affected the G(X) in these systems since PVME was shown to crosslink readily while PS was quite resistant to radiation crosslinking under the conditions employed. It was also shown that irradiation of the phase separated blends drastically slowed the rate of phase dissolution at 100°C, while having little effect on the glass transition behavior of this system.

6.5 REFERENCES

1. Bates, F.S. *Science,* 1991, **251**, 898.

2. Flory, P.J. *Principles of Polymer Chemistry,* Cornell University Press, Ithaca, NY, 1953.

3. Olabisi, O.; Robeson, L.M.; Shaw, M.T. *Polymer - Polymer Miscibility,* Academic Press, New York, NY, 1979.

4. Flory, P.J. *J. Am. Chem. Soc.,* 1965, **87**, 1833.

5. McMaster, L.P. *Macromolecules,* 1973, **6**, 760.

6. Nishi, T.; Wang, T.T.; Kwei, T.K. *Macromolecules,* 1975, **8**, 227.

7. Ubrich, J.M.; Larbi, F.B.L.; Halary, J.L.; Monnerie, L.; Bauer, B.J.; Han, C.C. *Macromolecules*, 1986, **19**, 810.

8. Briber, R.M.; Bauer, B.J. *Macromolecules,* 1988, **21**, 3296.

9. Tran-Cong, Q.; Nagaki, T.; Soen, T. *Macromolecules*, 1991, **24**, 1505.

10. Clough, R.L. in *Encycl. Polym. Sci. Eng.,* 2nd edition, John Wiley and Sons, New York, NY, 1988, **13**, 667.

CHAPTER VII

7.0 RECOMMENDATIONS FOR FUTURE WORK

7.1 Formation of Polymeric Microspheres

This study has illustrated that the production of polymeric microspheres by electron beam irradiation of polyaphrons containing a reactive monomer is feasible and some key parameters influencing the product properties have been identified. However, optimization of this process was not attempted. It is suggested that future work should involve attempts to improve this process with respect to optimizing the size distribution and physical properties of the microspheres for potential applications. Specifically, the following approaches should be considered:

1. Develop a new method for preparing the polyaphrons to narrow the resulting size distribution and minimize the average size of the crosslinked microspheres. A method which will increase the shear forces on the liquids in order to improve spreading is suggested. For example, a high speed blender, mixer, or shaker would significantly increase the shear forces developed during aphron formation as compared to shaking by hand. Larger shear forces may cause the relatively viscous monomer phase to spread more uniformly and thin to a greater extent prior to encapsulation by the aqueous phase. If this could be achieved, it would result in the production of smaller microspheres with a narrower size distribution than has been reported in this dissertation. This improvement is desirable because some applications require very uniform particle sizes, such as in drug delivery systems,

where the particles must be of uniform size to ensure a constant drug absorption rate.

2. Use different types of surfactants. Two different types of anionic surfactants were employed in this study. It is suggested that some nonionic and/or cationic surfactants be considered for use in the aqueous phase to determine the effects of surfactant type on the resulting product. Nonionic surfactants may be of particular interest because the electrostatic nature of the encapsulating aqueous film would be quite different due to the absence of charged moieties on the surfactant molecules. This may influence the spreading phenomena that occur during aphron formation, which may affect the final product properties.

3. Incorporate some different monomers into the polyaphron system in an attempt to produce microspheres with tailored physical properties. For example, a low viscosity acrylated polyurethane could be used to produce rubbery crosslinked particles, which may have potential applications for toughening glassy materials.

7.2 DSC Analysis of Irradiated LARC-CPI

The following suggestions are made for future work on the irradiation of LARC-CPI in order to more fully understand the response of this polymer to radiation exposure:

1. Perform a solid state ^{13}C NMR study on irradiated LARC-CPI with the intent to identify what types of molecular structures are created by radiation exposure. In particular, NMR analysis may be able to determine if there are crosslinked structures

in the irradiated polymer. Furthermore, the functional groups that are involved in the specific radiation chemistry may be identified and how they are altered as a result of irradiation. It should be realized however, that the NMR spectra of LARC-CPI has not been characterized to date, and hence some difficulties may be encountered in this approach. Unfortunately, the author cannot provide any suggestions for overcoming such problems, since experience with this technique is extremely limited.

2. Perform this type of study using gamma radiation in sealed ampules, etc. It would be valuable to compare results from a gamma radiation study with a electron beam radiation study so as to better understand the resulting differences. During electron beam processing, there is much less control over the radiation environment as compared to gamma irradiation. It would be of interest to determine how this affects the radiation degradation of this polymer (or any polymer) since most damage studies are performed using gamma radiation. This would be useful for future radiation damage studies with the electron beam because it would provide a basis for comparison with gamma radiation experiments. Furthermore, a gamma radiation study could provide information on the types of gases produced during the irradiation of LARC-CPI, which may be useful for gaining a better understanding of the radiation chemistry occurring in this polymer.

7.3 Reversal of Physical Aging By Electron Beam Irradiation

This study was somewhat exploratory in nature, as it illustrated a phenomena that has not been previously observed. Hence there is much work that could be done in this area. The following are several suggestions for future work that are worthy of consideration:

1. Look at the deaging behavior of a series of PMMA with varying molecular weights and corresponding end group concentrations. This would confirm or disprove the possibility of end groups reactions contributing to the sharp decrease in the endothermic peak area at the glass transition observed at very low doses.

2. Determine the radiation induced gas evolution behavior of polycarbonate. This information could be easily obtained by irradiating PC in a sealed ampule and subsequently analyzing the gases present in the ampule (i.e. a head space analysis). Specifically, determination of G(gas) values, types of gaseous products evolved, and the effect of dose and dose rate on these parameters would be helpful for gaining a better understanding of the origin of the observed deaging behavior of polycarbonate. Furthermore, a more thorough comparison could be made among the polymeric glasses used in this study with this information. This would provide a better understanding of the relationship between gas evolution and deaging, and whether gas evolution is indeed the cause of this observed phenomena.

3. Carry out dilatometry experiments to see if there is truly an increase in free volume resulting from radiation exposure. This would also be useful for determining

the efficiency of different gases in increasing free volume if gas evolution is indeed the origin of radiation induced deaging.

7.4 Irradiation of PS-PVME Blends

The following suggestions for future work are given with the intent of developing a better understanding of the irradiation of PS-PVME blends and the corresponding physical properties of these materials:

1. Consider the gelation behavior of PS-PVME blends that have been phase separated by a nucleation and growth mechanism and compare this with the results obtained in this study for the blends phase separated by spinodal decomposition. Since the morphology developed by a nucleation and growth mechanism is quite different from that of spinodal decomposition, it would be of interest to see how this would affect the subsequent gelation behavior.

2. Related to #1 above, consider the effect of phase separation temperature on the morphology of the blends and resulting gelation behavior. Altering the phase separation temperature within the spinodal region would change the composition of the resulting phases, and hence may have some influence on the gelation behavior.

3. Evaluate the physical and mechanical properties of the phase separated, irradiated blends with the motivation of developing potential applications for these materials. Spinodal decomposition of polymer blends results in the development of a rather unique morphology, which has been shown to be rendered quite stable by radiation crosslinking. By evaluating the physical and mechanical properties of these materials

and how some of the variables discussed affect these properties, an economical method for producing polymeric materials with unique and/or superior characteristics may be developed.

4. Develop a better understanding of the specific radiation chemistry of PVME in order to determine the energy transfer mechanisms that are operative during the irradiation of PS-PVME blends and why PS does not provide a protective effect against radiation exposure. Pulse radiolysis of PVME (and PS-PVME blends) may prove to be a useful technique for evaluating the specific radiation chemistry and what excited states, free radicals, etc. are produced during irradiation of these systems.

APPENDIX

A.1 Description of the Electron Beam Radiation Source and Dosimetry.

All experimental work described in this dissertation utilized an Energy Sciences Inc. (ESI) CB150 Electrocurtain as the electron beam radiation source. This system has a tungsten linear filament geometry as the electron source. The filament is encased in a beam control assembly which when energized, sets up an electric potential between the filamant and the extraction grid. The presence of the electric field results in the extraction of electrons from the filament and acceleration of the electrons towards a titanium foil window (see Figure A-1). The entire beam control assembly must be kept under high vacuum (10^{-5} - 10^{-7} torr). Hence, the foil window is necessary to allow for passage of the elctrons toward a conveyor system while maintaining proper vacuum in the beam assembly chamber. The beam control assembly operates at 350 Watts with an accelerating voltage of 175 kV. It should be noted that the electrons must pass through the foil window and several centimeters of atmosphere before impinging on the sample, so the energy of the incident electrons is actually slightly less than 175 kV. Under these conditions, organic materials with thicknesses of up to 5 mils may be processed with minimum variance in the depth - dose profile, which is ± 10 % for this type of electron beam source.

Unless otherwise noted, all samples processed are attached to a PET substrate which is taped to a metal plate. The plate is placed in a 6" x 6" aluminum tray on top of a wooden spacer. The wooden spacer is used to minimize the window to

sample distance. Once prepared, the aluminum tray is passed ubnder the electron beam at a constant predetermined velocity by the conveyor system. This system is equipped with a nitrogen purge which allows for processing in either air or under nitrogen. When processing under nitrogen, a Delta F Corp. trace oxygen analyzer is used to monitor the oxygen level in the conveyor chamber. When processing in air, an exhaust fan is used to remove ozone produced during irradiation. The conveyor system is completely self-shielded with lead plates and is interlocked such that if any radiation leak is detected, the system is automatically shut down.

The applied dose given to all samples was determined by the following equation:

$$D = \frac{Ixk}{S} \qquad [48]$$

where:

D = dose (megarads)

I = beam current (milliamps)

S = convweyor speed (ft/min)

k = 66.1 ± 2.3 ((Mrad ft/min)/mAmps))

This performance equation was developed from dosimetry measurements made on the system using Far West Technology radiochromic dosimeters. The dosimetry techniques are described in ESI Standard Procedure SP-821A. The conveyor speed is controlled by a dial setting and a calibration curve is used to determine the actual sample speed (see Figure A-2).

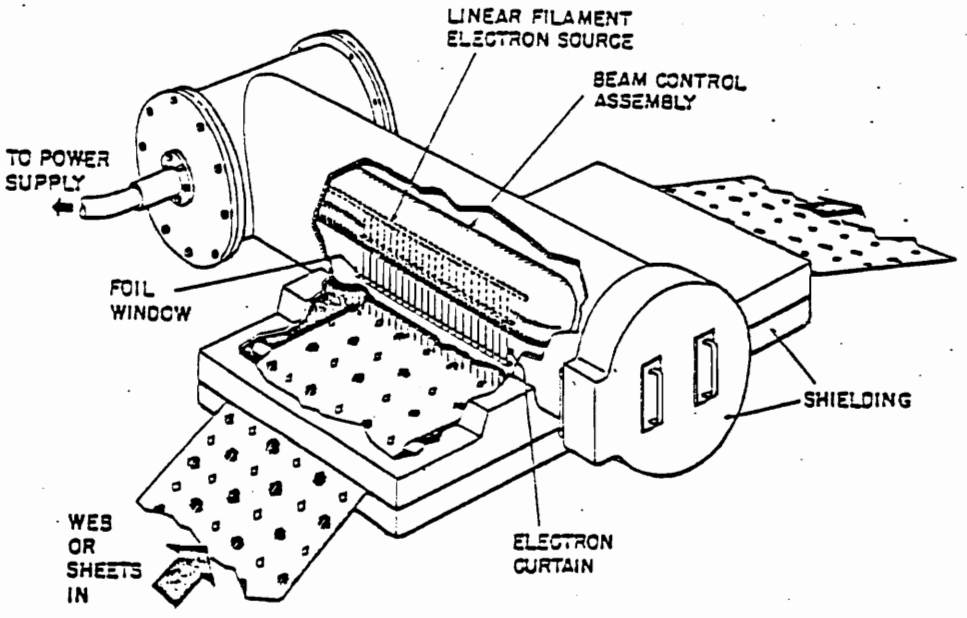

Figure A-1. Schematic drawing of the electron beam chamber and conveyor system in the ESI CB150 Electrocurtain.

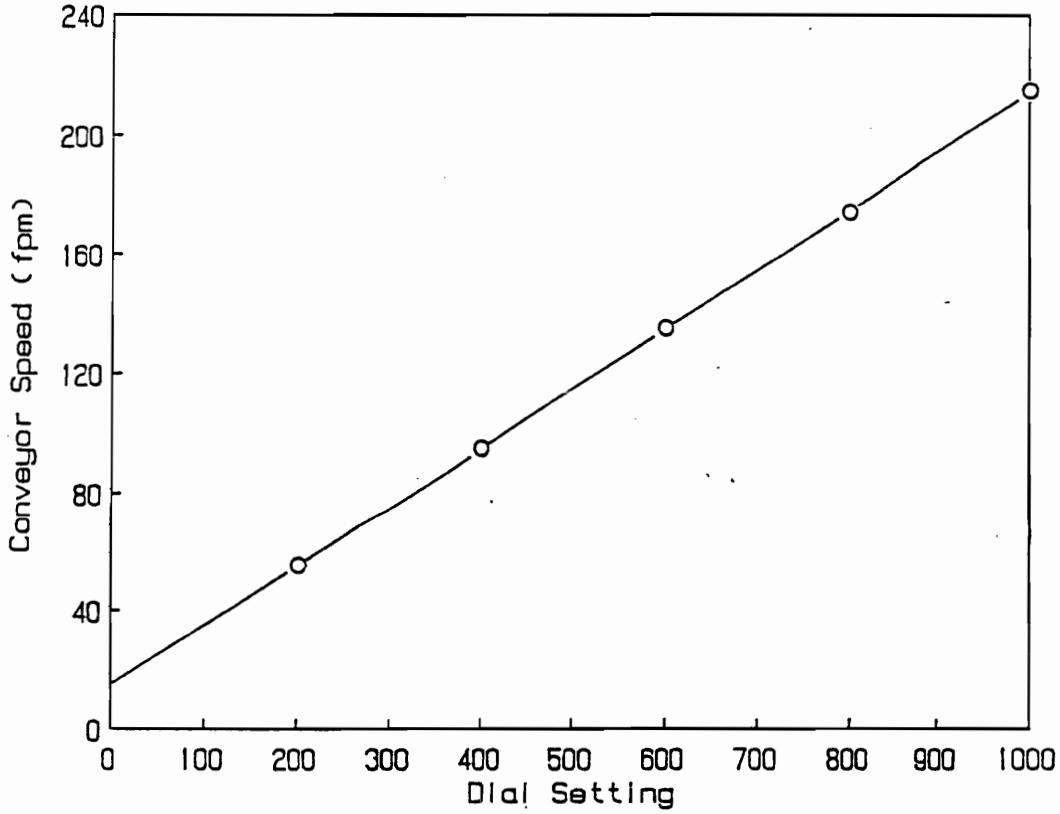

Figure A-2. Calibration curve for the conveyor speed controller.

VITA

Dale Curtis McHerron was born the youngest of three children and the only son of Lester and Elena McHerron on November 21, 1963 in Poughkeepsie, NY. His entire childhood was spent in Poughkeepsie until he graduated from Roy C. Ketcham High School in 1981. He then came to Virginia Tech to pursue an undergraduate degree in chemical engineering which he obtained in 1985. During this time he earned a black belt in Tae kwon do and was vice president of the Va. Tech Tae Kwon Do Club. He also joined Sigma Nu fraternity where he acted as academic chairman. After obtaining his undergraduate degree, he moved to Greenwood, SC where he worked for Milliken and Co. as a production manager and process engineer for three years. Here he developed an interest in polymeric materials and decided to return to school to pursue an advanced degree in this subject area. He returned to Virginia Tech to work under Dr. Garth Wilkes in the polymer characterization laboratory in the chemical engineering department, where this document was developed. He will now return to New York to work for IBM in the Advanced Thin Film Technology Group at East Fishkill. He has been an alpine skier for over twenty years and also currently enjoys mountain biking, camping and backpacking, and water sports.